

Making Light Work of Ligation: A Novel Toolbox for Photochemical Surface Design

Zur Erlangung des akademischen Grades eines
DOKTORS DER NATURWISSENSCHAFTEN
(Dr. rer. nat.)

Fakultät für Chemie und Biowissenschaften
Karlsruher Institut für Technologie (KIT) - Universitätsbereich

genehmigte
DISSERTATION
von

Dipl.-Chem. Thomas Paulöhl

aus
Ulm, Deutschland

Dekan: Prof. Dr. Martin Bastmeyer

Referent: Prof. Dr. Christopher Barner-Kowollik

Korreferent: Prof. Dr. Joachim Podlech

Tag der mündlichen Prüfung: 19.07.2013

Die vorliegende Arbeit wurde von September 2010 bis Mai 2013 unter Anleitung von Prof. Dr. Christopher Barner-Kowollik am Karlsruher Institut für Technologie (KIT) – Universitätsbereich angefertigt.

Ich erkläre hiermit, dass ich die vorliegende Doktorarbeit im Rahmen der Betreuung durch Prof. Dr. Christopher Barner-Kowollik, selbständig verfasst und keine anderen als die angegebenen Quellen und Hilfsmittel verwendet habe. Des Weiteren erkläre ich, dass ich mich derzeit in keinem laufenden Promotionsverfahren befinde, und auch keine vorausgegangenen Promotionsversuche unternommen habe.

Thomas Paulöhrl

Karlsruhe, den 31.05.2013

Abstract

The present thesis describes the development and application of novel light-induced approaches for the design of precisely modified surfaces with tailored chemical and biochemical properties at a molecular level. The established arsenal of photochemical methods confer inherently spatial temporal control and form – in their entirety – a facile toolbox for modular conjugations in solution and for spatially resolved immobilizations onto surfaces – including 3D resolved protein patterns on structurally complex microscaffolds – with high efficiency. The construction of advanced polymeric architectures is reported by combining thiol-ene chemistry with a polymeric backbone bearing photoreleasable thiols. Besides being a rapid and powerful tool for photochemical transformations, the *o*-nitrobenzyl moiety also enables – by considering the usual by-product as the actual product – for the first time to mildly confer spatio-temporal control to the realm of oxime ligation. Enhanced selectivity and fast reaction kinetics are features evidenced by utilizing a photochemical strategy avoiding photoremovable protecting moieties. Based upon the Diels-Alder trapping of photogenerated *o*-quinodimethanes, spatially constrained patterns of small-molecules, polymers and peptides bearing a pendant maleimide moiety are generated and imaged via time-of-flight secondary-ion mass spectrometry (ToF-SIMS). While the precise manipulation of surface chemistry even in a non-light protected environment represents alone a major step forward, the photochemical approach delivers unprecedented coupling performance at ambient temperature with inherent control over time and space, yet eschewing the use of a catalyst. Aside from the ability to achieve locally constrained surface immobilizations, the effort expended in their construction is of significant importance. A photochemical concept with a broadened scope is demonstrated by lifting the restriction to require a photoactive surface linker precisely tailored to specific needs. Based upon the facile photoactivation of a Diels-Alder cycloadduct in aqueous media or solid state, a novel light-induced approach allowing the photopatterning of peptides strictly composed of naturally occurring residues is reported. An alternative and very simple surface encoding protocol providing a facile means for the direct patterning of nucleophiles proceeds via the efficient trapping of photogenerated thioaldehydes. Ultimately, the 3D resolved multimolecular modification of complex microscaffolds, fabricated via direct laser writing (DLW), with a resolution close to one micron is achieved via two-photon activation and trapping of a latent diene.

Zusammenfassung

Die vorliegende Doktorarbeit beschreibt die Entwicklung neuer photochemischer Konzepte und deren Einsatz in der örtlich kontrollierten Modifikation von Oberflächen. Die chemischen Oberflächeneigenschaften konnten dabei auch für komplexe drei-dimensionale Mikrogerüste mit einer hohen Auflösung gezielt modifiziert werden. Zunächst wurde die *o*-nitrobenzyl Schutzgruppe für die Musterung von Oberflächen verwendet. Ein Benzaldehyd-Derivat, welches aufgrund seiner hohen Reaktivität typischerweise als unerwünschtes Nebenprodukt betrachtet wird, wurde hierbei für eine weitergehende Oximbildung eingesetzt. Eine lichtinduzierte Isomerisierungsreaktion wurde für die effiziente Bildung eines Diels-Alder Cycloaddukts eingesetzt und vermeidet Nebenreaktionen und den Einsatz von photochemischen Schutzgruppen. Die Oberflächenmusterungen wurden sowohl für Polymere als auch für Peptide mit Hilfe der Flugzeit-Sekundärionenmassen-spektrometrie (ToF-SIMS) nachgewiesen. Neben der Möglichkeit die Oberflächenchemie exakt zu kontrollieren bietet dieser Ansatz auch weitere Vorteile: C-C Bindungen können lichtinduziert und mit einer hohen Effizienz geknüpft werden, ohne dass Katalysatoren oder erhöhte Temperaturen notwendig werden. Neben der Kupplungseffizienz ist die örtliche Anbindung von unmodifizierten Substraten besonders erstrebenswert, da hierbei die synthetisch notwendigen Schritte für eine Oberflächenmusterung deutlich reduziert werden. Eine der entwickelten Strategien basiert auf einer Photoaktivierung eines Diels-Alder Cycloaddukts, welche auch in wässriger Lösung durchgeführt werden kann. Mit Hilfe dieses Verfahrens konnte die örtlich definierte Anbindung eines unmodifizierten c(RGDfK) Peptides in einer ToF-SIMS Studie nachgewiesen werden. Ein weiteres Oberflächenkodierungsverfahren basiert auf einer photochemischen Bildung von hochreaktiven Thioaldehyden, welche mit Nukleophilen direkt abgefangen werden können. Sowohl in Lösung als auch an der Oberfläche konnte mit Hilfe der Massenspektrometrie die Anbindung nachgewiesen und bildlich dargestellt werden. Dreidimensionale polymere Mikrogerüste, die mit dem Laserlithographiesystem (DLW) Verfahren hergestellt wurden, konnten mit dem entwickelten photoinduzierten Diels-Alder Oberflächenkodierungsverfahren mit verschiedenen Proteinen bis hin zu einer Auflösung von einem Mikrometer modifiziert werden. Letzteres Verfahren könnte zukünftig dazu dienen, ein besseres Verständnis von Zellen in realitäts-nähren drei-dimensionalen Umgebungen zu gewinnen.

Contents

1	Introduction	1
2	Photochemistry and Modular Synthetic Approaches - a Literature Review	5
2.1	Photochemistry – A Historical Perspective	5
2.2	Photoremovable Protecting Groups (PPGs)	9
2.3	Modularity in Modern (Polymer-) Chemistry	16
2.3.1	Uncatalyzed Alkyne-Azide Cycloaddition	18
2.3.2	(Hetero-)Diels-Alder Cycloaddition/Cycloreversion	20
3	Mass Spectrometry as a Versatile Characterization Technique in Solution and on Surface	25
3.1	Principles of Mass Spectrometry (MS)	25
3.1.1	Ionization Techniques	27
3.1.2	Mass Analyzers	28
3.2	Imaging Mass Spectrometry	29
3.2.1	Secondary Ion Mass Spectrometry (SIMS)	31
3.2.2	Desorption Electrospray Ionization (DESI)	32
4	Polymer Modification by <i>in situ</i> Phototriggered Deprotection and Thiolene Chemistry	33
4.1	Abstract	33
4.2	Introduction	34
4.3	Experimental Part	36
4.4	Results and Discussion	39
4.5	Conclusions	48
5	(Bio)Molecular Surface Patterning by Phototriggered Oxime Ligation	51
5.1	Abstract	51
5.2	Introduction	51
5.3	Experimental Part	52
5.4	Results and Discussion	59

5.5	Conclusions	66
6	Phototriggered Diels-Alder Surface (Bio)functionalization at Ambient Temperature	67
6.1	Abstract	67
6.2	Introduction	67
6.3	Experimental Part	69
6.4	Results and Discussion	75
6.5	Conclusions	83
7	Spatially Controlled Surface Immobilization of Non-Modified Peptides	85
7.1	Abstract	85
7.2	Introduction	86
7.3	Experimental Part	87
7.4	Results and Discussion	94
7.5	Conclusions	101
8	Spatially Controlled Surface Immobilization of Nucleophiles via Trapping of Thioaldehydes	103
8.1	Abstract	103
8.2	Introduction	103
8.3	Experimental Part	105
8.4	Results and Discussion	110
8.5	Conclusions	116
9	Three-Dimensional Microscaffolds Exhibiting Spatially Resolved Surface Chemistry	117
9.1	Abstract	117
9.2	Introduction	118
9.3	Experimental Part	119
9.4	Results and Discussion	124
9.5	Conclusions	132
10	Concluding Remarks and Outlook	133
10.1	Concluding Remarks	133
10.2	Outlook	135
11	Materials and Characterization	139
11.1	Materials	139
11.1.1	Materials Used in Chapter 4	139

11.1.2	Materials Used in Chapter 5	140
11.1.3	Materials Used in Chapter 6	140
11.1.4	Materials Used in Chapter 7	141
11.1.5	Materials Used in Chapter 8	142
11.1.6	Materials Used in Chapter 9	143
11.2	Photoreactions	144
11.3	Characterization	144
12	List of Abbreviations	149
	Bibliography	153
	Curriculum Vitae	175
	List of Publications and Conference Contributions	177
	Acknowledgment	181

1

Introduction

The construction of tailor-made functional materials has been greatly facilitated by the ability to generate precisely defined architectures via modern polymerization techniques and by assembling the resulting macromolecular building blocks covalently with unprecedented efficiency. Conjugation techniques providing modular synthetic pathways to previously inaccessible polymeric structures have to adhere to a number of – in the realm of polymer chemistry very harsh – criteria in order to earn the status of a *click* reaction, such as non-demanding reaction conditions and high efficiency.^[1,2] These characteristics are, however, not sufficient for applications that require a site-specific immobilization of (bio-)molecules onto two- or three-dimensional scaffolds.^[3] The recent years have therefore witnessed an increasing demand for protocols that allow for the efficient and mild modification of substrates at precisely defined positions.

Photoinduced approaches are particularly attractive since they inherently confer spatial/temporal control to covalent-bond-forming reactions or to desired molecular cleavages.^[4] The use of low-energetic light also provides a facile means to induce chemical transformations mildly without the need of (toxic) catalysts, additional reagents, or elevated temperatures. However, selectivity and efficiency issues^[5] are still associated with many photochemical reactions and their applicability in modular conjugations is yet to be demonstrated.

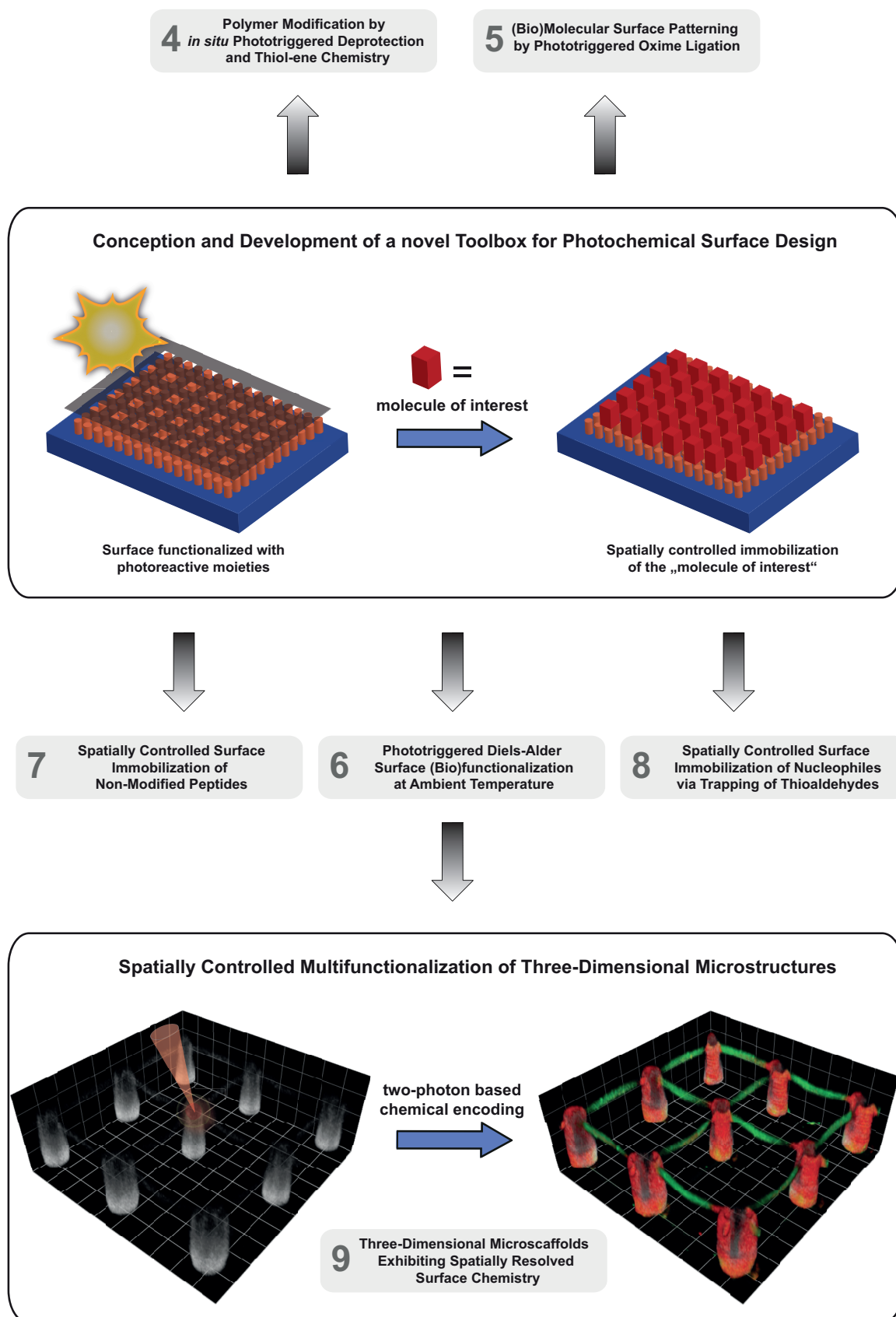
Striving to provide versatile surface patterning techniques with high efficiency and selectivity in benign solvents, the present thesis explores novel and resurrects seminal photochemical reactions. The developed approaches to construct patterns of (bio-) chemical substrates differ greatly regarding the involved chemistry. Generation of surface patterns will be demonstrated, for instance, by low-energy photodeprotection generating aldehyde as well as via Diels-Alder trapping of photogenerated *o*-quinodimethanes. The latter photoenol-mediated conjugation strategy is evidenced to possess many interesting features, including an enhanced selectivity and reactivity even in a non-light protected environment making it a first-class *click* reaction.

Of equal importance to the ability to achieve efficient locally constrained surface immobilizations is the ease with which they can be obtained. Indeed, considerable efforts are required for the preparation of surface anchors and substrates bearing appropriate coupling moieties. These compounds have to be precisely tailored to the concrete needs, thus limiting their versatility. To tackle this problem, two chapters of the present thesis address the design of novel photochemical systems able to efficiently react with functionalities inherently present in many substrates. To date, photochemical concepts that allow for direct amine-mediated patterning are rather rare and often involve extremely reactive intermediates, such as nitrenes or carbenes,^[6] which clearly results in limitations of selectivity or orthogonality. The investigations in the present thesis comprise, inter alia, the development of a novel light-triggered approach for the spatially controlled surface immobilization of non-modified peptides. Based upon the photoactivation of a Diels-Alder cyclo-adduct, the key step is evidenced to proceed smoothly in aqueous media. The efficient one-pot trapping of photogenerated thioaldehydes is demonstrated to be an alternative methodology for the direct and synthetically facile immobilization of nucleophiles.

The diverse set of photochemical approaches developed herein establish, in their entirety, a versatile toolbox for photopatterning in different contexts, yet with high efficiency. To gain comparable data, all reaction outcomes are determined via identical analytical methods; electrospray ionisation mass spectrometry (ESI-MS) for solution experiments and imaging time-of-flight secondary-ion mass spectrometry (ToF-SIMS) for the locally constrained composition analysis of solid substrates.

Direct laser writing (DLW) has emerged as a powerful technique for the fabrication of precisely defined three-dimensional (3D) polymeric microstructures.^[7,8] While these constructs represent a most significant step forward,^[9] the

recent years have witnessed an increasing demand to chemically functionalize the generated structures at pre-defined positions. One key idea of the current thesis is thus to combine advantageous features of the herein developed photoenol mediated immobilization technique with the high degree of spatial control achievable via two-photon absorption processes. Via this methodology, the locally constrained functionalization of precisely modified 3D polymeric microscaffolds with proteins will be demonstrated and the applicability of these constructs to mimic cell environments can be envisaged. An outline of the investigations addressed in the present thesis are depicted in Scheme 1.1.



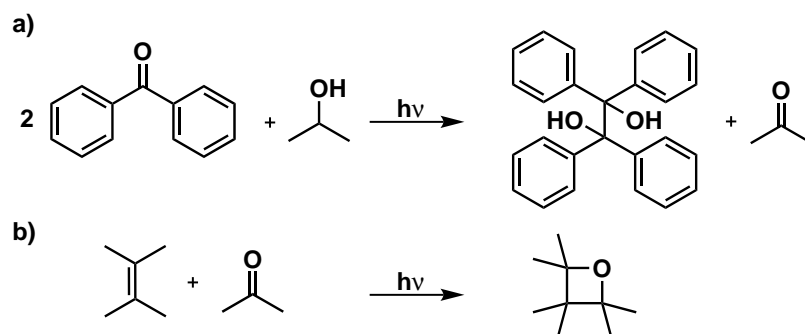
Scheme 1.1 Outline of the approaches that have been addressed in the present thesis. The numbers refer to the numbering of the respective chapters.

2

Photochemistry and Modular Synthetic Approaches - a Literature Review

2.1 Photochemistry – A Historical Perspective

In the early 20th century, Ciamician and Silber were one of the firsts to discover that not only thermal energy but also (sun-)light can be applied to initiate a chemical reaction.^[10-12] Maybe one of the most notable light-triggered transformations was the reduction of benzophenone to benzopinacol in propan-2-ol (see Scheme 2.1a).^[13,14] Shortly thereafter, Paternò and Chieffi reported the successful formation of four-membered oxetane rings by irradiation of carbonyl compounds with ultraviolet light and subsequent addition to alkenes (see Scheme 2.1b).^[15] Büchi and coworkers have reinvestigated this early work^[16] and since then the reaction is termed the Paternò-Büchi reaction. Several reports have been devoted to study the mechanism of the reaction and it is today widely acknowledged to involve a biradical intermediate.^[17] The synthetic application of this reaction is rich and, to mention just one example, Junckers and Conradi have recently demonstrated the modifications of aldehyde end-capped polymers with alkenes under UV irradiation.^[18] Concomitant with the success of synthetic photochemistry was the exploration of its theoretical background. Absorption of a definite quantity (a result derived by quantum me-



Scheme 2.1 Two early discovered photoreactions: the light triggered reduction of benzophenone to benzopinacol (a) and the Paternò-Büchi reaction (b).

chemical calculations) of energy can promote an electron to an excited (singlet) state. The fate of electronically excited states can be visualized in simplified terms in a Jabłoński diagram (see Figure 2.1).^[19,20] Note that in such a diagram the energy scale is plotted vertically and the horizontal lines represent vibrational states, e.g. of the ground- or the excited state (electronic states are depicted by thick-, vibrational states by thinner lines). The following radiative (straight arrows) and non-radiative (curly arrows) electronic transitions can occur:^[20]

- internal conversion (IC) is a very fast, radiationless and spin allowed transition from a higher to a lower electronic state, during which process the electronic excitation energy is converted into vibrational energy.^[21,22]
- radiationless decay can occur in form of a very fast energy cascade or via a

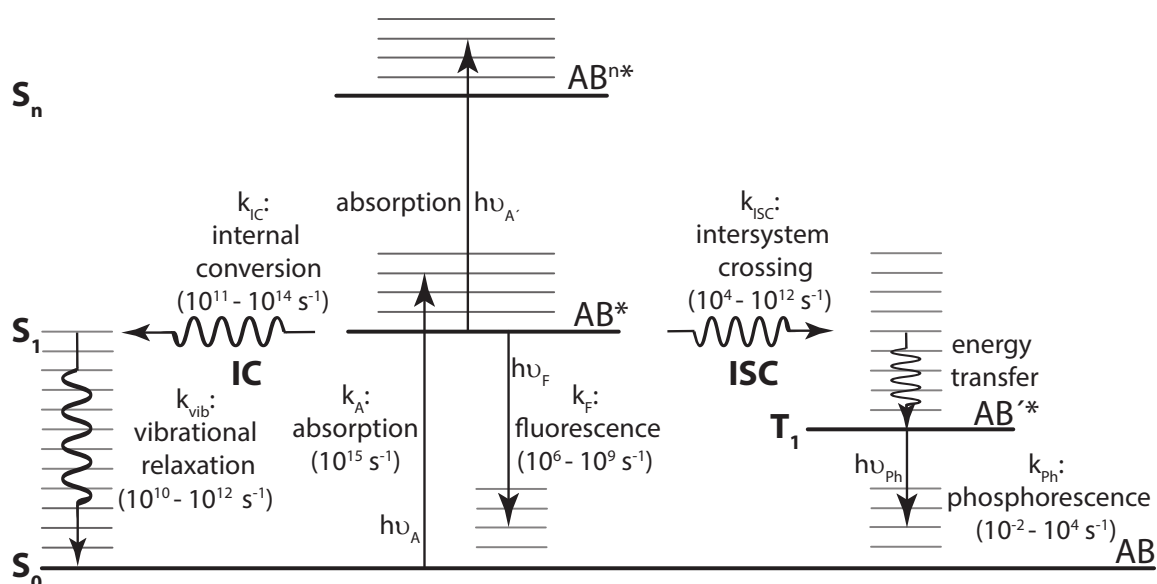


Figure 2.1 The Jabłoński diagram illustrates radiative (straight arrows) and non-radiative (curly arrows) electronic transitions in a molecule. Electronic states are depicted by thick-, vibrational states by thinner horizontal lines and the energy scale is plotted vertically. ISC = intersystem crossing, IC = internal conversion.

slower vibrational cascade. The obtained thermal / kinetic energy is transferred to the environment.^[23]

- intersystem crossing (ISC) is a spin-forbidden, radiationless process between two electronic states, which differ – in contrast to IC – in their spin multiplicity.^[24] Highly ISC efficiencies are obtained in cases where the S_1 - T_1 energy gap is small and a typical example is benzophenone ($ISC \approx 1$).^[25] Generally, ketones exhibit enhanced ISC rates, whereas the ones of olefins are almost about zero.^[20] After ISC crossing, the T_1 state (which is typically many orders of magnitude longer lived than the S_1 state) may return to the ground state S_0 , either by a radiationless process or by emission of light (phosphorescence).
- relaxation from an excited singlet state can occur to a vibrational low level of S_0 (but not to the vibrational ground state) by emission of light (fluorescence).^[26] In most cases, the wavelength of the emitted radiation is longer than that of the absorbed one and the relaxation occurs from the lowest excited state S_1 , although $S_2 \rightarrow S_0$ fluorescence has also been reported.^[27] Fluorescence can also be employed to measure the distance (typically in the range of 1 nm - 10 nm) between two chromophores and the mechanism is called Förster resonance energy transfer (FRET). The basic idea of the technique is the radiationless energy transfer of an excited donor molecule to an acceptor with an efficiency, which is inversely proportional to the sixth power of the distance.^[28]

Many chemical reactions proceed from the excited triplet state, as they can have lifetimes magnitudes higher than that of excited singlet states. As alluded to above, the ISC rates of ketones are typically high and it is therefore apparent that the photochemical reactions associated with ketones / aldehydes are extremely fruitful. Indeed, photoreactions involving carbonyls have received much attention since the early days of photochemistry and Norrish and coworkers were the first to systematically categorize the reactions after $n \rightarrow \pi^*$ excitation.^[29,30] The so-called Norrish type I reaction proceeds via an α -cleavage (preferentially – but not exclusively – from the triplet state) resulting in the formation of highly reactive acyl- and alkyl radicals (see Figure 2.2). Starting from these reactive species, the following reactions may occur:^[20] Recombination of the radicals (A), α -hydrogen abstraction (B), intermolecular hydrogen abstraction (C), and decarbonylation (D). One important example of a Norrish type I reaction is the light-induced decomposition of benzoin into benzoyl- and benzyl alcohol radicals, which both can act as initiators for radical polymerizations. Indeed, the net initiation efficiencies of benzoyl radicals and their respective methyl substituted analogues has been recently established via a post-polymerization analysis.^[31]

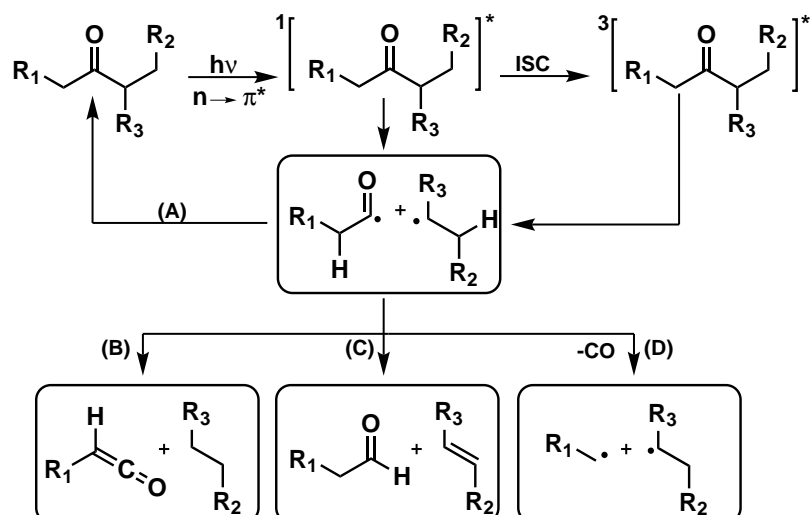


Figure 2.2 The Norrish type I process proceeds via an α -cleavage and results in the formation of highly reactive acyl- and alkyl radicals.

An alkyl ketone with a hydrogen atom in γ -position can undergo a light-triggered intramolecular [1,5]-H-shift and the reaction sequence is called a Norrish type II process (see Figure 2.3). The key species is a biradical, which can be formed from both the singlet or the triplet $n\pi^*$ state.^[32,33] The biradical character was confirmed via photoracemization and quenching experiments.^[33] Analysis of the obtained product mixture, which was found to include cyclization (F) and elimination (G),^[34] is another clear indication for the key intermediate.

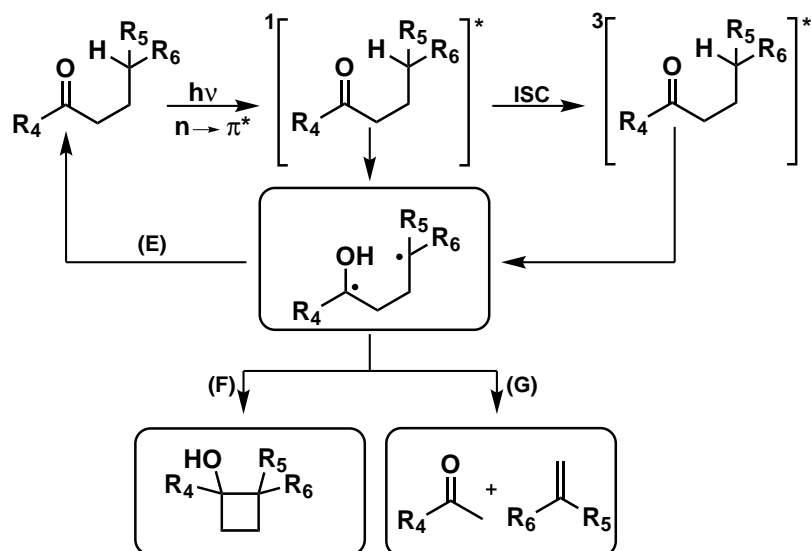


Figure 2.3 The Norrish type II proceeds via a light-triggered intramolecular [1,5]-H shift in the course of which the key species – a biradical – is formed.

2.2 Photoremovable Protecting Groups (PPGs)

Photoremovable protecting groups (PPGs) are typically employed to render – by chemical modification – a reactive functionality in a molecule inert.^[35,36] The initial molecular activity can subsequently – with spatial and temporal control – be restored via a light-trigger. In contrast to other protecting groups (PGs) in organic chemistry, the photolabile moiety can be cleaved upon a light stimulus without the need for any additional reagents.^[37] Such orthogonal and mild photolytic cleavage is particularly attractive for solid-supported organic synthesis^[38] and in the field of combinatorial library screening.^[39,40]

It is possible to identify several relevant criteria to evaluate the applicability of a novel PPG:^[41]

1. The PPG should be synthetically installable in a molecule with ease and – upon attachment – the relevant reactive functionality in a molecule should be rendered fully inert (under the given conditions).
2. The photodeprotection should be sufficiently fast, clean and highly efficient.
3. The efficiency of the photodeprotection is governed by the quantum yield ϕ and the absorption coefficient ϵ of the chromophore; thus the photoreaction should occur with high quantum yield ϕ and a strong absorbance at the excitation wavelength.
4. The absorbance spectrum of the reactive chromophore in the PPG should possess a sufficiently high absorption coefficient ϵ at wavelengths above 320 nm in order to avoid highly energetic and thus harmful irradiation, e.g., of the biological environment.
5. If the photoreaction is accompanied with photolytic by-products, they should **not**:
 - affect the system under investigation
 - be chemically reactive (e.g., formation of radicals should be avoided)
 - interfere with the on-going photolysis (e.g., generating secondary photolysis).
6. Ideally, the photoreaction should take place irrespective of the utilized solvent. For biological applications it is often sufficient when the photoreaction can proceed under physiological conditions.

Unfortunately, none of the literature known PPG can fully meet all these specifications and – with this said – it is clear that there is not one PPG which fits the specific needs and requirements of all applications. Despite this drawback, PPGs are still widely exploited in many research areas and many synonymous words exist, e.g., PPGs have also often been referred to the terms *caged* compounds or *cages*, especially when it comes to biochemistry. In this line, the light-initiated re-activation of a molecule is often referred to as uncaging. Figure 2.4 illustrates exemplarily a typical literature procedure for the caging and uncaging of amines in solution and on a surface.^[35] Prop-2-en-1-amine is protected by a base catalyzed reaction with 6-nitroveratryloxycarbonyl chloride (NVOC-Cl) – a commercially available reactant – in high yield (see Figure 2.4a). Light-triggered deprotection of the initial amine functionality is subsequently achieved via mild irradiation at 411 nm (see Figure 2.4b). However, it should be noted that the formation of the second photolysis product, namely *o*-nitrosobenzaldehyde, is typically – given by its high reactivity and strong absorbance – undesired and can induce the formation of numerous by-products, such as the formation of an imine, resulting from the phototriggered release of amine substrate and *o*-nitrosobenzaldehyde.^[42] Chapter 5 will discuss the problems associated with the *o*-nitrosobenzaldehyde in detail and will also demonstrate that the usual by-product can also be considered as the actual product for subsequent transformations. Nevertheless, the use of light as a trigger provides a straightforward means to obtain spatial and temporal control on a surface (see Figure 2.4c). In detail, silicon wafers were modified with the above described photoactive NVOC moiety via silane chemistry. Free amines are released only in the irradiated zone, which functionalities allow for subsequent chemical surface derivatization. PPGs have emerged in the literature in thousands of examples, which accounts for the immense importance attached to them. Several excellent reviews and perspectives have already been published covering their mechanistic aspects^[41] and applications in polymerization,^[43,44] organic synthesis,^[17,37,45] biochemistry,^[46–51] and biomedicine^[52,53]. PPGs are in many examples also applied to surfaces in order to gain spatial control for subsequent reactions, and del Campo *et al.* reviewed this topic very recently.^[36] Given the large number of PPGs (and their derivatives), the following will only focus on the two most widely employed PPGs, namely the *o*-nitrobenzyl- and the coumarin-4-ylmethyl moiety. For a more detailed overview over other important PPGs – e.g., *p*-hydroxyphenacyl (pHP) (see Scheme 2.2a),^[54] 2,5-dimethylphenacyl (DMP) (see Scheme 2.2b),^[55] and 3',5'-dimethoxybenzoin (DMB) (see Scheme 2.2c),^[56] to name but a few – the reader is referred to the above mentioned reviews including the up-to-date one by Klàn *et al.*^[57]

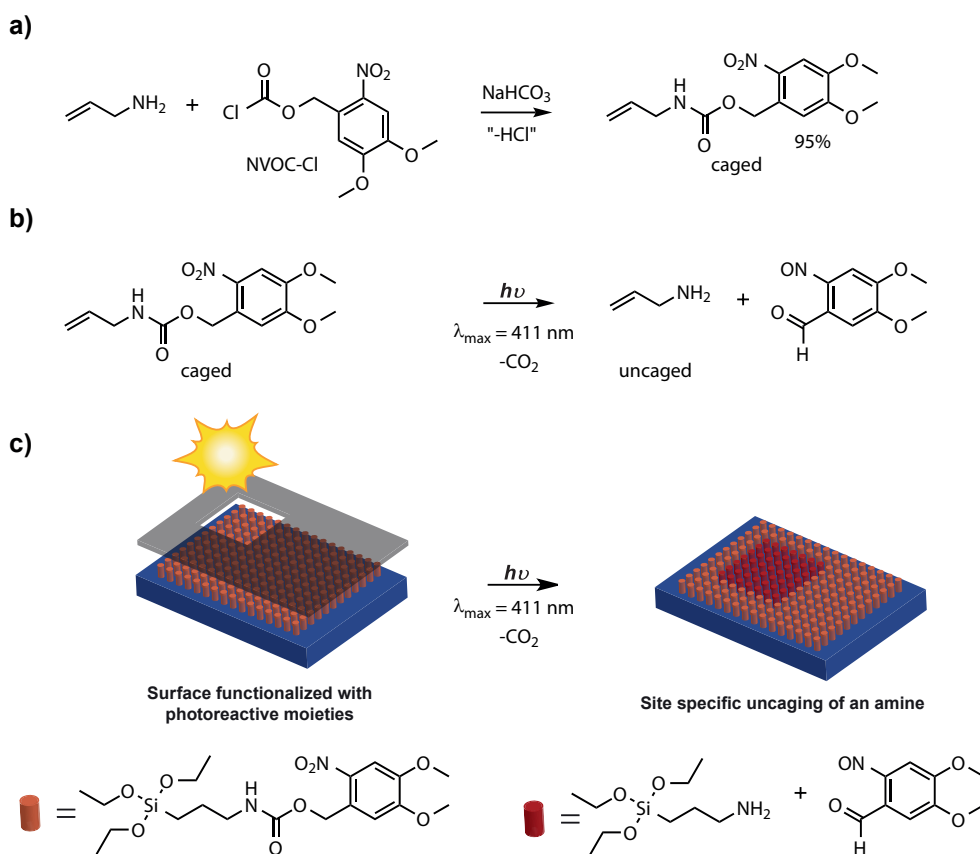
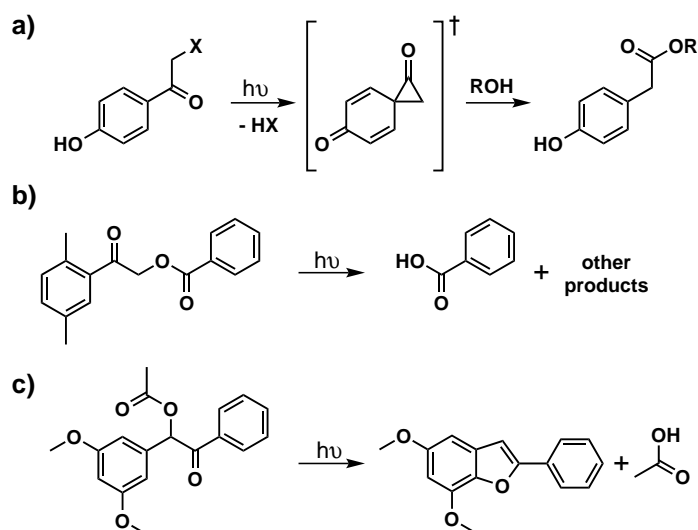


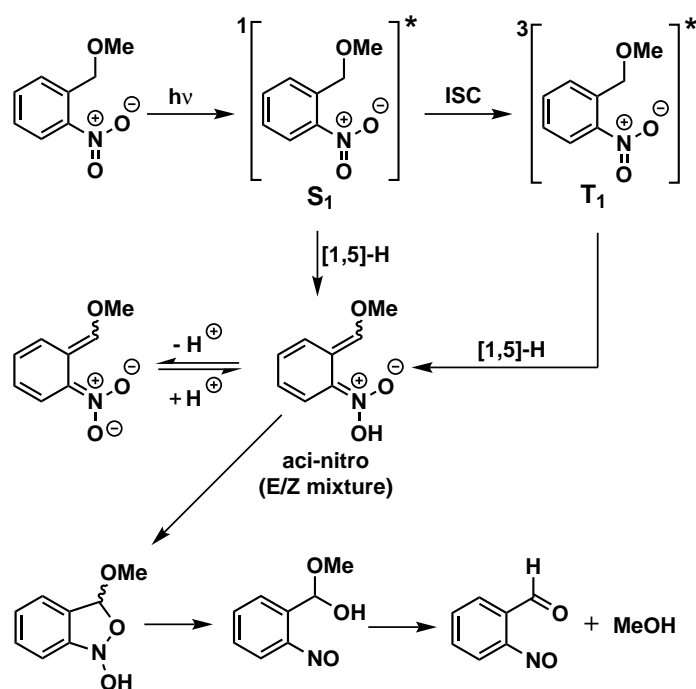
Figure 2.4 Example for the *caging* and *uncaging* of an amine functionality. Prop-2-en-1-amine is protected via a base catalyzed reaction with 6-nitroveratryloxycarbonyl chloride (NVOC-Cl) (a) and can be subsequently deprotected via mild irradiation at 411 nm (b). The concept can be translated to surface derivatization (c).^[35]



Scheme 2.2 Examples for PPGs less frequently employed than the *o*-nitrobenzyl- and the coumarin-4-ylmethyl group: the *p*-hydroxyphenacyl (pHP) (a),^[54] the 2,5-dimethylphenacyl (DMP) (b),^[55] and the 3',5'-dimethoxybenzoin (DMB)^[56] (c) moiety.^[57]

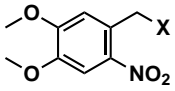
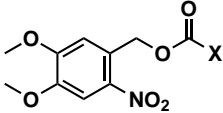
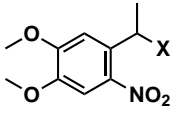
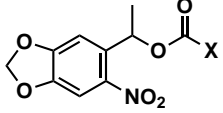
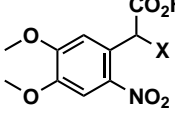
The *o*-Nitrobenzyl Photoremovable Protecting Group (PPG)

Of the myriad of PPGs which have been studied, the *o*-nitrobenzyl group is certainly the predominant one.^[57] One of the earliest studies on the photoisomerization of *o*-nitrobenzaldehyde to *o*-nitrosobenzoic acid dates back to 1901,^[10] however, it took seven decades until Woodward *et al.* could finally demonstrate the broad applicability of this PPG.^[42] Scheme 2.3 depicts the revised mechanism of the phototriggered release of methanol from 1-(methoxymethyl)-2-nitrobenzene.^[57–59] The main pathway after photon absorption of the substrate is the formation of an excited singlet state (S_1) which can subsequently undergo a [1,5]-H-shift to an aci-nitro intermediate. In minor amounts, the latter can also be formed via intersystem crossing to an excited triplet state (T_1) followed by a [1,5]-H-shift. In any case, an irreversible cyclization of the neutral^[60] aci-nitro compound to the 3-methoxybenzo[*c*]isoxazol-1(3*H*)-ol intermediate occurs, which in turn ring-opens to a hemiacetal intermediate. Hydrolysis of the latter releases methanol in a final reaction step, which is rate-determining for the overall sequence in aqueous media at neutral pH.^[58] Many different *o*-nitrobenzyl derivatives have been reported and Table 2.1 summarizes some commonly utilized ones. The absorbance maximum of *o*-nitrobenzyl cages can be red-shifted above 350 nm by utilizing 2-nitrobenzenes bearing two methoxy substituents in ortho and para position. Consequently, 4,5-dimethoxy-2-nitrobenzyl (DMNB) and 6-nitroveratryloxycarbonyl (NVOC) can both be deprotected via mild irradiation (at 365 nm) and are, indeed, the most frequently utilized cages among



Scheme 2.3 Revised photodeprotection mechanism of 1-(methoxymethyl)-2-nitrobenzene.^[57–59]

Table 2.1 A selection of common *o*-nitrobenzyl cages with red-shifted absorbance.

Structure	Name	Protected groups (selected examples)	λ_{\max} [nm]
	4,5-dimethoxy-2-nitrobenzyl (DMNB)	SH (X=SR) ^[61] OH (X=OR) ^[62] COOH (X=OCOR) ^[63]	≈ 355
	6-nitroveratryloxycarbonyl (NVOC)	NH ₂ (X=NHR) ^[35] OH (X=OR) ^[35]	≈ 355
	4,5-dimethoxy-2-nitrophenethyl (DMNPE)	HOPO ₃ R (X=OPO ₃ R) ^[64] OH (X=OR) ^[65] COOH (X=OCOR) ^[66]	≈ 355
	α -methyl-6-nitro-piperonyloxycarbonyl (MeNPOC)	NH ₂ (X=NHR) ^[67] OH (X=OR) ^[68]	≈ 345
	α -carboxy-4,5-dimethoxy-2-nitrobenzyl (CDMNB)	SH (X=SR) ^[69] OH (X=OR) ^[70] COOH (X=OCOR) ^[71]	≈ 355

the *o*-nitrobenzyl family. One important application of the NOVC moiety was developed by Fodor *et al.* when they performed a parallel chemical synthesis of peptides via a light-directed approach on a glass surface.^[72] In this approach, NVOC-protected amino acids were reacted at their 1-hydroxybenzotriazole (HOBT)-activated C-terminus with free amines on a glass surface. Subsequent irradiation released new amino-functionalities, which were again coupled to another amino acid. Finally, an array of 1024 peptides – each of which with a different amino acid sequence – was obtained by irradiation and iteration of the coupling procedure. Among the many *o*-nitrobenzyl derivatives which have been evaluated, it is worthwhile to further highlight three of them: the 4,5-dimethoxy-2-nitrophenethyl (DMNPE),^[64] the α -methyl-6-nitro-piperonyloxycarbonyl (MeNPOC)^[67] and the α -carboxy-4,5-dimethoxy-2-nitrobenzyl (CDMNB)^[70] derivative. In the first two cases, an α -methyl group was introduced in an attempt to gain higher quantum yields for the photoreaction. Indeed, the quantum yields of the different *o*-nitrobenzyl derivatives increased drastically (typical by a factor of 5) by addition of an α -methyl group, e.g., the quantum yield for the photodeprotection in acetonitrile

increases from 2-nitrobenzyl pivalate ($\Phi = 0.13$) to 1-(2-nitrophenyl)ethyl pivalate ($\Phi = 0.64$).^[73] Additionally, the acetophenone-type primary photolysis product was reported to be less toxic to the biological environment when compared to *o*-nitrosobenzaldehyde.^[74] Finally, α -carboxy-4,5-dimethoxy-2-nitrobenzyl (CDMNB) with its inherent α -carboxy group provides a much better water solubility of the photocage, which is an important feature for biological applications. An additional benefit of the CDMNB moiety is its high quantum yield upon irradiation at 365 nm ($\Phi = 0.17$, the value has to be compared to $\Phi = 0.0013$ of NVOC^[37]), and it is to be expected that it might find use in a wide range of biological applications.^[71] The cage, however, demonstrates one drawback: The competition between cleavage and decarboxylation during photolysis.^[69] In summary, the *o*-nitrobenzyl group has emerged as a powerful tool that can be used to cage a wide range of organic functionalities such as carboxy,^[69] amine,^[74] hydroxy,^[75] and thiol.^[76] Many precursors of the PPG are commercially available and, thus, the synthetic effort for the production of caged compounds is lowered. The underlying mechanism for the photocleavage of *o*-nitrobenzyl derivatives is well studied^[58] and proceeds - depending on the leaving group, solvent and the employed *o*-nitrobenzyl derivative - quite efficiently. The *o*-nitrobenzyl PPG possesses also some drawbacks: The main limitation stems from its photolytic by-product(s), e.g., *o*-nitrosobenzaldehyde, which is the most reactive one. These compounds are potentially cell-toxic and reduce the overall release yield by an internal light filter effect. The latter has been attributed to the transformation of the undesired photoproduct, *o*-nitrosobenzaldehyde, into an azobenzene derivative which indeed can absorb light more efficiently than the initial PPG.^[77]

The Coumarin-4-ylmethyl Photoremovable Protecting Group (PPG)

Givens and Matuszewski observed in 1984 that 7-methoxycoumarin-4-ylmethyl (7-MCM) diethyl phosphate undergoes highly efficient phototriggered reactions with nucleophiles.^[78] For instance, diethyl phosphate was replaced highly efficiently with methanol upon irradiation at 360 nm and Schade *et al.* proposed in 1999 a general mechanism of this photoreaction (see Figure 2.5).^[79] After light absorption, the excited singlet state can undergo heterolytic C–O bond cleavage. The S_N1 mechanism of the bond-breaking event was experimentally supported by employing ¹⁸O labeled water as a nucleophile. ESI-MS analysis demonstrated that only the coumarin based photolysis product contained ¹⁸O isotope whereas the liberated diethylphosphoric acid remained unlabeled.^[79] For good leaving groups (e.g., when a strong acid is released) the latter rate-determining step was found to exceed $10^9 s^{-1}$,^[86] which highlights an attractive feature of the coumarin-4-ylmethyl cages:

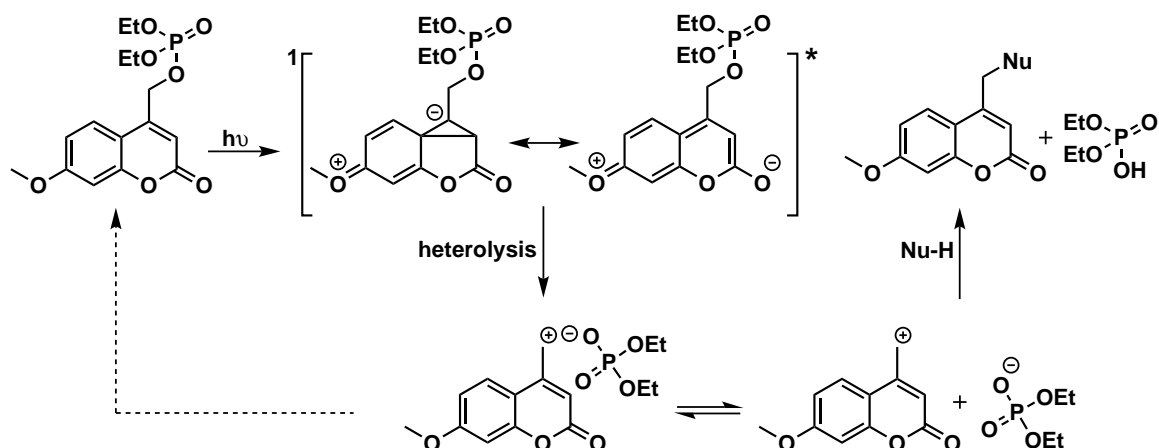


Figure 2.5 The general mechanism for the light-triggered release of a leaving group and subsequent attachment of a nucleophile (NuH) is illustrated by example of the photorelease of a phosphate from (7-methoxycoumarin-4-yl)methyl (7-MCM).^[57,79]

the remarkably fast release rates. The key intermediate, an ion pair of coumarinyl-methyl cation and phosphate anion,^[57] can either reform starting material or can undergo a reaction with nucleophiles. As it was the case for the *o*-nitrobenzyl PPG, several modifications of the coumarinylmethyl base structure have been evaluated in an attempt to further optimize its physical properties (e.g., water solvability,

Table 2.2 A selection of common coumarin-4-ylmethyl cages with red-shifted absorbance.

Structure	Name	Protected groups (selected examples)	λ_{\max} [nm]
	7-methoxycoumarin -4-ylmethyl (7-MCM)	HOPO ₃ R ₂ (X=PO ₃ R ₂) ^[79] HOOR (X=OCOR) ^[79] HOSO ₂ R (X=SO ₂ R) ^[79]	≈ 325
	6-bromo-7-hydroxycoumarin -4-ylmethyl (BHCM)	HOOR (X=OCOR) ^[80] NH ₂ R (X=CONHR) ^[80]	≈ 370
	6,7-bis(carboxymethoxy) coumarin-4-ylmethyl (BCMCM)	HOPO ₃ R ₂ (X=PO ₃ R ₂) ^[81] NH ₂ R (X=CONHR) ^[82]	≈ 340
	7-(diethylamino)coumarin -4-ylmethyl (DEACM)	HOPO ₃ R ₂ (X=PO ₃ R ₂) ^[83] HOOR (X=OCOR) ^[84] NH ₂ R (X=CONHR) ^[85]	≈ 395

absorbance at even longer wavelengths and quantum yield; see Table 2.2). The first generation of coumarin-4-ylmethyl cages, e.g., those based on 7-MCM, displayed unsatisfactory characteristics, such as blue-shifted absorption maxima and poor aqueous solubility. To address these issues, the 6-bromo-7-hydroxycoumarin-4-ylmethyl (BHCM) was designed,^[80] which moiety provides a bathochromic shift of the absorption maxima of 45 nm and a slightly enhanced water solubility. The latter could be further improved by appending carboxylates, e.g., in case of 6,7-bis(carboxymethoxy)coumarin-4-ylmethyl (BCMCM).^[81,82] Further development in this area led to the design of a second generation of coumarin-4-ylmethyl cages bearing an amino moiety. 7-(diethylamino)coumarin-4-ylmethyl (DEACM) is one of the most promising candidates within this class.^[83,84] Indeed, the modification led to a significant improvement of the entire photochemical system by shifting the absorbance maximum to nearly 400 nm^[86] while still providing one of the highest quantum yields among all coumarin derivatives. To conclude, the coumarin-4-ylmethyl cage presents many attractive features making it the PPG of choice in cases where fast release rates, strong absorbance at wavelengths above 390 nm, pro-fluorescent properties or a decent two-photon excitation cross-section are necessary. It presents, however, some drawbacks: moderate quantum yields, strong absorbing photo-products and stability issues in aqueous solutions.^[79]

2.3 Modularity in Modern (Polymer-) Chemistry

In 2001, Sharpless and colleagues established a promising framework of chemical reactions, which are tailor-made to efficiently generate complex structures.^[1] The novel philosophy is based upon modularity and orthogonality. This concept has undoubtedly marked a turning point in synthetic chemistry: Complex structures and architectures are no longer synthesized sequentially – as is the case in traditional organic synthesis – but are rather assembled out of smaller parts, the so-called building blocks, which can be linked via highly orthogonal and efficient chemical reactions. The fundamental basis for a *click* reaction is thus a strong thermodynamic driving force ($> 80 \text{ kJ}\cdot\text{mol}^{-1}$). Sharpless defined several other criteria for a reaction to earn the status of a *click* reaction:^[1]

- the reaction should proceed under simple reaction conditions with very high chemical yield.
- the process must be modular and wide in scope.
- readily available starting materials/reagents should be utilized and the reaction product must be stable under physiological conditions.

- the reaction should take place in either no solvent or a benign solvent such as water and the product should be obtained stereospecifically via a simple product isolation procedure.

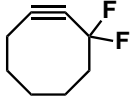
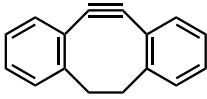
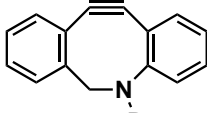
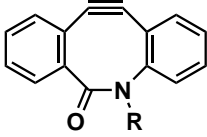
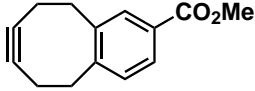
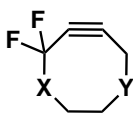
The above mentioned criteria have to be carefully weighed according to their relevance for the specific need. For the design of a variety of materials, for instance, a highly stereospecific ligation reaction might be a less important criterion. In cases where selective precipitation is not an option, product separation can be a challenging task in polymer chemistry. With this said, a new key condition arises directly for polymer-polymer ligation reactions: equimolarity.^[2] The development of the *click* philosophy was inspired by nature, where molecules are also created from relatively small building blocks. Proteins, for instance, arise from only 21 amino acids that are joined through amide linkages and self-assemble into the complex structure. This concept can be described as “*nature’s way of performing combinatorial chemistry*”^[87] and it can be utilized as a guiding principle for modern day chemistry. The fundamental principles of *click* chemistry have been widely adapted and, indeed, the generation of complex materials is nowadays highly dominated by modular synthetic pathways.^[88] *Click* chemistry has had significant impact on an incredible number of original articles. Many excellent reviews, perspectives and special issues have been published and the wide field of modular chemistry was further subdivided into these key areas: bioconjugation,^[89] materials science,^[90] drug discovery,^[91,92] and polymer chemistry,^[2,93] to name but a few.^[87] In summary, the advent of *click* chemistry has led to a paradigm shift in the design of modern polymeric architectures.^[94] Indeed, the modern day chemist has a number of tools available to carry out ultra rapid and mild conjugation chemistry with functionalities such as (in ascending order of importance): tetrazole–alkene,^[95] tetrazine–alkene,^[96] aminoxy–aldehyde/ketone,^[97] thiol–ene,^[98] (hetero-) dienophile–diene,^[99] and azide–alkyne,^[100] to name but a few.^[101] Within this framework of reactions, polymers can be viewed as molecular building blocks providing convenient modular access to complex architectures.^[102] Additionally, the *click* philosophy provided also solutions for the construction of many previously unattainable materials. Viewed from a more critical point-of-view, one has to recognize that numerous publications exist, in which *click* reactions have just been utilized to replace equally effective methods in order to benefit from the prestige attached to the *click* concept. One of the topics, however, in which traditional chemistry cannot compete with modular chemistry is the field of biomaterials. Indeed, the increasing demand for synthetic tools combining synthetic materials with biological systems is – given by the very strict requirements of mild, orthogonal, selective and non-harmful reaction conditions – a task tailor-made for *click* conjugations. Two widely employed tools for

mild and efficient conjugation of different functionalities will be highlighted in the following.

2.3.1 Uncatalyzed Alkyne-Azide Cycloaddition

The classical 1,3-dipolar cycloaddition between organic azides and terminal, non-activated alkynes leads – even at elevated temperatures – to the often rather sluggish formation of 1,2,3-triazoles. Thus, the reaction does not adhere to the above described set of *click* requirements. It was the discovery of a dramatic rate acceleration accompanied with regioselectivity under copper(I) catalysis by Medal and Sharpless,^[103,104] which made the cycloaddition suddenly the premier example of *click* reactions.^[105] Of special importance of the Huisgen azide–alkyne cycloaddition (CuAAC) is its bioorthogonal character. Azide and alkyne functionality are generally not present in natural systems and both moieties have been shown to be essentially inert to the many other functional groups in biological environments.^[106] Although the 1,2,3-triazole ring has proven to be inert to most chemical and thermal treatments, Bielawski and coworkers have recently demonstrated the ability to reverse the 1,3-dipolar cycloaddition by ultrasonification.^[107] As a consequence, synthetic modifications do not always require complex synthetic means, yet can sometimes be performed in a rather simple manner. The following drawbacks should be taken into consideration: (a) in this specific case, the cycloreversion is limited to 1,2,3-triazole rings which are functionalized with sufficiently long polymer chains on both sides, and (b) materials made by 1,3-azide-alkyne cycloadditions might fail if the applied stress exceeds a critical value.^[108] The toxicity of transition metal salts for *in vivo* applications has also led to a great deal of research to develop activated alkynes, which do not require a catalyst, while still providing extremely fast reaction kinetics at ambient temperature. One of the earliest examples of strain-promoted azide-alkyne cycloadditions (SPAAC) dates back to 1961, when Wittig and Krebs observed a very fast reaction between phenylazide and cyclooctynes without catalysis.^[109] It was not until 2004, that Bertozzi and coworkers resurrected this inspiring seminal work and demonstrated efficient coupling under physiological conditions and without apparent toxicity to living cells.^[110] Since then, many groups have harnessed the reactivity of cyclooctynes^[111] and the development of even stronger activated derivatives is still on-going (see Table 2.3). A reactivity enhancement for the cycloaddition of azides was achieved by Bertozzi and coworkers by creating difluorinated cyclooctyne (DIFO), a compound possessing electron-withdrawing fluorine substituents at the propargylic position.^[113] The accelerating effect has been recently studied in great detail and it is interesting to note that it is not based on an increased ring-strain, but rather on hyperconjugative interaction.^[118] A limiting

Table 2.3 A selection of activated cyclooctynes. The reactivities of the compounds are normalized to cyclooctyne and were determined from literature values of their respective second-order rate coefficients.^[112]

Structure	Name (abbreviation)	Inventor (year)	Reactivity [a.u.]
	cyclooctyne (OCT)	Bertozzi ^[110] (2004)	1
	difluorinated cyclooctyne (DIFO)	Bertozzi ^[113] (2008)	≈ 50 ^[111]
	dibenzocyclooctyne (DIBO)	Boons ^[114] (2008)	≈ 30 ^[112]
	aza-dibenzocyclooctyne (ADIBO)	van Delft, ^[115] Popik ^[116] (2010)	≈ 200 ^[112]
	biarylazacyclooctynone (BARAC)	Bertozzi ^[117] (2010)	≈ 500 ^[111]
	carboxymethylmonobenzocyclooctyne (COMBO)	Kele ^[112] (2012)	≈ 150 ^[112]
	<i>predicted compound</i>	Alabugin ^[111] (2012)	>> 500 ^[111]

factor in these novel technologies is, however, the inefficient, multi-step synthesis of DIFO and its derivatives.^[119] A different approach was taken by Boons (dibenzocyclooctyne (DIBO)),^[114] van Delft (aza-dibenzocyclooctyne (ADIBO))^[115] and Kele (carboxymethylmonobenzocyclooctyne (COMBO))^[112] with their respective coworkers. Following the strategy of reactant destabilization, the ring-strains have steadily increased, which has ultimately led to the development of the most reactive cyclooctyne derivative to date: biarylazacyclooctynone (BARAC).^[117] Although the latter compound allows for an extremely rapid coupling, e.g. *in vivo* for the imaging of azide-labeled biomolecules,^[120] one has to note a major drawback: the reactivity enhancement of highly ring-strained cyclooctynes comes at the price of their overall decreased stability.^[111] As a consequence, BARAC has to be kept refrigerated in a light protected environment.^[121] At this point, one has to acknowledge that nature

follows a superior strategy, which does not sacrifice stability for reactivity and is based on transition state stabilization. Alabugin and coworkers followed such a pathway and were able to predict – by a computational analysis of potential energy profiles – alkynes which are less strained, while still providing high reactivity.^[111] These encouraging theoretical results still have to be verified experimentally and have to be examined with regard to their practical applicability, especially as the accessibility of activated alkynes continues to be a problem.

2.3.2 (Hetero-)Diels-Alder Cycloaddition/Cycloreversion

Aside from catalyzed or uncatalyzed azide-alkyne ligation, the Diels-Alder (DA) reaction is another extremely powerful and widely utilized conjugation technique.^[122,123] In 1928, Diels and Alder fully characterized the cycloadduct formed from the reaction between cyclopentadiene and 1,4-benzoquinone.^[124] The cycloaddition generates in a thermally driven and concerted reaction a new cyclohexene ring in a highly regiospecific manner.^[125] The formation of the two new sigma bonds is suprafacial; thus stereochemical information of both reactants are transferred to the product(s). The Woodward-Hoffmann rules (originally stemming from concepts of orbital phase and symmetry of the frontier molecular orbitals (FMO)) can predict the regioselectivity of the DA reaction. Typically, the ‘para’ and ‘ortho’ positions are favored, a result which can be rationalized by taking the FMO coefficients of the sigma bond forming atoms into account.^[126] Moreover, the endo transition state is in many cases also preferred above the exo transition state,^[127] a result that is subject to on-going discussions. Different hypotheses are being discussed, such as secondary orbital interactions, electrostatic forces, solvent effects, and others.^[128] The versatility of Diels-Alder reactions stems also from the fact that it may be performed – depending on the electronic situation of the reactants – in different modes. Figure 2.6a depicts a fast and thermally reversible reaction between a functionalized electron poor dienophile (maleimide) and a diene, which is locked into its s-cis configuration (cyclopentadiene). The reaction has proven to be extremely effective and allows for the construction of cyclic polymers of high purity.^[129] The interaction between the HOMO of the diene and the LUMO of the dienophile constitutes the smallest energy gap and this situation is termed the normal electron demand DA reaction. The inverse case is depicted in Figure 2.6b. 1,2,4,5-tetrazine reacts in an exceptionally fast cycloaddition with trans-cyclooctene and, after the occurrence of a retro-DA (rDA) reaction, nitrogen is released as the only by-product. Finally, and in protic medium, the reaction product rearranges to the shown isomer. This reaction sequence has been recently proposed as a versatile method for ultrafast bioconjugation *in vivo*.^[130,131] One of the most widely

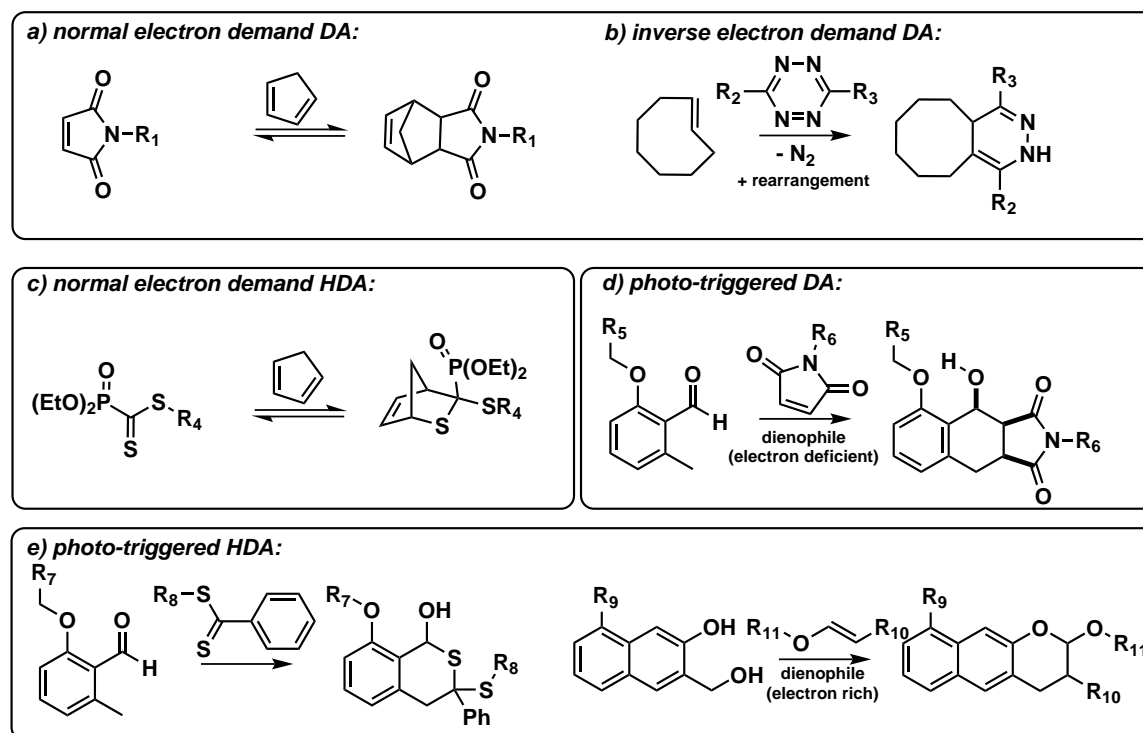


Figure 2.6 Diels-Alder reactions can be performed in different modes: with normal electron demand (a), with inverse electron demand (b), with a heterogenic atom being involved (c), with a light trigger (d), and via photoconjugation with heterogenic atom(s) being involved (left: dithiobenzoate, right: 3-(hydroxymethyl)-naphthalene-2-ol) (e).

utilized tetrazine-derivatives is (4-(1,2,4,5-tetrazin-3-yl)phenyl)methanamine, an asymmetrically substituted tetrazine derivative, which has shown excellent stability to water.^[96] Additionally, the Diels-Alder reaction can be performed with electron deficient hetero-dienophiles and considerable amount of research stated below has been conducted in the group of Barner-Kowollik. One important example allowing for the rapid and atom-economic construction of well-designed architectures is the hetero Diels-Alder (HDA) reaction of electron deficient dithioesters with cyclopentadiene (see Figure 2.6c).^[94] The highly reactive cyclopentadiene was utilized in this approach to allow for a reduction in the temperature range in which the forward and reverse HDA reaction can take place. Following from this concept, a reversible addition-fragmentation chain transfer (RAFT) agent, namely a phosphoryl dithioester (shown in the Figure), was trialed for its quantitative reversibility under thermal conditions and it was possible to map the reaction progress on a molecular level.^[102] Importantly, the dithioester has to fulfill a dual purpose: Besides serving as a versatile anchor for HDA cycloadditions, the dithioester has to also efficiently mediate / control the RAFT process. The versatile RAFT-HDA concept came into play at the synthesis of complex polymer architectures such as stars,^[132] for the modification of Si surfaces,^[133] for the modification of microspheres,^[134] and

for the construction of high molecular weight block copolymers.^[135] The efficient synthesis of the latter material was confirmed and visualized by employing 2D liquid adsorption chromatography at critical conditions (LACCC).^[136] The construction of self-healing materials via reversible bonding and debonding on demand is another upcoming research area. Cross-linked polymeric network have been shown to be formed at ambient temperature, whereas thermal treatment led – confirmed by SEC – to a rapid debonding.^[137] Similarly, a step-growth polymerization / depolymerization of a bis-diene with a bis-RAFT agent has been recently theoretically and experimentally assessed.^[138] Besides reversibility, the enhancement of the reaction rate is also an highly investigated research area. In this context, a HDA reaction featuring ultrafast kinetics has been reported and it is based on the Lewis acid promoted cycloaddition of cyclopentadienyl end-capped polymers, which are readily accessible via bromine substitution of ATRP polymers with nickelocene,^[139] to RAFT polymers featuring a pyridinyl dithioester end-group.^[99] Such a modular approach to access complex architectures has recently been shown to be rate-enhanced in water, thus allowing for the utilization of less reactive dienes without catalyst.^[140] Although this clearly marks a major step forward for the technology to be employed in biological systems, one has to note that up to now only a few electron deficient dithioesters are suitable candidates for efficient HDA reactions. Moreover, the dithioesters needs to serve a second role in order to be useful for atom-efficient couplings. They have to efficiently mediate/control the RAFT process and the aforementioned electron deficient RAFT agents can only perform this task for some monomer families: for acrylates (e.g., isobornyl acrylate^[135] or a protected glycomonomer^[140]) by employing benzyl pyridin-2-yl dithioformate, 2-hydroxyethyl acrylate^[140] by employing 2-cyanoprop-2-yl diethoxyphosphoryl dithioformate, and styrene^[99] by employing benzyl (diethoxyphosphoryl) dithioformate as chain-transfer agent. One way of tackling this problem is to employ an *in situ* formed, extremely reactive diene, which would allow for a HDA reaction with unactivated RAFT agents. Following from the inspiring work of Yang and Rivas,^[142] and the detailed studies of Sammes,^[143] Barner-Kowollik and coworkers have explored the photogeneration of hydroxy-*o*-quinodimethanes. It could be demonstrated that the latter highly reactive diene can be trapped by (hetero-)dienophiles, e.g. for the modular construction of block-copolymers via trapping with maleimides (see Figure 2.6d)^[144] or non-activated RAFT agents, such as 2-cyanopropyl dithiobenzoate (CPDB).^[145] The latter result marks a key point for the on-going development of novel ultrafast / catalyst-free HDA reactions, since it enables for the first time for the atom-efficient ligation with polymers prepared by conventional RAFT agents.^[145] The photoinduced isomerization of *o*-methyl-substituted aromatic ketones or aldehydes to *o*-quinodimethanes has been estab-

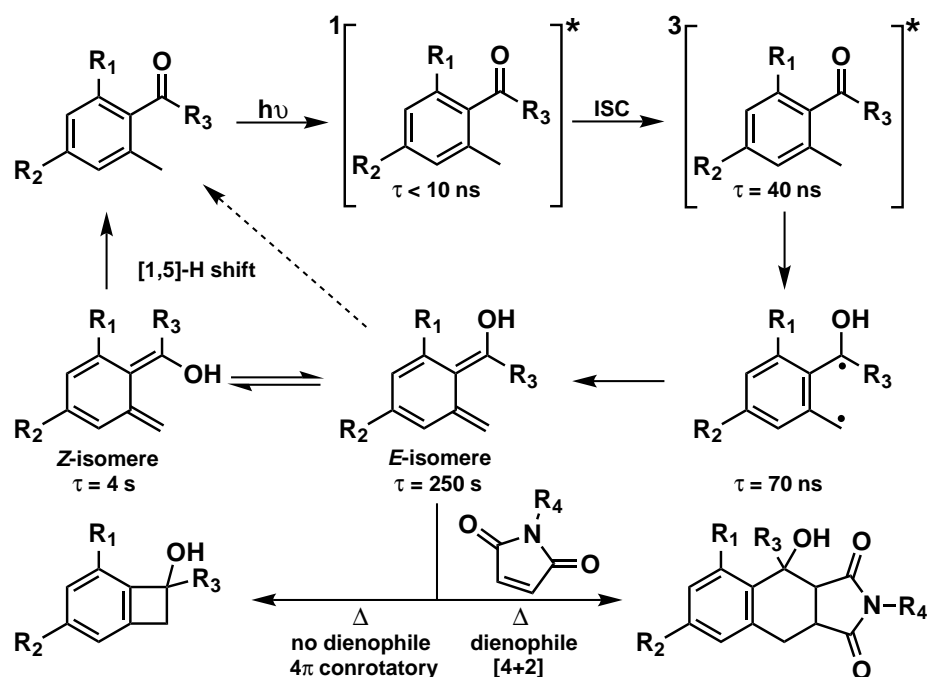


Figure 2.7 Mechanism for the photoinduced isomerization of *o*-methyl-substituted aromatic ketones or aldehydes to *o*-quinodimethanes presented by the example of 2,4-substituted benzophenone. The lifetimes of the involved species were assessed in degassed cyclohexane. ^[141]

lished with the aid of the flash photolysis technique by Porter and Tchir^[141,146] and others^[147,148] (see Figure 2.7). Light absorption leads to a short-lived singlet state via an $n \rightarrow \pi^*$ transition of the carbonyl. Subsequently, intersystem crossing (ISC) to the triplet state occurs, which is followed by a Norrish type II γ -hydrogen abstraction. The resulting biradical can either donate a electron,^[149] or – in the vast majority of cases – decay to the ground state photoenol, which is obtained as a *E/Z* mixture. While the *Z*-isomer is rather short lived and preferentially undergoes sigmatropic [1,5]-H shift, it is the long-lived *E*-isomer, which is responsible for subsequent thermally allowed reactions, e.g., the conrotatory ring-closure to cyclobutenol or the Diels-Alder cycloaddition.^[147,148] One of the main advantages of the photoenol system is its improved selectivity and orthogonality as well as a better handling in a non-light protected environment, the latter of which stems from the ability to regenerate the initial photoactive moiety via the sigmatropic [1,5]-H shift. The photoenol-mediated conjugation strategy possesses many interesting features, making it a first-class *click* reaction^[3] and Chapter 6 will demonstrate its ease and efficiency on surfaces. An alternative approach that generates highly reactive intermediates with short lifetimes via a light trigger, such as *o*-naphthoquinone methides, has been reported by Popik, Locklin, and coworkers.^[150] In this respect, the light-induced reaction of 3-(hydroxymethyl)-naphthalene-2-ol derivatives with vinyl ether moieties enabled for locally constrained surface immobilizations (see

Figure 2.6e)^[151-153] and exchangeable functionalization using thiols.^[154]

3

Mass Spectrometry as a Versatile Characterization Technique in Solution and on Surface

Since the early experiments of Thomson in the early 20th century,^[155] mass spectrometry (MS) has evolved into an extremely powerful and sensitive analytic tool for the identification of substrates in biology and chemistry.^[156] The current thesis utilizes mass spectrometry to assess the reaction outcomes of all developed photochemical approaches (Chapter 4-9). In detail, electrospray ionization mass spectrometry (ESI-MS) is employed for the experiments performed in solution and imaging time-of-flight secondary-ion mass spectrometry (ToF-SIMS) for the locally constrained composition analysis of solid substrates. The data acquired for each of the individual photochemical approaches can therefore be directly compared with each other. The following outlines the basic principles of mass spectrometry.

3.1 Principles of Mass Spectrometry (MS)

In contrast to low molecular weight components, the analysis of synthetic non-volatile macromolecules is a rather difficult task, since the polymer chains have to be introduced into the gas phase as ions without the occurrence of any fragmentation.^[157] It has been the development of soft ionization techniques, such as

electrospray ionization (ESI), matrix-assisted laser desorption ionization (MALDI), and – to a smaller extent – also atmospheric pressure chemical ionization (APCI) that leave the formed ions entirely intact, meeting the aforementioned demands of macromolecular ionization. Other ionization techniques, such as chemical ionization (CI), electron ionization (EI), fast atom bombardment (FAB), and field ionization (FI) tend to induce a stronger fragmentation of the analyte. One of the most basic purposes of a mass spectrometer is to determine the mass-to-charge ratios m/z of gaseous analyte ions and to display the results with their respective abundances in a mass spectrum.^[158] Four key components can be identified in a mass spectrometer (see Figure 3.1): The ionization source converts the analyte into gaseous ions, which are subsequently separated by their m/z ratio in the mass analyzer and are converted in the detector into an electrical signal.^[159] The data is in a last step computer processed and the final set of analytical data is constructed. The following will describe two of the most widely employed (soft) ionization techniques and mass analyzers. For a full overview over mass spectrometry in polymer chemistry the reader is referred to an up-to-date book^[160] as well as to several recent reviews articles.^[161,162]

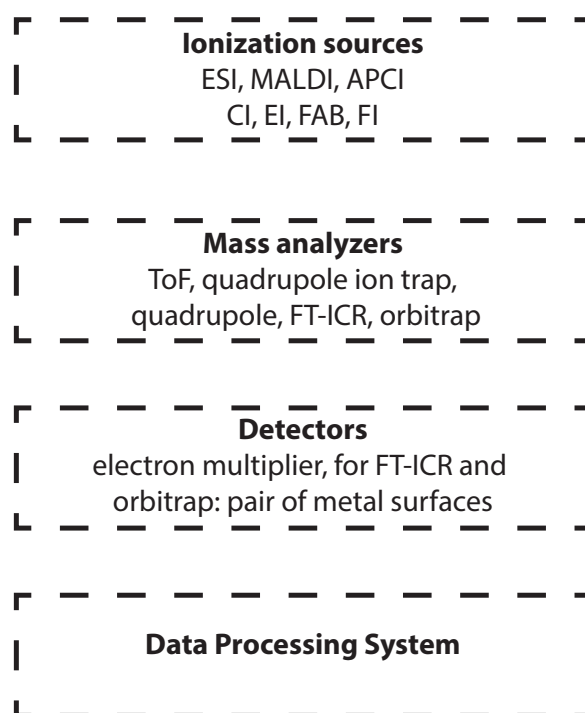


Figure 3.1 Four key components can be identified in a mass spectrometer: an ionization source, a mass analyzer, a detector and a data processing system. ESI = electrospray ionization, MALDI = matrix-assisted laser desorption ionization, APCI = atmospheric pressure chemical ionization, CI = chemical ionization, EI = electron ionization, FAB = fast atom bombardment, FI = field ionization, ToF = time-of-flight, and FT-ICR = Fourier transform ion cyclotron resonance.

3.1.1 Ionization Techniques

The Electrospray Ionization (ESI) technique

M. Dole *et al.* were the first to notice that an electrospray method can be utilized to produce macroions with well defined m/z values^[163] and in a follow up publication in 1970, details on the macroion structure were published.^[164] Although these initial results certainly laid the foundation of ESI-MS, it took another two decades till J. B. Fenn reported in a groundbreaking publication on the ESI-MS spectra obtained from large biomolecules and polymers.^[165] J. B. Fenn was awarded for his development the shared Nobel Prize in chemistry and the amount of publications on ESI-MS steadily increased. As alluded to earlier, ESI is a soft ionization technique and one benefits from two advantages: a) multiple charged ions are obtained, thus extending the reachable mass range (it is important to note that for polymeric samples, multiple charges do often lead to overlapping mass peaks. Pre-separation by size-exclusion chromatography (SEC) can help to diminish such a problem)^[166] and b) the fragmentation during ionization is reduced.^[167] Three fundamental steps can be identified during the ionization process:^[158,159,167,168]

- in an initial step, the analyte solution is forced through a capillary, which is held at a high voltage (≈ 4 kV). At the tip of the nozzle, highly charged droplets are produced and deformed by the applied strong electric force into a so-called Taylor cone.^[169]
- The charged droplets are sprayed from the tip of a needle and the solvent begins – often with the additional aid of elevated temperature and a stream of inert gas – to evaporate and the surface charge steadily increases. At some point, a critical ratio of surface charge to surface area is reached – the so-called Rayleigh limit – and the droplet explodes into smaller droplets.
- the shrinkage of charged droplets continues up to a point, where only desolvated (multiple) charged molecular ions in the gas phase are present. These ions are finally detected in the mass analyzer.^[168]

The Matrix-Assisted Laser Desorption Ionization (MALDI) technique

In addition to ESI, MALDI is another robust and often employed ionization technique that was first developed by Tanaka and Hillenkamp and which is often combined with a time-of-flight (ToF) detector.^[170,171] The analyte is co-crystallized with a large excess (typically the ratio between analyte and matrix molecules is in the range of $10^{-2} - 10^{-5}$ mol/mol) of a MALDI matrix (e.g., an organic aromatic acid). Upon bombardment with a (UV)-laser beam, desorption occurs and primarily

single charged ions are formed.^[158] The key to a successful mass experiment is the preparation of a suitable matrix / analyte mixture, which needs to fulfill a number of roles.^[172,173]

- the MALDI matrix has to strongly absorb radiation of the laser in order to ensure an efficient energy transfer.
- the analyte has to be embedded in a crystalline matrix, which also implies judicious choice of solvent to aid the crystallization process.
- the matrix has to be selected such as to ensure an efficient desorption and ejection of the analyte into the gas phase.
- the matrix ideally generates improved ionization pathways for the analyte, e.g., by acting as a proton donor or acceptor or by allowing the analyte to form alkali adducts.

The desorption and ionization process in MALDI is a less understood process compared to ESI. As a result, the usability of most matrices for specific applications has been determined empirically.^[172]

3.1.2 Mass Analyzers

The mass analyzer is the key component of every mass spectrometer and it can significantly differ in some performance characteristics, e.g., the mass resolving power, mass accuracy and mass limits.^[174] The following will focus on the two most widely employed mass analyzers, namely the Time-of-Flight (ToF) and the quadrupole mass filter. For a more detailed overview of other mass analyzers – e.g., the quadrupole ion trap,^[175] the Fourier transform ion cyclotron (FT-ICR),^[176] or the orbitrap^[177] to name but a few – the reader is referred to the above noted reviews. As alluded to above, a book chapter covering the most important mass analyzers has recently been published.^[174]

The Time-of-Flight (ToF) analyzer

The linear Time-of-Flight (ToF) analyzer is conceptually rather simple and is based on the relation that ion velocities in a static electric field are inversely related to their square root of m/z .^[178,179] The time necessary for ions with specific m/z ratios to travel through a field-free drift tube translates therefore directly into a mass spectrum.^[180] One of the problems associated with linear ToF was a low mass resolution stemming from a kinetic energy distribution of ions with the same m/z value.^[181] A reflectron^[182] retards ions according to their kinetic energy and

is employed in most contemporary ToF analyzers to compensate for the spread in ion velocities.^[174,180] The mass resolving power is hereby greatly enhanced. A ToF analyzer features an additional advantage of special importance for polymer chemists: the theoretically unlimited mass range in which it can operate^[183] and MALDI-ToF mass spectrometry, for instance, has been reported to make molar masses up to approximately 1 million Da accessible.^[184]

The quadrupol mass filter

A quadrupol device consists of four rods operated at a direct current voltage U that is superimposed by an alternating voltage V . The resulting stable or unstable trajectories of charged species with a given m/z value can be described by second order differential equations and depend, among others, on the magnitude of both voltages.^[185] By electronically changing the magnitude of these voltages, only certain ions with a specific m/z ratio lead to stable trajectories (such stability regions of ions can be illustrated in a Mathieu diagram)^[180] and can pass through the mass filter to the detector. Quadrupol mass filters are perhaps the most widely employed mass analyzers based on their mechanical simplicity (low cost) and the possibility to couple this continuous and non-pulsed method to liquid chromatography (LC) systems.

3.2 Imaging Mass Spectrometry

Imaging mass spectrometry is an extremely powerful tool that combines attractive features of solution based mass spectrometry (rapid, specific, and sensitive identification of analytes) with additional information on their spatial distribution on a solid substrate.^[186] Principally there are two modes in which chemical composition and spatial information can be deduced from a sample: via the microprobe- or via the microscope technique.^[186,187] In the microprobe modus, spatial and chemical information is gained by ionization of a highly localized region of the solid substrate and by correlation of its position with the corresponding mass spectrum. An image of the molecular composition can be reconstructed by moving the substrate in x/y direction. As a consequence, the spatial resolution is governed by the focusing capability of the ionization beam. The mentioned resolution limitation is reduced in the technically more complex microscope mode in which the spatial origin of an ion is transmitted through its trajectory. The spatial information is calculated by the use of appropriate ion optics and a position sensitive mass detector.^[187] In contrast to the similar imaging capabilities of fluorescence microscopy, imaging mass spectrometry is a method that does not require molecule-specific tags and provides additionally

detailed information on the chemical composition. The analysis and imaging of surfaces via mass spectrometry requires an efficient desorption or sputtering and subsequent ionization of the analyte into the gas phase without significant fragmentation.^[183] Three techniques have proven themselves to be particularly efficient in meeting such demands and some characteristics of them are depicted in Table 3.1. They are based upon the exposure or bombardment of the solid sample with a laser beam (imaging matrix-assisted laser desorption ionization imaging mass spectrometry (imaging MALDI)), a flux of charged droplets (desorption electrospray ionization (DESI)), or an ion beam (secondary ion mass spectrometry (SIMS)). The obtained free ions from the surface are finally separated according to their m/z value in one of the available mass analyzers (see also Chapter 3.1.2) and much to the success of imaging mass spectrometry is owed to the many improvements that have been applied previously to modern mass spectrometers. The short period between the discovery of the MALDI process (see also Chapter 3.1.1) and the first MALDI imaging publication by Caprioli *et al.*^[192] accounts for their high conceptual similarity. In fact, images are obtained by moving the sample along the x/y axis and by recording mass spectra of each position. A detailed description of imaging MALDI can be found in the literature and the reader is referred to the reviews and perspectives covering this topic.^[186,187,193–195] The following section will focus on two other powerful tools for the imaging of molecular distributions on surface that have emerged, namely SIMS and DESI.

Table 3.1 Three desorption/sputtering methods that are generally utilized in imaging mass spectrometry (IMS).^[187] MALDI = matrix-assisted laser desorption ionization, DESI = desorption electrospray ionization, SIMS = secondary ion mass spectrometry.

Name	Ionization method (energy/constituent)	Lateral resolution	Mass limit
imaging MALDI	laser beam	30-100 μm ^[188]	\approx 30 kDa ^[189]
DESI	charged solvent droplets (\approx 2 eV) ^[190]	\approx 150 μm ^[190]	up to \approx 60 kDa ^[187]
SIMS	primary ion beam (5-25 keV) ^[183]	\approx 100 nm ^[188]	typically <1000 Da ^[187] but up to 10000 Da ^[191] (with significant fragmentation)

3.2.1 Secondary Ion Mass Spectrometry (SIMS)

Secondary ion mass spectrometry (SIMS) utilizes an energetic (5-25 keV)^[183] ion beam to sputter / ionize the surface of a solid substrate and the ion source operated early on with a high primary ion dose in the so-called dynamic SIMS mode. The analysis of surface elements and the profiling of surface depths (high ion doses can remove up to 10 monolayers per second)^[196] via dynamic SIMS was widely used, however, the ion beam caused severe damage and made the method unsuitable for molecular analysis in the uppermost surface layer. The years after 1970 were devoted to reduce the damage of the pulsed primary ion bombardment to a minimum by applying a low-ion dose ($< 10^{13}$ ions·cm⁻², referred to as the “static SIMS limit”).^[197] Only a small fraction of surface atoms are statistically bombarded with primary ions under these conditions. As a consequence, the probability of a surface area to receive an particle impact twice, which would result in the detection of ions/fragments that do not originate from the uppermost one to three monolayers, is significantly reduced. Benninghoven followed this less-destructive surface analysis approach and his pioneering work led to the development of static SIMS.^[198-200] The time-of-flight (ToF) analyzer (see Chapter 3.1.2) is most commonly utilized for a SIMS experiment, as it can detect all of the secondary ions in parallel if the primary ion source provides very short pulse widths.^[183] (Static) ToF-SIMS offers many substantial benefits over other surface characterization techniques:^[197]

- extremely high surface sensitivity (uppermost 1-2 nm of the solid substrate)
- very low detection limits
- excellent spatial resolution (≈ 100 nm).^[188] It is important to note that an ion beam can be focused much sharper (≈ 50 nm) than it is possible with a light beam (≈ 1 μ m).^[196]
- mapping of the chemical composition (imaging capabilities) by rastering the ion beam across the surface.
- direct (no further preparative pre-requirements, e.g., a matrix) characterization of the surface composition.

The above-mentioned advantages make imaging ToF-SIMS an extremely powerful tool that has been selected in the current thesis for the characterization of all surface patterns that have been generated via the investigated novel photochemical approaches (see Chapters 5, 6, 7 and 8). The most important downside of SIMS is perhaps its much harsher ionization condition as compared to MALDI or DESI. As a result, extensive fragmentations are observed if the molecular weight of surface

bound substrates exceed molecular weights of $1000 \text{ g}\cdot\text{mol}^{-1}$ and the interpretation of the resulting mass spectra is often a very complicated task. The combination of fragmentation and ionization difficulties limits the mass range and it seems to be nearly impossible to detect intact proteins with SIMS.^[201]

3.2.2 Desorption Electrospray Ionization (DESI)

The composition analysis via SIMS requires an ultra-high vacuum and its application for the sampling of sensitive biological substrates is therefore severely constrained. Cooks and coworkers introduced a novel technique termed desorption electrospray ionization (DESI) in 2004, which allows for the identification of analytes weakly bound to a surface according to their spatial distribution at atmospheric pressure and under ambient conditions.^[202,203] Although the desorption process of DESI is not yet fully understood, simulations^[204] on the collision of charged droplets with thin films favor the so-called “droplet pick-up”^[203,205] mechanism.^[206] A microscopic liquid layer is formed by directing a spray of charged (micro)-droplets onto a solid substrate and the weakly bound analyte dissolves in it partially. The collision with subsequent droplets leads to the emission of secondary charged droplets and – after evaporation of the solvent – the free gaseous ions are analyzed in the mass spectrometer. Besides offering a method for ambient ionization, three other beneficial characteristics have particularly proven their usefulness in a range of applications:^[205]

- the fragmentation of complex biological substrates is drastically reduced by utilizing a low energy / projectile ratio (2 eV).^[190]
- no surface pretreatment is required, making DESI a high throughput technique.
- DESI offers good sensitivity (in the order of 1 nanogram [ng] deposited on 1 cm^2 , however SIMS can detect up to 1 femtogram [fg] deposited on 1 cm^2)^[190] and selectivity. In contrast to SIMS, the latter can be enhanced by MS/MS experiments.

The use of a low energy / projectile ratio makes DESI unrivalled for the detection of intact biological substrates,^[207] but it also constrains the molecular compositions analysis to substrates that are weakly bound to the surface. The current thesis investigates the construction of molecular patterns that are generated by the phototriggered formation of covalent bounds and DESI is therefore not the preferred analytical method. In contrast to the excellent spatial resolution that can be achieved by SIMS ($< 100 \text{ nm}$),^[188] the one of DESI is currently limited to $\approx 150 \text{ }\mu\text{m}$.^[190]

4

Polymer Modification by *in situ* Phototriggered Deprotection and Thiol-ene Chemistry*

4.1 Abstract

A novel and efficient methodology for the light-triggered release of thiols at ambient temperature is presented, which can be utilized for the *in situ* modification of polymeric backbones prepared via radical polymerization. Initially, a model reaction on poly(ethylene glycol) methyl ether was examined via size exclusion chromatography coupled to electrospray ionization-mass spectrometry (SEC/ESI-MS) to establish the photodeprotection feasibility of 2-nitrobenzyl thioether moieties in the presence of variable activators or catalysts employed in Michael-type or radical thiol-ene chemistries, respectively. When 0.01 eq. of dimethylphenylphosphine is employed, disulfide coupling is reduced to its minimum and quantitative phototriggered formation of thiol-capped poly(ethylene glycol) methyl ether species is observed after a 16 hour irradiation period at 320 nm by a low-cost light source. The concept is extended to polymer backbone modification by atom transfer radical polymerization of the novel photosensitive monomer: 2-((3-((2-

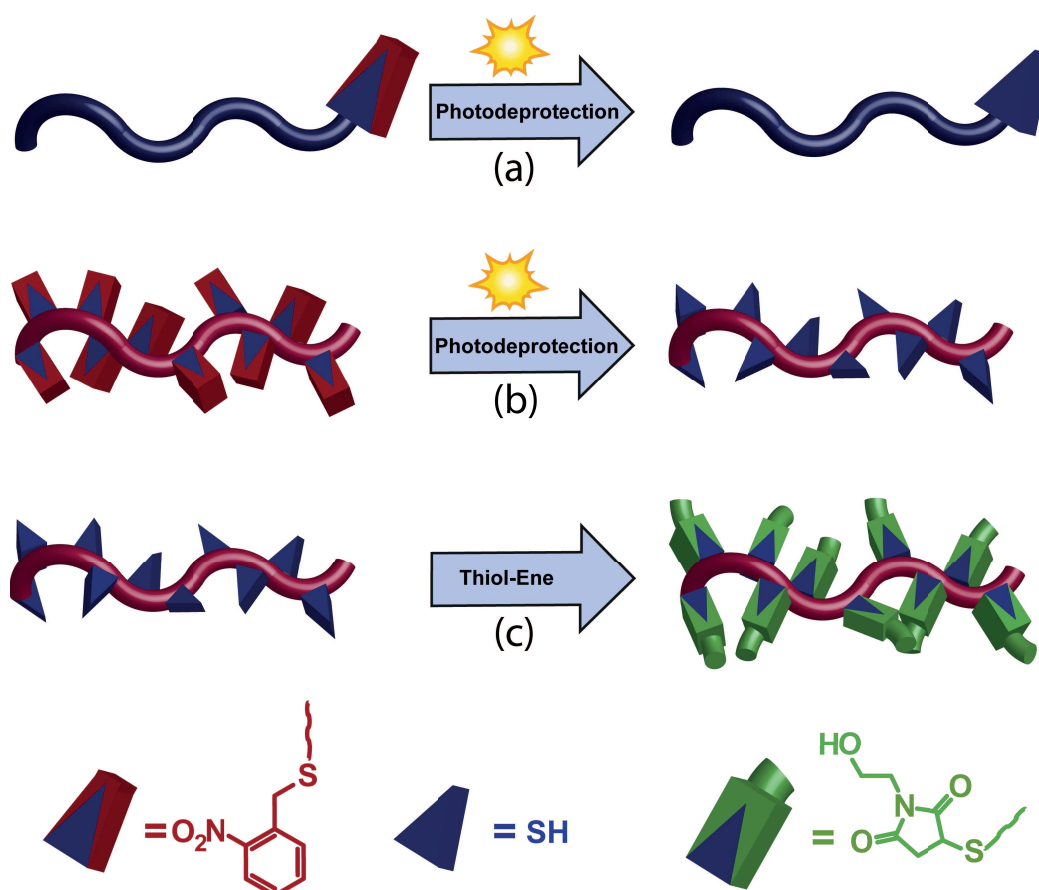
* Parts of this Chapter were reproduced from Ref. 208 by permission of the Royal Society of Chemistry.

nitrobenzyl)thio)propanoyl)oxy)ethyl methacrylate containing the 2-nitrobenzyl thioether moiety. Homopolymers ($4700 \text{ g}\cdot\text{mol}^{-1} \leq M_n \leq 20000 \text{ g}\cdot\text{mol}^{-1}$, $1.29 \leq PDI \leq 1.40$) containing one protected thiol per repeating unit were obtained and, upon a light stimulus ($\lambda_{\text{max}} = 320 \text{ nm}$), thiol entities are released along the lateral polymer chain. The photodeprotection process is mapped by exploiting the increased absorbance of the photocleaved *o*-nitrosobenzaldehyde molecules at 345 nm and UV-Vis data suggests a quantitative backbone deprotection after a 16 hour irradiation time period. Further *in situ* functionalization of polymeric backbone is achieved via base-catalyzed maleimide-thiol addition at ambient temperature and its outcome is evidenced by virtue of a decreased signal intensity of the 2-nitrobenzyl thioether moiety and the appearance of characteristic product protons in NMR spectroscopy.

4.2 Introduction

The recent combination of living/controlled polymerization techniques with powerful post-polymerization strategies has allowed for the preparation of an astonishing diversity of functional materials with tailored physical, chemical, and mechanical properties.^[90,209–211] Aside from Cu-catalyzed azide-alkyne *click* chemistry,^[2] thiol-ene ligation reactions have been widely investigated as a convenient conjugation technique in macromolecular science.^[98,101,212,213] Indeed, the modern day chemist benefits from the inherent versatility of Michael-type thiol-ene conjugations owing to its tolerance to various reaction conditions, its high efficiency and relative orthogonality, its rapid reaction kinetics with a well defined reaction pathway, and – in the case of the radical-type thiol-ene conjugation – also to its robust photoinitiation capability even in the presence of oxygen.^[214] The synthesis of fourth-generation dendrimers with exceptional efficiency by Hawker and colleagues is conceivably the most convincing example to date demonstrating *click* attributes,^[215] which make thiol-ene chemistry amenable to applications ranging from dental resins and hydrogels to versatile materials for soft imprint lithography.^[216] Although radical thiol-ene should not be proposed as a straightforward conjugation tool for polymer-polymer conjugation reactions^[217] (with its much harsher set of *click* conditions), both variants, the radical-initiated and base/nucleophile-catalyzed thiol-ene chemistry, are ubiquitous in ligation chemistry. Besides conjugation techniques, mercapto groups feature specific interactions with metals^[218,219] and the development of technologies involved in preparing thiol-functionalized macromolecules is becoming increasingly important. However, the controlled incorporation of thiol groups into polymer chains remains challenging due to their role as chain-transfer agents in the radical polymerization process and in disulfide formation. The first – rather limited

– approach to convert the bromine end group of atom transfer radical polymerization (ATRP)-made polystyrene to the corresponding thiol end group was carried out by Garamszegi *et al.*^[220] Very recently, Liras *et al.*^[221] developed this concept further by employing thioacetate followed by a controlled hydrolysis in which the employed functionalization system proved to be essentially inert to the multitude of ester functional groups that exist in poly(methacrylates).^[222,223] However, for both these transformations rather severe conditions are required, e.g., hydrolysis requires reflux under basic conditions for many hours and may not be applicable when more sensitive systems are studied. Milder approaches towards thiol-capped polymers encompass the use of 2,4-dinitrofluorobenzene, a protection group, which can be quantitatively removed by an excess of mercaptoethanol.^[224] Thiol functionalization can also be obtained in high yield by posttreatment of polymers synthesized by reversible addition fragmentation chain transfer polymerization (RAFT): dithio- or trithiocarbonate groups inherently present in these polymers can be converted into thiols by hydrolysis,^[225] aminolysis,^[226,227] or metal hydride reduction.^[228]



Scheme 4.1 Proposed strategy for polymer backbone functionalization. Detailed investigation of the phototriggered deprotection of the 2-nitrobenzyl thioether moiety on a PEG chain-end functionalized model system (a) and on the polymeric backbone (b). Highly efficient thiol-maleimide ligation chemistry allows subsequently for the polymer backbone modification (c).

Although being successful, all of the above transformations are limited to polymer end-group modifications. In search of a way to increase functionalization and to obtain a thiol-functionalized polymer backbone, the incorporation of the 2-nitrobenzyl thioether moiety into a monomer as a photodeprotectable source of thiols was explored (see Scheme 4.1 for an overview of the proposed strategy). In addition, the use of light would also provide a facile means to obtain spatial and temporal control over the thiol release for polymer conjugation reactions, including those with sensitive biomolecules.

4.3 Experimental Part

Synthesis and Polymerization of a Photodeprotectable Monomer

Synthesis of 3-((2-nitrobenzyl)thio)propanoic acid **1**

2.46 g (23.18 mmol, 1.0 eq.) 3-mercaptopropionic acid was dissolved in 20 mL acetone and 2.04 g (51 mmol, 2.2 eq.) NaOH dissolved in 14 mL water was added. The solution was cooled to 0 °C and 5.00 g (23.14 mmol, 1.0 eq.) 2-nitrobenzyl bromide dissolved in 20 mL acetone was slowly added. After stirring for 30 min, the yellow solution was allowed to warm to ambient temperature and was stirred for 4 hours. The solvents were removed under reduced pressure and the residue was redissolved in a mixture of 20 mL DCM and 20 mL of water. The aqueous phase was washed with dichloromethane and subsequently acidified with 10 % aqueous HCl. The resulting dispersion was extracted with 2 × 30 mL DCM. The organic extracts were combined and dried over sodium sulfate. The solvent was removed under reduced pressure yielding a brown-colored crude product. Subsequent two-fold recrystallization in a 1:40 v/v acetone/hexane mixture yielded 2.73 g (11.23 mmol, 49 %) of an off-white solid. ¹H NMR (250 MHz, DMSO); [δ , ppm]: 12.28 (s, 1H, COO H), 8.00 (d, 1H, ArH), 7.74-7.49 (m, 3H, 3 × -ArH), 4.07 (s, 2H, -ArCH₂), 2.57 (t, 2H, -SCH₂), 2.45 (t, 2H, -SCH₂CH₂).

Synthesis of 2-((3-((2-nitrobenzyl)thio)propanoyl)oxy)ethyl methacrylate **4**

1.71 g (7.09 mmol, 0.99 eq.) of **1** was dissolved in 20 mL DCM. 0.93 g (7.15 mmol, 1.0 eq.) hydroxyethylmethacrylate (HEMA), 2.0 g (9.69 mmol, 1.4 eq.) DCC, and 86 mg (0.71 mmol, 0.1 eq.) DMAP were added. The mixture was allowed to stir at ambient temperature overnight. Precipitated urea was removed by filtration and the solvent under reduced pressure. Purification by flash chromatography (silica gel, 1:2 v/v ethyl acetate/hexane) yielded 1.4 g (3.9 mmol, 56 %) of **4** as a yellow oil. ¹H NMR (400 MHz, CDCl₃); [δ , ppm]: 8.01 (d, J = 8.1 Hz, 1H, ArH), 7.61-7.36

(m, 3H, 3 × -ArH), 6.14-6.09 (m, 1H, -CH), 5.61-5.57 (m, 1H, -CH), 4.34 (s, 4H, 2 × -OCH₂), 4.08 (s, 2H, -ArCH₂), 2.71 (t, *J* = 6.8 Hz, 2H, -SCH₂CH₂CO), 2.59 (t, *J* = 7.1 Hz, 2H, -SCH₂CH₂CO), 1.95-1.92 (m, 3H, -CH₃). ¹³C NMR (101 MHz, CDCl₃); [δ, ppm]: 171.61, 167.23, 148.87, 136.02, 134.02, 133.19, 132.01, 128.43, 126.26, 125.55, 62.55, 62.41, 34.51, 33.69, 33.69, 27.00, 18.40.

ATRP polymerization of **4**

6.8 mg CuBr (48 μmol, 1.0 eq.) was introduced into a dried Schlenk tube, which was subsequently sealed with a rubber septum, evacuated and backfilled with nitrogen. A solution of 1.7 g (4.8 mmol, 100 eq.) of **4** in anisole (50 wt. %) and 11.9 μL (58 μmol, 1.2 eq.) PMDETA were introduced into another Schlenk tube, which was equipped with a rubber septum. The monomer solution was deoxygenated by three consecutive freeze-pump-thaw cycles and subsequently transferred to the first Schlenk tube via a cannula. The tube was finally placed in a thermostatic oil bath held at 80 °C. After the polymerization mixture reached the desired temperature, EBiB (8.4 μL, 58 μmol, 1.2 eq.) was added. The polymerization was stopped after 8.5 hours by cooling the mixture in an ice bath and exposure to oxygen. The mixture was passed through a short column of neutral alumina to remove the copper catalyst. The polymer **5b** was isolated by two-fold precipitation in cold diethyl ether. SEC/THF: *M*_n = 20000 g·mol⁻¹, PDI = 1.40. (Molecular weights relative to PMMA are reported in the current contribution.) The reaction conditions and reagent concentrations for obtaining polymers **5a** and **5c** can be found in Table 4.2.

Synthesis and Photodeprotection of a PEG Model System

Synthesis of a PEG model system **2**

0.50 g (2.10 mmol, 1.0 eq.) of **1**, 0.84 g (*M*_n = 2000 g mol⁻¹, 0.42 mmol, 0.2 eq.) poly(ethylene glycol) methyl ether, and 0.47 g DCC (2.30 mmol, 1.10 eq.) were dissolved in 10 mL of dry DCM. 26 mg (0.21 mmol, 0.10 eq.) DMAP was added and the solution was stirred overnight. Precipitated urea was filtered off and the solvent was removed under reduced pressure. The polymer was obtained by redissolution in THF followed by two-fold precipitation in diethyl ether. SEC/THF (GPC data are based on polystyrene standard calibration): *M*_n = 3100 g·mol⁻¹, PDI = 1.02. Since the SEC is calibrated with polymers having a different solution behavior and SEC/ESI-MS analysis revealed a clean reaction product, the theoretical *M*_n value of 2250 g·mol⁻¹ was used for calculations in the model reactions.

Photodeprotection of a PEG model system 2

3.0 mg (1.3 μmol , 1.0 eq.) of **2** were dissolved in 4 mL DCM and aliquoted into headspace vials (Pyrex, diameter 20 mm), which were crimped air-tight using SBR seals with a PTFE inner liner. The solution was deoxygenated by bubbling nitrogen through for 10 min. The flasks were subsequently irradiated for 16 hours by revolving around a compact low-pressure fluorescent lamp (Arimed B6, Cosmedico GmbH, Stuttgart, Germany) emitting at 320 nm (for more details see Chapter 11.2). The solvent was evaporated after the reaction, 2 mL THF was added and the slightly yellow solution was analyzed immediately via SEC/ESI-MS. The procedure was repeated with additionally added thiol-ene catalysts in the following manner: DCM stock solutions of 100 μL (in 10 mL DCM) TEA, 50 mg (in 10 mL DCM) DMPA, and 10 μL (in 50 mL DCM) DMPP were prepared. A small volume of each stock solution was then added to model system **2** as follows: (a) 19 μL (1.0 eq.) of TEA, (b) 70 μL (1.0 eq.) DMPA, and (c) 9.5 μL (0.01 eq.) DMPP.

Polymer Backbone Modification via Photochemistry and Thiol-Ene Ligation**NMR analysis of the photodeprotection and subsequent thiol-ene ligation reaction of **5c****

5c (40.0 mg, 8.5 mmol) was dissolved in 40 mL DCM and 12.1 μL (0.01 eq. with respect to thiol-protected moieties on polymeric backbone) DMPP was added. The solution was aliquoted into 10 headspace vials in the same manner as above. The flasks were subsequently irradiated for timed intervals by revolving around a compact low-pressure fluorescent lamp (Arimed B6, Cosmedico GmbH, Stuttgart, Germany) emitting at 320 nm (for more details see Chapter 11.2). A stir bar, 84.0 mg (5.0 eq.) of 1-(2-hydroxyethyl)-1*H*-pyrrole-2,5-dione and 166 mL (10 eq.) of TEA were subsequently added to the yellow-orange colored solution and stirred overnight (16 h). The solvent was evaporated after the reaction and 50 mL of 1:1 v/v chloroform/water were added. The mixture was extracted two times with 10 mL of chloroform, dried over sodium sulfate and the solvent was evaporated. The resulting solid was redissolved in 1 mL of dichloromethane and precipitated into 8 mL of cold diethyl ether. The obtained solid was filtered and dried under vacuum.

SEC analysis of the photodeprotection and subsequent thiol-ene ligation reaction of **5c**

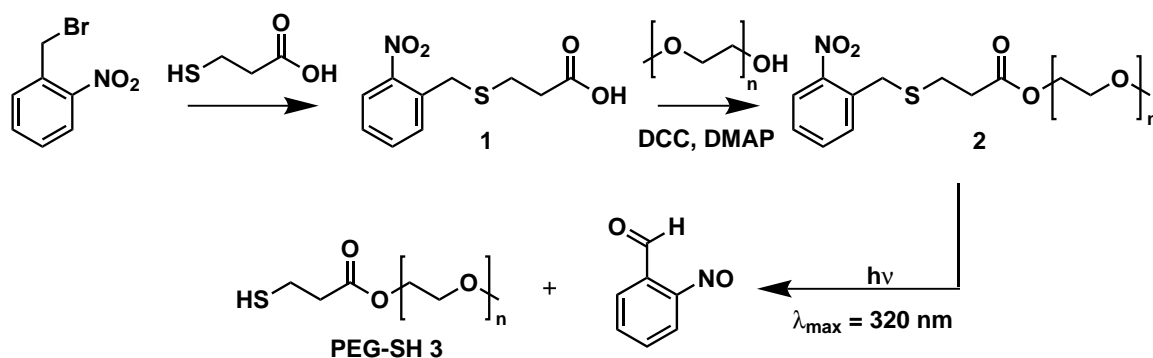
4.0 mg **5c** was dissolved in 40 mL DCM and aliquoted into headspace vials. DMPP (0.01 eq. with respect to thiol-protected moieties on polymeric backbone) was added. The solutions were deoxygenated by purging with nitrogen for 10 min. The flasks were subsequently irradiated for different periods of time in the aforementioned

photoreactor. The solvent was evaporated after the reaction, 2 mL THF was added and the SEC trace was obtained by the further addition of 1.0 mg of the disulfide reducing agent DTT.

4.4 Results and Discussion

Photodeprotections on a PEG Chain-End Functionalized Model System

In order to obtain detailed insights into the photodeprotection and *in situ* thiol-ene reactions, a model system **2** (see Scheme 4.1a) was synthesized as mass spectrometry already proved to be a rather facile and efficient method for the assessment of PEG chain-end modification.^[229] The photodeprotection experiments were carried out at ambient temperature by irradiation of a dichloromethane solution of the model system **2** with a 36 W compact fluorescent lamp (see Scheme 4.2 and the Experimental Part for details). Figure 4.1a and b depict the ESI-MS spectra of the protected thiol end-capped polymer **2** alongside that of the unprotected thiol reaction product PEG-SH **3**, respectively. Such thiol-capped polymers can readily form undesired disulfide,^[230] whose occurrence could be observed in the current system in minor amounts. Additionally, the model reaction was examined to establish the feasibility of simultaneous ambient temperature deprotection and thiol-ene functionalization. For this purpose, the deprotection of **2** was attempted in the presence of initiators/catalysts required for the thiol-ene to take place: 2,2-dimethoxy-2-phenylacetophenone (DMPA), a photoinitiator for radical thiol-ene addition on the one hand, and triethylamine (TEA) and dimethylphenylphosphine (DMPP) for Michael-type thiol-ene addition on the other hand. In addition to their catalytic role in Michael-type addition,^[231–233] phosphines are also known to reduce disulfide bonds,^[234] thus DMPP could have a dual role in the current study. A recent kinetic study of the photochemical reaction mechanism of *o*-nitrobenzyl



Scheme 4.2 Introduction of a photodeprotectable thiol end group on PEG and subsequent UV deprotection.

compounds revealed a strong pH and solvent dependence,^[58] which could be qualitatively confirmed in the current study. Indeed, the addition of one equivalent of TEA (with respect to the thiol-protected moiety) completely prevented any photodeprotection reaction and only the starting material could be observed in the mass spectrum (Figure 4.1c). Aside from the base-catalyzed thiol-ene addition, the possibility of a photoinitiated radical addition was considered. The introduction of one equivalent of DMPA into the deprotection experiment mixture yielded – besides the desired main product PEG-SH **3** – major side-products (Figure 4.1d). Furthermore, the radically initiated thiol-ene reaction features the inconvenience of initiating a parallel polymerization process when homopolymerizable alkenes are used. Although in minor quantities, disulfide formation due to radical coupling was also observed. Following from this, DMPP was employed in the current study to eliminate disulfide coupling. Figure 4.1e clearly indicates the quantitative formation of the desired thiol-capped species PEG-SH **3** in the presence of 0.01 eq. (with

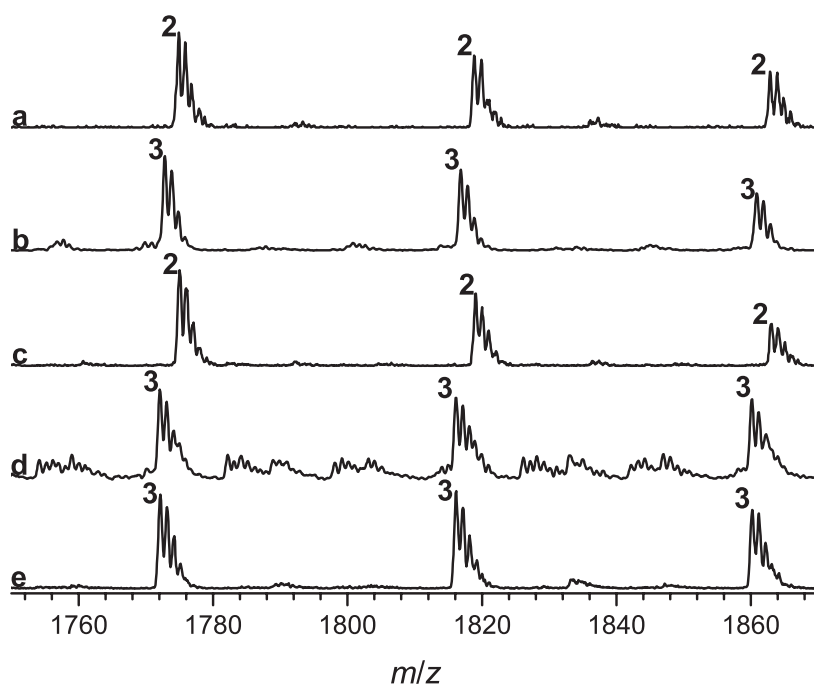


Figure 4.1 SEC/ESI-MS spectra of **2** (a), **2** after 16 hour UV irradiation ($\lambda_{\max} = 320$ nm) in the absence of any catalyst (b), in the presence of 1 eq. TEA (c), 1 eq. DMPA (d), and 0.01 eq. DMPP (e).

Table 4.1 Experimental and theoretical m/z values for the first peaks in the isotopic distribution of Figure 4.1 and Figure 4.2 in the m/z range between 1810 and 1855.

$m/z_{\text{expt.}}$	ion assignment	formula	$m/z_{\text{theor.}}$	$\Delta m/z$
1818.9	2 _(n=35) + Na ⁺	[C ₈₁ H ₁₅₃ HNao ₃₉ S] ⁺	1819.9	0.1
1816.0	3 _(n=38) + Na ⁺	[C ₈₀ H ₁₆₀ HNao ₄₀ S] ⁺	1816.0	0.0

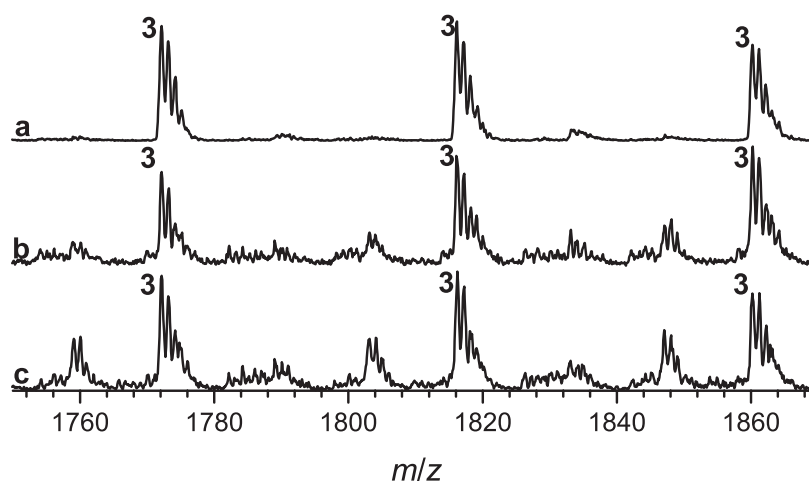
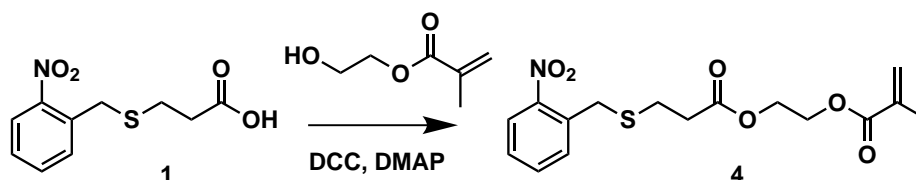


Figure 4.2 SEC/ESI-MS spectra of **2** after UV irradiation in presence of 0.01 eq. (a), 0.2 eq. (b) and 0.5 eq. of DMPP (with respect to thiol-protected functionality) (c).

respect to thiol-protected moiety) of DMPP without notable disulfide formation. However, it should be noted that the use of reactive phosphine in non-catalytic amounts resulted in by-product formation corresponding to phosphine-conjugated species (see Figure 4.2). Such monoaddition of phosphine (e.g., onto vinyl groups) has also been clearly identified by Li *et al.* in the presence of an excess of DMPP or tris (2-carboxyethyl)phosphine.^[233] Following the promising results performing the photoreaction in the presence of catalytic amounts of DMPP and the known high efficiency of photoinitiated radical thiol-ene reactions, it was initially tried to perform both – the photodeprotection and photoinitiated thiol-ene reaction – simultaneously. Unfortunately, besides the desired ligation product, numerous side-products were also obtained in such an *in situ* photodeprotection of **2** in the presence of 10 eq. ethyl vinyl ether (the vinyl ether double bond was chosen because of its high reactivity toward thiols^[213]), whose formation could not be avoided. To sum up, the conditions utilized in Figure 4.1e (a 16 hour photodeprotection period in the presence of 0.01 eq. DMPP) yielded optimal results. In order to avoid by-product formation during polymer backbone modification, the efforts were directed towards a two-step *in situ* process: (i) photodeprotection in the absence of an ene while utilizing the optimized conditions of Figure 4.1e and (ii) nucleophilic thiol-ene reaction.

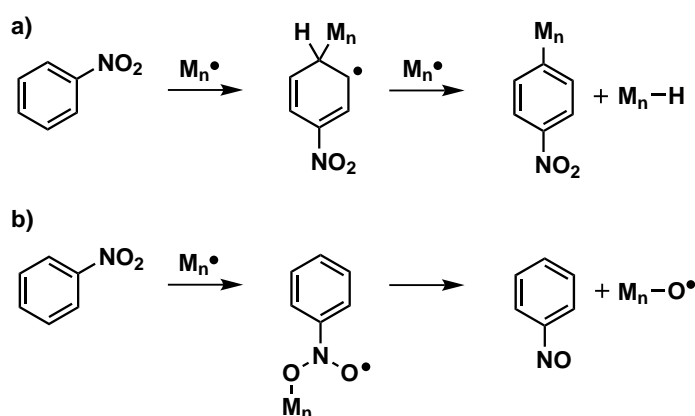
Investigation of the Photodeprotection on a Polymeric Backbone

To demonstrate the effectiveness of the concept to functionalize polymer backbones, a novel photodeprotectable monomer was prepared via esterification of **1** (Scheme 4.3). In fact, the incorporation of *o*-nitrobenzyl esters into polymers for the photoinduced cleavage of covalent bonds is well known in polymer science, e.g., in star polymers,^[235] (block) copolymers,^[236–238] and biodegradable polymers.^[239]



Scheme 4.3 Synthetic route towards the photodeprotectable monomer 4.

However, monomers containing such photodegradable groups are challenging to polymerize by living/controlled polymerization techniques due to their sensitivity. Indeed, the nitro-aromatic group can act as an inhibitor/retardant^[240] in the polymerization process via the attack of the propagating radical at the aromatic ring or at the nitro moiety.^[241] Attack on the aromatic ring yields a radical, which can react with either monomer or terminate with another propagating species (see Scheme 4.4). In case of a reaction of the propagating radical with the nitro moiety, subsequent cleavage to nitrosobenzene and another radical occurs, both of which can again react with another propagating species. Alternatively, nitro aromatic compounds can also produce radicals above 80 °C in concentrations sufficiently high enough to perturb the living/controlled polymerization process.^[242] It was recently confirmed in the group of Barner-Kowollik that the *o*-nitrobenzyl moiety strongly affects polymerization of acrylamides in both a free radical- and a RAFT polymerization.^[243] In contrary, the nitro-aromatic group has only very little effect on the polymerization of methacrylates.^[244] Following from this, the controlled homopolymerization of *o*-nitrobenzyl methacrylates is possible and has, indeed, been recently reported by Gohy *et al.*^[245] via RAFT (up to 60 % conversion) and via ATRP (up to 30 % conversion). In both cases retardation was not observed and the most promising results were obtained by employing ATRP for the polymerization of



Scheme 4.4 Proposed mechanism for the radical termination observed for nitro-aromatic compounds during polymerization. The propagating radical can attack at the aromatic ring (a) and at the nitro moiety (b).^[240,241]

o-nitrobenzyl methacrylate with a ratio of [monomer]/[CuBr]/[EBiB]/[PMDETA] = 200:1:1:1 in 33 wt. % anisole. Although their *o*-nitrobenzyl ester clearly differs from the thioether **4** in terms of structure, the above findings still provided a good starting point for the current system. Polymer **5a** with a number-average molecular weight of 13000 g·mol⁻¹ and a PDI of 1.3 was obtained under these conditions. The variable other studied conditions and the corresponding results for the ATRP polymerization of **4** are summarized in Table 4.2. The low-conversion and low-molecular-weight polymer **5c** was prepared in order to perform ESI-MS analysis. In perfect agreement with the presence of still-fully protected lateral groups, NMR analysis revealed for all precipitated polymers (**5a**, **5b**, and **5c**) a 4:6 integration ratio of the phenyl protons f and g to the protons d, d', and e (see Figure 4.3). Thus, the *o*-nitrobenzyl group showed to be essentially inert to the polymerization process employed. As the presence of fully intact photodegradable moieties on the polymeric backbone is essential for the concept of light-triggered polymer backbone modification, an additional ESI-MS analysis on polymer **5c** was subsequently performed (not shown). The analysis revealed major by-products, which might be formed during the ESI-MS analysis in

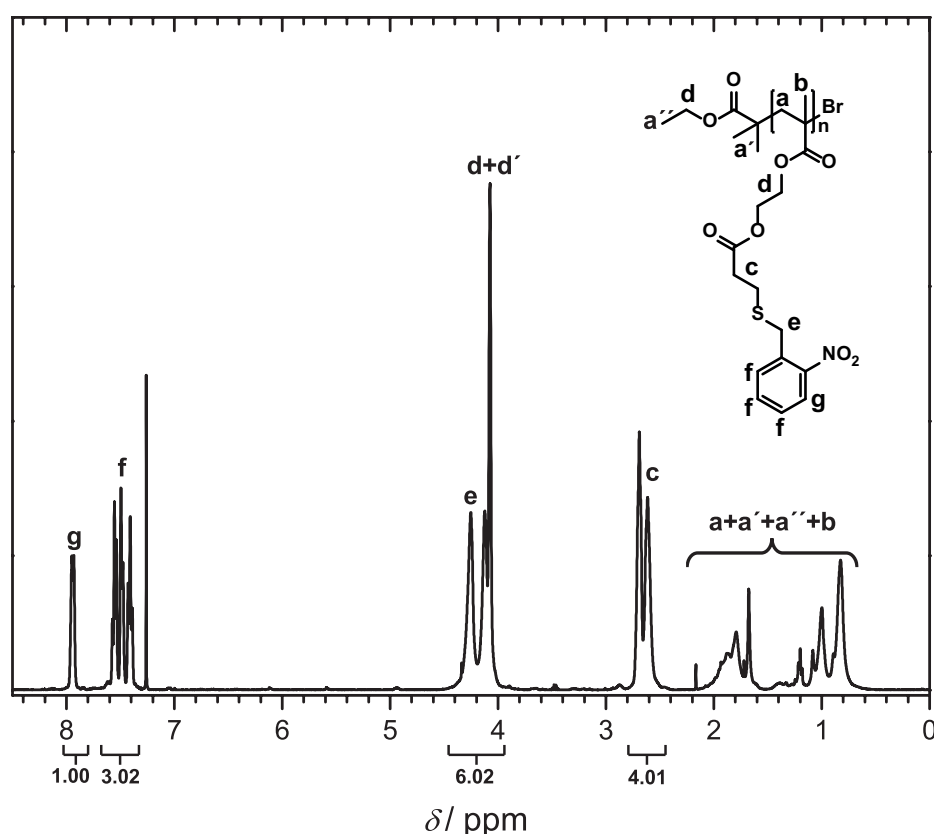


Figure 4.3 ¹H NMR spectrum in CDCl₃ of the precipitated polymer **5c** obtained by ATRP of **4** in anisole (50 wt. %) at 80 °C ([**4**]/[CuBr]/[EBiB]/[PMDETA] = 100:1:1.2:1.2). The integration ratio of the phenyl protons f and g to the protons d, d', and e is 4:6, which is expected for a fully protected backbone and a large repeating unit n.

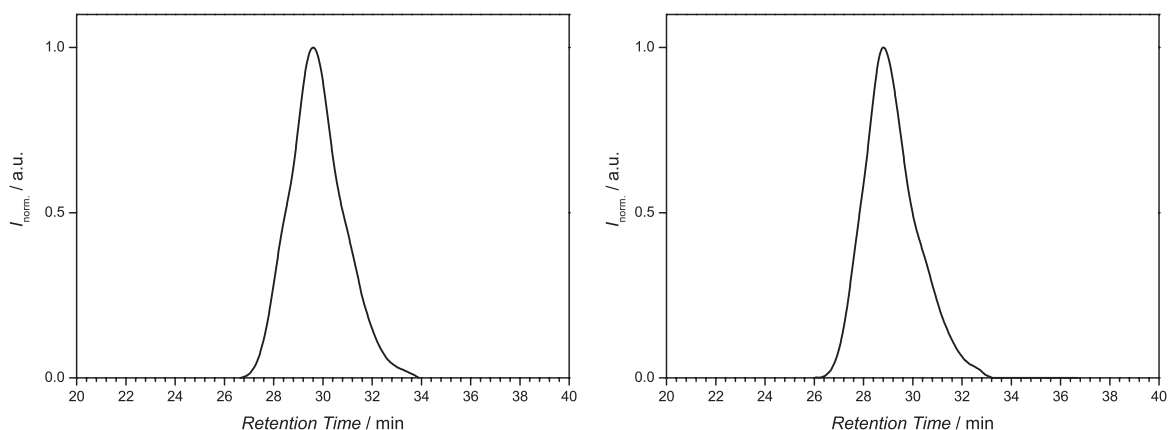
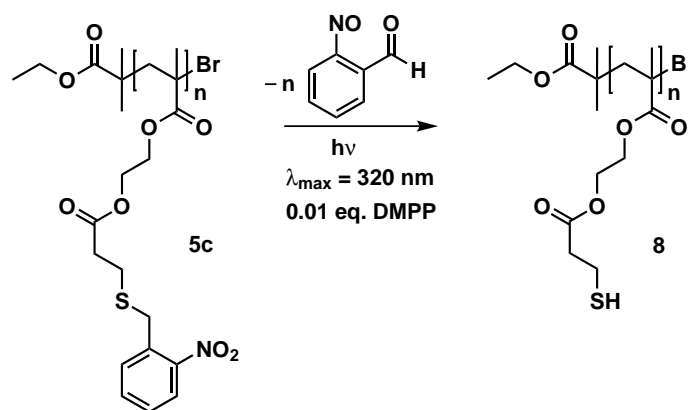


Figure 4.4 SEC traces for the ATRP polymers **5a** (left) and **5b** (right). Conditions and the corresponding results for the ATRP polymerization of **4** are summarized in Table 4.2.

the ionization process. Indeed, the latter has been previously reported (i.e. lactonization^[246,247] and disproportionation^[248]); regardless, these by-products importantly differ only in their polymeric end-group and are, as such, of no significance in the investigation of polymer backbone modification. Moreover, during ESI-MS analysis of the polymer **5c**, only species corresponding to the expected repeating unit of photomonomer **4** were found, which underpins the existence of a clearly defined polymer backbone with intact lateral photodegradable groups. Subsequently, the photocleavage ability of the protected thiol groups present on the polymer backbone was examined. For this purpose, UV-Vis spectroscopy was employed to monitor the photodeprotection rates. During the photodeprotection, each lateral group is expected to release one *o*-nitrosobenzaldehyde molecule, which is known to exhibit a maximum absorbance near 345 nm (see Scheme 4.5).^[58,249] In this line, timed UV irradiation ($\lambda_{\text{max}} = 320$ nm) of **5c** in DCM led to a clear increase in absorbance at 345 nm corresponding to the release of *o*-nitrosobenzaldehyde molecules (see Figure 4.5). After irradiation for 16 hours, the UV spectrum remained unchanged and the release of thiol entities on the polymeric backbone is assumed to be quantitative. To further confirm the primary deprotection of **5c** by irradiation in DCM in the presence of 0.01 eq. of DMPP, a comparative SEC analysis between the photoprotected polymer **5c** and the photodeprotected polymer **8** was performed. Figure 4.6 depicts

Table 4.2 Conditions and results for the ATRP of **4**.

Entry	2/CuBr/EBiB/PMDETA	Solvent (wt %)	Time/h	$M_n/\text{g}\cdot\text{mol}^{-1}$	M_w/M_n
5a	200/1/1/1	Anisole (33 %)	15.0	13000	1.34
5b	100/1/1.2/1.2	Anisole (50 %)	8.5	20000	1.40
5c	100/1/1.2/1.2	Anisole (50 %)	0.8	4700	1.29



Scheme 4.5 Photodeprotection of the ATRP-synthesized polymer **5c** by UV irradiation ($\lambda_{\text{max}} = 320 \text{ nm}$). The released *o*-nitrosobenzaldehyde molecule exhibits a strong absorbance at 345 nm.

a clear shift towards lower molecular weights, an outcome that was expected for multiple releases of *o*-nitrosobenzaldehyde molecules. However, it is not possible to draw conclusions via a numerical comparison since the polymers before and after deprotection have certainly a very different hydrodynamic behavior. NMR analysis of the obtained deprotected polymer proved to be troublesome as typical thiol reducing agents (e.g., dithiothreitol(DTT)) with their inherent thiol moieties would clearly falsify the NMR results. Without the addition of reducing agent and due to the presence of multiple thiol groups in high concentrations, fast formation of insoluble, highly crosslinked networks occurred from extensive disulfide bonding

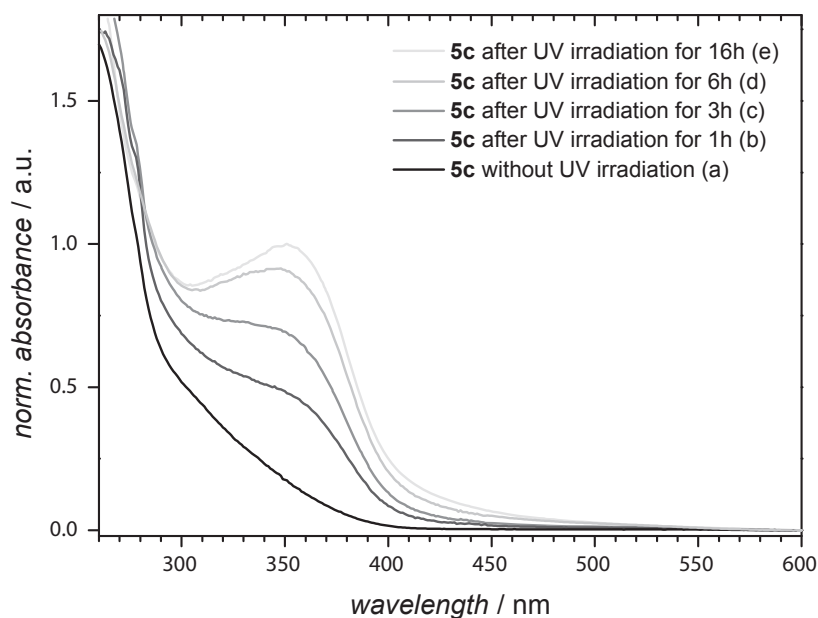


Figure 4.5 Overlay of UV-vis spectra of **5c** ($2 \times 10^{-4} \text{ mol}\cdot\text{L}^{-1}$) during photodeprotection with 0.01 eq. DMPP in DCM after timed offline UV irradiation ($\lambda_{\text{max}} = 320 \text{ nm}$, 36 W): without irradiation (a), and with irradiation for 1 h (b), 3 h (c), 6 h (d) and 16 h (e). Prolonged irradiation ($>16 \text{ h}$) did not change the absorbance significantly.

under oxygen. The accomplishment of polymer backbone modification by thiol-ene chemistry being the main goal, it was consequently decided to perform the rather facile NMR analysis after final backbone modification, which would of course also support the formation of lateral thiol entities on the polymeric backbone **8**. Additionally, the deprotection rates can be optimized when utilizing a lamp emitting at lower wavelengths. However, the occurrence of a UV-C degradation process in poly(methyl methacrylate)^[250] was previously reported and – with having conjugations with UV-C sensitive biomolecules in mind – it was decided to perform all further photodeprotections with the standard UV-B light source ($\lambda_{\max} = 320$ nm).

Polymer Backbone Modification by Phototriggered Deprotection and Thiol-ene Chemistry

Quantitative polymer backbone modifications are – in contrast to the polymeric end-group – rather rare in polymer chemistry and difficult to achieve given the sheer amount of possible side reactions and steric hindrance. As a consequence, *in situ* polymer backbone modification of the deprotected polymer **8** was performed by a Michael-type thiol-maleimide reaction (see Scheme 4.6 for the overall strategy to modify polymer backbone). This reaction is perhaps – together with Diels-Alder cycloadditions utilizing cyclopentadiene^[99,139] – one of the most efficient *click* reactions to date.^[211,251,252] For this purpose, the maleimide 1-(2-hydroxyethyl)-1*H*-pyrrole-2,5-dione **9** was synthesized according to a previously reported procedure.^[213,253]

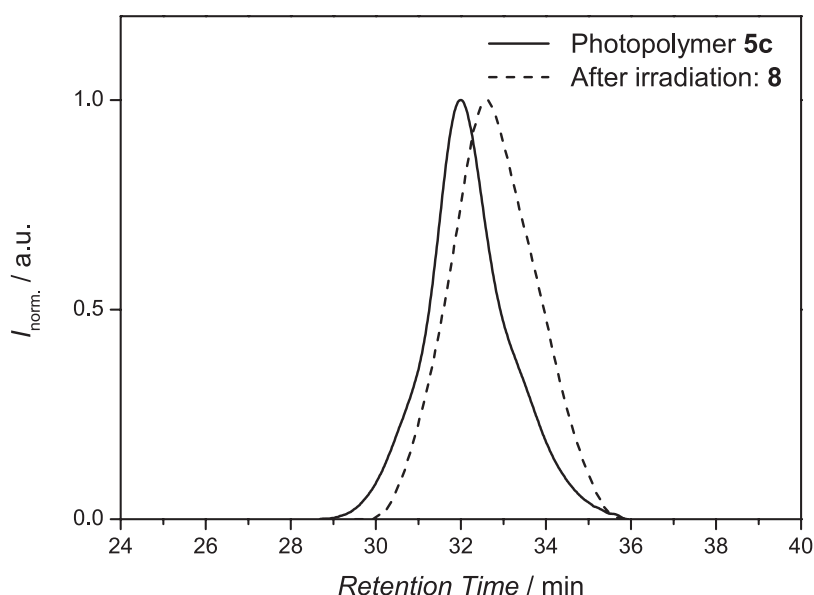
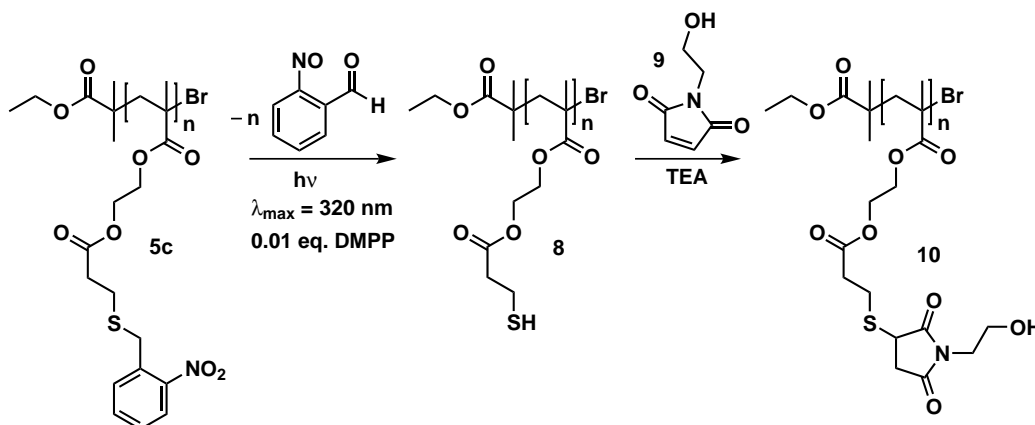


Figure 4.6 Overlay of the size-exclusion chromatograms of **5c** before and after a 16 hour UV irradiation ($\lambda_{\max} = 320$ nm) in DCM. The clear shift to lower molecular weights is attributed to the loss of the photosensitive 2-nitrobenzyl moiety. Disulfide reducing agent dithiothreitol (DTT) was added to **8** before SEC measurement to prevent cross linking.



Scheme 4.6 Strategy for the one-pot photodeprotection of the 2-nitrobenzyl thioether moiety with UV light and subsequent thiol-ene backbone modification with **9**.

The substance possesses the advantage of being water-soluble, which is interesting since an excess of **9** as well as the known byproduct formed by hydrolysis of the maleimide group^[254] can be straightforwardly removed after the thiol-ene reaction by washing with water and precipitation. Additionally, product formation can be simply assessed by NMR analysis in the final polymer thanks to distinctive protons at 3.7 ppm. To confirm the ability to modify the polymer backbone, the thiol-maleimide reaction of the deprotected polymer **8** was subsequently performed with the *N*-modified maleimide **9**. Importantly, the final polymer **10** is insensitive to oxygen, soluble in chloroform and does not form disulfide bridges. ¹H NMR spectroscopic analysis reveals the occurrence of photodeprotection by virtue of the relative decrease in signal intensity of the protons g and f as well as the appearance of characteristic product protons i, i', h, and h' (see signal changes from Figure 4.7a-c). Given the high efficiency of the thiol-maleimide reaction, free lateral thiol groups in the final polymer **10** were not detected; however, one can observe the occurrence of non-quantitative photodeprotection after the 16 hours irradiation time interval by the clear visibility of protons g and f (corresponding to the 2-nitrobenzyl thioether moiety) in Figure 4.7b. The requirement of prolonged irradiation is likely connected to the higher concentrations (e.g., $(10^{-2} \text{ mol}\cdot\text{L}^{-1})$) utilized in the NMR study, as the released *o*-nitrosobenzaldehyde molecules exhibit a high absorbance near the deprotection wavelength. The very low signal intensity of proton g clearly confirms that nearly quantitative photodeprotection was achieved after an increased photodeprotection time of 60 hours. Due to the presence of product protons d, d', i and i' it can be concluded that polymer backbone modification by performing the *in situ* ambient temperature thiol-maleimide reaction was achieved at least to some extent (Figure 4.7c). However it should be noted that the quantification remains a challenging task since one can not fully exclude possible side-reactions

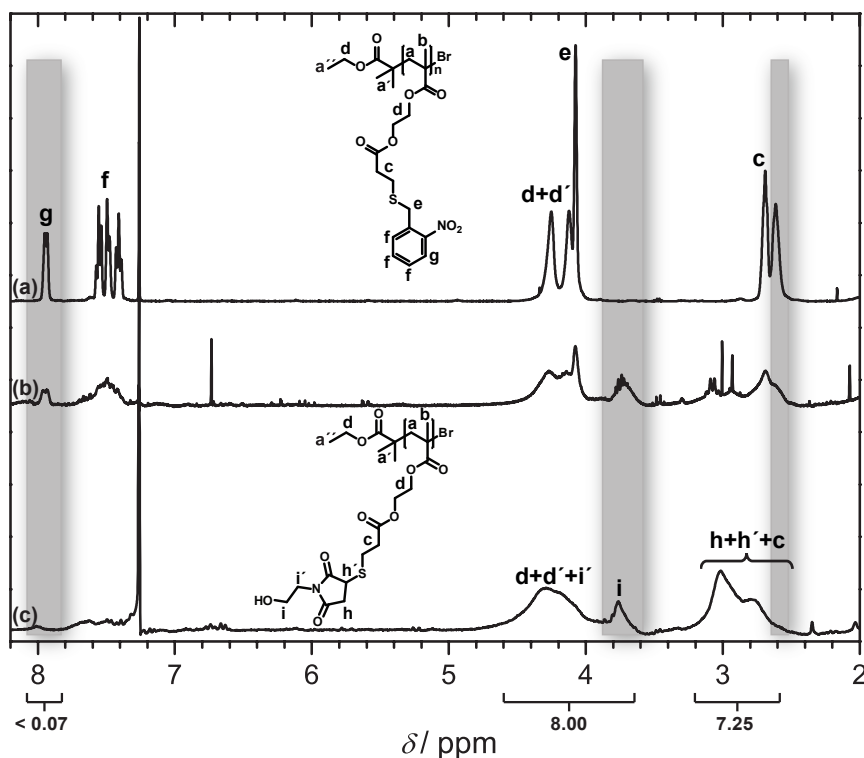


Figure 4.7 ^1H NMR spectra of **5c** in CDCl_3 . **3** before irradiation (a), after 16 hour irradiation ($\lambda_{\text{max}} = 320 \text{ nm}$) and one-pot thiol-ene backbone modification with **9** (b), and after 60 hour irradiation and one-pot thiol-ene backbone modification with **9** (c).

such as disulfide coupling of the polymeric side-chains bearing lateral thiols after photodeprotection or reactions of the *o*-nitrosobenzaldehyde moiety with released thiols.

4.5 Conclusions

In summary, a novel method generating thiols on polymers via protection chemistry was demonstrated using the well-known *o*-nitrosobenzyl moiety and a deprotection low-cost light source. When polymer end group modification is targeted, a quantitative formation of thiol-capped poly(ethylene glycol) methyl ether could be achieved. The photodeprotection has been shown to be essentially inert to catalytic amounts of DMPP and neither disulfide nor other by-product formation could be observed. Furthermore, the concept was extended to polymer backbone modification by the atom transfer radical polymerization of a novel monomer bearing an *o*-nitrosobenzyl thioether moiety. According to NMR and ESI-MS analysis, the photodegradable groups of the obtained polymer remain intact during the polymerization. The photodeprotection is mapped by exploiting the increased absorbance of photocleaved *o*-nitrosobenzaldehyde molecules at 345 nm and UV/Vis data suggest – in agreement with a clear shift to lower molecular weights in GPC analysis – a quantitative

release of thiol entities along the lateral polymer chain after a 16 hour irradiation time interval. Crosslinking of the obtained thiol-functionalized backbone presented an issue in the presence of oxygen and led to insoluble networks. However, it can be envisaged that such behavior could be utilized for the preparation of photocrosslinkable gels. Such network formation can be prevented by *in situ* reaction of the obtained thiol-functionalized polymer with Michael-type acceptors such as maleimides. Finally, polymer backbone modification was achieved by irradiation for 60 hours and subsequent nucleophilic thiol-maleimide addition.

5

(Bio)Molecular Surface Patterning by Phototriggered Oxime Ligation*

5.1 Abstract

Making light work of ligation: A novel method utilizes light for oxime ligation chemistry. A quantitative, low-energy photodeprotection generates aldehyde, which subsequently reacts with aminoxy moieties. The spatial control allows patterning on surfaces with a fluoro marker and GRGSGR peptide, and can be imaged by time-of-flight secondary-ion mass spectrometry (ToF-SIMS).

5.2 Introduction

Photolabile moieties are widely employed in organic chemistry and beyond as a powerful tool for breaking bonds without the need for any additional reagents.^[37] Such orthogonal and mild photolytic cleavage is particularly attractive for solid-supported organic synthesis,^[38] in the field of combinatorial library screening,^[39] and for the tracking of molecular dynamics in biological systems.^[255] Of the myriad of photocleavable protecting groups which have been studied, the *o*-nitrobenzyl group is certainly the predominant one since it enables the caging of a wide range

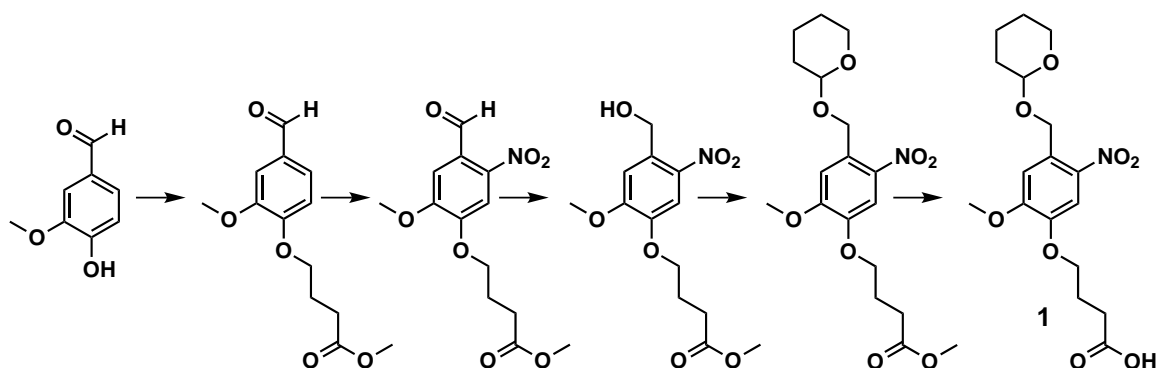
* Parts of this Chapter were reproduced from Ref. 40 by permission of John Wiley and Sons.

of functionalities, such as carboxy,^[69] amine,^[74,256] hydroxy,^[75] and thiol.^[208,243] In addition, the use of light as a trigger provides a straightforward means to obtain spatial and temporal control over a desired molecular cleavage,^[47] which has found significant attention in constructing patterns of multiple cell lines,^[257] the production of 3D structured materials for tissue scaffolds,^[258] and the photocaging of active compounds^[41,259] for instance. Furthermore, the precise positioning of *o*-nitrobenzyl groups in polymer chains has allowed for the controlled alteration of polymer properties upon light stimulus, as demonstrated by the fabrication of cytocompatible 3D hydrogels that can photodegrade^[260] or photorelease peptides,^[261] amphiphilic dendrimer-based photodestructible micelles,^[262] or photocleavable block copolymers to produce functionalized nanoporous films,^[263] to name but a few.^[44]

5.3 Experimental Part

Synthesis of a Universal Photoactive Precursor

The synthetic strategy for the synthesis of a photoactive precursor is outlined in Scheme 5.1.



Scheme 5.1 Strategy for the synthesis of 4-(2-methoxy-5-nitro-4-(((tetrahydro-2*H*-pyran-2-yl)oxy)methyl)phenoxy)butanoic acid **1**.

Synthesis of methyl 4-(4-formyl-2-methoxyphenoxy)butanoate

The synthesis was performed according to a slightly modified literature procedure.^[264] 8.90 g (58.5 mmol, 1.06 eq.) 4-hydroxy-3-methoxybenzaldehyde (vaniline), 9.89 g (55.0 mmol, 1.0 eq.) methyl 4-bromobutanoate, and 10.2 g (73.8 mmol, 1.34 eq.) potassium carbonate were dissolved in DMF (40 mL). The mixture was stirred at ambient temperature for 16 hours, after which time the resulting solution

was poured into chilled water (200 mL) and allowed to precipitate for 15 min at 0 °C. The solid was filtered off, washed with water, redissolved in dichloromethane, and dried over magnesium sulfate. The solvent was removed under reduced pressure to yield 12.2 g (48.4 mmol, 88 %) of a white solid. ^1H NMR (400 MHz, CDCl_3); [δ , ppm]: 9.83 (s, 1H, $-\text{CHO}$), 7.46-7.36 (m, 2H, $-\text{ArH}$), 6.97 (d, $J = 8.1$ Hz, 1H, $-\text{ArH}$), 4.15 (t, $J = 6.3$ Hz, 2H, $-\text{OCH}_2$), 3.96 (s, 3H, $-\text{ArOCH}_3$), 3.79 (s, 3H, $-\text{COOCH}_3$), 2.55 (t, $J = 7.2$ Hz, 2H, $-\text{CH}_2\text{COO}$), 2.24-2.15 (m, 2H, $-\text{OCH}_2\text{CH}_2\text{CH}_2$). ^{13}C NMR (101 MHz, CDCl_3); [δ , ppm]: 191.03, 173.52, 153.94, 150.02, 130.26, 126.86, 111.70, 109.43, 67.96, 56.10, 51.80, 30.41, 24.37. ATR-FTIR: The ester (1726 cm^{-1}) and the aldehyde (1679 cm^{-1}) moieties are visible. ESI-MS: $[\text{M}+\text{Na}]^+$: $m/z_{\text{expt.}} = 275.2$; $m/z_{\text{theo.}} = 275.1$.

Synthesis of methyl 4-(4-formyl-2-methoxy-5-nitrophenoxy)butanoate

The synthesis was performed according to a modified literature procedure.^[264] 9.4 g (37.3 mmol, 1.0 eq.) methyl 4-(4-formyl-2-methoxyphenoxy)butanoate was added slowly to a precooled ($-2\text{ }^\circ\text{C}$) solution of nitric acid (70 %, 140 mL) and stirred at $-2\text{ }^\circ\text{C}$ for 3 hours. It is important to note that – depending on the temperature of the nitration reaction – ipso substitution of the formyl moiety occurs. The resulting solution was poured into chilled water (500 mL) and allowed to precipitate for 15 min at $0\text{ }^\circ\text{C}$ (note: since saponification of the product can occur under these conditions, the precipitation time should be kept as short as possible). The product was filtered, washed with water, and dissolved in dichloromethane. The organic layer was dried over magnesium sulfate. The solvent was removed under reduced pressure to yield 7.7 g (25.9 mmol, 69 %) of a slightly yellow powder. The product contains 5 mol % of the ipso byproduct (methyl 4-(2-methoxy-4,5-dinitrophenoxy)butanoate) and 2 mol % of starting material, both of which can be readily removed in the following synthetic step(s). ^1H NMR (400 MHz, CDCl_3); [δ , ppm]: 10.43 (s, 1H, $-\text{CHO}$), 7.61 (s, 1H, $-\text{ArH}$), 7.42 (s, 1H, $-\text{ArH}$), 4.21 (t, $J = 6.3$ Hz, 2H, $-\text{OCH}_2$), 3.99 (s, 3H, $-\text{ArOCH}_3$), 3.69 (s, 3H, $-\text{COOCH}_3$), 2.56 (t, 2H, $-\text{CH}_2\text{COO}$), 2.24-2.15 (m, 2H, $-\text{OCH}_2\text{CH}_2\text{CH}_2$). ^{13}C NMR (101 MHz, CDCl_3); [δ , ppm]: 187.76, 173.18, 153.48, 151.70, 143.91, 125.51, 109.04, 108.13, 68.61, 56.64, 51.79, 30.18, 24.09. ATR-FTIR: The ester (1736 cm^{-1}) and the aldehyde (1679 cm^{-1}) moieties are visible. ESI-MS: $[\text{M}+\text{Na}]^+$: $m/z_{\text{expt.}} = 320.2$; $m/z_{\text{theo.}} = 320.1$.

Synthesis of methyl 4-(4-(hydroxymethyl)-2-methoxy-5-nitrophenoxy)butanoate

The synthesis was performed according to a modified literature procedure.^[265] 1.50 g (39.7 mmol, 1.5 eq.) sodium borohydride was slowly added at $0\text{ }^\circ\text{C}$ to a solution of 7.7 g (25.9 mmol, 1.0 eq.) methyl 4-(4-formyl-2-methoxy-5-nitrophenoxy)butanoate in EtOH/THF 1:1 v/v (100 mL). After 3 h, all solvents were removed in vacuo and

the residue was suspended in water (50 mL) and dichloromethane (50 mL). The aqueous layer was extracted two times with dichloromethane (2×50 mL) and the combined organic layers were dried over magnesium sulfate. The solvent was removed under reduced pressure. In order to increase the overall yield and to remove partially saponified products, methanol (100 mL) and 50 mg tosylic acid were added to the residue. The solution was stirred at room temperature over night. The solvent was removed in vacuo and the residue was suspended in water (50 mL) and dichloromethane (50 mL). The aqueous layer was extracted two times with dichloromethane (2×50 mL) and the combined organic layers were dried over magnesium sulfate. The solvent was removed under reduced pressure to yield a yellow solid as a raw product, which was purified by column chromatography on silica gel using hexane/ethyl acetate = 1:1 ($R_f = 0.6$) and finally 5.22 g (4.81 mmol, 75 %) of a slightly yellow powder were obtained. ^1H NMR (400 MHz, CDCl_3); [δ , ppm]: 7.69 (s, 1H, -ArH), 7.16 (s, 1H, -ArH), 4.12 (t, $J = 6.3$ Hz, 2H, $-\text{OCH}_2$), 3.97 (s, 3H, $-\text{ArOCH}_3$), 3.70 (s, 3H, $-\text{COOCH}_3$), 2.55 (t, $J = 7.4$ Hz, 2H, $-\text{CH}_2\text{COO}$), 2.29 (bs, 1H, OH), 2.24-2.15 (m, 2H, $-\text{OCH}_2\text{CH}_2\text{CH}_2$). ^{13}C NMR (101 MHz, CDCl_3); [δ , ppm]: 173.16, 154.32, 147.20, 139.68, 132.38, 110.23, 109.58, 68.30, 62.84, 56.40, 51.74, 30.50, 24.27. ATR-FTIR: The ester (1736 cm^{-1}) and the primary alcohol (3538 cm^{-1}) moieties are visible. The aldehyde moiety at (1679 cm^{-1}) has been removed. ESI-MS: $[\text{M}+\text{Na}]^+$: $m/z_{\text{expt.}} = 322.1$; $m/z_{\text{theo.}} = 322.1$.

Synthesis of methyl 4-(2-methoxy-5-nitro-4-(((tetrahydro-2H-pyran-2-yl)oxy)methyl)phenoxy)butanoate

860 mg (2.9 mmol, 1.0 eq.) methyl 4-(4-(hydroxymethyl)-2-methoxy-5-nitrophenoxy)butanoate was dissolved in 10 mL of dichloromethane. Subsequently, 365 mg (4.3 mmol, 1.5 eq.) 3,4-dihydro-2H-pyran and 72 mg (0.6 mmol, 0.2 eq.) pyridinium chloride were added. After the yellow solution was stirred at ambient temperature for 2 h, the solvent was removed under reduced pressure and the obtained orange oil was redissolved in diethyl ether (120 mL). The solvent was filtered and the crude product was obtained after evaporation of the solvent as an orange solid. Recrystallization of the raw product in diethyl ether (5 mL) removed the byproduct of step 2 and 540 mg (1.4 mmol, 48 %) of a white solid were obtained after filtration. Note: Alternatively, the product can be obtained by purification by column chromatography on silica gel using hexane/ethyl acetate = 3:2 ($R_f = 0.5$). ^1H NMR (400 MHz, CDCl_3); [δ , ppm]: 7.70 (s, 1H, -ArH), 7.31 (s, 1H, -ArH), 5.15 (d, $J = 15.7$ Hz, 1H, $-\text{ArCH}_2\text{O}$), 4.94 (d, $J = 15.8$ Hz, 1H, $-\text{ArCH}_2\text{O}$), 4.81-4.77 (m, 1H, $-\text{OCHO}$), 4.12 (t, $J = 6.3$ Hz, 2H, $-\text{ArOCH}_2$), 3.96 (s, 3H, $-\text{ArOCH}_3$), 3.90-3.80 (m, 1H, $-(\text{OCH})\text{CH}_2$), 3.70 (s, 3H, $-\text{COOCH}_3$), 3.63-3.52 (m, 1H, $-(\text{OCOH})\text{CH}_2$), 2.56

(t, $J = 7.2$ Hz, 2H, $-\text{CH}_2\text{COO}$), 2.26-2.11 (m, 2H, $-\text{OCH}_2\text{CH}_2\text{CH}_2$), 2.00-1.34 (m, 6H, $-(\text{OCHO})(\text{CH}_2)_3$). ^{13}C NMR (101 MHz, CDCl_3); [δ , ppm]: 173.48, 154.20, 146.87, 139.38, 131.11, 110.12, 109.58, 99.04, 68.41, 66.31, 62.86, 56.37, 51.84, 30.78, 30.53, 25.50, 24.45, 19.87. ATR-FTIR: The ester (1736 cm^{-1}) moiety is clearly visible. The primary alcohol moiety at (3538 cm^{-1}) has been removed. ESI-MS: $[\text{M}+\text{Na}]^+$: $m/z_{\text{expt.}} = 406.2$; $m/z_{\text{theo.}} = 406.2$. Elemental analysis: Calculated (%): C: 56.39; N: 3.65; H: 6.57. Found (%): C: 56.45; N: 3.52; H: 6.53.

Synthesis of 4-(2-methoxy-5-nitro-4-(((tetrahydro-2H-pyran-2-yl)oxy)methyl)phenoxy)butanoic acid 1

370 mg (1.0 mmol, 1.0 eq.) methyl 4-(2-methoxy-5-nitro-4-(((tetrahydro-2H-pyran-2-yl)oxy)methyl)phenoxy) butanoate was dissolved in dichloromethane (18 mL) and 130 mg (3.25 mmol, 3.25 eq.) sodium hydroxide dissolved in methanol (2 mL) was added. The resulting solution, which turned orange, was stirred for 18 hours. The solvent was removed under reduced pressure and water/dichloromethane 1:1 v/v (100 mL) was added. The water phase was extracted and was acidified with 3 % HCl. The organic phase was washed two times with water, dried over magnesium sulfate and the solvent was removed under reduced pressure to yield 269 mg (0.7 mmol, 70 %) of a slightly yellow solid. ^1H NMR (400 MHz, acetone- d_6); [δ , ppm]: 7.73 (s, 1H, $-\text{ArH}$), 7.41 (s, 1H, $-\text{ArH}$), 5.07 (d, $J = 15.3$ Hz, 1H, $-\text{ArCH}_2\text{O}$), 4.59 (d, $J = 15.2$ Hz, 1H, $-\text{ArCH}_2\text{O}$), 4.81-4.77 (m, 1H, $-\text{OCHO}$), 4.20 (t, $J = 6.3$ Hz, 2H, $-\text{ArOCH}_2$), 3.99 (s, 3H, $-\text{ArOCH}_3$), 3.90-3.80 (m, 1H, $-(\text{OCH})\text{CH}_2$), 3.59-3.48 (m, 1H, $-(\text{COH})\text{CH}_2$), 2.57 (t, $J = 7.2$ Hz, 2H, $-\text{CH}_2\text{COO}$), 2.26-2.11 (m, 2H, $-\text{OCH}_2\text{CH}_2\text{CH}_2$), 1.96-1.46 (m, 6H, $-(\text{OCHO})(\text{CH}_2)_3$). ^{13}C NMR (101 MHz, acetone- d_6); [δ , ppm]: 174.23, 155.05, 148.03, 141.42, 131.16, 111.27, 110.29, 99.20, 69.11, 66.46, 62.50, 56.60, 31.25, 30.43, 29.75, 26.20, 25.28, 20.10. ATR-FTIR: The carboxylic acid (1701 cm^{-1}) moiety is visible. The ester moiety at (1736 cm^{-1}) has been removed. ESI-MS: $[\text{M}+\text{Na}]^+$: $m/z_{\text{expt.}} = 392.2$; $m/z_{\text{theo.}} = 392.1$.

Synthesis of a Photoactive Surface Linker

Synthesis of 4-(2-methoxy-5-nitro-4-(((tetrahydro-2H-pyran-2-yl)oxy)methyl)phenoxy)-*N*-(3-(triethoxysilyl)propyl)butanamide

119 mg (0.32 mmol, 1.0 eq.) 4-(2-methoxy-5-nitro-4-(((tetrahydro-2H-pyran-2-yl)oxy)methyl)phenoxy)butanoic acid 1 was added to a Schlenk tube and dry THF (6 mL) was added. 53 μL (0.38 mmol, 1.2 eq.) triethylamine was added at $0\text{ }^\circ\text{C}$ and the solution was purged with nitrogen for 5 min. 41 μL (0.43 mmol, 1.4 eq.) ethyl chloroformate was added and the solution was stirred further at $0\text{ }^\circ\text{C}$ for

4 h. Subsequently, 79 μL (0.34 mmol, 1.1 eq.) 3-(triethoxysilyl)propan-1-amine were added and the solution was stirred over night at ambient temperature. The solution was filtered and the solvent was evaporated. Ethyl acetate was added and the organic layer was washed with water. The organic layer was dried over magnesium sulfate and the solvent was removed under reduced pressure. The crude product was redissolved in ethylacetate:hexane = 3:1 and purified by column chromatography (SiO_2 , ethyl acetate/hexane 3:1 v/v; $R_f = 0.5$). 65 mg (0.11 mmol, 34 %) 4-(2-methoxy-5-nitro-4-(((tetrahydro-2H-pyran-2-yl)oxy)methyl)phenoxy)-N-(3-(triethoxysilyl)propyl)butanamide was obtained as a slightly yellow solid. ^1H NMR (400 MHz, CDCl_3); [δ , ppm]: 7.71 (s, 1H, -ArH), 7.32 (s, 1H, -ArH), 5.83 (bs, 1H, -CONH), 5.15 (d, $J = 15.7$ Hz, 1H, -Ar CH_2O), 4.94 (d, $J = 15.7$ Hz, 1H, -Ar CH_2O), 4.77 (s, 1H, -OCHO), 4.12 (t, $J = 5.5$ Hz, 2H, -Ar OCH_2), 3.97 (s, 3H, -Ar OCH_3), 3.95-3.85 (m, 1H, -(OCH) CH_2), 3.86-3.77 (m, 6H, -SiO(CH_2) $_3$), 3.62-3.52 (m, 1H, -(OCOH) CH_2), 3.32-3.22 (m, 2H, -CONH CH_2), 2.40 (t, $J = 7.0$ Hz, 2H, - CH_2COO), 2.26-2.14 (m, 2H, -O $\text{CH}_2\text{CH}_2\text{CH}_2$), 1.95-1.50 (m, 6H, -(OCHO)(CH_2) $_3$), 1.28-1.16 (m, 9H, -O $\text{CH}_2(\text{CH}_3)_3$), 0.67-0.59 (s, 2H, -Si CH_2). ^{13}C NMR (101 MHz, CDCl_3); [δ , ppm]: 172.00, 139.41, 131.05, 110.11, 98.98, 77.42, 77.16, 76.84, 68.78, 66.33, 62.96, 58.59, 56.37, 42.05, 33.02, 30.99, 25.63, 23.08, 19.93, 18.58, 15.35, 7.94. ATR-FTIR: The amid (1632 cm^{-1}) moiety is visible. The carboxylic moiety at (1736 cm^{-1}) has been removed. ESI-MS: $[\text{M}+\text{Na}]^+$: $m/z_{\text{expt.}} = 595.4$; $m/z_{\text{theo.}} = 595.3$. Elemental analysis: Calculated (%): C: 54.53 N: 4.89 H: 7.74. Found (%): C: 54.08 N: 4.83 H: 7.80.

Synthesis of a Photoactive Test System

NOTP-containing poly(ethylene glycol) 2

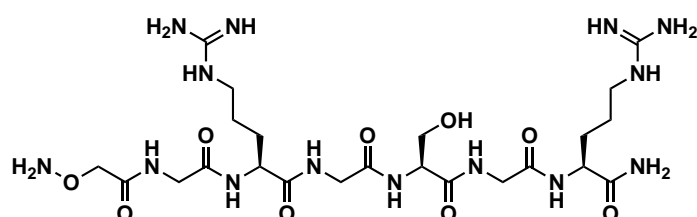
80 mg (0.22 mmol, 4.4 eq.) 4-(2-methoxy-5-nitro-4-(((tetrahydro-2H-pyran-2-yl)oxy)methyl)phenoxy)butanoic acid, 100 mg ($M_n = 2000\text{ g}\cdot\text{mol}^{-1}$, 0.050 mmol, 1.0 eq.) poly(ethylene glycol) methyl ether and 33 mg (0.67 mmol, 3.0 eq.) DCC were dissolved in dry DCM (10 mL). 7 mg (0.06 mmol, 1.2 eq.) DMAP was added and the solution was stirred overnight. Precipitated urea was filtered off and the solvent was removed under reduced pressure. Polymer 2 was obtained by re-dissolution in THF followed by precipitation in diethyl ether. The final polymer was re-dissolved in distilled water, filtered through a 0.45 mm PTFE (teflon) standard GPC filter (to remove any traces of urea or starting material) and the water was removed upon freeze-drying. SEC/THF (GPC data is based on polystyrene standard calibration): $M_n = 3400\text{ g}\cdot\text{mol}^{-1}$, PDI = 1.02. Since the SEC is calibrated with polymers having a different solution behavior and SEC/ESI-MS analysis revealed a clean reaction product, the theoretical $M_n = 2320\text{ g}\cdot\text{mol}^{-1}$ was used for calculations in the model

reactions in solution.

Synthesis of an aminoxy end-capped peptide

The synthesis of the peptides was carried out at the Humboldt Universität (Berlin) in the group of Prof. Dr. Hans Börner by Maria Meißler.

Synthesis of (2-aminoxy)acetamido-Gly-Arg-Gly-Ser-Gly-Arg-NH₂



Scheme 5.2 Chemical structure of the (2-aminoxy)acetamido-Gly-Arg-Gly-Ser-Gly-Arg-NH₂ peptide

The peptide synthesis was performed on an Applied Biosystems ABI 433a peptide synthesizer in a 0.25 mmol scale, using an AM Rink-Amid resin as solid support. Fmoc-amino acid derivatives were coupled following standard ABI-FastMoc protocols (single coupling, no capping) in NMP, facilitated by HBTU/DIPEA. After final Fmoc removal half of the resin (0.125 mmol) was transferred to a 10 mL syringe reactor. 47.8 mg (0.25 mmol, 2.0 eq.) tBoc-2-(aminoxy)acetic acid was activated with 130.1 mg (0.25 mmol, 2.0 eq.) PyBOB and 85 μ L (0.5 mmol, 4.0 eq.) DIPEA (0.5 mmol, 4.0 eq.). The tBoc-2-(aminoxy)acetic acid was double coupled with bench top protocols for two times 3.5 h at room temperature to ensure quantitative conversion as proved with colorimetric Kaiser-test. Afterwards the resin was washed with NMP and DCM and dried overnight under vacuum at 25 °C. The product could be liberated from the resin with TFA/DCM/TES 30:69:1 v/v % (100 mL) for 2 h, followed by removing the Pbf protecting groups in the absence of the resin by a treatment with 50 mL of TFA/H₂O/TES 95:4:1 v/v % for 2 h to obtain the fully deprotected peptide. The peptide was isolated by diethyl ether precipitation, centrifugation, and lyophilization from water. Molecular characterization was performed by ¹H NMR in deuterated trifluoroacetic acid, ATR-FTIR, and ESI-MS in MeCN/water mixture of 3:1 (1 % AcOH): ¹H NMR (500 MHz, d-TFA); [δ , ppm]: 5.05-4.96 (m, 1H), 4.94-4.87 (m, 1H), and 4.85-4.67(m, 3H) correspond to α -CH^{Arg}, α -CH^{Ser}, OCH₂), 4.40-4.22 (m, 7H, β -CH₂^{Ser}, α -CH^{Gly}), 4.20- 4.10 (m, 1H, β -CH₂^{Ser}) 3.42-3.28 (m, 4H, δ -CH₂^{Arg}), 2.16-2.04 (m, 2H, β -CH₂^{Arg}), 2.01-1.74 (m, 6H, β -CH₂^{Arg}, γ -CH₂^{Arg}). ATR-FTIR: ν [cm⁻¹] 3281 (m, Amid A), 1651 (vs, Amid-I),

1539 (s, Amid-II), 1418 (w), 1199 (m), 1131 (m), 837 (m), 802 (w), 721 (m). ESI-MS: $[M+H]^+$: $m/z_{\text{expt.}} = 661.5$; $m/z_{\text{theo.}} = 661.3$.

Phototriggered Experiments in Solution

Photodeprotection of NOTP-containing poly(ethylene glycol) 2

1.0 mg (0.43 μmol , 1.0 eq.) of **2** of was dissolved in dichloromethane (1 mL) and aliquoted into a headspace vial (Pyrex, diameter 20 mm), which was crimped airtight using SBR seals with a PTFE inner liner. The solution was deoxygenated by purging with nitrogen for 2 minutes. The flask was subsequently irradiated for 3 minutes by revolving around a compact low-pressure fluorescent lamp (Osram Delux L Blue UVA 18W, OSRAM AG, München, Germany) emitting at 370 nm (± 30 nm, 18 W) at a distance of 40-50 mm in a custom-built photoreactor (see Figure 11.1). The solvent was evaporated under ambient conditions. THF (0.5 mL) was added and the solution with polymer **3** was analyzed immediately via SEC/ESI-MS (see Figure 5.1) and UV-Vis spectroscopy (see Figure 5.1).

Surface Modifications

Cleaning and preactivation of the Si wafers

All Si wafers were cleaned three successive times by ultrasonification for 10 min in acetone, chloroform, ethanol and finally dried under an nitrogen stream. Pre-activation of the surfaces was achieved by separately placing them in small glass vials containing acidic piranha solution (sulfuric acid 95 % / aqueous hydrogen peroxide 35 % 3:1 v/v) for 60 min at 100 °C in a shaker. Caution: piranha solution is an extremely strong oxidant and should be handled very carefully! The Si wafers were subsequently washed und ultrasonificated with distilled water for 10 minutes and dried under an nitrogen stream.

Silanization of Si wafers with NOTP-containing silane

Preactivated substrates were placed separately in small glass vials containing a solution of NOTP-containing silane (1 mg, 1.7 μmol) dissolved in anhydrous toluene (1 mL). They were subsequently heated to 50 °C for 16 hours in a shaker. The wafers were subsequently ultrasonicated in dry toluene (10 mL, 10 min) and dichloromethane (10 mL, 10 min) to remove any physisorbed silane.

Spatially controlled photodeprotection

A mask (see Figure 11.2) was placed onto a NOTP-functionalized Si wafer. The latter was placed into the headspace vial, which was crimped air-tight using SBR seals with PTFE inner liner. The solution was deoxygenated by purging with nitrogen for 3 min. The flasks were subsequently irradiated for 3 minutes in a photoreactor (see Figure 11.1). After irradiation, the mask was removed. The wafer was subsequently rinsed with dichloromethane and sonicated for 5 min in acetone to remove any possibly physisorbed material. The wafer was finally dried under a nitrogen stream.

Spatially controlled surface functionalization with O-((perfluorophenyl)methyl)hydroxylamine

1 mg O-((perfluorophenyl)methyl)hydroxylamine hydrochloride was dissolved in DMF (1 mL) and a photodeprotected silicon wafer from the last step was added into a small vial, which was placed in a shaker for 16 hours. The wafer was subsequently rinsed with DMF and sonicated for 10 min in acetone to remove any physisorbed material. The wafer was finally dried under a nitrogen stream.

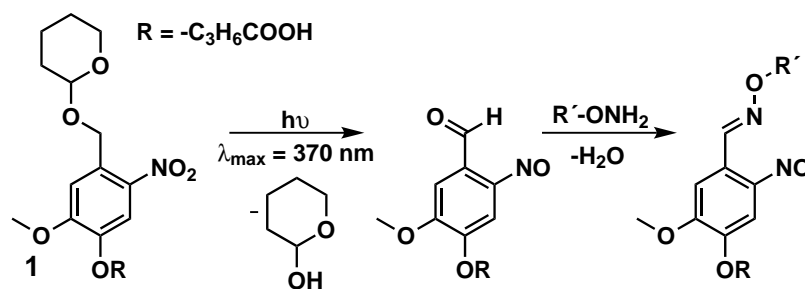
Spatially controlled surface functionalization with (2-aminooxy)acetamido-Gly-Arg-Gly-Ser-Gly-Arg-NH₂

In a headspace vial (Pyrex, diameter 20 mm), (2-aminooxy)acetamido-Gly-Arg-Gly-Ser-Gly-Arg-NH₂ (1 mg) was dissolved in DMF (1 mL) and a photodeprotected silicon wafer from the last step was added into a small vial, which was placed in a shaker for 16 hours. The wafer was subsequently rinsed with DMF and sonicated for 10 min in acetone to remove any physisorbed material. The wafer was finally dried under a nitrogen stream. The wafer was subsequently washed with distilled water and finally dried under a nitrogen stream.

5.4 Results and Discussion

The underlying mechanism for the photocleavage of *o*-nitrobenzyl derivatives is well studied^[58] and typically leads to the release of the protecting group in the form of a nitrosobenzaldehyde derivative as a byproduct.^[266] The idea presented herein, however, is to take advantage of this photoreleased aldehyde moiety for oxime formation (see Scheme 5.3).^[267] In other words, to consider the usual byproduct as the actual product. As alluded to above, the use of light will also provide a facile means to confer spatial and temporal control to the increasingly employed oxime-based click chemistry. To date, only Maynard and coworkers have reported molecular patterns employing oxime ligation, however the reaction requires rather

harsh conditions, such as electron-beam or photoacid generator-based photolithographies.^[268–270] Interestingly, the method presented herein proceeds at less-energetic wavelengths (UVA) than light-triggered strategies recently reported, which are based on the nitrile imine-ene 1,3-dipolar cycloaddition (UVC),^[271] on the Diels-Alder cycloaddition of *o*-quinodimethanes^[3] or 3-(hydroxymethyl)naphthalene-2-ol derivatives (UVB).^[151,152] Altogether, these different techniques form a versatile toolbox for photopatterning in different contexts, yet all with high efficiency under ambient conditions. The current approach proceeds in two steps: a) a fast and mild photodeprotection and b) the subsequent oxime ligation reaction (see Scheme 5.3). The 2-[(4,5-dimethoxy-2-nitrobenzyl)oxy]tetrahydro-2*H*-pyranyl (NOTP) scaffold in compound **1** was selected as a novel highly reactive photocleavable moiety based on its overall kinetics – photocleavage quantum yield of *o*-nitroveratryl ethers is one order of magnitude higher than that of most other *o*-nitro-veratryl derivatives^[255] – as well as for the ease of incorporation of the (tetrahydropyran-2-yl)oxy group through dihydropyran (see the Experimental Chapter for a full synthetic procedure). Initial model reactions were performed in solution on a poly(ethylene glycol) methyl ether (PEG) functionalized with **1**, a system amenable to mass spectrometry, a method which allows the detection of potential side-product formation with much higher sensitivity and specificity than ¹H NMR spectroscopy.^[229] A low-cost compact fluorescent lamp ($\lambda_{\max} = 370$ nm, 18 W) was employed as the UVA source for the photodeprotection. The outcome of the deprotection is shown in Figure 5.1, which depicts the mass spectrum of the fully photodeprotected nitrosobenzaldehyde capped PEG **3**. Complete cleavage upon mild irradiation was typically achieved within only 3 min at ambient temperature (see also Figure 5.1 middle for UV spectra). Subsequently overnight reaction of **3** with hydroxylamine hydrochloride resulted in the desired aldoxime **4** (see Figure 5.2). The presence of a small quantity of impurities may also be observed, which can all be assigned to the multiple side reactions undergone by the nitroso moiety,^[272] for example, dimerization yielding **5**, two- and four-electron reduction leading to **6** and **8**, or



Scheme 5.3 Photoinduced cleavage of a 2-((4,5-dimethoxy-2-nitrobenzyl)oxy)tetrahydro-2*H*-pyranyl (NOTP) derivative and subsequent oxime ligation with hydroxylamine derivatives.

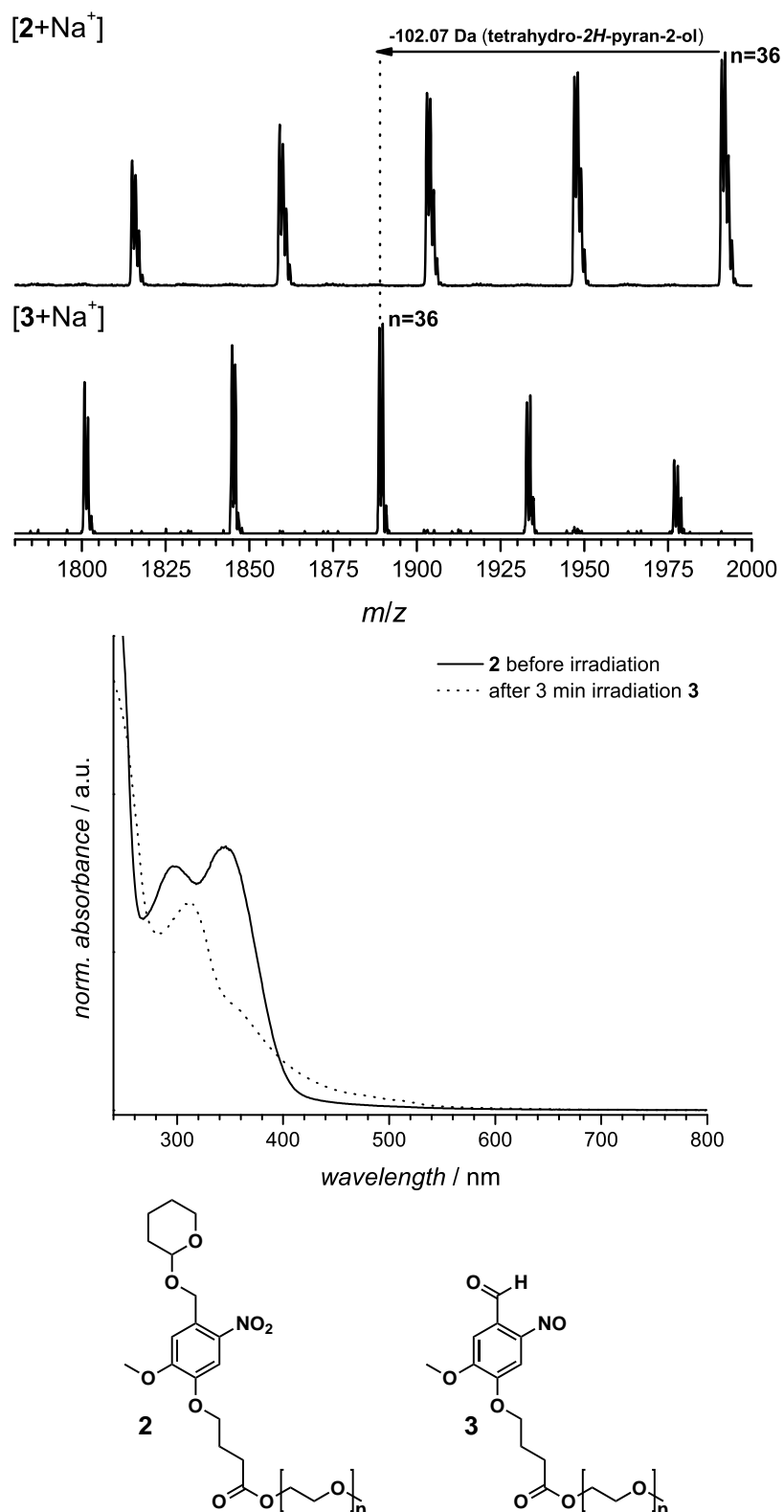
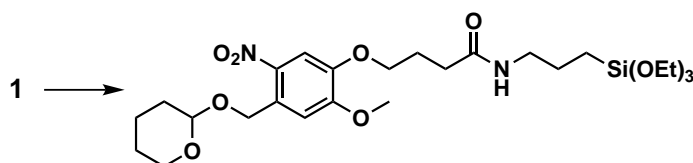


Figure 5.1 ESI-MS spectra of NOTP-capped poly(ethylene glycol) methyl ether before (top), UV-Vis spectra of **2** in dichloromethane ($2 \cdot 10^{-4} \text{ mol L}^{-1}$) before and **3** after irradiation ($\lambda_{\text{max}} = 370 \text{ nm}$, 18 W) for 3 min (middle). Bottom: Structural formulae for starting compound **2** and photoproduct **3**.

Table 5.1 Experimental and theoretical m/z values for the isotopic distribution of Figure 5.1 in the m/z range between 1875 and 1925

$m/z_{\text{expt.}}$	ion assignment	formula	$m/z_{\text{theor.}}$	$\Delta m/z$
1903.0	$2_{n=34} + \text{Na}^+$	$[\text{C}_{86}\text{H}_{161}\text{NNaO}_{42}]^+$	1903.0	0.0
1888.8	$3_{n=35} + \text{Na}^+$	$[\text{C}_{85}\text{H}_{159}\text{NNaO}_{42}]^+$	1889.0	0.2

subsequent condensation generating **7**. Owing to the undesirable nitroso-centered reactions this strategy is not suitable for polymer-polymer conjugation in solution, as such reactions are subject to a stringent set of click requirements.^[2] However, it is noteworthy that all the products derived from the reaction between **3** and hydroxylamine contain the desired oxime bond. Consequently, when the reaction sequence is performed on a surface, no influence on the grafting density or the spatial control is to be expected. These findings, as well as the light-based nature of the conjugation technique, was the occasion to translate it to the spatially constrained grafting of molecules onto surfaces to produce molecular patterns. The synthetic route to functionalize silicon surfaces is straightforward. A NOTP-functionalized silane was prepared (Scheme 5.4), dissolved in anhydrous toluene, and used to treat activated silicon wafers. Upon successful silanization, the photopatterning was achieved by irradiation of the silicon wafer covered with a shadow mask for 3 min (the UV dose can be estimated to be lower or comparable to that of the most efficient soft photopatterning techniques^[273,274]). Subsequently, the mask was removed and the silicon wafer was immersed in a solution of O-[(perfluorophenyl)methyl] hydroxylamine hydrochloride, which was utilized as a molecular marker to spatially map the locally constrained surface grafting (Figure 5.4a). In order to confirm that the employed silanization technique does not destroy the NOTP species, we performed a test experiment in which the NO_2 (peak at 406.6 eV)^[275] and NH (peak at 399.8 eV)^[276] XPS spectra of purely adsorbed (see Figure 5.3a) 4-(2-methoxy-5-nitro-4-(((tetrahydro-2H-pyran-2-yl)oxy)methyl)phenoxy)-N-(3-(triethoxysilyl)propyl)butanamide was compared with the ones in which silanization (see Figure 5.3b) has been performed. The presence of NO_2 moieties in similar ratios was clearly confirmed in both cases. Figure 5.3c depicts the clear disappearance of the NO_2 peak after irradiation of the

**Scheme 5.4** Synthesis of the NOTP-functionalized silane. Reagents: ethyl chloroformate, triethylamine, 3-(triethoxysilyl)propan-1-amine, THF.

NOTP silanized sample, which corresponds to a full photodeprotection of the surface. Figure 5.3d evidences the F1s XPS spectra of a Si-wafer after NOTP silanization and Figure 5.3e after performing the spatially controlled surface functionalization with O-((perfluorophenyl)methyl)hydroxylamine. The main peak in the F1s spectrum at 688.4 eV can be assigned to fluorine atoms (C-F).^[277] Thus, the spectrum shows a drastically increased intensity of fluorine atoms after the phototriggered procedure, which clearly indicates successful coupling. Successful surface derivatization of a NOTP-capped surface was also confirmed by time-of-flight secondary ion mass spectrometry (ToF-SIMS), which is a powerful and highly sensitive technique for the spatially resolved analysis of molecular patterns on solid substrates.^[196] In contrast to traditional fluorescence imaging, ToF-SIMS data also provides detailed information on the chemical composition, essential for analysis of non-fluorescent (bio)-molecules. A ToF-SIMS composition analysis of the nitro and fluorine con-

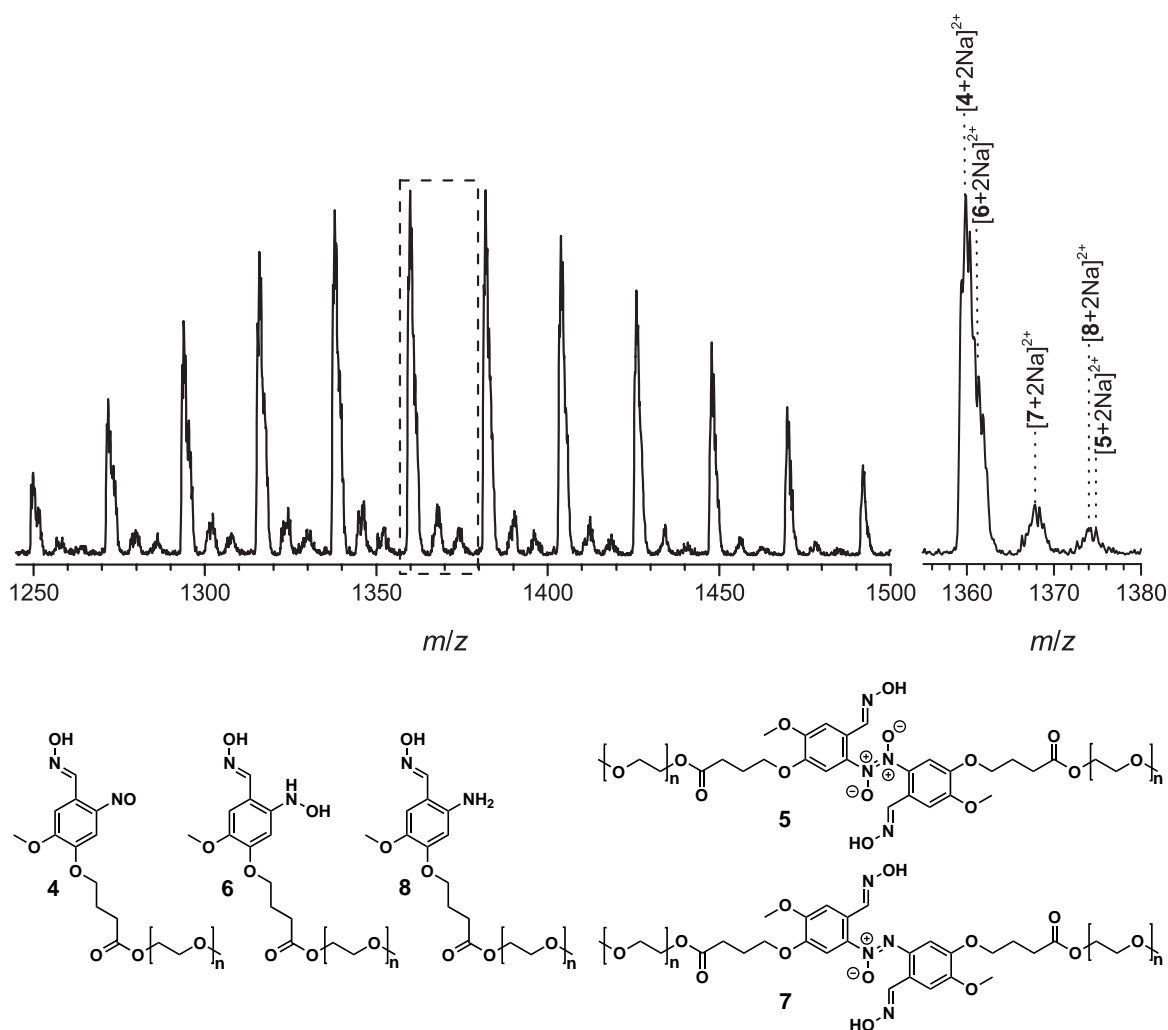
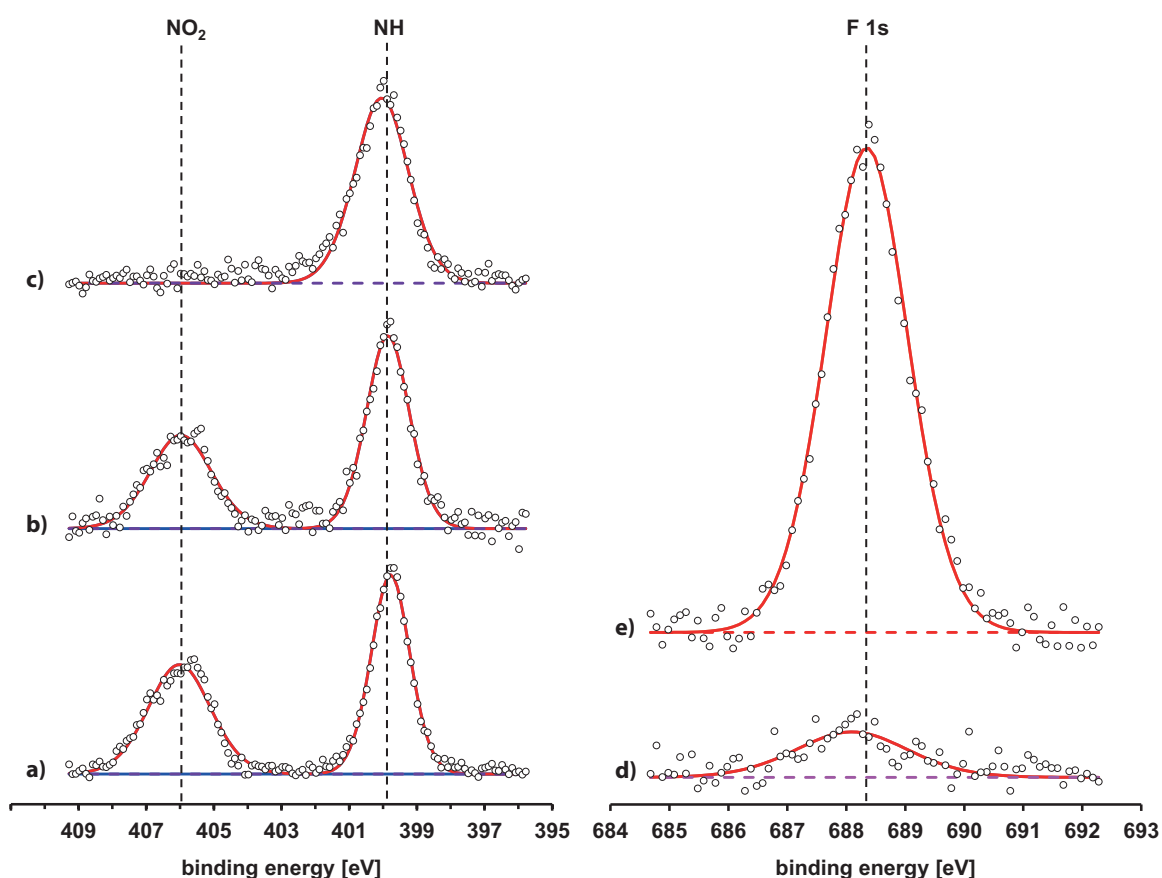


Figure 5.2 ESI-MS spectrum of nitrosobenzaldehyde-capped poly(ethylene glycol) methyl ether **3** after reaction with hydroxylamine hydrochloride to form **4**. Species **5**, **6+8**, and **7** can be assigned to dimerization, reduction, and condensation of the nitroso moiety, respectively.

Table 5.2 Experimental and theoretical m/z values for the isotopic distribution of Figure 5.2 in the m/z range between 1379 and 1400

$m/z_{\text{expt.}}$	ion assignment	formula	$m/z_{\text{theor.}}$	$\Delta m/z$
1381.6	$4_{n=55} + 2\text{Na}^{2+}$	$[\text{C}_{123}\text{H}_{236}\text{N}_2\text{Na}_2\text{O}_{61}]^{2+}$	1381.8	0.2
1397.7	$5_{n=48} + 2\text{Na}^{2+}$	$[\text{C}_{124}\text{H}_{228}\text{N}_4\text{Na}_2\text{O}_{61}]^{2+}$	1397.7	0.0
1382.9	$6_{n=55} + 2\text{Na}^{2+}$	$[\text{C}_{123}\text{H}_{238}\text{N}_2\text{Na}_2\text{O}_{61}]^{2+}$	1382.8	0.1
1389.9	$7_{n=48} + 2\text{Na}^{2+}$	$[\text{C}_{124}\text{H}_{228}\text{N}_4\text{Na}_2\text{O}_{60}]^{2+}$	1389.7	0.2
1396.8	$8_{n=56} + 2\text{Na}^{2+}$	$[\text{C}_{125}\text{H}_{242}\text{N}_2\text{Na}_2\text{O}_{61}]^{2+}$	1396.8	0.0

**Figure 5.3** Comparison of NO_2 and NH spectra of Si-substrates after pure adsorption of NOTP-silane (a) and after silanization (b). The NO_2 moiety fully disappeared after irradiation (c). Peak heights have been normalized to maximum intensity. Comparison of $\text{F}1s$ of Si-substrates after NOTP silanization (d) and after performing the phototriggered oxime ligation strategy with O-((perfluorophenyl)methyl)hydroxylamine hydrochloride (e). Peak heights have been normalized to the $\text{N}1s$ peak intensity of the NH component.

tents on the surface after irradiation and functionalization readily reproduced the shadow mask structures with a good spatial resolution between irradiated and non-irradiated areas. Indeed, only the non-irradiated zone showed the presence of nitrite (NO_2^-) – a fragment initially present in the protected molecule – while only the irradiated part exhibited fluorine functionalization, as demonstrated by

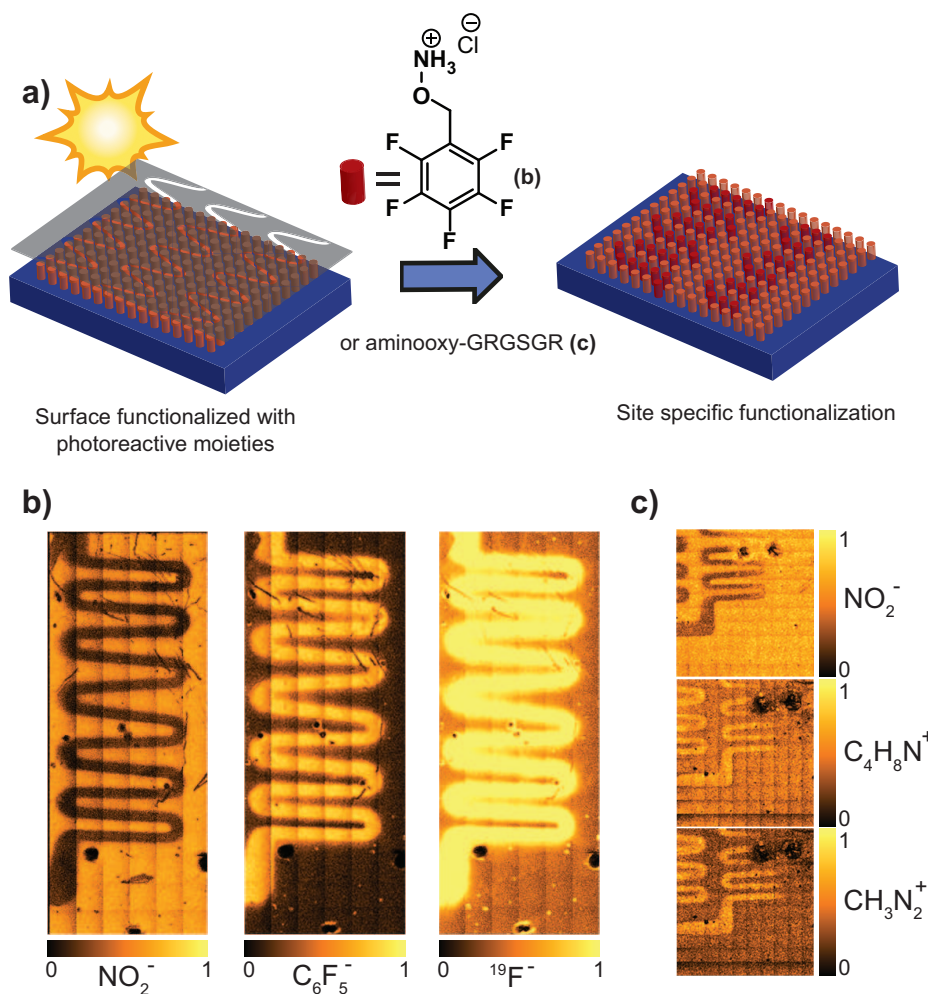


Figure 5.4 Schematic representation of the photodeprotection of Si wafers (blue) functionalized with NOTP (orange) using a shadow mask (gray), and subsequent patterning with O-[(perfluorophenyl)-methyl] hydroxylamine hydrochloride (a). ToF-SIMS images after photodeprotection (left) and oxime ligation with the fluoro marker (center and right) (b). ToF-SIMS images after photodeprotection and oxime ligation with aminoxy-GRGSGR (structure included in Scheme 5.2) (c).

the detection of F^- and C_6F_5^- ions, after immersion of the wafer in the solution of O-[(perfluorophenyl)methyl] hydroxylamine hydrochloride (Figure 5.4b). To also demonstrate the feasibility of a covalent and site specific attachment of biomolecules by this phototriggered approach, a freshly prepared NOTP-functionalized wafer was irradiated and treated with a solution of (2-aminoxy) acetamido Gly-Arg-Gly-Ser-Gly-Arg peptide (GRGSGR). ToF-SIMS again provided evidence that the peptide was immobilized in a pattern corresponding to the mask features (Figure 5.4c). In that case, composition analysis was based on the presence of CH_3N_2^+ and $\text{C}_4\text{H}_8\text{N}^+$ ions, characteristic secondary ions for arginine-containing peptides.^[278–280]

5.5 Conclusions

In summary, the highly efficient phototriggered deprotection of a novel *o*-nitrobenzyl acetal at 370 nm was presented. The strategy allows not only the quantitative and extremely rapid photorelease of aldehyde functionalities, but also for the first time the spatial control over the *click*-type oxime ligation using mild conditions. Indeed, the two-step procedure was translated to the fabrication of patterned silicon surfaces. The site-specific attachment of aminoxy- functionalized (bio)molecules, that is, a small marker molecule and a peptide, was confirmed by ToF-SIMS. It can be envisaged that the introduced technique can be extended to the generation of functional patterned substrates to study/control cell behavior. However, the potentially cell toxic nitroso group should be first neutralized, e.g., with glutathione.^[281]

6

Phototriggered Diels-Alder Surface (Bio)functionalization at Ambient Temperature*

6.1 Abstract

A photoconjugation strategy based on light-triggered Diels-Alder addition of *o*-quinodimethanes is compatible with biomolecules and proceeds rapidly at ambient temperature without the need of a catalyst. Spatial control was confirmed by photopatterning of a small-molecule ATRP initiator, a polymer, and a peptide in a time-of-flight secondary-ion mass spectrometry (ToF-SIMS) investigation.

6.2 Introduction

The recent years have witnessed a substantial increase of activity in the modification of materials by the highly efficient chemical methods often referred to as *click* chemistry.^[1,2] The set of reactions belonging to this class exhibit specific features such as fast reaction kinetics, high yields, orthogonal reactivity, and tolerance to a wide range of solvents. However, in some applications featuring surface patterns

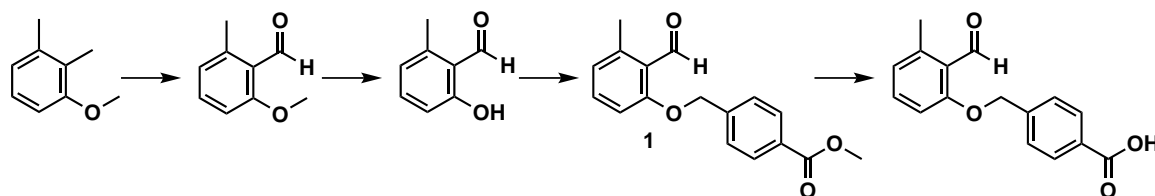
* Parts of this Chapter were reproduced from Ref. 3 by permission of John Wiley and Sons.

or three-dimensional scaffolds, these characteristics are not sufficient, because spatial control is also required. Furthermore, temporal control of chemical reactions could offer the significant advantage of triggering reactions at any time, which would be particularly interesting when a specific sequence of events is required. The use of light as a temporal and spatial trigger has very recently been adapted to *click* methods.^[152] For instance, Bowman and coworkers reported patterns of hydrogels fabricated by azide-alkyne cycloaddition cross-linking initiated by the phototriggered reduction of Cu(II) into Cu(I), the latter being the catalyst for the reaction.^[282] However, their method presents the disadvantage of involving many species, such as the different copper species and the radical photoinitiator required to generate Cu(I). Although no such effect was reported, these species are able to diffuse in the medium and could hinder its spatially resolved character. The same applies to the widely used photoinitiated radical thiol-ene and thiol-yne reactions.^[98,283] The key to achieve full spatial control is to immobilize one of the two components and to directly activate it. Popik, Locklin, and coworkers followed such a path when they used immobilized cyclopropanone-masked cyclooctynes.^[284] Under UV light, decarbonylation occurs, releasing strained alkynes reacting rapidly with azides in solution and producing fluorophore patterns. Following the inspiring work of Lin and coworkers,^[95,285] who resurrected the seminal work of Huisgen and Sustmann,^[286] Barner-Kowollik and coworkers have recently explored the photogeneration of nitrile imines from immobilized diaryl tetrazoles to pattern different polymers on cellulose by 1,3-dipolar cycloaddition with maleimide-functionalized macromolecules.^[271] Importantly, the same group has additionally introduced a novel procedure for *click* conjugations based on the Diels-Alder addition of hydroxy-*o*-quinodimethanes (photoenols) generated by photoisomerization of *o*-methylphenyl ketones or aldehydes (for a detailed mechanism see also Figure 2.7 in Chapter 2) and demonstrated its ease and efficiency in light-induced conjugations of polymeric building blocks.^[144,287] The latter strategy fulfills the harsh set of *click* conditions required for polymer-polymer ligation.^[2]

The present chapter describes a novel photochemical methodology with enhanced chemical selectivity and orthogonality while still providing fast reaction kinetics. These features allow for the highly efficient generation of surface patterns, yet in presence of diverse amino acid residues and in a non-light protected environment. The concept avoids the use of photoremovable protecting groups (PPG) and is based on the photogeneration and trapping of a highly reactive intermediate.

6.3 Experimental Part

Synthesis of a Universal Photoactive Precursor



Scheme 6.1 Overall strategy for the synthesis of methyl 4-((2-formyl-3-methylphenoxy)methyl)benzoic acid.

Synthesis of 2-hydroxy-6-methylbenzaldehyde

6.8 g (50.0 mmol, 1.0 eq.) 2-methoxy-6-methylbenzaldehyde^[288,289] was dissolved in 60 mL dichloromethane. 20.0 g (150.0 mmol, 3.0 eq.) AlCl_3 was cautiously added to the yellow solution and the mixture was stirred at ambient temperature over night. The color changed from yellow over red to a dark brown. Excess of aluminium chloride was cautiously quenched with water; the aqueous layer was extracted three times with dichloromethane and dried over sodium sulfate. The solvent was removed under reduced pressure and 4.72 g (31.5 mmol, 63 %) of a dark brown oil was obtained. In order to obtain an increased overall yield for **1**, the raw product was used directly in the next step without further purification. $^1\text{H NMR}$ (250 MHz, CDCl_3); [δ , ppm]: 11.90 (s, 1H, OH), 10.32 (s, 1H, CHO), 7.42–7.32 (m, 1H, ArH), 6.84–6.68 (m, 2H, ArH), 2.60 (s, 3H, $-\text{ArCH}_3$).

Synthesis of methyl 4-((2-formyl-3-methylphenoxy)methyl)benzoate **1**

3.36 g (24.7 mmol, 1.0 eq.) 2-hydroxy-6-methylbenzaldehyde and 5.74 g (25.19 mmol, 1.02 eq.) 4-(bromomethyl) benzoate were dissolved in acetone (170 mL; the solvent has been predried over sodium sulfate). To this solution, 5.1 g (37.1 mmol, 1.5 eq.) potassium carbonate and 100 mg (0.38 mmol, 0.015 eq.) 18-crown-6 were added. The mixture was stirred at 40 °C over night. After filtration, the solvent was removed under reduced pressure, the residue was re-dissolved in 100 mL of dichloromethane/water (1:1 v/v) and acidified with aqueous HCl (3 %). The aqueous layer was extracted two more times with dichloromethane (2 × 30 mL) and the combined organic layers were dried over sodium sulfate. The solvent was removed under reduced pressure, 50 mL of 7:1 v/v hexane/ethyl acetate was added and 3.5 g (12.32 mmol, 50 %) essentially pure **1** precipitated after cooling in

the fridge. The product was obtained as a solid after filtration and drying under reduced pressure. ^1H NMR (250 MHz, acetone- d_6); [δ , ppm]: 10.73 (s, 1H, CHO), 8.06 (d, $J = 8.4$ Hz, 1H, ArH), 7.68 (d, $J = 8.3$ Hz, 1H, ArH), 7.45 (t, $J = 8.2$ Hz, 1H, ArH), 7.13 (d, $J = 8.4$ Hz, 1H, ArH), 6.89 (d, $J = 7.7$ Hz, 1H, ArH), 5.38 (s, 2H, $-\text{OCH}_2$), 3.89 (s, 3H, $-\text{ArCOOCH}_3$), 2.52 (s, 3H, $-\text{ArCH}_3$).

Synthesis of methyl 4-((2-formyl-3-methylphenoxy)methyl)benzoic acid

1.83 g (6.44 mmol, 1.0 eq.) of **1** was dissolved in 90 mL of dichloromethane and 770 mg (19.3 mmol, 3.0 eq.) sodium hydroxide dissolved in 10 mL methanol were added. The reaction mixture was stirred over night at ambient temperature. The solvents were removed under reduced pressure and the residue was subsequently redissolved in 140 mL dichloromethane/water (1:1 v/v). The organic layer was extracted with water, all water layers were combined and acidified with aqueous HCl (3 %) to pH 3. The aqueous layer was subsequently extracted 3 times with dichloromethane and the combined organic layers were dried over sodium sulfate. The solvent was removed under reduced pressure and 1.3 g (4.81 mmol, 75 %) of a white powder was obtained. ^1H NMR (250 MHz, acetone- d_6); [δ , ppm]: 10.74 (s, 1H, CHO), 8.05 (d, $J = 8.4$ Hz, 1H, ArH), 7.68 (d, $J = 8.4$ Hz, 1H, ArH), 7.45 (t, $J = 8.1$ Hz, 1H, ArH), 7.13 (d, $J = 8.4$ Hz, 1H, ArH), 6.89 (d, $J = 7.6$ Hz, 1H, ArH), 5.39 (s, 2H, $-\text{OCH}_2$), 2.52 (s, 3H, $-\text{ArCH}_3$).

Synthesis of a Photoactive Surface Linker

Synthesis of the photoactive silane **6**

330 mg (1.22 mmol, 1.0 eq.) methyl 4-((2-formyl-3-methylphenoxy)methyl)-benzoic acid and 9 mL of dry THF was added to a Schlenk tube. 200 μL of triethylamine were subsequently added. The solution was purged with nitrogen for 5 min, 140 μL (1.47 mmol, 1.2 eq.) ethyl chloroformate was added at 0 °C and stirred further at 0 °C for 4 h. 300 μL (1.38 mmol, 1.13 eq.) 3-(triethoxysilyl)propan-1-amine were added and the solution was stirred over night. The solution was filtered and the solvent was evaporated, ethylacetate was added and the organic layer was washed with water, water + sodium hydroxycarbonate, water and water + sodiumchloride. The organic layer was dried over magnesium sulfate and the solvent was removed under reduced pressure. The crude product was re-dissolved in ethylacetate:hexane = 1:1 and purified by column chromatographie (SiO_2 , ethylacetate / hexane 1:1 v/v; $R_f = 0.5$). 235 mg (0.5 mmol, 41 %) of **6** were obtained as a white solid. ^1H NMR (400 MHz, CDCl_3); [δ , ppm]: 10.74 (s, 1H, CHO), 7.80 (d, $J = 8.1$ Hz, 2H, ArH), 7.48 (d, $J = 8.1$ Hz, 2H, ArH), 7.36 (t, $J = 8.4$ Hz, 1H, ArH), 6.85 (dd, $J = 8.0$ Hz, 5.3 Hz, 2H,

ArH), 6.55 (bs, 1H, NH), 5.21 (s, 2H, $-\text{OCH}_2\text{Ar}$), 3.77 (q, $J = 7.0$ Hz, 6H, $-\text{SiO}(\text{CH}_2)_3$), 3.48 (dd, $J = 12.9$ Hz, 6.6 Hz, 2H, $-\text{NHCH}_2$), 2.58 (s, 3H, $-\text{ArCH}_3$), 1.86–1.68 (m, 2H, $-\text{SiCH}_2\text{CH}_2$), 1.27–1.17 (m, 9H, $-\text{OCH}_2(\text{CH}_3)_3$), 0.70 (d, $J=7.4$, 2H, $-\text{SiCH}_2$). ^{13}C NMR (101 MHz, CDCl_3); [δ , ppm]: 192.24, 167.22, 162.14, 142.41, 139.68, 134.90, 134.55, 127.49, 124.8, 123.8, 110.50, 70.11, 58.61, 42.36, 22.97, 21.62, 18.44, 7.96.

Synthesis of the Maleimido End-capped Peptides

The synthesis of the peptides was carried out at the Humboldt Universität (Berlin) in the group of Prof. Dr. Hans Börner.

Synthesis of maleimido-GRGSGR

The peptide synthesis was performed on an Applied Biosystems ABI 433a peptide synthesizer in a 0.25 mmol scale using an AM Rink-Amid resin solid support. Fmoc-amino acid derivatives were coupled following standard ABI-Fastmoc protocols (single coupling, no capping) in NMP facilitated by HBTU/DIPEA. After final Fmoc removal, the resin was transferred to a 10 mL syringe reactor, where 133.2 mg (0.5 mmol, 2.0 eq.) MPS was double coupled with bench top protocols for twice 2 h at room temperature. Afterwards the resin was washed with NMP and DCM and dried overnight under vacuum at 25 °C. Cleavage from the resin was performed with TFA/DCM/TES 30:69:1 v/v for 1 h, followed with TFA/ H_2O /TES 95:4:1 v/v for 2 h to remove the Pbf protection group and obtain the fully deprotected peptide. Peptide **4** was isolated by diethylether precipitation, centrifugation, and three-fold lyophilization from water. Molecular characterization was performed by ESI-MS (see Figure 6.4a). $M_{\text{exp.}}(\mathbf{4}+\text{H}^+) = 739.5$ and $M_{\text{theo.}}(\mathbf{4}+\text{H}^+) = 739.4$.

Synthesis of maleimido-GRGDS

The synthesis for the maleimido-GRGDS peptide (including the employed materials) is described in Chapter 7.3.

Phototriggered Experiments in Solution

Irradiation procedure

The samples to be irradiated were placed on a metallic disk revolving around a compact low-pressure fluorescent lamp (Arimed B6, Cosmedico GmbH, Stuttgart, Germany) emitting at 320 nm (± 30 nm, 36 W, the emission spectrum of the employed compact low-pressure fluorescent lamp is included in Figure 6.1) at a distance of 40–50 mm in a custom-built photoreactor (see Figure 11.1).

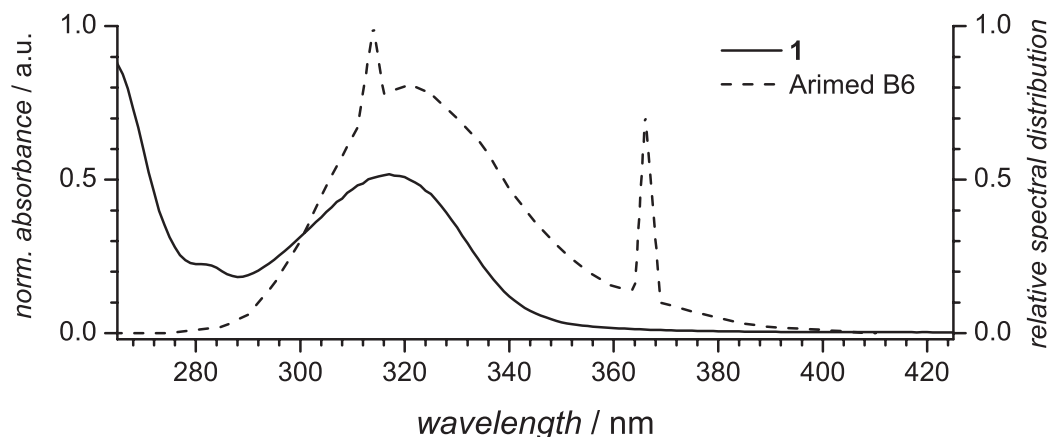


Figure 6.1 UV-Vis spectrum of photoenol precursor **1** ($5 \cdot 10^{-3} \text{ mol} \cdot \text{L}^{-1}$) in dichloromethane and the spectral distribution of the employed compact low-pressure fluorescent lamp (36 W, Arimed B6, $\lambda_{\text{max}} = 320 \text{ nm}$).

Phototriggered reaction with maleimide

3.3 mg (1.35 μmol , 1.0 eq.) of **2** and 1.31 mg (13.5 μmol , 10.0 eq.) maleimide were dissolved in 5 mL acetonitrile and aliquoted in four different headspace vials (900 μL in each one, Pyrex, diameter 20 mm), which were crimped air-tight using SBR seals with PTFE inner liner. The solution was deoxygenated by purging with nitrogen for 10 min. The flasks were subsequently irradiated for a) 5 min, b) 10 min, c) 15 min, and d) 20 min by revolving around a compact low-pressure fluorescent lamp (Arimed B6, Cosmedico GmbH, Stuttgart, Germany) emitting at 320 nm ($\pm 30 \text{ nm}$, 36 W, the emission spectrum of the employed compact low-pressure fluorescent lamp is included in Figure 6.1) at a distance of 40-50 mm in a custom-built photoreactor (see Figure 11.1). The solvents were evaporated under vacuum after the reaction, THF (0.5 mL) was added in each vial and the four solutions were analyzed immediately via SEC/ESI-MS (see Figure 6.2).

Phototriggered reaction of *N*-(5-fluoresceinyl)maleimide

1.0 mg (0.41 μmol , 1.0 eq.) of **2** and 0.5 mg (1.2 μmol , 3.0 eq.) *N*-(5-fluoresceinyl)maleimide were dissolved in 2 mL DMF and aliquoted in a headspace vial (Pyrex, diameter 20 mm), which was crimped air-tight using SBR seals with PTFE inner liner. The solution was deoxygenated by purging with nitrogen for 10 min. The flask was subsequently irradiated for 2 h by revolving around a compact low-pressure fluorescent lamp (Arimed B6, Cosmedico GmbH, Stuttgart, Germany) emitting at 320 nm ($\pm 30 \text{ nm}$, 36 W, the emission spectrum of the employed compact low-pressure fluorescent lamp is included in Figure 6.1) at a distance of 40-50 mm in a custom-built photoreactor (see Figure 11.1). The solvent was evaporated under vacuum after the reaction, 0.5 mL of THF was added and the solution was analyzed

immediately via SEC/ESI-MS (see Figure 6.3).

Phototriggered reaction of maleimido-GRGSGR 4

0.24 mg (0.82 μmol , 1.2 eq.) of **1** and 0.5 mg (0.68 μmol , 1.0 eq.) of **4** were dissolved in a mixture of 250 μL phosphate buffered saline (PBS) and 750 μL of acetonitrile and placed into a headspace vial, which was crimped air-tight using SBR seals with PTFE inner liner. The solution was deoxygenated by purging with nitrogen for 10 min. The flask were subsequently irradiated for 120 min by revolving around a compact low-pressure fluorescent lamp (Arimed B6, Cosmedico GmbH, Stuttgart, Germany) emitting at 320 nm (± 30 nm, 36 W, the emission spectrum of the employed compact low-pressure fluorescent lamp is included in Figure 6.1) at a distance of 40-50 mm in a custom-built photoreactor (see Figure 11.1). The reaction solution was directly analyzed via ESI-MS (see Figure 6.4a). Identical results were obtained for maleimide-GRGDS **4** (see Figure 6.4b).

Surface Modifications

Cleaning and preactivation of the silicon wafers

All Si wafers and glass substrates were cleaned three successive times by ultrasonification for 15 min in chloroform, acetone, and ethanol. Preactivation of the surfaces was achieved by separately placing them in small glass vials containing acidic piranha solution (sulfuric acid 95 % / aqueous hydrogen peroxide 35 % 3:1 v/v) for 60 min at 100 °C. **Caution: piranha solution is an extremely strong oxidant and should be handled very carefully!**

Silanization of Si wafers with FMP-containing silane 6

Preactivated substrates were placed separately in small glass vials containing a solution of 10 mg (22.1 μmol) of FMP-containing silane **6** in 2 mL anhydrous toluene. They were subsequently heated to 50 °C for 2 h without stirring. The solution was brought to ambient temperature and the wafers were left immersed for another 12 h. The wafers were subsequently ultrasonicated in 10 mL dry toluene (10 min), 10 mL acetone (5 min), and finally 10 mL ethanol (5 min) to remove any physisorbed silane.

Spatially controlled surface functionalization with bromine-containing maleimide 7

10 mg (34.6 μmol) of **7** was dissolved in 4 mL DCM in a headspace vial (Pyrex, diameter 20 mm). A mask (see Figure 11.2 in the Materials Chapter) was placed onto a FMP-functionalized Si wafer. The latter was placed into the headspace vial,

which was crimped air-tight using SBR seals with PTFE inner liner. The solution was deoxygenated by purging with nitrogen for 10 min. The flasks were subsequently irradiated for 2 h in the photoreactor. After irradiation, the mask was removed. The wafer was subsequently rinsed with acetone and sonicated 5 min in acetone to remove any possibly physisorbed material. The wafer was finally dried under a nitrogen stream.

Spatially controlled sequential surface functionalization

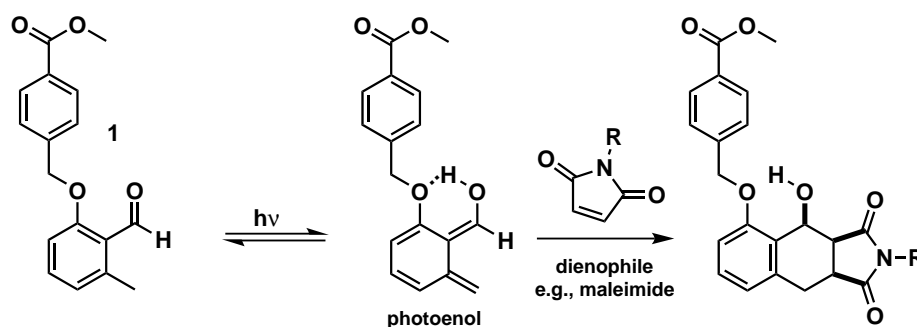
a) 20 mg of **8** was dissolved in 4 mL DCM in a headspace vial (Pyrex, diameter 20 mm). A mask was placed onto a FMP-functionalized Si wafer. The latter was placed into the headspace vial, which was crimped air-tight using SBR seals with PTFE inner liner. The solution was deoxygenated by purging with nitrogen for 10 min. The flasks were subsequently irradiated for 2 h in the photoreactor. After irradiation, the mask was removed. The wafer was subsequently rinsed with acetone and sonicated 5 min in acetone to remove any possibly physisorbed material. The wafer was finally dried under a nitrogen stream. b) 10 mg (34.6 μmol) of **7** was dissolved in 4 mL DCM in a headspace vial (Pyrex, diameter 20 mm). The Si wafer from a) patterned with **8** was placed in the headspace vial, which was crimped air-tight using SBR seals with PTFE inner liner. The solution was deoxygenated by purging with nitrogen for 10 min. The flasks were subsequently irradiated for 2 h in the photoreactor (see Figure 11.1). After irradiation, the mask was removed. The wafer was then rinsed with acetone and sonicated 5 min in acetone to remove any possibly physisorbed material. The wafer was finally dried under a nitrogen stream.

Spatially controlled surface (bio-)functionalization with **4**

4 mg (5.4 μmol) of maleimido-GRGSGR **4** was dissolved in 2 mL acetonitrile/PBS 3:1 v/v in a headspace vial (Pyrex, diameter 20 mm). A mask was placed onto a FMP-functionalized Si wafer. The latter was placed into the headspace vial, which was crimped air-tight using SBR seals with PTFE inner liner. The solution was deoxygenated by purging with nitrogen for 10 min. The flasks were subsequently irradiated for 2 h in the photoreactor. After irradiation, the mask was removed. The wafer was then rinsed with acetone and sonicated 5 min in acetone. The wafer was subsequently placed in distilled water for 2 h and finally dried under a nitrogen stream.

6.4 Results and Discussion

After performing a screening study of potential photoenol candidates, the 2-formyl-3-methylphenoxy (FMP) moiety has been identified to be an even more efficient precursor compared to the previously reported 2-methylbenzophenone derivative.^[144] Promotion of the Diels-Alder endo addition occurs based on hydrogen bond formation in the photoenol intermediate by increasing both its lifetime and the amount of formed (Z)-isomer (Scheme 6.2), which is, in contrast to the (E)-isomer,^[143,290-292] highly reactive towards dienophiles (for example, a maleimide derivative). Initial model reactions (see Figure 6.2) were performed in solution, as mass spectrometry of samples in solution is an efficient method for identifying potential side-product formation with much higher sensitivity than for example ¹H NMR spectroscopy.^[40,229] A 36 W compact fluorescent lamp at the absorbance maximum of FMP ($\lambda_{\text{max}} = 320$ nm, see Figure 6.1) was employed as UV source. The outcome of such an investigation is shown in Figure 6.2, which depicts the mass spectra of starting FMP-capped poly(ethylene glycol) methyl ether before irradiation **2** alongside the photostable Diels-Alder cycloadduct **3**. Full conversion with maleimides is – in acetonitrile or dichloromethane – typically achieved in less than 15 minutes at ambient temperature. Importantly, the photoinduced reactions were also compatible with polar solvents needed for the phototriggered reaction of otherwise insoluble compounds, e.g., *N*-(5-fluoresceinyl)maleimide. Figure 6.3 shows the phototriggered reaction of **2** with *N*-(5-fluoresceinyl)maleimide in DMF. It should, however, be noted that longer irradiation times are typically required with these polar solvents for quantitative product formation, especially when the reaction is performed in water. As water-borne catalyst-free conjugation reactions are highly interesting for biological applications, attention was placed on the attachment of biomolecules such as peptides. Figure 6.4 depicts the mass spectra of a maleimido-GRGSGR peptide **4** before and after **5**, and maleimide-GRGDS be-



Scheme 6.2 Photoinduced isomerization of a 2-formyl-3-methylphenoxy (FMP) derivative **1** and subsequent Diels-Alder [4 + 2] cycloaddition with a dienophile.

fore and *clicked*-GRGDS after photoconjugation with a low-molecular-weight FMP derivative **1**. In detail, **4** was irradiated in the presence of **1** (1:1.2 mol/mol) in acetonitrile/phosphate-buffered saline (PBS, 3:1 v/v) and, again, a quantitative formation of the expected Diels-Alder adduct was observed. The model reactions in solution provided a proof-of-principle that phototriggered (bio)conjugation can be achieved without catalyst yet with high efficiency. The light-based nature of

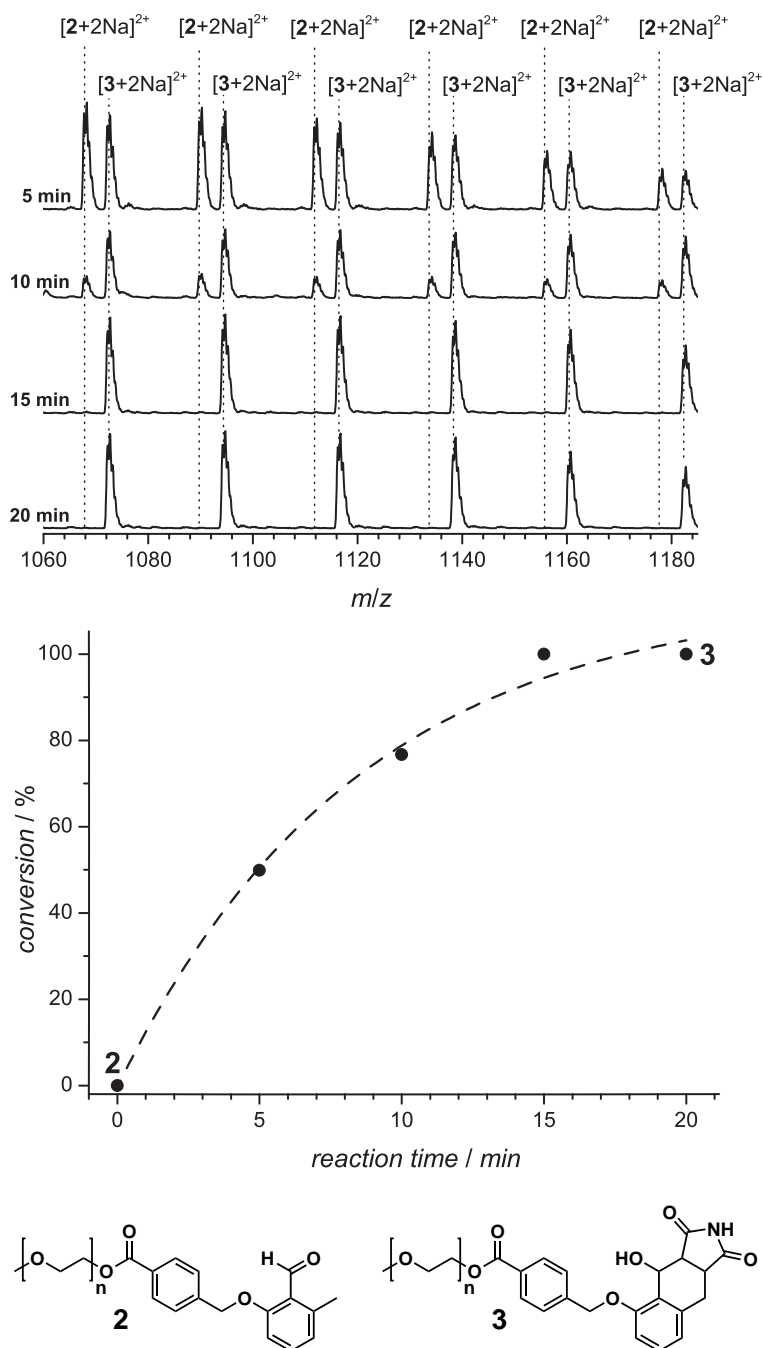
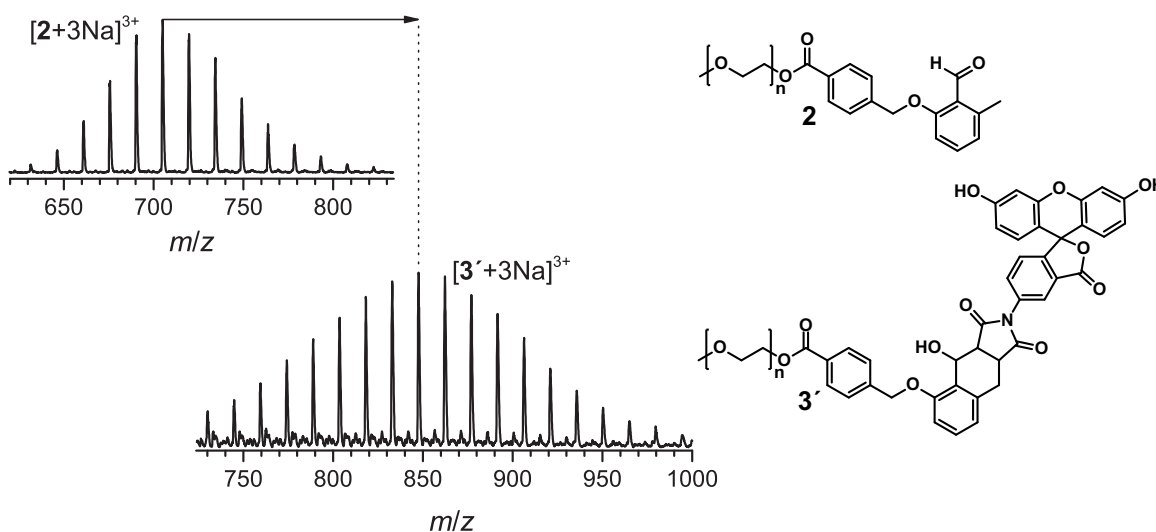


Figure 6.2 SEC/ESI-MS investigation of the photo-triggered reaction ($\lambda_{\max} = 320$ nm) of model system **2** with maleimide (1:10 mol/mol) in acetonitrile. Full conversion was observed within 15 min reaction time. Note: The reaction kinetics in dichloromethane (not shown) are similar to those observed in acetonitrile.

Table 6.1 Experimental and theoretical m/z values for the first peak in the isotopic distribution of Figure 6.2 in the m/z range between 1060 and 1080.

$m/z_{\text{expt.}}$	ion assignment	formula	$m/z_{\text{theor.}}$	$\Delta m/z$
1067.8	$2_{(n=41)} + 2\text{Na}^{2+}$	$[\text{C}_{99}\text{H}_{180}\text{Na}_2\text{O}_{45}]^+$	1067.6	0.2
1072.2	$3_{(n=39)} + 2\text{Na}^{2+}$	$[\text{C}_{99}\text{H}_{175}\text{Na}_2\text{NO}_{45}]^+$	1072.1	0.1

the conjugation technique is supposed to be an efficient means to provide spatially constrained grafting of molecules onto surfaces to obtain molecular patterns. Very recently, Popik *et al.* presented surface grafting by photoinduced hetero-Diels-Alder reaction onto vinyl ether coated slides involving a type of chemistry similar to the current system.^[152] However, the photoreactive moiety used was present as a soluble species, which is detrimental with respect to the spatial resolution. The method also requires multistep incorporation of the photoactive 3-hydroxymethyl-2-naphthol moiety for each different coupling. In contrast, the key idea presented in the current study is the immobilization of the photoactive FMP moiety directly onto the surface to perform spatially resolved *in situ* grafting of maleimide derivatives, for

**Figure 6.3** SEC/ESI-MS spectra of the phototriggered reaction of **2** with *N*-(5-fluoresceinyl)maleimide (1:3 mol/mol) in DMF. ESI-MS analysis confirmed full conversion within 2 h irradiation time ($\lambda_{\text{max}} = 320$ nm).**Table 6.2** Experimental and theoretical m/z values for the peak maximum in the isotopic distribution of Figure 6.3.

$m/z_{\text{expt.}}$	ion assignment	formula	$m/z_{\text{theor.}}$	$\Delta m/z$
704.8	$2_{(n=40)} + 3\text{Na}^{3+}$	$[\text{C}_{97}\text{H}_{176}\text{Na}_3\text{O}_{44}]^+$	704.7	0.1
847.3	$3'_{(n=40)} + 3\text{Na}^{3+}$	$[\text{C}_{121}\text{H}_{189}\text{Na}_3\text{NO}_{51}]^+$	847.1	0.2

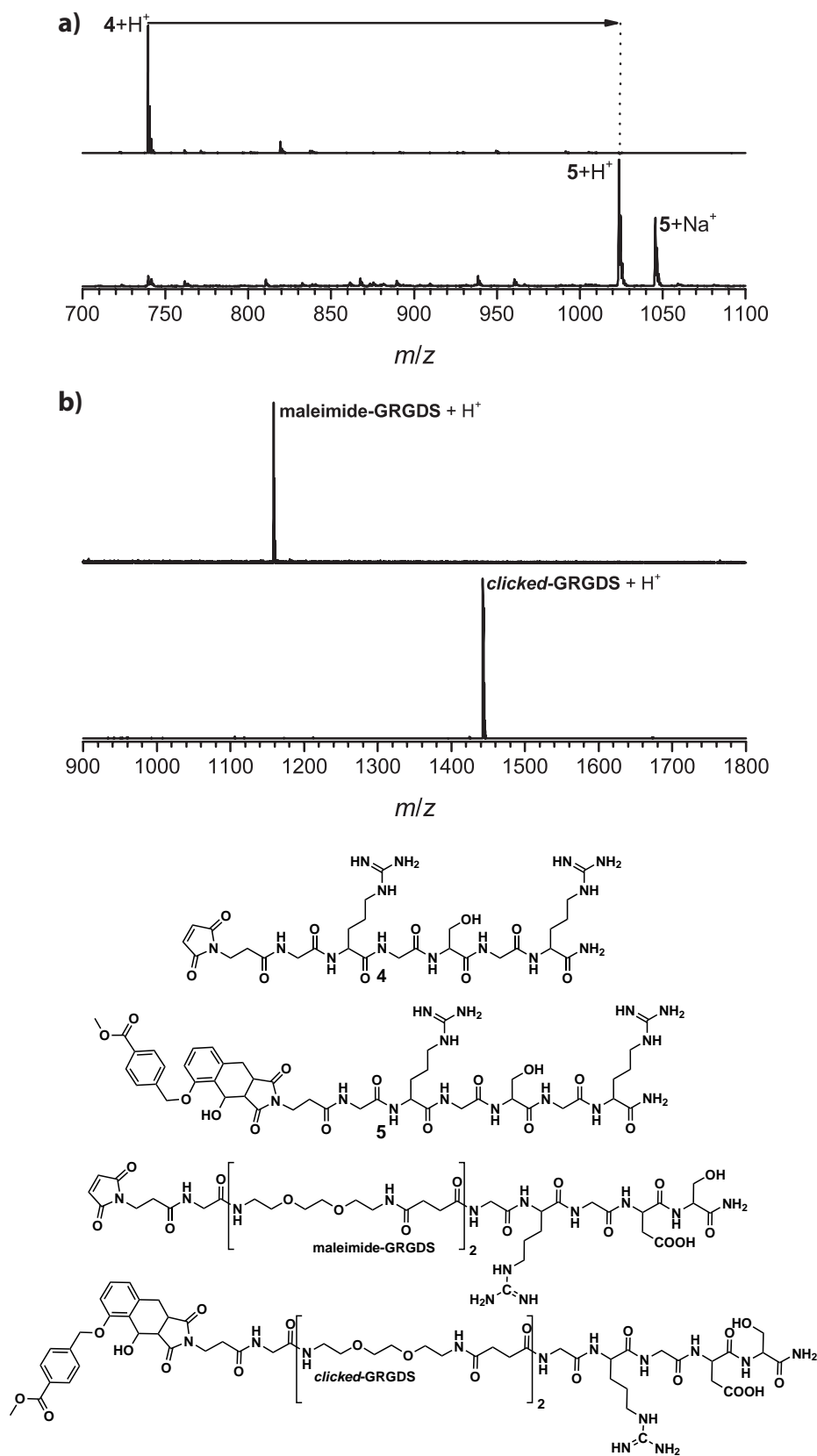
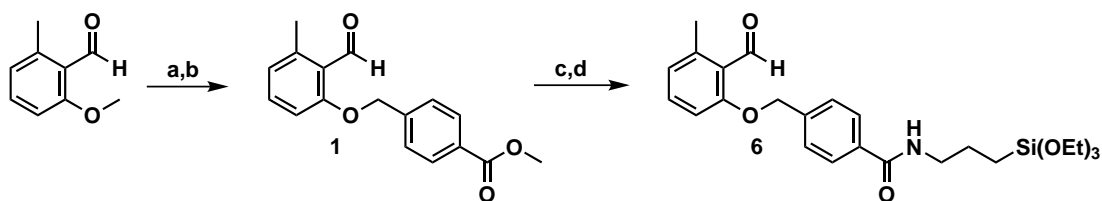


Figure 6.4 ESI-MS spectra of maleimido-GRGDS peptide before **4** and after **5** photoconjugation with FMP derivative **1** (a), and maleimido-GRGDS before and *clicked*-GRGDS after photoconjugation with FMP derivative **1** (b).

Table 6.3 Experimental and theoretical m/z values for the isotopic distribution of Figure 6.4a in the m/z range between 700 and 1100 and for the isotopic distribution of Figure 6.4b in the m/z range between 900 and 1800.

$m/z_{\text{expt.}}$	ion assignment	formula	$m/z_{\text{theor.}}$	$\Delta m/z$
739.5	4 + H ⁺	[C ₂₉ H ₄₆ N ₁₄ O ₁₀] ⁺	739.4	0.1
761.4	4 + Na ⁺	[C ₂₈ H ₄₆ N ₁₄ NaO ₁₀] ⁺	761.3	0.1
1023.6	5 + H ⁺	[C ₄₅ H ₆₃ N ₁₄ O ₁₄] ⁺	1023.5	0.1
1045.6	5 + Na ⁺	[C ₄₅ H ₆₂ N ₁₄ NaO ₁₄] ⁺	1045.6	0.1
1158.6	maleimide-GRGDS + H ⁺	[C ₄₆ H ₇₆ N ₁₅ O ₂₀] ⁺	1158.5	0.1
1442.7	clicked-GRGDS + H ⁺	[C ₆₃ H ₉₂ N ₁₅ O ₂₄] ⁺	1442.6	0.1

example sensitive biomolecules. With the existence of a broad spectrum of readily available maleimido-functionalized (bio)molecules one also avoids the complicated incorporation of the photoactive species mentioned above. The synthetic route to functionalize silicon surfaces is rather straightforward. The FMP-functionalized silane **6** was prepared (Scheme 6.3), dissolved in anhydrous toluene, and reacted with activated silicon wafers. Figure 6.5 depicts the C 1s and Br 3d X-ray photoelectron spectroscopy (XPS) spectra of a Si-wafer after FMP silanization with **6**. The C 1s spectrum convincingly demonstrates successful silanization (see Figure 6.5a, left). The main peak in the C 1s spectrum at 285.0 eV is assigned to hydrocarbon atoms (C-C, C-H), the components at 286.5 eV and 287.9 eV are assigned to the C-O / C-N and C=O groups, respectively.^[276,293] The weak peak at 291.1 eV is well-known for the $\pi - \pi^*$ transition in aromatic compounds. The corresponding Br 3d spectrum indicates the absence of bromine. Upon confirmation of effective surface silanization, the light-directed Diels-Alder cycloaddition was performed on the surface using different maleimide derivatives. After the phototriggered reaction with **7**, one can clearly detect the bromine at Br 3d_{5/2} = 70.2 eV binding energy (Figure 6.5b, right), which is assigned to a bromine / quaternary carbon bond.^[294,295] This finding and the appearance of the additional component at 289.0 eV, attributed to the O-C=O group, clearly indicate the coupling of the maleimide



Scheme 6.3 Synthesis of the FMP-functionalized silane **6**. Reagents and conditions: AlCl₃, CH₂Cl₂ (a); 4-bromomethylbenzoate, K₂CO₃, acetone (b); NaOH, CH₂Cl₂/methanol (9:1 v/v) (c); ethyl chloroformate, 3-triethoxysilylpropan-1-amine, THF (d).

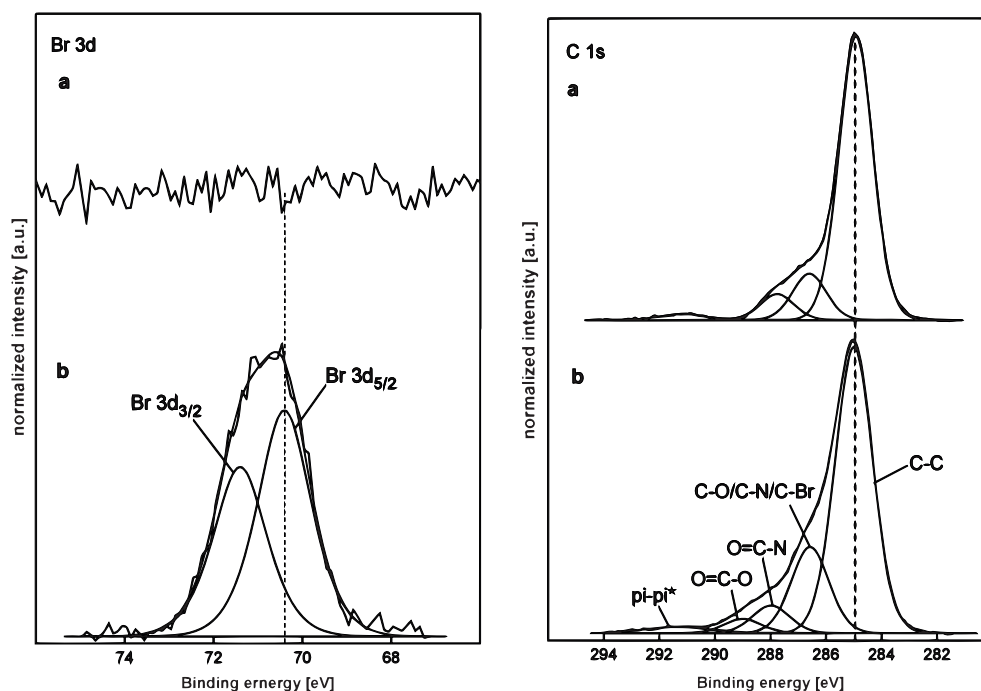


Figure 6.5 Comparison of Br 3d (left) and C 1s (right) XPS spectra of FMP silanized Si-substrates (a) and after the subsequent phototriggered Diels-Alder surface grafting of bromine containing maleimid derivative **7** (b). Peak heights have been normalized to maximum intensity.

derivative **7**. Imaging Time-of-Flight Secondary Ion Mass Spectrometry (ToF-SIMS) is a commonly utilized and sensitive technique that allows for the highly spatially resolved analysis of molecular patterns on solid substrates.^[296] In particular, bromine compounds with their inherent isotopic pattern can be unambiguously detected by ToF-SIMS; therefore, the bromine-containing dienophile **7** was utilized in the current study as a molecular marker to spatially map the locally constrained surface grafting. The photopatterning was achieved by irradiation of the functionalized silicon wafers immersed in a solution of **7** by utilizing two shadow masks: first a macroscopic structure with a square cut into a metal plate and then one with a micropattern (Figure 6.6). After the phototriggered reaction, it is not necessary to deactivate or cap the remaining FMP groups on the surface, as the formation of reactive diene species formed during irradiation is fully reversible. The FMP surface is also photochemically inert (in the absence of a dienophile during irradiation, no chemical changes of the FMP layer were detectable by ToF-SIMS) and only reacts in the presence of a suitable dienophile, thus simplifying preparation, handling, and storage. Subsequent ToF-SIMS composition analysis of the bromine content on the surface readily reproduced the shadow mask structures (Figure 6.6b) of irradiated and non-irradiated areas with good spatial resolution. This type of pattern could potentially be used to grow polymers by surface-initiated metal-catalyzed radical polymerization in a “grafting-from” approach.^[297] In fact, the enormous applicabil-

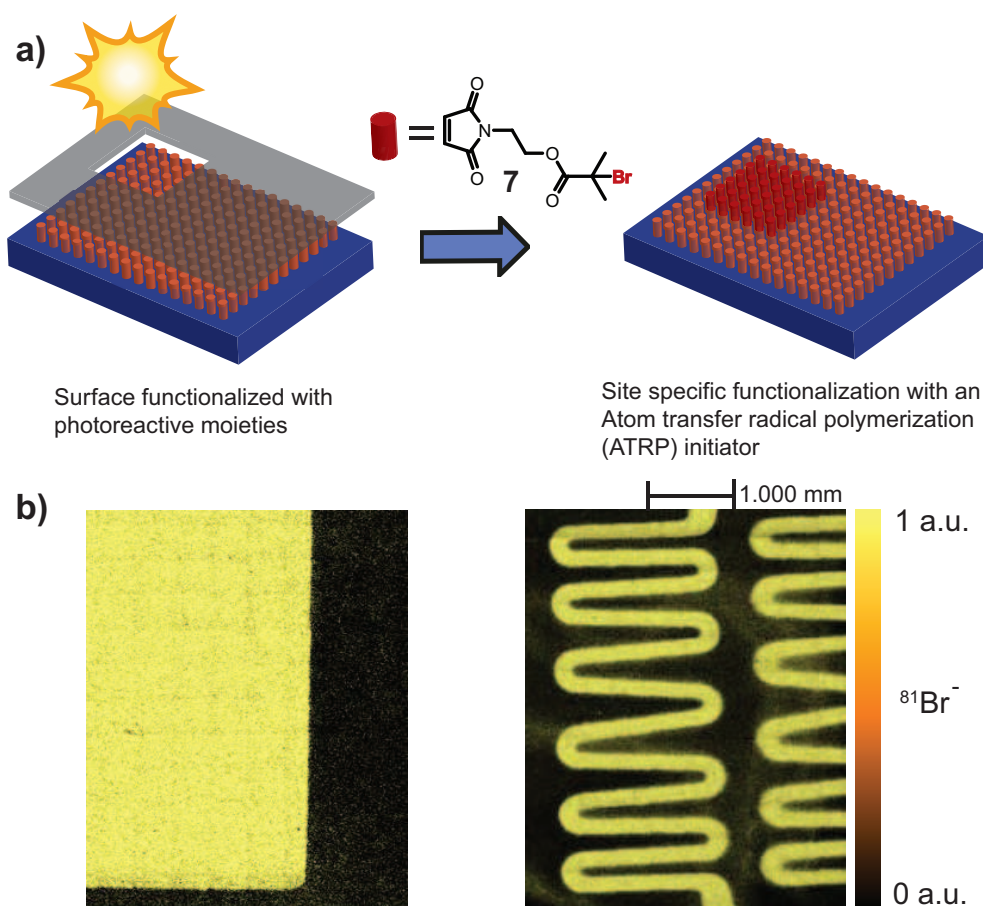


Figure 6.6 Representation of the phototriggered Diels-Alder surface grafting of bromine-containing maleimide derivative **7** (a). ATRP=atom transfer radical polymerization. ToF-SIMS images of silicon wafers patterned with **7** utilizing two shadow masks (see Figure 11.2 in the Materials Chapter) (b).

ity of polymer surface patterns at different length scales is well-known in research fields including tissue engineering, cell biology, and medicinal science.^[298] Apart from the aforementioned “grafting-from” approach, the phototriggered strategy can also be utilized to directly functionalize a surface with polymers. The “grafting-to” approach was performed by irradiation of a freshly prepared FMP surface with maleimido-capped poly(ethylene glycol) methyl ether (PEG-Mal) **8** in a “grafting-to” approach (Figure 6.7a) and characteristic mass fragments of PEG were only found in the irradiated square (Figure 6.7b, left), thus confirming the site-specific immobilization. PEG is commonly used to locally reduce non-specific binding and to spatially control adhesive and non-adhesive areas on surfaces.^[299] Importantly, the initial photoreactivity of non-irradiated FMP-functionalized areas is retained and can be utilized for further Diels-Alder functionalization with a second dienophile. In this context, a preformed PEG-patterned surface received a subsequent flood exposure in presence of **7**. Successful sequential photopatterning was again verified by a bromine and PEG composition analysis (Figure 6.7b). To additionally

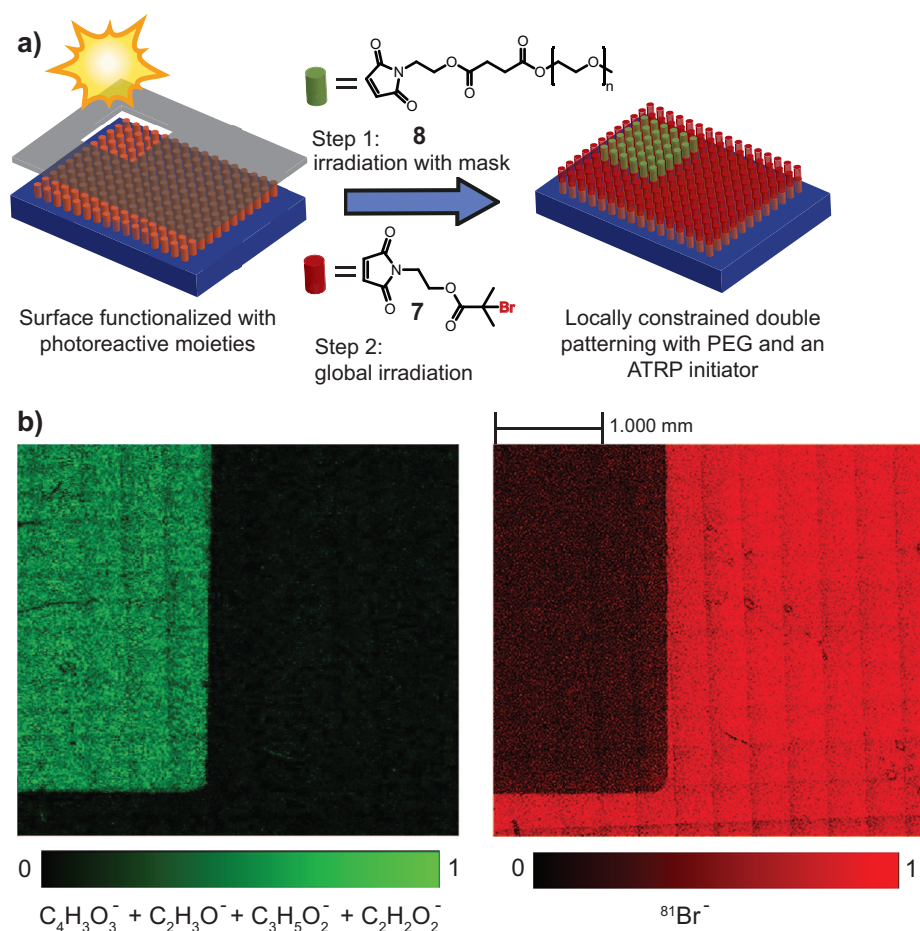


Figure 6.7 Representation of the phototriggered double patterning of ω -maleimido poly(ethylene glycol) **8** and ATRP initiator **7** (a). ToF-SIMS images demonstrating successful photopatterning of **8** (left). The initial photoreactivity is retained on non-irradiated parts and can be reutilized for further Diels-Alder functionalization by global irradiation with **7** (right) (b).

demonstrate the feasibility of covalent and site-specific attachment of peptides by this phototriggered approach (which also avoids protection chemistry), a freshly prepared FMP-functionalized surface was irradiated with maleimido-GRGSGR **4** in acetonitrile/PBS (3:1 v/v). ToF-SIMS again provided evidence that the peptide was immobilized in a patterned way that corresponded to the mask features. In that case, composition analysis was based on the presence of $C_4H_8N^+$, a secondary-ion characteristic for peptides (Figure 6.8).^[300] The successful biopatterning was also confirmed by characteristic mass fragments for the arginine groups of **4** for example ($C_4H_{11}N_3^+ + C_5H_8N_3^+ + C_5H_{11}N_4^+$).

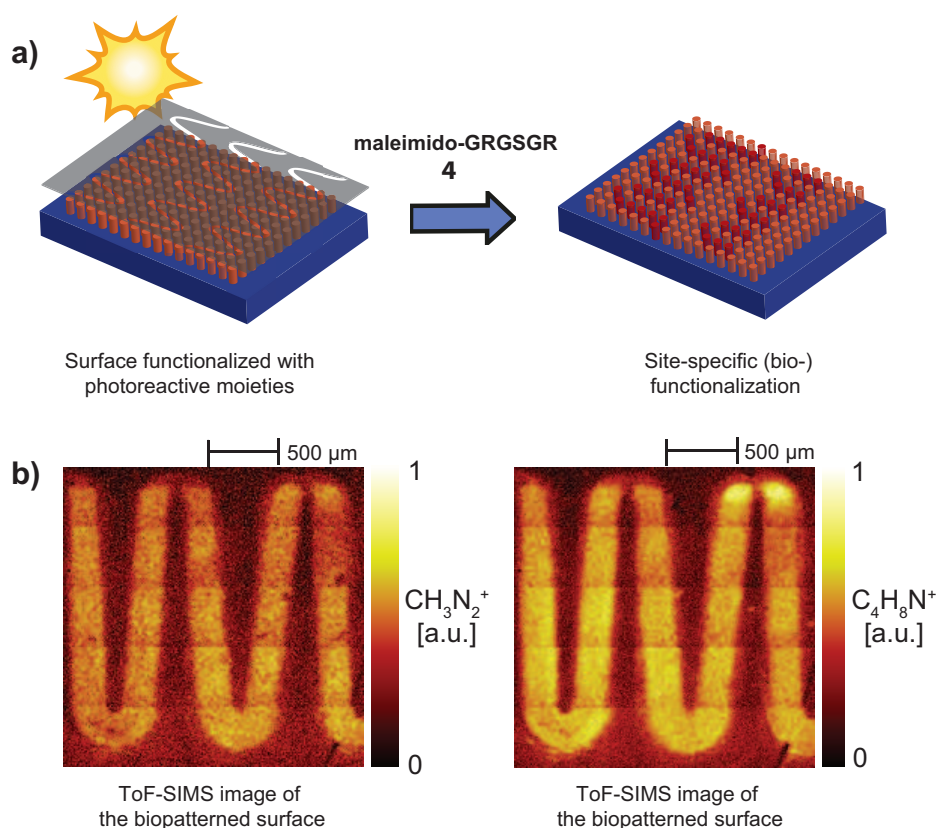


Figure 6.8 Representation of the locally constrained biofunctionalization on a surface (a). ToF-SIMS images for the bioconjugation with maleimido-GRGSGR **4** (b).

6.5 Conclusions

The photoenol-mediated conjugation strategy possesses many interesting features, making it a first-class *click* reaction. It can proceed rapidly at ambient temperature in a wide range of (polar) solvents. No catalyst is required and no byproduct is formed, and thus no purification steps are required. Most importantly, control over time and space is inherent owing to its light-induced nature. Herein, the high efficiency and speed of the phototriggered Diels-Alder (bio)conjugation was demonstrated in solution as well as on a surface by means of the covalent attachment of three dienophiles: a small molecule ATRP initiator, a polymer, and a peptide. It can be envisaged that this procedure can be utilized for many applications ranging from the photolithographic grafting of conductive polymers for LED development to the generation of a variety of complex architectures, including polymer-protein conjugates.

7

Spatially Controlled Surface Immobilization of Non-Modified Peptides*

7.1 Abstract

A novel platform utilizing light as a facile means to provide spatio-temporal control for the direct covalent immobilization of peptides possessing exclusively natural aminoacid residues is presented. The strategy is based on the utilization of a phencyclone derivative acting as a potent diene for the highly efficient Diels-Alder formation of the photoactive precursor. The cycloadduct in turn can be activated at ambient temperature via a facile one-pot *in situ* decarbonylation/dehydrogenation reaction triggered by mild irradiation for 2 hours. The obtained triphenylene-imide is capable of undergoing ring-opening reactions with amines. In contrast to previously reported phototriggered strategies, which require complex multi-step synthesis of surface anchors functionalized with photochemically active moieties and individual modifications of (biologically) relevant substrates, the synthetic effort in the current approach is reduced to a minimum by employing a *click* reaction for the formation of the photoactive species and the inherent amine functionality

* Parts of this Chapter were reproduced from Ref. 301 by permission of John Wiley and Sons.

of biomolecules for spatially controlled ligation. Successful patterning on surfaces with an amine-functionalized bromine marker and a genuine c(RGDfK) peptide was evidenced by imaging time-of-flight secondary-ion mass spectrometry (ToF-SIMS).

7.2 Introduction

Controlled surface modification via the precise positioning of chemical functionalities or relevant biomolecules holds significant promise for advances in ever-growing research areas such as biointerface science, point-of-care applications, biosensors, and nanotechnology.^[302–304] Among the myriad of modification techniques which have been developed, photochemical approaches play a key role. They contribute not only significant way to the existing repertoire of carbon-carbon bond-forming reactions,^[305] yet also inherently confer spatio-temporal control to chemical reactions and are as such highly appealing for the generation of carbohydrate-,^[306] DNA fragment,^[307] or multiple cell line patterns.^[257] The use of light has a tremendous influence on the way biomaterials scientists can perform experiments, e.g., to control the photodegradation of hydrogels^[261,308] or the activity of cells.^[309,310] The modern day chemist has a number of protocols available for spatially controlled surface grafting, which mostly rely on the release of appropriate functional groups upon a light stimulus, such as azide-reactive cyclooctynes or aminooxy-reactive aldehydes.^[40,311] A novel approach that photogenerates highly reactive intermediates with short lifetimes, such as *o*-naphthoquinone methides, has also been reported.^[151] Regeneration of the initial photoactive moiety occurs via hydration, often resulting in improved selectivity and orthogonality as well as a better handling in a non-light protected environment. Popik, Locklin, and coworkers have followed such a path when they used 3-(hydroxymethyl)-naphthalene-2-ol derivatives with vinyl ether moieties for covalent surface derivatization.^[152,153] In our team, the ease and efficiency of the photoisomerization of *o*-methylbenzaldehyde to *o*-quinodimethanes was demonstrated in light-induced modular ligation of conventional RAFT polymers and in spatially controlled surface grafting (see Chapter 6).^[3,145] Altogether, these different photoreactions form a versatile toolbox for photopatterning in different contexts, yet with high efficiency. A limiting factor of their applicability in novel technologies is, however, that all of the aforementioned transformations involve complex multi-step synthesis of surface anchors functionalized with photochemical active moieties and, often even more challenging, individual modifications of the (biological) relevant substrates with appropriate coupling functionalities. These compounds have to be precisely tailored to the concrete needs, thus limiting their versatility.

The present chapter introduces a technology for providing spatio-temporal control for the direct covalent immobilization of peptides possessing exclusively natural amino acid residues by means of their inherent amine functionality. In contrast to the photoisomerization of *o*-methylbenzaldehyde (see Chapter 6), the current strategy represents a photochemical approach that can be performed with ease in water, in solid state, and without employing inert gas.

7.3 Experimental Part

Synthesis of a Universal Photoactive Precursor

Synthesis of 1,3-bis(4-methoxyphenyl)propan-2-one

1,3-Bis(4-methoxyphenyl)propan-2-one was synthesized according to a modified literature procedure:^[312] 2.14 g (11.2 mmol, 1.2 eq.) 1-ethyl-3-(3-dimethylaminopropyl)carbodiimide (EDC) hydrochloride was added to 1.59 g (9.6 mmol, 1.0 eq.) 4-methoxyphenyl acetic acid and 1.50 g (12.3 mmol, 1.3 eq.) 4-(dimethylamino)pyridine (DMAP) in 30 mL pre-dried dichloromethane. The resulting solution was stirred at ambient temperature for 2 days. The reaction mixture was diluted with 30 mL water and the organic layer was subsequently washed with 2 × 30 mL diluted aqueous HCl and 2 × 30 mL with saturated aqueous NaHCO₃. The organic layer was dried over magnesium sulfate. The solvent was removed under reduced pressure to yield a yellow solid. The product was recrystallized in 50 mL EtOH/hexane 1:2 v/v to yield 440 mg (1.6 mmol, 17 %) of the product as colorless needles. ¹H NMR (400 MHz, CDCl₃); [δ , ppm]: 7.05 (d, J = 8.6 Hz, 4H, 2 × 2 × -ArH), 6.84 (d, J = 8.6 Hz, 4H, 2 × 2 × -ArH), 3.78 (s, 6H, 2 × -OCH₃), 3.63 (s, 4H, 2 × -ArCH₂). ¹³C NMR (101 MHz, CDCl₃); [δ , ppm]: 206.72, 158.86, 130.71, 126.31, 114.35, 55.47, 48.26.

1,3-bis(4-methoxyphenyl)-2*H*-cyclopenta[*l*]phenanthren-2-one (MCPO) 1

The synthesis was performed according to a literature procedure from 9,10-phenanthrenequinone and 1,3-bis(4-methoxyphenyl)propan-2-one as starting materials.^[313] Spectral data were in accordance with those previously reported in the literature.^[314] ESI-MS: [1+H]⁺: $m/z_{\text{expt.}}$ = 443.3; $m/z_{\text{theo.}}$ = 443.2.

Synthesis of maleimide functional GRGDS peptide 2

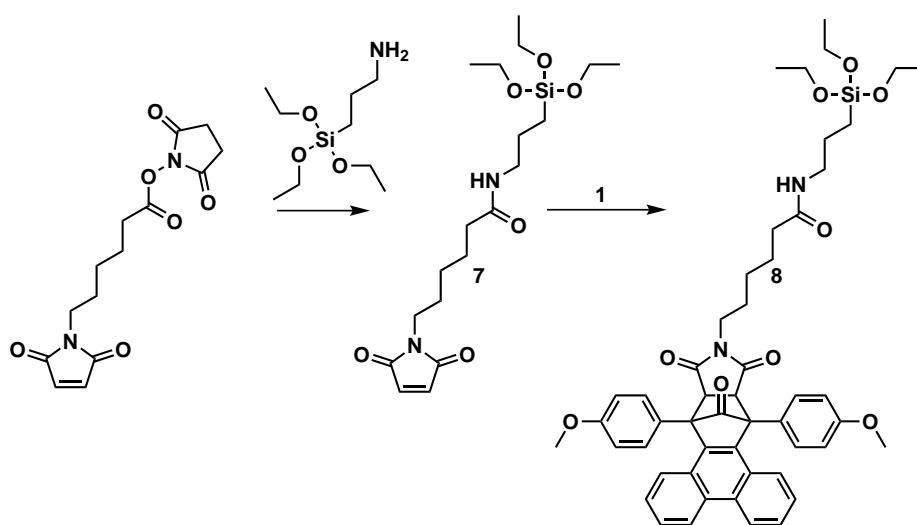
The synthesis of the peptide was carried out at the Humboldt Universität (Berlin) in the group of Prof. Dr. Hans Börner by Katharina Linkert. The peptide synthesis was performed on an Applied Biosystems 433a peptide synthesizer in a 0.1 mmol scale. A TentaGel[®] rink-amide linker resin (SRAM) with 0.23 mmol·g⁻¹ capacity was used as solid support. Fmoc-amino acid derivatives were coupled following standard ABI-Fastmoc protocols (no capping, single coupling of amino acids Axx1-5, double coupling of Axx6 and Fmoc-4-(2-(2-(2-aminoethoxy)ethoxy)ethylamino)-4-oxobutanoic acid). Coupling was performed in *N*-methyl-2-pyrrolidone (NMP) and facilitated by 2-(1*H*-benzotriazol-1-yl)-1,1,3,3-tetramethyluronium hexafluorophosphate (HBTU) / *N,N'*-diisopropylethylamine (DIPEA). After final Fmoc removal the resin was transferred to a 40 mL glass reactor, where 3-maleimidopropionic acid (MPA) was coupled twice at ambient temperature (first coupling: MPA (0.5 mmol, 5.0 eq.), (benzotriazol-1-yloxy)tripyrrolidinophosphonium hexafluorophosphate (PyBOP, 0.5 mmol, 5.0 eq.), DIPEA (1 mmol, 10.0 eq.), 1 h and second coupling: MPA (0.2 mmol, 2.0 eq.), PyBOP (0.2 mmol, 2eq.) and DIPEA (0.4 mmol, 4.0 eq.) for 2 h; in-between both coupling steps the resin was washed with NMP). Finally, the resin was washed with NMP, NMP/dichloromethane (DCM), and was dried overnight under vacuum at 25 °C. Cleavage of the product from the resin was performed with TFA/DCM/triethylsilane (TES) 50:47.5:2.5 v/v % for 2 h, followed by TFA/H₂O/TES 96:2.5:2.5 v/v % for 2 h to remove the 2,2',4,6,7-pentamethyldihydrobenzofuran-5-sulfonyl (Pbf) protection groups. The fully deprotected peptide was isolated by ether precipitation centrifugation, twice reprecipitation from TFA in diethyl ether and lyophilization from water as a colorless product. The chemical structure and its high purity were confirmed by LC-ESI mass spectrometry and ¹H NMR. ESI-MS: [2+H]⁺: $m/z_{\text{expt.}} = 1158.6$; $m/z_{\text{theo.}} = 1158.5$.

Synthesis of c(RGDfK)

The synthesis of the peptides was carried out at the Humboldt Universität (Berlin) in the group of Prof. Dr. Hans Börner by Katharina Linkert. The peptide synthesis was performed according to previously described procedures.^[315] c(RGDfK) was synthesized in a 0.1 mmol scale. A TentaGel[®] resin with hydroxytrityl linker (TentaGel[®] S-Trt-OH) and a loading of 0.25 mmol·g⁻¹ was converted to the active chloride by 3 h heating to 60 °C with a large excess of freshly distilled acetyl chloride in dry toluene under inert gas atmosphere. The first amino acid (aspartic acid) was coupled via γ -carboxyl group by agitating the activated resin with a solution of Fmoc-Asp-OAll (2.5 eq.) and *N,N*-diisopropyl ethylamine (DIPEA) (3 eq.) in dry dichloromethane (DCM) for 1.5 h. The resin was capped by washing three times

with dry DCM/MeOH/DIPEA (80:15:5 v/v %). The following amino acid derivatives were coupled in an automated fashion on an Applied Biosystems 433a peptide synthesizer by following standard ABI-Fastmoc protocols (single coupling, capping and final Fmoc on). Coupling was performed in *N*-methyl-2-pyrrolidone (NMP) and facilitated by 2-(1*H*-benzotriazol-1-yl)-1,1,3,3-tetramethyluronium hexafluorophosphate (HBTU) / DIPEA. After assembly of the amino acids, the resin was transferred to a 40 mL glass reactor to perform the on-resin cyclisation step. For that purpose, the C-terminal allyl ester protective group was removed with Pd(PPh₃)₄ in CHCl₃/AcOH/*N*-methyl morpholine (37:2:1 v/v %) under an inert gas atmosphere by gentle agitation for 2 h. After washing the resin five times with DIPEA/dimethyl formamide (DMF) (5:95 v/v %) and five times with 5 %- diethyldithiocarbamic acid sodium salt in DMF the *N*-terminal Fmoc group was cleaved with piperidine/DMF (1:4 v/v %). The on-resin cyclisation was performed for 48 h in NMP and facilitated by (7-azabenzotriazol-1-yloxy)tripyrrolidinophosphonium hexafluorophosphate (PyAOP) (2 eq.) and DIPEA (2 eq.). Subsequently, the resin was carefully washed with NMP, DCM and dried overnight under vacuum at 25 °C. Cleavage of the product from the resin was performed with TFA/H₂O/triethylsilane (TES) (93:5:2 v/v %) to obtain the completely deprotected peptide. c(RGDfK) was isolated by diethyl ether precipitation, centrifugation and lyophilization from water. The chemical structure and high purity was confirmed by LC-ESI mass spectrometry. ESI-MS: [M+H]⁺: $m/z_{\text{expt.}} = 604.5$; $m/z_{\text{theo.}} = 604.3$.

Synthesis of a Photoactive Surface Linker



Scheme 7.1 Strategy for the synthesis of 6-(2,5-dioxo-2,5-dihydro-1*H*-pyrrol-1-yl)-*N*-(3-(triethoxysilyl)propyl)hexanamide **7**.

The synthetic strategy for the synthesis of a photoactive precursor is outlined in Scheme 7.1.

Synthesis of 6-(2,5-dioxo-2,5-dihydro-1*H*-pyrrol-1-yl)-*N*-(3-(triethoxysilyl)-propyl)-hexanamide 7

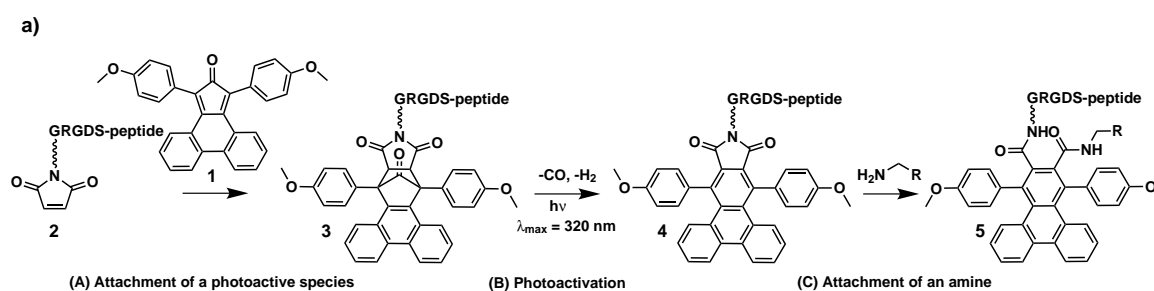
First, the synthesis of 2,5-dioxopyrrolidin-1-yl 6-(2,5-dioxo-2,5-dihydro-1*H*-pyrrol-1-yl)hexanoate was performed according to a literature procedure.^[316] Spectral data were in accordance with those previously reported in the literature.^[316,317] Alternatively, the compound is also commercially available from Sigma Aldrich. **7** was subsequently synthesized according to a slightly modified literature procedure:^[318] 165 mg (0.75 mmol, 1.0 eq.) (3-aminopropyl)triethoxysilane was added to a solution of 230 mg (0.75 mmol, 1.0 eq.) of 2,5-dioxopyrrolidin-1-yl-6-(2,5-dioxo-2,5-dihydro-1*H*-pyrrol-1-yl)hexanoate in 15 mL dry THF. The resulting solution was stirred over night under an nitrogen atmosphere. The solvent was removed under reduced pressure and the residue was purified by column chromatography (Si-gel, eluent: CH₂Cl₂/acetone 8:1). 210 mg (0.51 mmol, 68 %) of the product was obtained as a colorless viscous liquid. ¹H NMR (400 MHz, CDCl₃); [δ , ppm]: 6.68 (s, 2H, 2 \times -CH), 5.69 (bs, 1H, -NH), 3.93-3.61 (m, 6H, -SiO(CH₂)₃), 3.56-3.41 (m, 2H, -NCH₂), 3.31-3.10 (m, 2H, -CONHCH₂), 2.14 (t, *J* = 6.4, 13.8 Hz, 2H, -NHCOCH₂), 1.72-1.48 (m, 6H, -NCH₂CH₂CH₂, -SiCH₂CH₂), 1.36-1.24 (m, 2H, -NHCOCH₂CH₂), 1.26-1.13 (m, 9H, -SiOCH₂(CH₃)₃), 0.62 (t, *J* = 6.5, 9.7 Hz, 2H, -SiCH₂). ¹³C NMR (101 MHz, CDCl₃); [δ , ppm]: 172.66, 170.97, 134.20, 58.60, 41.93, 37.76, 36.72, 28.40, 26.51, 25.29, 23.04, 18.43, 7.89.

Synthesis of 6-(9,13-bis(4-methoxyphenyl)-10,12,14-trioxo-9a,10,12a,13-tetrahydro-9*H*-9,13-methanophenanthro[9,10-*f*]isoindol-11(12*H*)-yl)-*N*-(3-(triethoxysilyl)propyl)-hexanamide 8

60 mg (0.14 mmol, 1.0 eq.) of **7** and 90 mg (0.20 mmol, 1.4 eq.) of **1** were dissolved in 10 mL of dichloromethane and stirred (light-protected) at ambient temperature for 24 hours. The solvent was removed under reduced pressure and the residue was suspended in 5 mL of methanol. The mixture was filtered through a 0.45 mm PTFE standard GPC filter (to remove excess of **1**) and the essentially pure product was purified by column chromatography (Si-gel, eluent: ethyl acetate). 60 mg (0.064 mmol, 46 %) of **8** were obtained as a colorless solid. ¹H NMR (400 MHz, CDCl₃); [δ , ppm]: 8.59 (d, *J* = 8.5 Hz, 2H, -Ar*H*), 8.16 (d, *J* = 8.6 Hz, 2H, -Ar*H*), 7.52-7.41 (m, 2H, -Ar*H*), 7.25-7.11 (m, 6H, -Ar*H*), 7.05 (dd, *J* = 8.7 Hz, 2.4 Hz, 2H, -Ar*H*), 6.90 (dd, *J* = 8.7 Hz, 2.8 Hz, 2H, -Ar*H*), 5.30 (t, *J* = 5.6 Hz, 1H, -NH), 4.27 (s, 2H, 2 \times -NCOCH), 3.90 (s, 6H, 2 \times -ArOCH₃), 3.75 (q, *J* = 7.0 Hz, 6H, -SiO(CH₂)₃),

3.11 (dd, $J = 13.0, 6.9$ Hz, 2H, $-\text{CONCH}_2$), 2.86-2.72 (m, 2H, $-\text{NHCH}_2$), 1.64-1.47 (m, 4H, $-\text{CONHCH}_2\text{CH}_2$, $-\text{CONCH}_2\text{CH}_2$), 1.47-1.39 (m, 2H, $-\text{NHCOCH}_2$), 1.15 (t, $J = 7.0$ Hz, 9H, $-\text{SiOCH}_2(\text{CH}_3)_3$), 0.90-0.72 (m, 2H, $-\text{CONCH}_2\text{CH}_2\text{CH}_2$), 0.62-0.47 (m, 2H, $-\text{NHCOCH}_2\text{CH}_2$), 0.26-0.14 (m, 2H, $-\text{SiCH}_2$). ^{13}C NMR (101 MHz, CDCl_3); [δ , ppm]: 197.71, 174.53, 172.58, 159.72, 133.50, 132.04, 131.35, 130.44, 127.16, 126.80, 126.65, 125.98, 123.17, 114.86, 114.31, 62.77, 58.61, 55.50, 44.92, 41.87, 38.51, 35.92, 26.15, 25.45, 24.58, 23.16, 18.46, 7.91.

Phototriggered Experiments in Solution



Scheme 7.2 Overall concept for light-triggered modifications of the GRGDS peptide **2**: Formation of the photoactive precursor **3** by efficient Diels-Alder cycloaddition with phencyclone derivative **1** (A), the fast and mild photoactivation of **3** yielding the triphenylene imide-based compound **4** (B) and subsequent nucleophilic attachment of primary amines resulting in **5** (C).

Construction of the photoactive peptide **3**

2.50 mg (2.15 μmol , 1.0 eq.) of **2** and 1.24 mg (2.80 μmol , 1.3 eq.) of **1** were dissolved in 3 mL of MeCN/ H_2O 7:1 v/v and the reaction mixture was stirred in a light-protected environment for 2 days. The solvent was removed under reduced pressure, methanol was added, and the mixture was filtered through a 0.45 mm PTFE standard GPC filter (to remove any traces of starting material). **3** was obtained quantitatively (3.45 mg, 2.15 μmol) after removing the solvent (see Figure 7.1).

Two-step photoactivation

0.080 mg (0.051 μmol , 1.0 eq.) of **3** were dissolved in 0.5 mL of MeCN/ H_2O 1:1 v/v and irradiated for 120 minutes by revolving around a compact low-pressure fluorescent lamp (Arimed B6, Cosmedico GmbH, Stuttgart, Germany) emitting at 320 nm (± 30 nm, 36 W, the emission spectrum of the employed compact low-pressure fluorescent lamp is included in Figure 7.2) at a distance of 40-50 mm in a custom-built photoreactor (see Figure 11.1).

- experiment A: acetic acid (2 % v/v) was added and the solution was directly analyzed via ESI-MS (see Figure 7.3c).
- experiment B: the solvent was removed from a freshly deprotected solution (procedure see above) and 0.05 mg (0.46 μmol , 9.0 eq.) of 1,4-benzoquinone in 0.5 mL of acetonitrile were added. The reaction mixture was stirred for 17 hours, the solvent was removed, 0.5 mL of MeCN/H₂O 1:1 v/v and acetic acid (2 % v/v) were added and the solution was analyzed via ESI-MS (see Figure 7.3d). Only the product **4** stemming from both decarbonylation and dehydrogenation was observed.

One-step *in situ* photoactivation

0.16 mg (0.10 μmol , 1.0 eq.) of **3** and 0.033 mg (0.3 μmol , 3.0 eq.) 1,4-benzoquinone was dissolved in 0.5 mL of distilled water and aliquoted into a headspace vial (Pyrex, diameter 20 mm), which was crimped air-tight using SBR seals with PTFE inner liner. The solution was deoxygenated by purging with nitrogen for 2 minutes. The flask was subsequently irradiated for 120 minutes by revolving around a compact low-pressure fluorescent lamp (Arimed B6, Cosmedico GmbH, Stuttgart, Germany) emitting at 320 nm (\pm 30 nm, 36 W, the emission spectrum of the employed compact low-pressure fluorescent lamp is included in Figure 7.2) at a distance of 40-50 mm in a custom-built photoreactor (see Figure 11.1). After irradiation, 0.5 mL MeCN and acetic acid (2 % v/v) was added and the solution were directly analyzed via ESI-MS (see Figure 7.1). Note: An excess of 1,4-benzoquinone should be avoided since it can react slowly with the hydroxyl group of serine. This problem can be circumvented by adding MeOH into the irradiation mixture.

Attachment of 2-(4-fluorophenyl)ethanamine

0.04 mg (0.025 μmol , 1.0 eq.) of **4** was dissolved in 1 mL methanol and placed in a small glass vial. 3.54 mg (25 μmol , 1000 eq.) 2-(4-fluorophenyl)ethanamine was added and the mixture was placed on a shaker (45 °C, 300 rpm) for 16 hours. The solvent was removed, 0.5 mL of MeCN/ H₂O 1:1 v/v and one drop of acetic acid was added (reasoning for the use of a higher amount of acetic acid as usual is that excess of amine needs to be protonated first. Otherwise sodium adducts form, e.g., of the peptide (carboxyl group is deprotonated and exchanged with sodium). The mixture was directly analyzed by ESI-MS (see Figure 7.1).

Surface Modifications

Cleaning and preactivation of the Si wafers

All Si wafers and glass substrates were cleaned three successive times by ultrasonication for 10 min in acetone, chloroform, and ethanol. Preactivation of the surfaces was achieved by separately placing them in small glass vials containing acidic piranha solution (sulfuric acid 95 % / aqueous hydrogen peroxide 35 % 3:1 v/v) for 60 min at 100 °C. **Caution: piranha solution is an extremely strong oxidant and should be handled very carefully!** The Si wafers were subsequently washed and ultrasonicated in distilled water for 10 minutes and dried under a nitrogen stream.

Silanization of Si wafers with MCPO

Preactivated substrates were placed separately in small glass vials containing a solution of 1.5 mg (1.7 μmol) of MCPO-containing silane **8** in 0.5 mL anhydrous toluene. They were subsequently heated to 50 °C for 2 h on a shaker (300 rpm). The solution was brought to ambient temperature and the wafers were left immersed over-night. The wafers were subsequently ultrasonicated in 10 mL dry toluene (5 min) and 10 mL acetone (5 min) to remove any physisorbed silane. Afterwards, a Tof-SIMS analysis was performed (see Figure 7.5).

Spatially controlled surface functionalization with 2-(4-bromophenyl)ethanamine

Two masks were trialed for this experiment. First, a shadow mask featuring waved structures (see Figure 11.2) and, secondly, one featuring repeating squares with 50 μm pitches in x,y. The respective mask was placed onto a MCPO-functionalized Si wafer, which was subsequently irradiated (no inert gas, ambient temperature, no solvent) by a compact low-pressure fluorescent lamp (Arimed B6, Cosmedico GmbH, Stuttgart, Germany) emitting at 320 nm (± 30 nm, 36 W, the emission spectrum of the employed compact low-pressure fluorescent lamp is included in Figure 7.2) for 3 hours in a custom photoreactor (see Figure 11.1). After irradiation, the mask was removed and a solution of 5 mg (46 μmol) 1,4-benzoquinone in 4 mL of dichloromethane was added and placed in a shaker (300 rpm) for 18 hours at ambient temperature. The wafer was subsequently rinsed with dichloromethane and sonicated for 5 min in acetone to remove any possibly physisorbed material. The wafer was finally dried under a nitrogen stream. 100 mg (0.50 mmol) 2-(4-bromophenyl)ethanamine was dissolved in 4 mL methanol and a photodeprotected silicon wafer from the last step was added into a small vial, which was placed in a shaker held at 45 °C for 40 hours. The wafer was subsequently rinsed with methanol and sonicated for 5 min in fresh methanol to remove any physisorbed material. The wafer was finally dried under a nitrogen stream.

Spatially controlled surface functionalization with c(RGDfK)

A mask (see Figure 11.2) was placed onto an MCPO-functionalized Si wafer, which was subsequently irradiated (no inert gas, ambient temperature, no solvent) by a compact low-pressure fluorescent lamp (Arimed B6, Cosmedico GmbH, Stuttgart, Germany) emitting at 320 nm (\pm 30 nm, 36 W, the emission spectrum of the employed compact low-pressure fluorescent lamp is included in Figure 7.2) for 3 hours in a custom photoreactor (see Figure 11.1). After irradiation, the mask was removed and a solution of 5 mg (46 μ mol) of 1,4-benzoquinone in 4 mL of dichloromethane was added and placed in a shaker (300 rpm) for 18 hours at ambient temperature. The wafer was subsequently rinsed with dichloromethane and sonicated for 5 min in acetone to remove any possibly physisorbed material. The wafer was finally dried under a nitrogen stream. 3 mg (5.0 μ mol, 1.0 eq.) of c(RGDfK) and 0.77 mg (6.0 μ mol, 1.2 eq.) of *N,N*-diisopropylethylamine (DIPEA) were dissolved in 1 mL DMF and the photoactivated silicon wafer was added into a small vial, which was placed in a shaker held at 45 °C for 42 hours. The wafer was subsequently rinsed with DMF, placed in fresh DMF for 2 hours at ambient temperature and finally sonicated for 5 min in DMF to remove any physisorbed material. The wafer was finally dried under a nitrogen stream. The final set of ToF-SIMS images were obtained after removing ionic contamination (e.g., Na⁺) by washing and sonication with HPLC grade water (see Figure 7.5).

7.4 Results and Discussion

The idea of the current study is to use potent dienes, namely phencyclone derivatives, as a novel platform for light-triggered modifications. In detail, the approach proceeds in three steps: (A) a versatile and highly efficient Diels-Alder-based formation of a photoactive precursor, (B) a fast and mild photoactivation to induce spatio-temporal control and (C) the nucleophilic attachment of amines (see Figure 7.1a). The construction of patterns of non-modified biomolecules such as peptides and proteins by means of their inherent amine functionality would be highly desirable,^[319,320] especially if the procedure does not involve extremely reactive intermediates such as radicals, which would clearly result in limitations of selectivity and orthogonality. Upon performing a screening study of potential phencyclone candidates, the easily synthesizable^[314] 1,3-bis(4-methoxyphenyl)-2H-cyclopenta[1]phenanthren-2-one (MCPO) **1** compound was identified to be the most efficient precursor (not shown). Initial model reactions were performed in solution on a maleimide-functionalized GRGDS peptide **2**, since the maleimido peptide already utilized in Chapter 6 can help to evaluate the possibility of performing

the proposed reaction sequence in the presence of diverse amino acid residues in polar solvents. The synthetic procedure for the attachment of the photoactive moiety is straightforward and was achieved by stirring **2** with **1** (1.05 molar eq. of **1**,

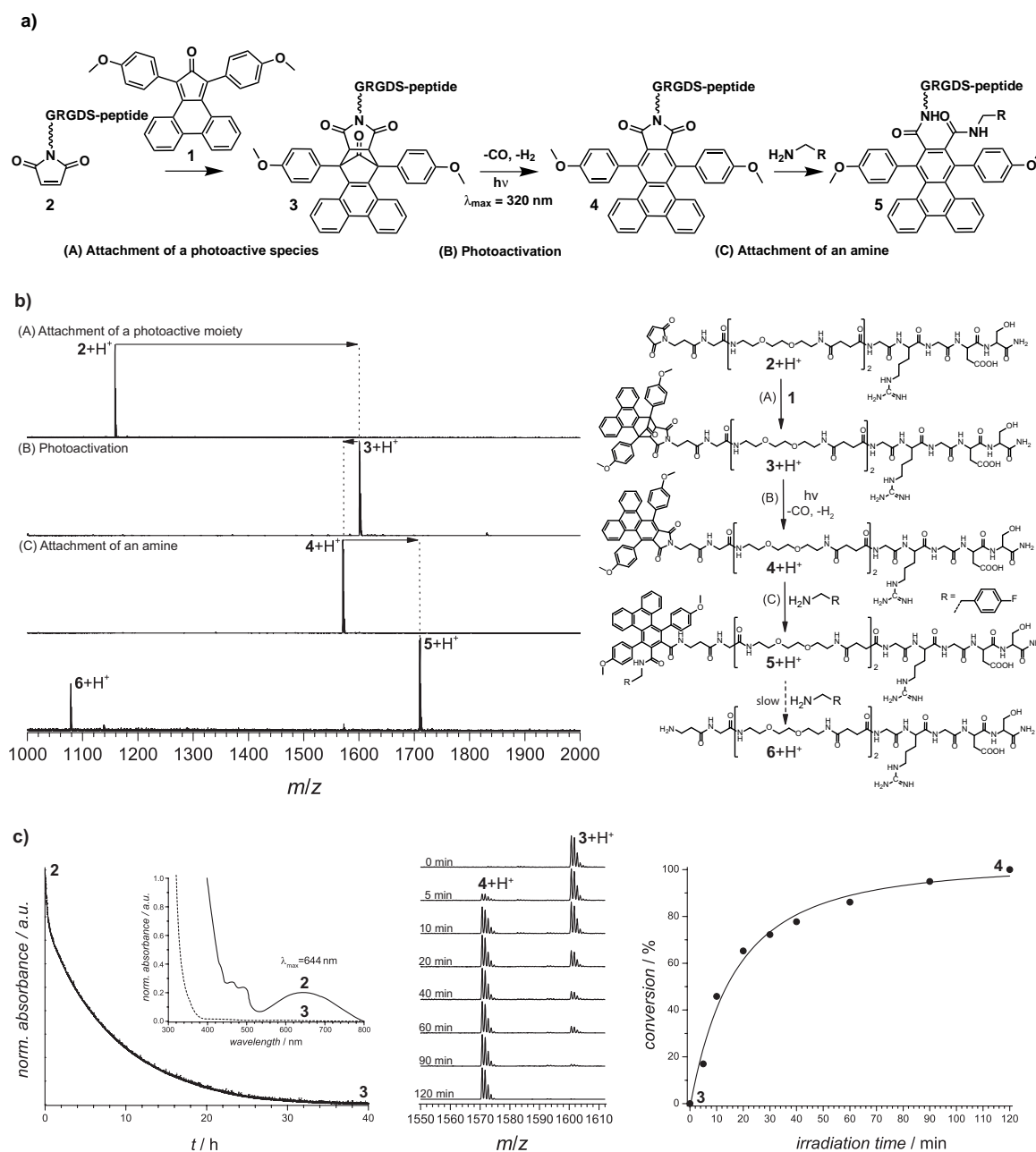


Figure 7.1 Overall concept for light-triggered modifications of the GRGDS peptide **2** (a). ESI-MS spectra of a maleimide end-capped GRGDS peptide **2** and after reaction with phencyclone derivative **1** (1.05 eq.). Subsequent decarbonylation and dehydrogenation to **4** was performed in water by an *in situ* photoreaction (2 h, 320 nm) in the presence of 3 eq. of 1,4-benzoquinone. Amine attachment to **5** was achieved by ring opening employing an excess of an amine derivative at 45 °C (b). Kinetic investigations of the Diels-Alder attachment of **1** by UV-Vis spectroscopy (left) and of the *in situ* activation before **3** and after **4** irradiation in the presence of 3 eq. of 1,4-benzoquinone (middle). An integration of the mass spectral abundances shows that quantitative conversion of species is achieved after 120 min reaction time (right) (c).

Table 7.1 Experimental and theoretical m/z values for the isotopic distribution of Figure 7.1 and Figure 7.3 in the m/z range between 1000 and 2000 and in the m/z range between 1500 and 1640, respectively.

$m/z_{\text{expt.}}$	ion assignment	formula	$m/z_{\text{theor.}}$	$\Delta m/z$
1158.6	2 + H ⁺	[C ₄₆ H ₇₆ N ₁₅ O ₂₀] ⁺	1158.5	0.1
1600.7	3 + H ⁺	[C ₇₇ H ₉₈ N ₁₅ O ₂₃] ⁺	1600.7	0.0
1570.7	4 + H ⁺	[C ₇₆ H ₉₆ N ₁₅ O ₂₂] ⁺	1570.7	0.0
1572.8	4* + H ⁺	[C ₇₆ H ₉₈ N ₁₅ O ₂₂] ⁺	1572.7	0.1
1709.8	5 + H ⁺	[C ₈₄ H ₁₀₆ FN ₁₆ O ₂₂] ⁺	1709.8	0.1
1078.6	6 + H ⁺	[C ₄₂ H ₇₆ N ₁₅ O ₁₈] ⁺	1078.5	0.1

MeCN/H₂O 7:1 v/v). In this context, UV-Vis spectroscopy is a useful technique for the online measurement of the concentration of **1**, which is colored by virtue of its $n \rightarrow \pi^*$ transition. The progress of the cycloaddition reaction could thus be monitored by measuring the loss of the long-wavelength absorbance of the phencyclone chromophore in the visible spectrum (644 nm, see Figure 7.1c, left) while the whole of the initially completely dark green reaction lost its colour within 40 hours reaction time indicating the efficient consumption of **1**. It should be noted that the rather slow cycloaddition can be accelerated by employing an excess of **1**, which is insoluble in methanol or water and can thus be readily removed from the reaction mixture by filtration. As a further test for a successful attachment of the photoactive precursor, an ESI-MS analysis was performed. Figure 7.1b depicts the mass spectra of the starting GRGDS peptide **2** alongside the quantitatively formed Diels-Alder cycloadduct **3**. Upon confirming the successful attachment of the photoactive species, the attention was turned to systematically investigating the photochemical behavior of the latter by employing a low cost 36 W compact fluorescent lamp ($\lambda_{\text{max}} = 320$ nm, see Figure 7.2) as the UV source. In general, bridged carbonyl compounds such as norbornen-7-one derivatives can eliminate carbon monoxide upon heating or mild irradiation.^[313,321] In the case of **3** light-triggered decarbonylation was observed, accompanied by a small amount of dehydrogenation product **4**. In order to produce the fully conjugated triphenylene-imide **4** in a quantitative manner, one can perform an one-pot *in situ* decarbonylation / dehydrogenation photoreaction. In detail, **3** was irradiated at ambient temperature in water for 2 hours in the presence of 1,4-benzoquinone (1:3 mol/mol). Inspection of the ESI-MS spectra in Figure 7.1b reveals a full peak shift of 30 amu towards lower mass-to-charge ratios, which corresponds to the loss of CO and H₂. A kinetic investigation was performed of which the result is shown in Figure 7.1c (middle). Complete disappearance of the quasimolecular ion [3+H]⁺ leaving [4+H]⁺ demonstrates that full conversion

was achieved after less than 120 min irradiation time at ambient temperature. The photoreaction can be performed in various solvents (including pure water), via a two step procedure (adding the dehydrogenation agent after the light-triggered decarbonylation, see Figure 7.3) and via the utilization of different dehydrogenation agents (e.g., alkylmaleimides, not shown). In a nutshell, in all of these cases an efficient transformation from the photoprotected compound **3** to photodeprotected **4** was observed in a quantitative and solvent independent manner. Secondary photolysis, which can be a major issue in the widely employed *o*-nitrobenzyl photoprotecting moiety,^[58] is avoided even after prolonged irradiation by means of the overall high photolytic and thermal stability of all products, which are namely CO, H₂, and the triphenylene-imide **4**. The latter moiety is, however, capable of undergoing ring-opening reactions with amines in analogy to the well-known phthalimide system.^[322] Inspection of Figure 7.1b reveals the successful formation of monoadduct of 2-(4-fluorophenyl)ethanamine **5** as the main product whereas double attachment resulted in cleavage and a small fraction of amine end-capped peptide **6**. The solution-based experiments convincingly demonstrate the highly efficient attachment of a photoactive precursor which avoids complex synthesis, its rapid and quantitative photoactivation, and its efficient catalyst-free coupling with amines. All in all, these findings form a significant contribution in the field of light-triggered approaches. A limiting factor of the approach in solution is, however, the necessity to employ an excess of amine to efficiently ring-open the triphenylene-imide **4**. The current strategy is thus not the system of choice in cases where product separation is difficult, e.g., when polymer-polymer conjugations are targeted. However, the full strength of the given platform for light-directed functionalization is evidenced when the reaction sequence is performed on a surface. Excess of amine reagent is

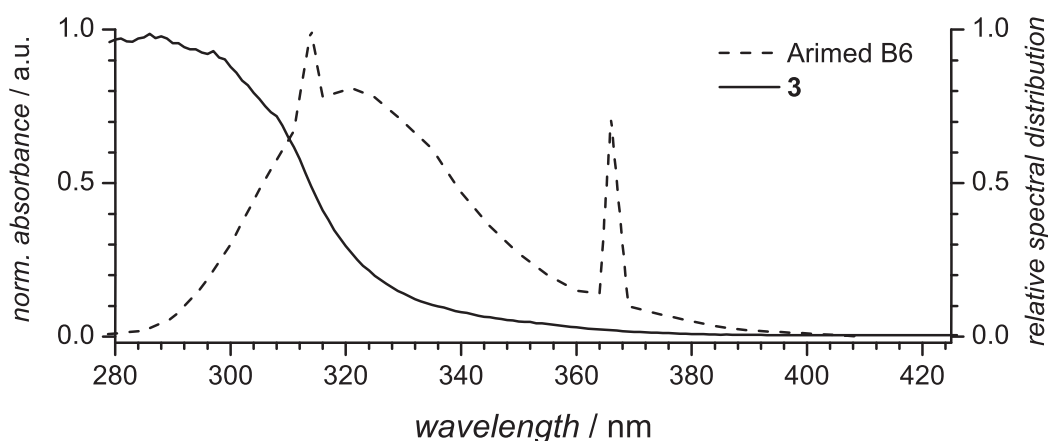


Figure 7.2 UV-Vis spectrum of Diels-Alder cycloadduct **3** ($1.6 \cdot 10^{-4} \text{ mol} \cdot \text{L}^{-1}$) in MeCN/H₂O 7:1 v/v and the relative spectral distribution of the employed compact low-pressure fluorescent lamp (36 W, Arimed B6, $\lambda_{\text{max}} = 320 \text{ nm}$).

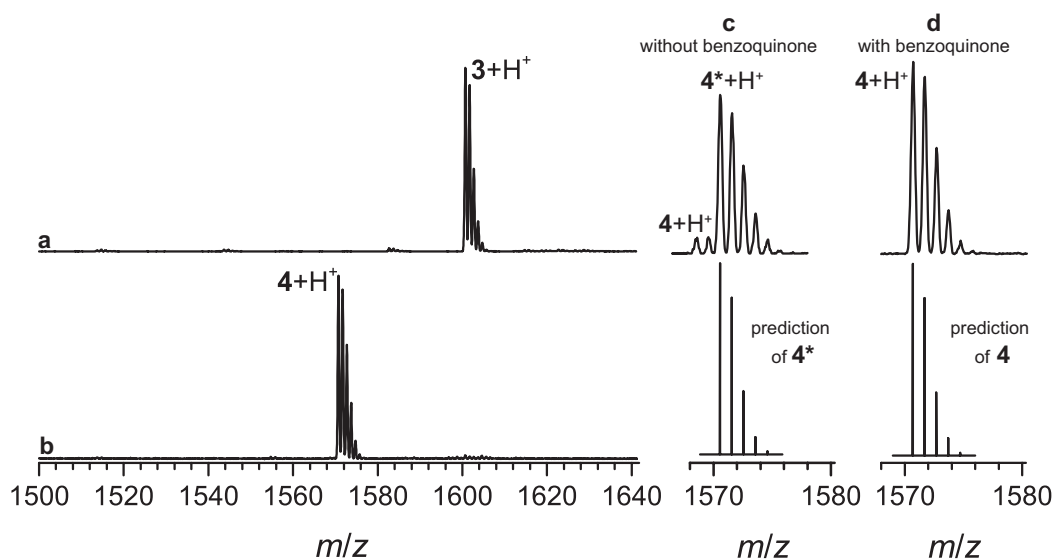


Figure 7.3 ESI-MS spectra of **3** before (a) and after irradiation and over-night stirring with 1,4-benzoquinone (b). Zoom-in of the ESI-MS spectra after irradiation without over-night stirring with 1,4-benzoquinone (c) and with over-night stirring with 1,4-benzoquinone 3 eq. (d).

easily removed via simple washing and double nucleophilic ring-opening by amines is – due by steric hindrance – less pronounced. Yet, the latter event would result in cleavage and an automatic removal from the surface. These findings and the potential ability to pattern non-modified biomolecules by means of their inherent

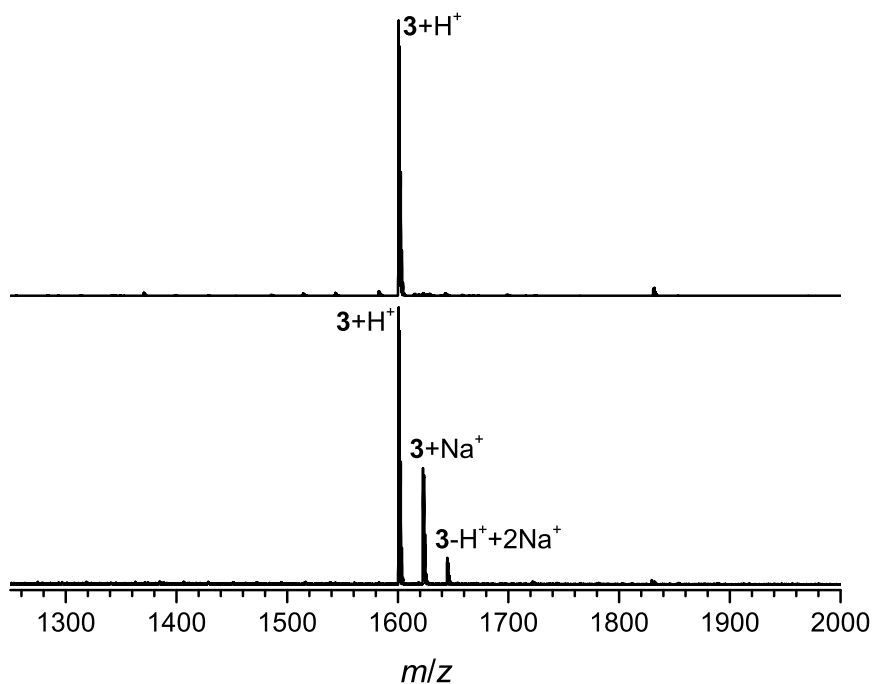
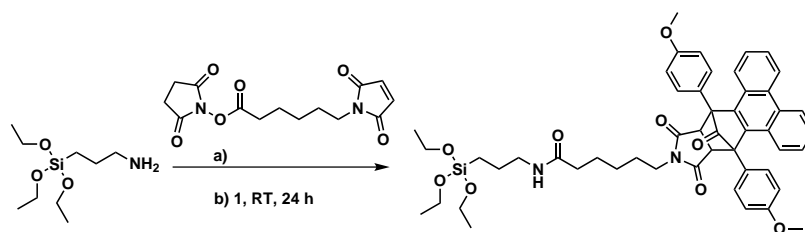


Figure 7.4 ESI-MS spectra of **3** before and after addition of 2-(4-fluorophenyl)ethanamine. The non-irradiated compound **3** was found to be fully stable under the standard amine attachment conditions (45 °C, 16 - 30 hours, shaker 300 / min).



Scheme 7.3 Synthesis of the MCPO-functionalized silane. Reagents: 3-(maleimido)propionic acid *N*-hydroxysuccinimide ester (a); **1**, THF, RT (b)

amine functionality prompted us to translate it to the spatially constrained grafting of molecules onto surfaces to produce molecular patterns. The clear dichotomy between the photoactivation and the chemical attachment in the current strategy would also allow for the construction of patterns of light-sensitive (bio)molecules that cannot be obtained by more conventional strategies. Importantly and being the basis for any spatially resolved grafting of molecules onto surfaces, the non-irradiated photosensitive precursor **3** was found to be fully inert in the presence of excess 2-(4-fluorophenyl)ethanamine at 45 °C (see Figure 7.4). The synthetic route to functionalized silicon surfaces is straightforward. A maleimide end-capped silane was prepared from commercially available substances (see Scheme 7.3) and was converted to the MCPO end-capped silane via a Diels-Alder cycloaddition with **1**. Finally the silane was dissolved in anhydrous toluene and employed to treat activated silicon wafers. Upon successful silanization, the photopatterning was achieved by irradiation of the silicon wafers for 3 hours under normal atmospheric conditions (no inert gas, ambient temperature) and without solvent. Two shadow masks were utilized for the locally constrained surface activation: one featuring squares with 50 μm pitches in x/y coordinates and one with a macroscopic pattern. After irradiation, patterning was achieved by immersing the silicon wafers in a 1,4-benzoquinone solution (dehydrogenation) and finally in a methanolic solution of the respective amine for 18 hours at 45 °C. Analysis of the photopatterning was achieved by imaging time-of-flight secondary-ion mass spectrometry (ToF-SIMS), which is a highly sensitive technique for the spatially resolved analysis of molecular patterns on solid substrates.^[3,296] A ToF-SIMS composition analysis of the surface reproduced the shadow mask structures with a good spatial resolution (edge steepness: 4.5 μm) between irradiated and non-irradiated areas (see Figure 7.5b, top). Indeed, only the non-irradiated zone showed the presence of the Diels-Alder cycloadduct ($\text{C}_{35}\text{H}_{24}\text{NO}_5^-$) – the full fragment of which is initially present in the protected molecule – while only the irradiated squares exhibited a fragment at 30 amu lower mass-to-charge ratio, corresponding to triphenyleneimide ($\text{C}_{34}\text{H}_{22}\text{NO}_4^-$) which is formed by loss of H_2 and CO . Bromine compounds with their inherent isotopic pattern can be unambiguously detected by ToF-SIMS, therefore, the pho-

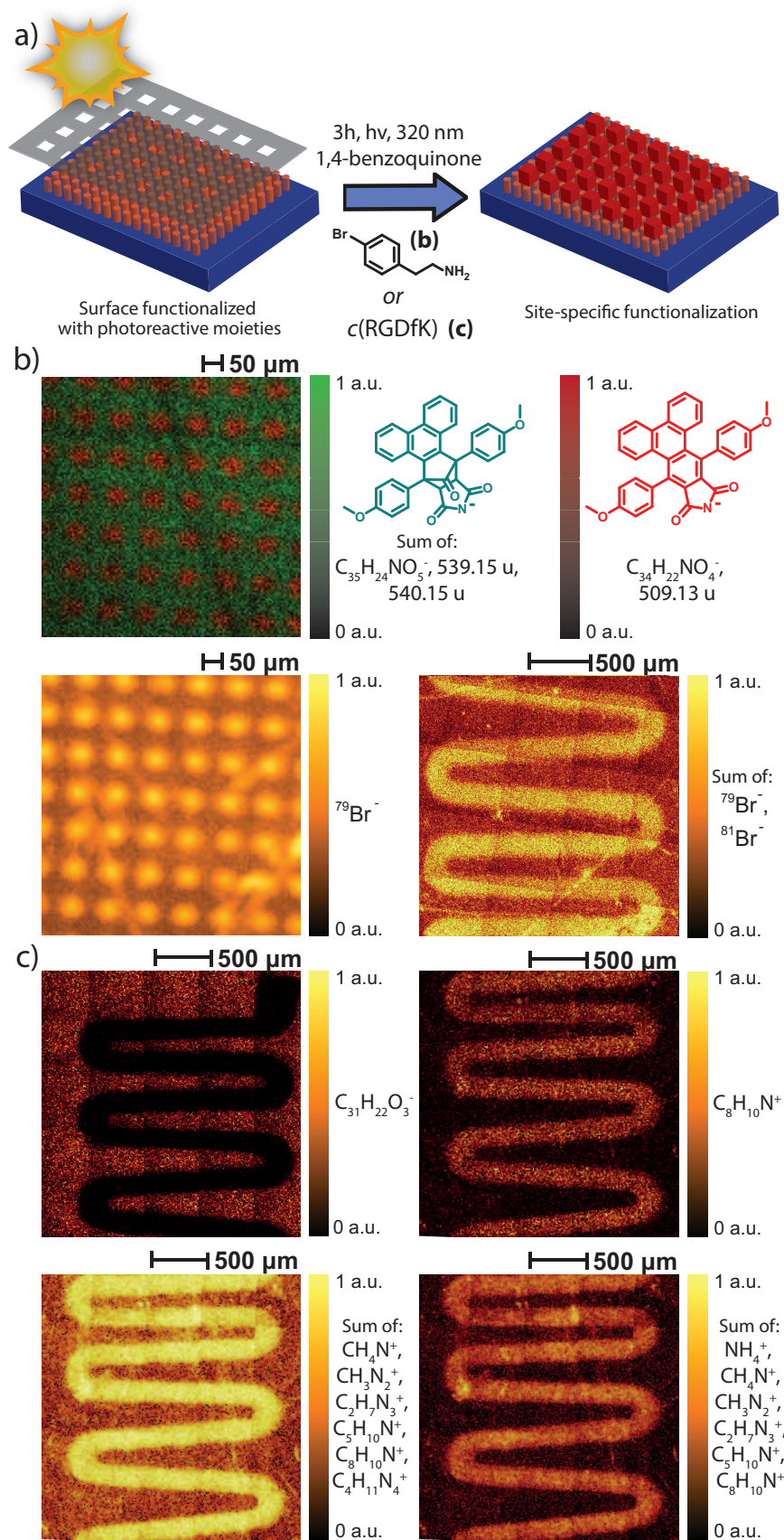


Figure 7.5 Representation of the phototriggered surface grafting of bromine-containing amine (a). ToF-SIMS images of silicon wafers patterned with 2-(4-bromophenyl)ethanamine utilizing two shadow masks (b). ToF-SIMS images of silicon wafers patterned with c(RGDfK) utilizing a shadow mask (c).

topatterned wafer was immersed in a solution of 2-(4-bromophenyl)ethanamine as a molecular marker to spatially map the amine-reactive areas. Clearly, only the irradiated part exhibited bromine functionalization after immersion of the wafer in the solution of 2-(4-bromophenyl)ethanamine (Figure 7.5b, bottom). To additionally demonstrate the feasibility of a covalent and spatially resolved attachment of non-modified peptides by this phototriggered approach, the irradiation/dehydrogenation procedure of the amine compound (irradiation: no inert gas, ambient temperature, no solvent; dehydrogenation via a 1,4-benzoquinone solution) was repeated for a freshly prepared MCPO-functionalized wafer. Finally, the surface was treated with a solution of *N,N*-diisopropylethylamine (DIPEA) and the extracellular matrix protein-mimicking c(RGDfK) peptide. Note that this time – in contrast to the initial solution experiments where the peptide was bearing the photoactive moiety – a non-modified peptide was employed able to react with photoactivated substrates via its lysine residue. In a ToF-SIMS analysis, the successful photodeprotection was confirmed via a negative contrast for the Diels-Alder cycloadduct ($C_{35}H_{24}NO_5^-$, not shown) as well as by its retro-Diels-Alder follow-up product 1 ($C_{31}H_{22}O_3^-$, see Figure 7.5c top left) formed during analysis. ToF-SIMS also provided evidence that the peptide was immobilized in a pattern corresponding to the mask features. In that case, composition analysis was based on the presence of $CH_3N_2^+$ and $C_8H_{10}N^+$ (Figure 7.5c, top right), characteristic secondary ions for arginine or phenylalanine-containing peptides, respectively.^[279,280,323] Sums of all positive ion fragments which can be assigned to the peptide are depicted in Figure 7.5c.

7.5 Conclusions

In the present chapter, a novel technique allowing the photopatterning of peptides strictly composed of naturally occurring residues, was introduced. The possibility to employ natural peptides is the first important feature since it avoids the expensive preparation or purchase of non-natural amino acids or the modification of peptide C- or N termini. In addition, the synthetic route towards the relevant photoreactive compounds is technically simple and achieved at a rather low cost. Finally, the photopatterning sequence itself involves catalyst-free and rather mild conditions. The photoreaction is fully compatible with all investigated solvents including water, avoids the formation of harmful photolysis by-products, and can be performed under ambient atmosphere and temperature. The combination of these features renders the present system extremely attractive for industrially relevant peptide micro- or nanoarray fabrication.

8

Spatially Controlled Surface Immobilization of Nucleophiles via Trapping of Thioaldehydes*

8.1 Abstract

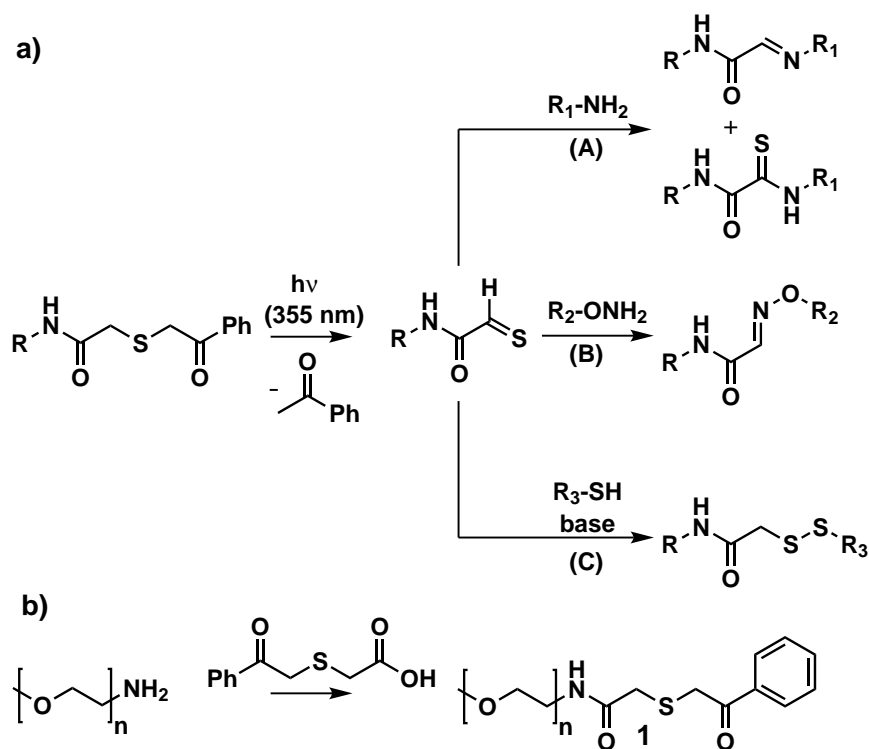
A novel and very simple photochemical strategy that utilizes light to provide spatio-temporal control for the direct covalent immobilization of nucleophiles is presented. The concept is based upon the efficient trapping of photogenerated thioaldehydes by amines, hydroxylamines, and thiols. Surface patterns of polymers and small molecules bearing pendant amine-, hydroxylamine- or thiol moieties were successfully generated and imaged in a time-of-flight secondary-ion mass spectrometry (ToF-SIMS) investigation.

8.2 Introduction

The ability to generate patterns of various substrates holds significant promise in highly investigated research areas such as sensor design and microelectronics.^[325] Among the tools that can meet such demands, light based systems can induce

* Parts of this Chapter were reproduced from Ref. 324 by permission of the Royal Society of Chemistry.

surface changes mildly without the need of any reagent and are thus particularly attractive.^[37] As an additional benefit one gains spatio-temporal control, which serves as a fundamental basis for micro- and nanofabrication applications. One of the strategies which allows for a site-specific immobilization is based on photoprotecting chemistry.^[36,57] A desired bond-cleavage occurs upon a light stimulus and a reactive functionality, initially rendered inert by a photoprotecting group, can subsequently be released and employed for further functionalization. In this line, the photogeneration of azide-reactive oxa-dibenzocyclooctynes,^[284,326] alkene-reactive nitrile imines,^[95,285] and hydroxylamine reactive aldehydes (see Chapter 5)^[40] have been recently reported. An alternative approach is the photogeneration of highly reactive intermediates with short lifetimes, such as *o*-naphthoquinone methides^[150,151] or *o*-quinodimethanes,^[3,145] which can be efficiently trapped by (hetero) dienophiles (see Chapter 6). The initial photoactive moieties are regenerated resulting in an enhanced selectivity and orthogonality even in a non-light protected environment. As already stated in Chapter 7, the effort expended in the construction of patterns of various substrates is mostly dependent on the synthesis of a photoactive surface anchor and a substrate bearing an appropriate coupling moiety. As the preparation of the latter can often be a challenging exercise, the attention was turned to systematically investigating



Scheme 8.1 Overall strategy for the attachment of amines (A), hydroxylamines (B) and thiolates (C) to photogenerated thioaldehydes (a). Synthesis of a photoactive model system (b).

systems that are able to efficiently react with functionalities inherently present in many substrates. As a starting point, the highly efficient photofragmentation of phenacyl sulfides^[327] and the utilization of the resulting heterodienophile in Diels-Alder reactions with dienes, has been recently reported in the group of Barner-Kowollik.^[328] A comparatively little explored method to achieve efficient conversions of thioaldehydes is the use of nucleophiles as trapping agents. Amines, for instance, yield the corresponding imines, which are partially susceptible to oxidation by sulfur species to form thioamide fragments (Scheme 8.1a, pathway A).^[329] In contrast, the *in situ* reaction with hydroxylamines affords oximes, which are less prone to sulfur oxidation (Scheme 8.1a, pathway B). Finally, thiolates react with thioaldehydes to afford disulfide bridges in good yields (Scheme 8.1a, pathway C).^[330]

The idea of the current study is to exploit the above mentioned trapping of thioaldehydes by nucleophiles to provide a simple and universal platform for light-triggered surface modifications at ambient temperature. In contrast to the photochemical approach described in the previous chapter, the present strategy establishes a one-pot *in situ* procedure for the direct and synthetically facile immobilization of nucleophiles. The generation of a highly reactive intermediate (thioaldehyde) translates into facile reactions kinetics and, consequently, the amount of necessary reacting substrate can be reduced from 1000 eq. (see Chapter 7) to 2 eq. in the present approach. The downsides of the approach are a rather limited chemical selectivity and the incompatibility to polar solvents.

8.3 Experimental Part

Synthesis of *N*-octadecyl-2-((2-oxo-2-phenylethyl)thio)acetamide

600 mg (2.9 mmol, 1.0 eq.) phenacyl thioacetic acid, 770 mg (2.9 mmol, 1.0 eq.) octadecan-1-amine and 850 mg (4.40 mmol, 1.5 eq.) EDC hydrochloride were dissolved in 10 mL predried DCM. 100 mg (0.82 mmol, 0.12 eq.) DMAP was added and the solution was stirred overnight. The reaction mixture was diluted with 30 mL of water and the organic layer was subsequently washed with 2 × 30 mL of diluted aqueous HCl and 2 × 30 mL of saturated aqueous NaHCO₃. The organic layer was dried over magnesium sulfate. The solvent was removed under reduced pressure and 580 mg *N*-octadecyl-2-((2-oxo-2-phenylethyl)thio)acetamide (1.3 mmol, 45 %) was obtained as a white solid after recrystallization from ethanol. ¹H NMR (400 MHz, CDCl₃); [δ , ppm]: 7.96 (d, *J* = 7.9 Hz, 2H, -ArH), 7.61 (t, *J* = 7.2 Hz, 1H, -ArH), 7.49 (t, *J* = 7.5 Hz, 2H, -ArH), 6.76 (bs, 1H, -CONH), 3.95 (s, 2H, -ArCOCH₂),

3.29-3.18 (m, 4H, $-\text{CONHCH}_2$, $-\text{NHCOCH}_2$), 1.55-1.43 (m, 2H, $-\text{CONHCH}_2\text{CH}_2$), 1.36-1.14 (m, 28H, $14 \times -\text{CH}_2$), 0.88 (t, $J = 6.4$ Hz, 3H, $-\text{CH}_3$). ^{13}C NMR (101 MHz, CDCl_3); [δ , ppm]: 194.31, 168.02, 135.13, 134.02, 129.01, 40.05, 38.31, 36.15, 32.07, 29.9-29.4, 27.07, 22.83, 14.26. ESI-MS: $[\text{M}+\text{Na}]^+$: $m/z_{\text{expt.}} = 484.4$; $m/z_{\text{theo.}} = 484.3$.

Synthesis of phenacyl sulfide (FAS) mono-functional amino end-capped poly(ethylene)glycol methyl ether **1**

126 mg (0.6 mmol, 4.0 eq.) phenacyl thioacetic acid, 250 mg (0.15 mmol, 1.0 eq.) mono-functional amino end-capped poly(ethylene)glycol methyl ether (mPEG-amine, $M_n \approx 1000 \text{ g}\cdot\text{mol}^{-1}$), and 62 mg (0.30 mmol, 2.0 eq.) DCC were dissolved in 5 mL pre-dried DCM. 7 mg (0.06 mmol, 0.40 eq.) DMAP was added and the solution was stirred overnight. Precipitated urea was filtered off and the solvent was removed under reduced pressure. The polymer **1** was obtained by re-dissolution in DCM and by precipitation in cold diethyl ether. To remove the starting material, the solid was suspended in 3 mL de-ionized water and filtered through a 0.45 mm PTFE standard GPC filter (note: this step drastically reduced the overall yield). 22 mg of polymer **1** were obtained by removing the solvent via freeze-drying. Note: The procedure can also be performed by exchanging the coupling reagent DCC with EDC hydrochloride (3 eq.). After the reaction, the product mixture (dissolved in DCM) is diluted with water and the organic layer is washed with diluted aqueous HCl ($2 \times 10 \text{ mL}$) and saturated aqueous NaHCO_3 ($2 \times 10 \text{ mL}$). Analysis of the FAS-capped polymer was performed by SEC/ESI-MS (see Figure 8.2).

Phototriggered Experiments in Solution

Phototriggered reaction of **1** with 2-(4-bromophenyl)ethanamine

A solution of 0.5 mg (4.2 μmol , 1.0 eq.) of **1** and 0.17 mg (8.4 μmol , 2.0 eq.) 2-(4-bromophenyl)ethanamine in 2 mL of dichloromethane were added into a headspace vial, which was crimped air-tight using SBR seals with PTFE inner liner. The solution was deoxygenated by purging with nitrogen for 3 min. The flask was subsequently irradiated for 1 hour by revolving around a compact low-pressure fluorescent lamp (Philips CLEO Compact PL-L: $\lambda_{\text{max}} = 355 \text{ nm}$, see Figure 8.1) at a distance of 40-50 mm in a custom-built photoreactor (see Figure 11.1). After irradiation, the solvent was removed under reduced pressure and the sample was subjected to SEC/ESI-MS analysis (see Figure 8.2).

Phototriggered reaction of mPEG-amine with *N*-octadecyl-2-((2-oxo-2-phenylethyl)thio)acetamide

A solution of 0.5 mg ($M_n \approx 1000 \text{ g}\cdot\text{mol}^{-1}$, 0.50 μmol , 1.0 eq.) mPEG-amine and 2.3 mg (5.0 μmol , 10.0 eq.) *N*-octadecyl-2-((2-oxo-2-phenylethyl)thio)acetamide in 1 mL of dichloromethane was added into a headspace vial, which was crimped air-tight using SBR seals with PTFE inner liner. The solution was deoxygenated by purging with nitrogen for 3 min. The flask was subsequently irradiated for 3 hours by revolving around a compact low-pressure fluorescent lamp (Philips CLEO Compact PL-L: $\lambda_{\text{max}} = 355 \text{ nm}$, see Figure 8.1) at a distance of 40-50 mm in a custom-built photoreactor (see Figure 11.1). After irradiation, the solvent was removed under reduced pressure and the sample was subjected to SEC/ESI-MS analysis (see Figure 8.3).

Phototriggered reaction of 1 with *O*-(2,3,4,5,6-pentafluorobenzyl)hydroxylamine hydrochloride

A solution of 0.5 mg (0.42 μmol , 1.0 eq.) of **1** and 0.21 mg (0.84 μmol , 2.0 eq.) *O*-(2,3,4,5,6-pentafluorobenzyl)hydroxylamine hydrochloride in 2 mL of acetonitrile (prepared from stock solutions) was added into a headspace vial, which was crimped air-tight using SBR seals with PTFE inner liner. The solution was deoxygenated by purging with nitrogen for 3 min. The flask was subsequently irradiated for 1 hour by revolving around a compact low-pressure fluorescent lamp (Philips CLEO Compact PL-L: $\lambda_{\text{max}} = 355 \text{ nm}$, see Figure 8.1) at a distance of 40-50 mm in a custom-built photoreactor (see Figure 11.1). After irradiation, the solvent was removed under reduced pressure and the sample was subjected to SEC/ESI-MS analysis (see Figure 8.2).

Phototriggered reaction of 1 with (4-bromophenyl)methanethiol

A solution of 0.5 mg (0.42 μmol , 1.0 eq.) of **1**, 0.17 mg (0.84 μmol , 2.0 eq.) (4-bromophenyl)methanethiol and 0.13 mg (1.0 μmol , 2.4 eq.) DIPEA in 2 mL of dichloromethane (prepared from stock solutions) was added into a headspace vial, which was crimped air-tight using SBR seals with PTFE inner liner. The solution was deoxygenated by purging with nitrogen for 3 min. The flask was subsequently irradiated for 1 hour by revolving around a compact low-pressure fluorescent lamp (Philips CLEO Compact PL-L: $\lambda_{\text{max}} = 355 \text{ nm}$, see Figure 8.1) at a distance of 40-50 mm in a custom-built photoreactor (see Figure 11.1). After irradiation, the solvent was removed under reduced pressure, 50 μL of hydrogen peroxide was added to reverse disulfide reduction and the sample was subjected to SEC/ESI-MS analysis (see Figure 8.2).

Surface Modifications

Cleaning and preactivation of the silicon wafers

All Si wafers and glass substrates were cleaned three successive times by ultrasonification for 15 min in chloroform, acetone, and ethanol. Preactivation of the surfaces was achieved by separately placing them in small glass vials containing acidic piranha solution (sulfuric acid 95 % / aqueous hydrogen peroxide 35 % 3:1 v/v) for 60 min at 100 °C. **Caution: piranha solution is an extremely strong oxidant and should be handled very carefully!**

Silanization of Si wafers with FAS-containing silane

Preactivated substrates were placed separately in small glass vials containing a solution of 2.0 mg (4.8 μmol) FAS-containing silane dissolved in 0.5 mL of anhydrous toluene. They were subsequently heated to 50 °C for 2 hours on a shaker (300 rpm) and held overnight at RT. The wafers were subsequently ultrasonicated for 2 minutes in 10 mL of dry toluene and for 2 minutes in 10 mL DCM to remove any physisorbed silane.

Spatially controlled surface modification with 2-(4-bromophenyl)ethanamine

A mask (see Figure 11.2) was placed onto a FAS-functionalized Si wafer. The latter was placed into a headspace vial, which was crimped air-tight using SBR seals with PTFE inner liner. A solution of 10 mg (0.05 mmol) 2-(4-bromophenyl)ethanamine in 4 mL of dichloromethane was added and deoxygenated by purging with nitrogen for 3 min. The flask was subsequently irradiated for 1 hour by revolving around a compact low-pressure fluorescent lamp (Philips CLEO Compact PL-L: $\lambda_{\text{max}} = 355$ nm, see Figure 8.1) at a distance of 40-50 mm in a custom-built photoreactor (see Figure 11.1). After irradiation, the mask was removed. The wafer was subsequently rinsed and sonicated in dichloromethane for 3 minutes and in acetone for 3 minutes to remove any possibly physisorbed material. The wafer was finally dried under a nitrogen stream and afterwards, a ToF-SIMS analysis was performed (see Figure 8.4).

Spatially controlled surface modification with mPEG-amine

A mask (see Figure 11.2) was placed onto a FAS-functionalized Si wafer. The latter was placed into a headspace vial, which was crimped air-tight using SBR seals with PTFE inner liner. A solution of 10 mg mPEG-amine ($M_n \approx 1000 \text{ g}\cdot\text{mol}^{-1}$, 0.01 mmol) in 4 mL of dichloromethane was added and deoxygenated by purging with nitrogen for 3 min. The flask was subsequently irradiated for 1 hour by revolving around a compact low-pressure fluorescent lamp (Philips CLEO Compact PL-L: $\lambda_{\text{max}} = 355$

nm, see Figure 8.1) at a distance of 40-50 mm in a custom-built photoreactor (see Figure 11.1). After irradiation, the mask was removed. The wafer was subsequently rinsed and sonicated in dichloromethane for 3 minutes and in acetone for 3 minutes to remove any possibly physisorbed material. The wafer was finally dried under a nitrogen stream and afterwards, a ToF-SIMS analysis was performed (see Figure 8.4).

Spatially controlled surface modification with (4-bromophenyl)methanethiol

A mask (see Figure 11.2) was placed onto a FAS-functionalized Si wafer. The latter was placed into a headspace vial, which was crimped air-tight using SBR seals with PTFE inner liner. A solution of 10 mg (0.05 mmol) (4-bromophenyl)methanethiol in 4 mL of dichloromethane and 7.75 mg (0.06 mmol) DIPEA was added and deoxygenated by purging with nitrogen for 3 min. The flask was subsequently irradiated for 1 hour by revolving around a compact low-pressure fluorescent lamp (Philips CLEO Compact PL-L: $\lambda_{\max} = 355$ nm, see Figure 8.1) at a distance of 40-50 mm in a custom-built photoreactor (see Figure 11.1). After irradiation, the mask was removed. The wafer was subsequently rinsed and sonicated in dichloromethane for 3 minutes and in acetone for 3 minutes to remove any possibly physisorbed material. The wafer was finally dried under a nitrogen stream and afterwards, a ToF-SIMS analysis was performed (see Figure 8.4).

Spatially controlled surface modification with O-(2,3,4,5,6-pentafluorobenzyl)-hydroxylamine hydrochloride

A mask (see Figure 11.2) was placed onto a FAS-functionalized Si wafer. The latter was placed into a headspace vial, which was crimped air-tight using SBR seals with PTFE inner liner. A solution of 10 mg (0.04 mmol) O-(2,3,4,5,6-pentafluorobenzyl)hydroxylamine hydrochloride in 4 mL of acetonitrile was added and deoxygenated by purging with nitrogen for 3 min. The flask was subsequently irradiated for 1 hour by revolving around a compact low-pressure fluorescent lamp (Philips CLEO Compact PL-L: $\lambda_{\max} = 355$ nm, see Figure 8.1) at a distance of 40-50 mm in a custom-built photoreactor (see Figure 11.1). After irradiation, the mask was removed. The wafer was subsequently rinsed and sonicated in acetonitrile for 3 minutes and in acetone for 3 minutes to remove any possibly physisorbed material. The wafer was finally dried under a nitrogen stream and afterwards, a ToF-SIMS analysis was performed (see Figure 8.5).

8.4 Results and Discussion

Although the ultimate aim is to immobilize substrates by means of nucleophilic additions to photogenerated thioaldehydes on surfaces, the reactions were initially performed on a model system in solution in order to assess in detail all reaction products via electrospray ionisation mass spectrometry (ESI-MS). Since amide linkages are less prone to undergo nucleophilic reactions than esters, the model system **1** was prepared by coupling of commercially available mono-functional amino end-capped poly(ethylen)glycol methyl ether (mPEG-amine, $M_n \approx 1000 \text{ g}\cdot\text{mol}^{-1}$) with 2-((2-oxo-2-phenylethyl)thio)acetic acid (Scheme 8.1b). A 36 W compact fluorescent lamp ($\lambda_{\text{max}} = 355 \text{ nm}$; see Figure 8.1) was employed as UV source for the photofragmentation of the phenacyl sulfide (FAS) end-capped polymer **1**. The latter was irradiated for 1 hour in the presence of the respective nucleophile (2 molar eq.) in degassed dichloromethane (unless otherwise stated). The outcome of the model reactions is shown in Figure 8.2, which depicts the single charged mass spectra of starting FAS-capped polymer before irradiation **1** alongside with the photostable nucleophilic addition adducts. After the photoinduced transformation of **1** with 2-(4-bromophenyl)ethanamine, one can clearly observe two dominant species in the product spectrum, which can be assigned to the expected formation of imine **2** and thioamide fragment **2'**. Both species contain – based upon the characteristic isotopic pattern of their signal (see also the zoom-in region, Figure 8.2 right) – bromine and, consequently, no influence on the grafting density is to be expected on a surface. Similar success was met in cases when the polymer is not bearing the photoactive moiety, e.g., in the photoconjugation of an octadecan chain bearing a lateral FAS moiety (in molar excess) with mPEG-amine. As a

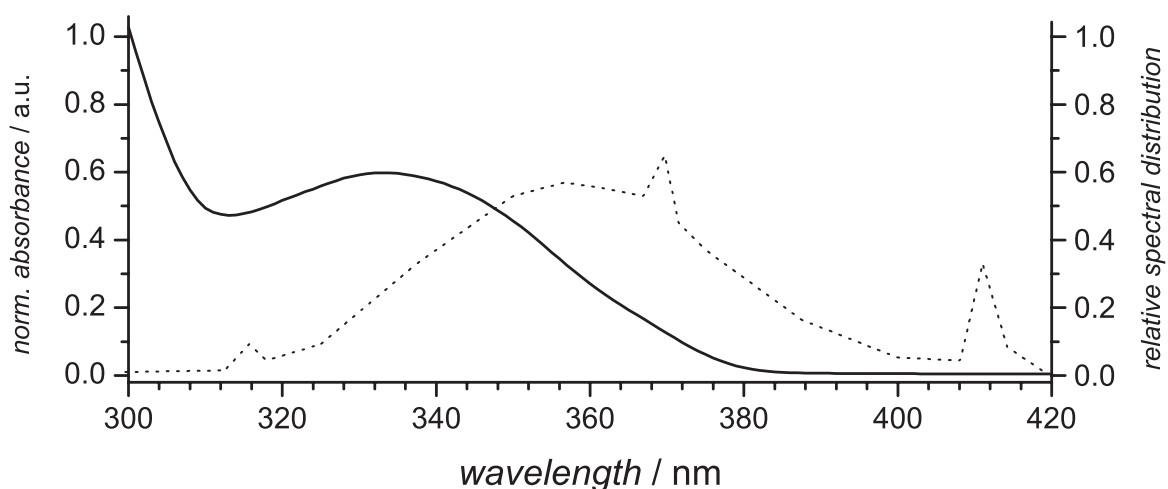


Figure 8.1 Emission spectrum of the employed compact low-pressure fluorescent lamp (36W, Philips CLEO Compact PL-L: $\lambda_{\text{max}} = 355 \text{ nm}$, dotted line). Absorption spectrum of *N*-octadecyl-2-((2-oxo-2-phenylethyl)thio)acetamide ($0.022 \text{ mol}\cdot\text{L}^{-1}$, solid line line).

result of the higher concentration of sulfur species, the corresponding thioamide fragment **5'** was obtained as the main product (see Figure 8.3). Quantitative conversions with *in situ* photogenerated thioaldehydes can be achieved by treatment with hydroxylamines. Specifically, **1** was irradiated for 1 hour with 2 molar eq. of O-(2,3,4,5,6-pentafluorobenzyl)hydroxylamine hydrochloride in degassed acetonitrile and an ESI-MS analysis revealed a full peak shift towards higher mass-to-charge ratios. Complete disappearance of the quasimolecular ion $[1+\text{Na}]^+$ leaving $[3+\text{Na}]^+$ demonstrates that full conversion was achieved after less than 1 hour irradiation time at ambient temperature by mild irradiation at 355 nm. As alluded to earlier, the formation of a disulfide can be expected for the photoconjugation of **1** with (4-bromophenyl)methanethiol by employing *N,N*-diisopropylethyl-amine (DIPEA).

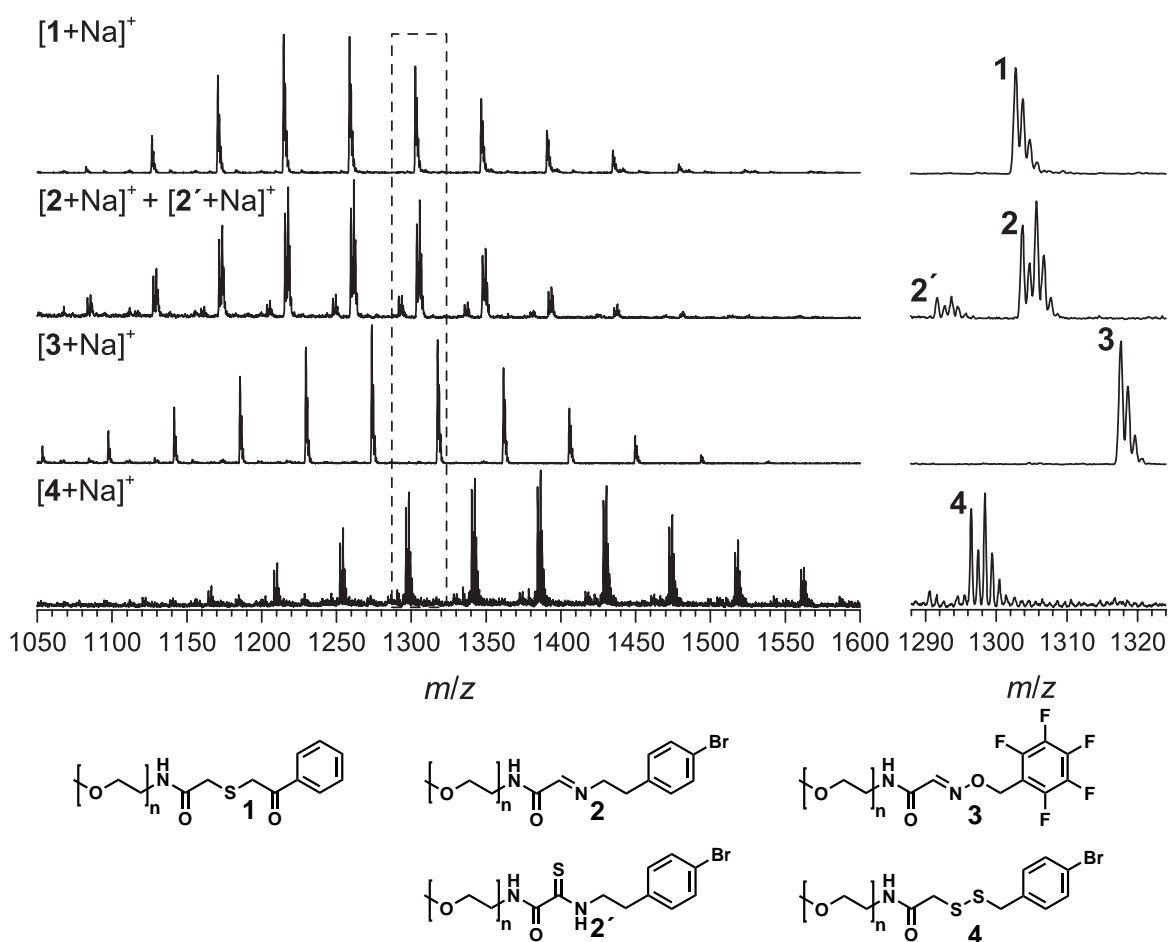


Figure 8.2 ESI-MS single charged spectra of a phenacyl sulfide (FAS) end-capped polymer **1** and after irradiation for 1 hour with nucleophiles (2 molar eq.). The reaction with 2-(4-bromophenyl)ethanamine yields imine **2** and the thioamide **2'** (note the characteristic isotopic pattern of the bromine species **2** and **2'**), whereas quantitative formation of **3** was observed for the one-pot *in situ* photoconjugation with O-(2,3,4,5,6-pentafluorobenzyl)hydroxylamine hydrochloride. Disulfide **4** was formed by treatment with (4-bromophenyl)methanethiol and *N,N*-diisopropylethylamine (DIPEA). Note also the characteristic isotopic pattern of the bromine species of **4**.

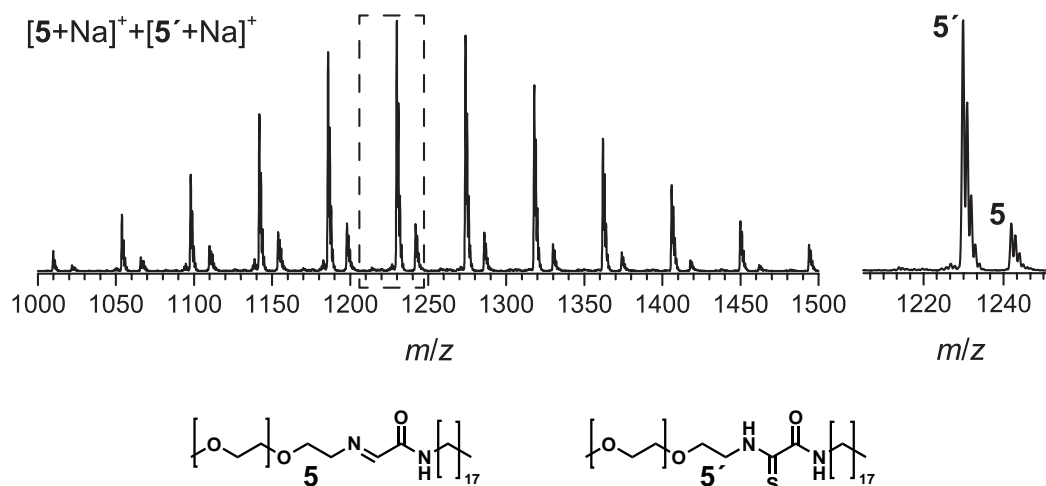
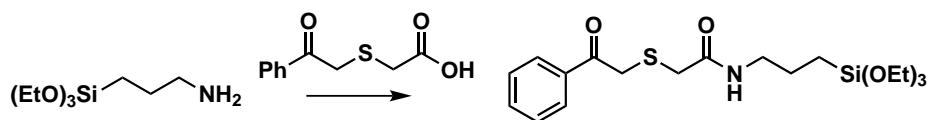


Figure 8.3 Phototriggered reaction of **1** with 10 eq. of *N*-octadecyl-2-((2-oxo-2-phenylethyl)thio)acetamide.

Table 8.1 Experimental and theoretical m/z values for the isotopic distribution of Figure 8.2 and Figure 8.3 in the m/z range between 1280 and 1325.

$m/z_{\text{expt.}}$	ion assignment	formula	$m/z_{\text{theor.}}$	$\Delta m/z$
1302.7	1 _(n=24) + Na ⁺	[C ₅₉ H ₁₀₉ NNaO ₂₆ S] ⁺	1302.7	0.0
1303.7	2 _(n=23) + Na ⁺	[C ₅₇ H ₁₀₅ BrN ₂ NaO ₂₄] ⁺	1303.6	0.1
1291.7	2' _(n=22) + Na ⁺	[C ₅₅ H ₁₀₁ BrN ₂ NaO ₂₃ S] ⁺	1291.6	0.1
1317.7	3 _(n=23) + Na ⁺	[C ₅₆ H ₉₉ F ₅ N ₂ NaO ₂₅] ⁺	1317.6	0.1
1296.5	4 _(n=22) + Na ⁺	[C ₅₄ H ₁₀₀ BrNNaO ₂₃ S ₂] ⁺	1296.5	0.0
1285.9	5 _(n=20) + Na ⁺	[C ₆₃ H ₁₂₆ N ₂ NaO ₂₂] ⁺	1285.9	0.0
1317.9	5' _(n=20) + Na ⁺	[C ₆₃ H ₁₂₆ N ₂ NaO ₂₂ S] ⁺	1317.8	0.1

Indeed, inspection of Figure 8.2 (bottom) confirms the successful formation of **4** and the characteristic isotopic pattern of bromine is again a clear indication of the successful reaction between starting material and thiolate. It should be noted that the raw mixture contains – in equilibrium – the disulfide **4** and, via reductive cleavage, the corresponding thiols. The depicted mass spectrum was obtained after addition of a small amount of hydrogen peroxide and the disulfide reduction was indeed reversed, yet at the expense of a slightly increased baseline noise. The experimental and theoretical m/z values of all shown species in Figure 8.2 are presented in Table 8.1 and are in excellent agreement with each other. The solution based experiments have demonstrated the simple and highly efficient one-pot coupling of amines, hydroxylamines and thiols to photogenerated thioaldehydes at ambient temperature. However, the technique should not be proposed as a novel *click* procedure as it involves an extremely reactive intermediate that translates into a rather limited selectivity and orthogonality. The current strategy is thus not the



Scheme 8.2 Synthesis of a FAS-functionalized silane. Reagents: ethyl chloroformate, triethylamine, 3-(triethoxysilyl)propan-1-amine, THF.

system of choice if a selective coupling to a substrate with a diverse set of chemical functionalities is targeted. The full strength of the light-directed functionalization methodology is evidenced when the reaction is performed with a mono-functional (amine, thiol, or hydroxylamine) substrate that incorporates additionally only moieties (e.g., hydroxy, carboxy, ether, amide or ester) that have been previously found to be essentially inert to the presence of thioaldehydes.^[327,328,331] If the selectivity issue has been taken into consideration, one can benefit from a highly efficient one-pot *in situ* coupling procedure that enables the spatially constrained grafting of molecules onto surfaces to produce molecular patterns. The synthetic route towards a photoreactive FAS surface linker is technically simple and is achieved at low cost (see Scheme 8.2). Surfaces were decorated with photoactive groups by treating activated silicon wafers with the obtained FAS-silane. Subsequent irradiation for 1 hour at 355 nm was performed by employing a shadow mask in the presence of degassed solutions of 2-(4-bromophenyl)ethanamine (a), mPEG-amine (b), and (4-bromophenyl)methanethiol with DIPEA (c), respectively. The locally constrained surface modification was confirmed via imaging time-of-flight secondary-ion mass spectrometry (ToF-SIMS), which is an extremely surface sensitive method that does not require molecule-specific tags while still providing excellent imaging capabilities (lateral resolutions of less than 100 nm have been reported).^[190,196,199] By comparison to desorption electrospray ionization (DESI), which is another emerging technique to perform imaging mass spectrometry, it allows also for the mapping of the chemical composition of solid substrates that are strongly bound (e.g., covalently attached) to the surface.^[190] A detailed comparison of the different surface sensitive mass spectrometric techniques may be found in the characterization Chapter 3. The harsher ionization conditions of SIMS induce a stronger fragmentation of surface species leading to an often challenging interpretation of the resulting mass spectra. Therefore, it is beneficial to base the composition analysis on fragments that are unambiguously detected by ToF-SIMS, such as bromine compounds with their inherent isotopic pattern. Figure 8.4a depicts the composition analysis of the surface after photoconjugation with 2-(4-bromophenyl)ethanamine; the shadow mask structures were reproduced with a good spatial resolution between irradiated and non-irradiated areas. The same irradiation sequence can also be applied for the locally constrained immobilization of poly(ethylene) glycol, which is a non-toxic

confirmed the successful immobilization by identification of several characteristic^[332] poly(ethylene)glycol mass fragments CH_3O^+ , $\text{C}_2\text{H}_4\text{O}^+$, $\text{C}_2\text{H}_5\text{O}^+$ (in positive ion mode) and CH_3O^- , $\text{C}_2\text{H}_3\text{O}^-$, $\text{C}_2\text{H}_2\text{O}_2^-$ (in negative ion mode, see Figure 8.4b) in the irradiated area. Another photocoupling procedure investigated herein involves the formation of disulfides by reaction of an FAS surface with thiolates e.g., (4-bromophenyl)methanethiol in the presence of DIPEA. Indeed, mass fragments that are characteristic for the disulfide (S_2^- , not shown) and for the bromine containing thiol (Br^- , see Figure 8.4c) were identified via imaging mass spectrometry only in the irradiated area. Consequently, the current approach enables the preparation of locally constrained disulfide decorated surfaces – the potential of which to efficiently anchor (bio)molecules bearing pendant thiols or disulfides has been recently reported^[333] – via a facile one-step irradiation procedure. An alternative conjugation technique that has found wide application is based on the rapid formation of oximes under nucleophilic catalysis.^[334] Chapter 5 has already demonstrated the ability to additionally confer spatial control to oxime ligation by utilizing the photorelease of aldehyde functionalities from the *o*-nitrobenzyl photoprotecting group.^[40] Secondary photolysis or side-reactions based on the concomitant formation of a nitroso moiety are, however, disadvantages. The alternative approach described here enables the rapid and quantitative oxime formation from photogenerated thioaldehydes with hydroxylamines without the need for a catalyst. In detail,

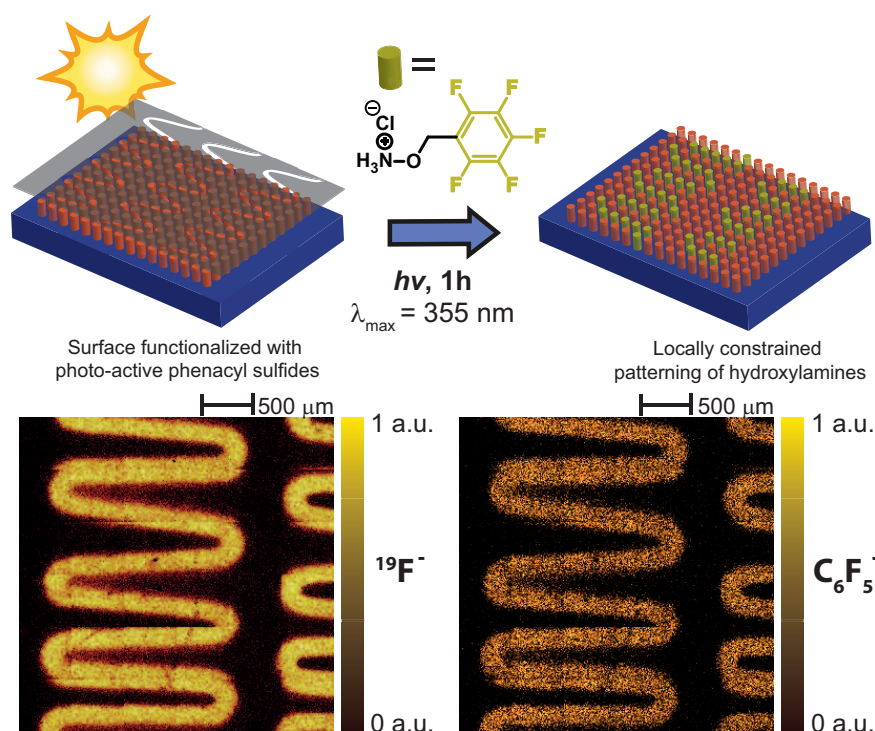


Figure 8.5 ToF-SIMS composition analysis of fluorine and C_6F_5^- species of silicon wafers patterned with O-(2,3,4,5,6-pentafluorobenzyl)-hydroxylamine hydrochloride in degassed acetonitrile.

a freshly prepared FAS functionalized Si-wafer was irradiated in the presence of O-(2,3,4,5,6-pentafluorobenzyl)hydroxylamine hydrochloride at 355 nm for 1 hour utilizing a shadow mask in degassed acetonitrile. In this case again, the substrate was efficiently immobilized in a pattern corresponding to the mask features as demonstrated by the detection of F⁻ and C₆F₅⁻ (see Figure 8.5).

8.5 Conclusions

In summary, it was demonstrated by electrospray ionisation mass spectrometry (ESI-MS) that photogenerated thioaldehydes can be efficiently trapped by amines, hydroxylamines, and thiols. The one-step coupling procedure can be translated to the fabrication of patterned silicon surfaces and requires only minimum (synthetic) effort. Site-specific attachments of a polymer and small molecules bearing pendant amines, hydroxylamines, and thiols were evidenced by imaging time-of-flight secondary-ion mass spectrometry (ToF-SIMS). The surface patterns are constructed without a catalyst, at ambient temperature and by mild irradiation at 355 nm. Functionalities that are inherently present in many substrates can be utilized, thus avoiding expensive synthetic modifications. The technology presented herein provides a simple and cost efficient methodology for the direct generation of functional patterned substrates.

9

Three-Dimensional Microscaffolds Exhibiting Spatially Resolved Surface Chemistry*

The results described in the present chapter stem from a collaboration within the context of a larger research program. In particular, the experimental work of preparing and encoding the surfaces was carried out by Benjamin Richter (AG Bastmeyer) while the organic and polymer synthesis was carried out by the candidate in close collaboration with Dr. Guillaume Delaittre (AG Barner-Kowollik). Figure 9.1 and Figure 9.2 have been prepared by Dr. Delaittre, Figure 9.3 and Figure 9.7 by the candidate, while all other Figures are from B. Richter.

9.1 Abstract

Materials applications have always strongly relied on mechanical properties. Nevertheless, in the last decade the chemical properties of materials – in particular at interfaces and surfaces – have increasingly gained importance. Producing materials with a uniform surface chemistry is usually straightforward yet challenges appear when partial, and particularly spatially defined, functionality is required. Diverse

* Parts of this Chapter were reproduced from Ref. 335 by permission of the John Wiley and Sons.

techniques have been developed and employed for two-dimensional (2D) chemical micro- and nanopatterning,^[336] e.g., photolithography,^[4,337] micro-contact printing,^[338] nanoimprint lithography,^[339] electron beam lithography,^[340] or dip-pen nanolithography.^[341] For more complex applications, three-dimensional (3D) materials that are well-defined at the micro- to the nanoscale are required. Herein it is shown that by combining two-photon polymerization with an efficient surface photochemistry, also amenable to two-photon activation, it is possible to generate structurally complex 3D microstructures with 3D resolved chemical patterns. Specifically microscaffolds with lattice constants of 10-20 microns are patterned with multiple protein ligands and polymers with a resolution close to one micron using a phototriggered cycloaddition.

9.2 Introduction

While macroscopic 3D printing is currently becoming mainstream, only very few techniques are available in research laboratories to produce finer 3D structures. Direct laser writing (DLW) is one that has recently emerged. DLW relies on the multi-photon absorption of photoresists to yield complex microstructures, usually via a two-photon polymerization process.^[7,8,342] While the competition for the highest resolution is strong,^[343-345] only very few studies reported on the covalent manipulation of the surface chemistry of DLW-produced materials and certainly not in a spatially defined way.^[346] Controlling this aspect would allow for the first time a genuine chemical patterning in 3D. Until now, multi-photon patterning of hydrogel films (0.5-1.5 mm thickness)^[347] was arguably the method which had reached the highest degree of spatial chemical resolution, yet control over the shape and mechanical properties of such materials remains poor. It is for instance not possible to generate freestanding structures with overhanging features and the accessible range of elastic moduli is reduced. Applications of these patterned hydrogels are therefore typically limited to biomaterials for cell biology and tissue engineering.^[348-350] Using DLW certainly enables a significantly higher degree of control over 3D architectures and mechanical properties. Recently a method was reported where two different photoresists, thereby providing two distinct surface properties, were combined to produce microstructures with well-controlled heterogeneous surface properties such as protein/cell adhesion or repellency.^[351] The first photoresist was used to construct the main framework which was immersed in the second photoresist that was subsequently exposed on top of the framework at predefined positions. However, the aforementioned method yields topographically inhomogeneous features which can be non-desirable in a number of applications. In a similar way, Fourkas and coworkers had previously employed two photoresists

to produce binary 3D structures of which one domain could be chemically modified.^[352] Herein, a single inorganic-organic hybrid photoresist, Ormocomp, is used which possesses elastic properties^[353] and is amenable to the surface grafting of reactive functional handles by a simple silanization step, owing to the presence of siloxane bonds. Via this method a homogeneous topography can be maintained without discernible feature size changes of the DLW-made microstructure.

9.3 Experimental Part

Synthesis of maleimide-functionalized poly(oligo(ethylene glycol) methacrylate) (Mal-POEGMA)

0.0410 g (414 μmol , 1.0 eq.) CuCl was introduced into a 10 mL Schenk tube which was sealed with a septum. The tube was subsequently evacuated and back-filled with nitrogen (5 cycles). In a 5 mL round-bottom flask, 1.4999 g (5.0 mmol, 12.5 eq.) OEGMA, 0.1428 g (399 μmol , 1.0 eq.) Fur-Mal-ATRP, and 0.1256 g (804 μmol) Bpy were dissolved in 1.91 mL ethanol. The mixture was deoxygenated by bubbling nitrogen over a period of one hour, after which it was introduced into the Schlenk tube via a cannula. The tube was directly after complete transfer placed in an oil bath at 60 °C for 165 min. The polymerization was stopped by cooling the tube and exposing its content to air (conversion determined by ^1H NMR: 96 %). After precipitation in diethyl ether and drying, the polymer was re-dissolved in toluene and the resulting solution was refluxed during 6 h, after which toluene was evaporated and the title compound obtained as a pale yellow oil (0.5843 g) after drying under vacuum overnight. $M_n[\text{SEC}] \approx 7000 \text{ g}\cdot\text{mol}^{-1}$, PDI = 1.29; $M_n[^1\text{H NMR}] \approx 6600 \text{ g}\cdot\text{mol}^{-1}$ (based on the comparison of the signal integrals of the maleimide end group vinyl protons at 6.7-6.8 ppm and the repeat unit ester protons at 3.95-4.25 ppm).

Phototriggered Test Experiments in Solution

Photoenol reaction with Mal-Bt in DMF

0.7 mg (0.29 μmol , 1.0 eq.) of **1** and 0.38 mg (0.84 μmol , 2.9 eq.) Mal-Bt were dissolved in dry DMF (1 mL) and aliquoted into a headspace vial (Pyrex, diameter 20 mm), which was crimped air-tight using SBR seals with PTFE inner liner. The solution was deoxygenated by purging with nitrogen for 2 min. The flask was subsequently irradiated for 2 hours by revolving around a compact low-pressure fluorescent lamp (Arimed B6, Cosmedico GmbH, Stuttgart, Germany) emitting at 320 nm (± 30 nm, 36 W, the emission spectrum of the employed compact low-

pressure fluorescent lamp and the UV-Vis spectrum of the photoenol species is depicted in Figure 6.1) at a distance of 40-50 mm in a custom-built photoreactor (see Figure 11.1). The solvent was evaporated under vacuum after the reaction, THF (0.5 mL) was added to the vial, and the solution was analyzed via SEC/ESI-MS (Figure 9.3 and Table 9.1).

Photoenol reaction with Mal-BG in DMF

0.3 mg (0.17 μmol , 1.0 eq.) of **1** and 0.30 mg (0.60 μmol , 3.5 eq.) Mal-BG were dissolved in dry DMF (1 mL) and aliquoted in a headspace vial (Pyrex, diameter 20 mm), which was crimped air-tight using SBR seals with PTFE inner liner. The solution was deoxygenated by purging with nitrogen for 2 min. The flask was subsequently irradiated for 2 hours by revolving around a compact low-pressure fluorescent lamp (Arimed B6, Cosmedico GmbH, Stuttgart, Germany) emitting at 320 nm (± 30 nm, 36 W, the emission spectrum of the employed compact low-pressure fluorescent lamp and the UV-Vis spectrum of the photoenol species is depicted in Figure 6.1) at a distance of 40-50 mm in a custom-built photoreactor (see Figure 11.1). The solvent was evaporated under vacuum after the reaction, THF (0.5 mL) was added to the vial, and the solution was analyzed via SEC/ESI-MS (Figure 9.7 and Table 9.2).

Fabrication and Functionalization of 3D Microscaffolds

3D microscaffold fabrication

For the fabrication of the 3D structures a commercially available DLW system is used (Photonic Professional, Nanoscribe GmbH) equipped with a 100 \times , NA (numerical aperture) = 1.4 oil-immersion objective. Typical average laser powers in the DLW process were 10-20 mW (in front of the microscope lens) and the typical piezoscanning velocity was 100 $\mu\text{m s}^{-1}$, leading to a typical total writing time of ca. 3 min for all scaffolds shown in Figure 9.5 to Figure 9.9. To enhance the adhesion of the microscaffolds to the glass substrate surface, plasma-cleaned coverslips were treated with 3-(trimethoxysilyl)propyl methacrylate (1 mM in toluene) for 1 h, rinsed in water, and dried with nitrogen. Ormocomp photoresist (already containing a photoinitiator) was drop-cast onto the coverslip and the 3D microscaffolds, including marker structures, were fabricated. After exposure, the scaffolds were developed in a 1:1 mixture of 4-methyl-2-pentanone and isopropyl alcohol, rinsed in isopropyl alcohol, and dried with nitrogen gas.^[351]

Photoenol functionalization of DLW microscaffolds

The microscaffold-bearing coverslips were plasma cleaned (10 min, argon gas) and covered with a solution of photoenol-functionalized silane Si-PE (1 mM in toluene). After 1h the coverslips were cleaned with water and dried with nitrogen gas.

Two-photon laser covalent surface functionalization of photoenol-functionalized DLW microscaffolds

The coverslips were placed in a home-built direct laser writing system consisting of a Ti:sapphire oscillator (Spectraphysics MaiTai HP) pumping an optical parametric oscillator (Spectraphysics Inspire HF100), an electro-optical modulator, a 100 \times , NA = 1.4 oil-immersion objective (Leica HCX PL APO 100 \times /1.4-0.7 OIL CS), a piezo-actuator stage (Physik Instrumente P-527.3CL), and a camera.^[354] A drop of a solution of maleimide derivative (0.1 and 0.6 mM in DMF, for Mal-Bt and Mal-BG, respectively) is then deposited on the scaffold. By using a ring made of PDMS it is ensured that the solution does not flow and evaporate too fast. The marker structure (Figure 9.5) was used to align the coverslips in the lateral plane. The vertical position was automatically adjusted by finding the glass-solvent interface using a confocal detection of reflected laser light. After the writing process, the coverslips were washed in DMF for at least 30 min, rinsed in isopropyl alcohol, and dried with nitrogen.

Imaging of Molecular Patterns by Staining through Protein Conjugation

Passivation

In order to prevent unspecific adsorption of the staining protein molecules and to ensure a reliable staining, the parts which were not irradiated during the patterning step were subsequently passivated. For the samples shown in Figure 9.4 and Figure 9.6 a covalent surface passivation was performed and obtained by flood irradiation. A solution of Mal-PEG (Figure 9.4) or POEGMA (Figure 9.6) (1 mM in DMF) was dropcast onto the coverslip and irradiated for 2 h with UV light (Hönle UVAHAND 250). The coverslips were subsequently washed in DMF for at least 30 min, rinsed in isopropyl alcohol, and dried with nitrogen. For the sample shown in Figure 9.8, no passivation step was necessary since the microscaffold was entirely functionalized with biotin and benzylguanine. Interestingly, for the microscaffolds depicted in Figure 9.9 passivation of the non-irradiated areas was possible by a homogeneous non-covalent method, i.e., using a passivating copolymer that binds onto the whole glass coverslip and microscaffold. In other words, the biotin and benzylguanine motifs were still accessible for complexation and reaction, respectively,

when buried in passivating poly(ethylene glycol) strands. For that purpose the glass coverslip was covered with a solution of PEG-PPG-PEG copolymer (Pluronic[®] F-108) (10 % w/w in water) for 1 h at room temperature.

Staining

For the (strept)avidin-mediated staining of the biotinylated patterns (red fluorescence), the samples were washed three times for 10 min in phosphate buffer saline (PBS), and incubated for 30 min at ambient temperature with Av-Rho or SA_v-Cy3 (1:100 in PBS). The samples were then washed three times for 10 min in PBS. To prepare the SNAP-GFP solution for the staining of the benzylguanine patterns a stock solution (46.4 mM) was taken from the -80 °C freezer and mixed with hepes buffer saline (HBS) to obtain a 4 mM concentration of SNAP-GFP. To discard eventual aggregates, the 4 mM solution was centrifugated for 10 min at 4 °C at 13000 rpm. The supernatant was subsequently mixed in a 1:1 ratio with Pluronic[®] F-108 (10 % w/w in water). Pluronic[®] F-108 prevents aggregation during the incubation, similarly to the case of bovine serum albumin for immunofluorescence staining of cells. The samples were washed three times for 10 min in HBS, incubated for 2 h at ambient temperature with the SNAP-GFP/Pluronic[®] F-108 solution, washed three times for 10 min in HBS, fixed for 10 min with 4 % paraformaldehyde in PBS and washed three times for 10 min in PBS. The coverslips were finally immersed in Mowiol (Hoechst) containing 1 % n-propyl gallate for fluorescence confocal microscopy.

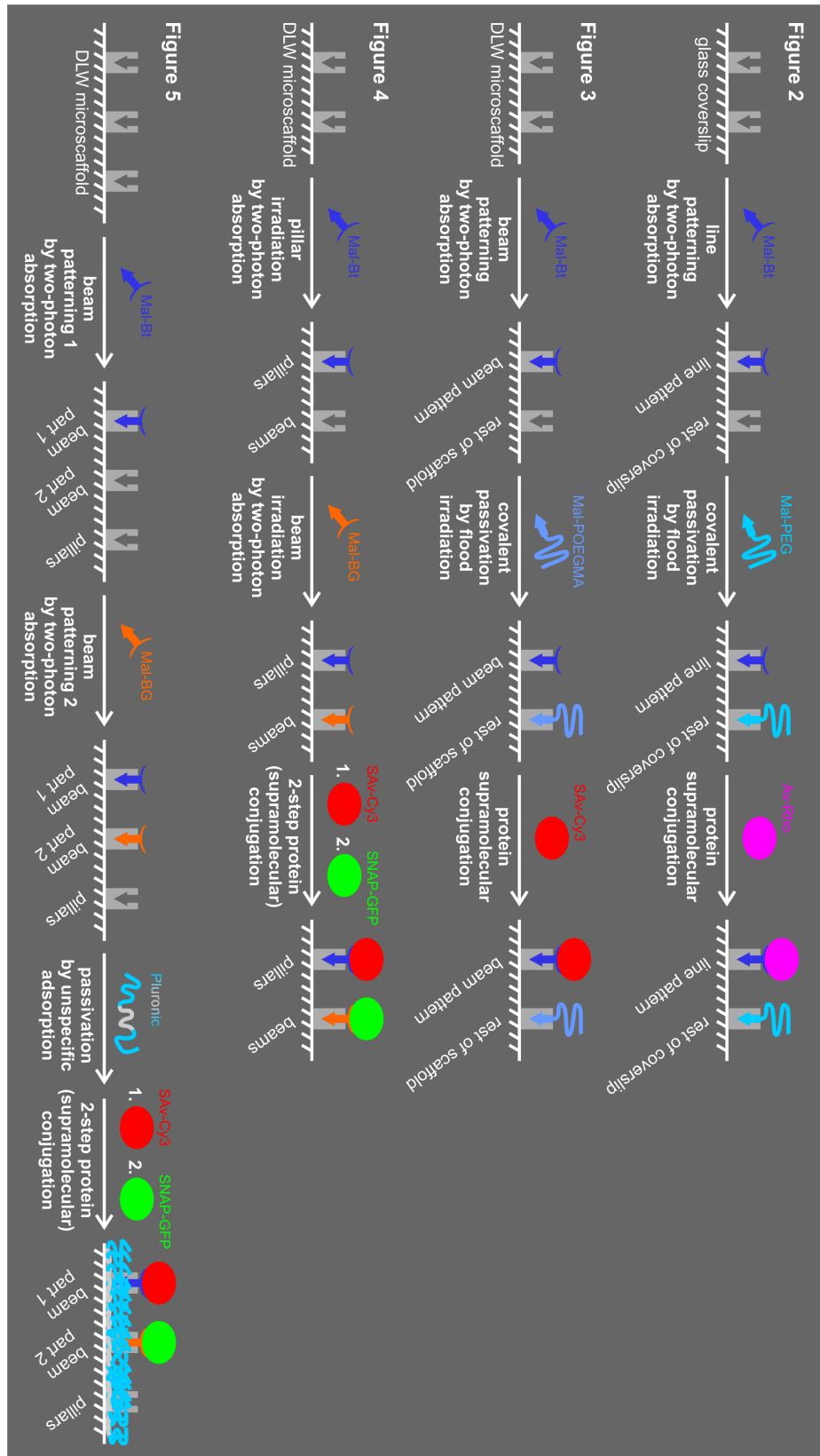


Figure 9.1 Schematic representation of the experimental sequences involved in the production of the different patterns displayed in the main text. Note that for the sake of simplicity washing steps are not represented.

9.4 Results and Discussion

One of the few possibilities, if not the only, to trigger the reaction of the functional handles present at the surface of the material only at pre-determined locations is to employ photoreactive groups that can be involved in a multi-photon – at least a two-photon – absorption process and to utilize an experimental setup similar to that of DLW, i.e., a femtosecond-pulsed laser. Furthermore, considering the short timeframe for light activation inherent to the scanning nature of this method, the photochemistry involved should be rather efficient. It has been recently shown, in solution but also on flat surfaces, that phototriggered cycloadditions are sufficiently effective.^[271,328] Particularly, 2-methylbenzaldehyde derivatives are latent dienes (photoenols, PE) that can be activated by UV light to react quantitatively with activated alkenes such as maleimides in a Diels-Alder cycloaddition.^[3,144] The idea was thus to homogeneously coat laser-writtenOrmocomp microscaffolds with latent photoenol molecules using the silane derivative Si-PE (Figure 9.2a-b) and to trigger the reaction with maleimides at specific locations by simultaneous absorption of two visible-frequency photons (Figure 9.2b-c). In a first phase it was necessary to assess the behavior of the photoenol moiety in two-photon absorption. Therefore, a flat glass coverslip was silanized with Si-PE that was subsequently covered with a solution of maleimide-functionalized biotin (Mal-Bt, Figure 9.2), allowing for further staining by supramolecular conjugation with fluorescently-labeled (strept)avidin. The reactivity of Mal-Bt towards the photoenol moiety was first assessed in a solution experiment (Figure 9.3 and Table 9.1). Biotin patterning was thus performed by femtosecond-pulsed irradiation at various wavelengths (560-700 nm, intervals of 20 nm). The biotin patterns were revealed by dipping the glass slide in a solution of rhodamine-labeled avidin (Av-Rho) and observed by confocal fluorescence microscopy (Figure 9.4a). Passivation of the non-biotinylated areas – to avoid non-specific protein adsorption – was achieved by covering the glass slide with a solution of maleimide-functionalized poly(ethylene glycol) (Mal-PEG) and flood irradiation using a standard laboratory UVA lamp (refer to Chapter 9.3 and Figure 9.1 for the full experimental procedure). For each wavelength the average laser power was varied from 0 to 19.75 mW (intervals of 0.25 mW, columns from the bottom right corner to the top left one) and for each laser power, i.e., within each column, the line spacing was varied from 5 μm to 0.25 μm . It was observed that for each wavelength the maximum of fluorescence was reached at approx. 5 mW. For yet higher laser powers (in the three upper column groups) the fluorescence intensity does not significantly increase. The smallest line spacing that could be resolved under the microscope after staining was 2 μm (Figure 9.4b), i.e., the maximal experimental resolution lies between 1 and 2 microns. It should be noted that

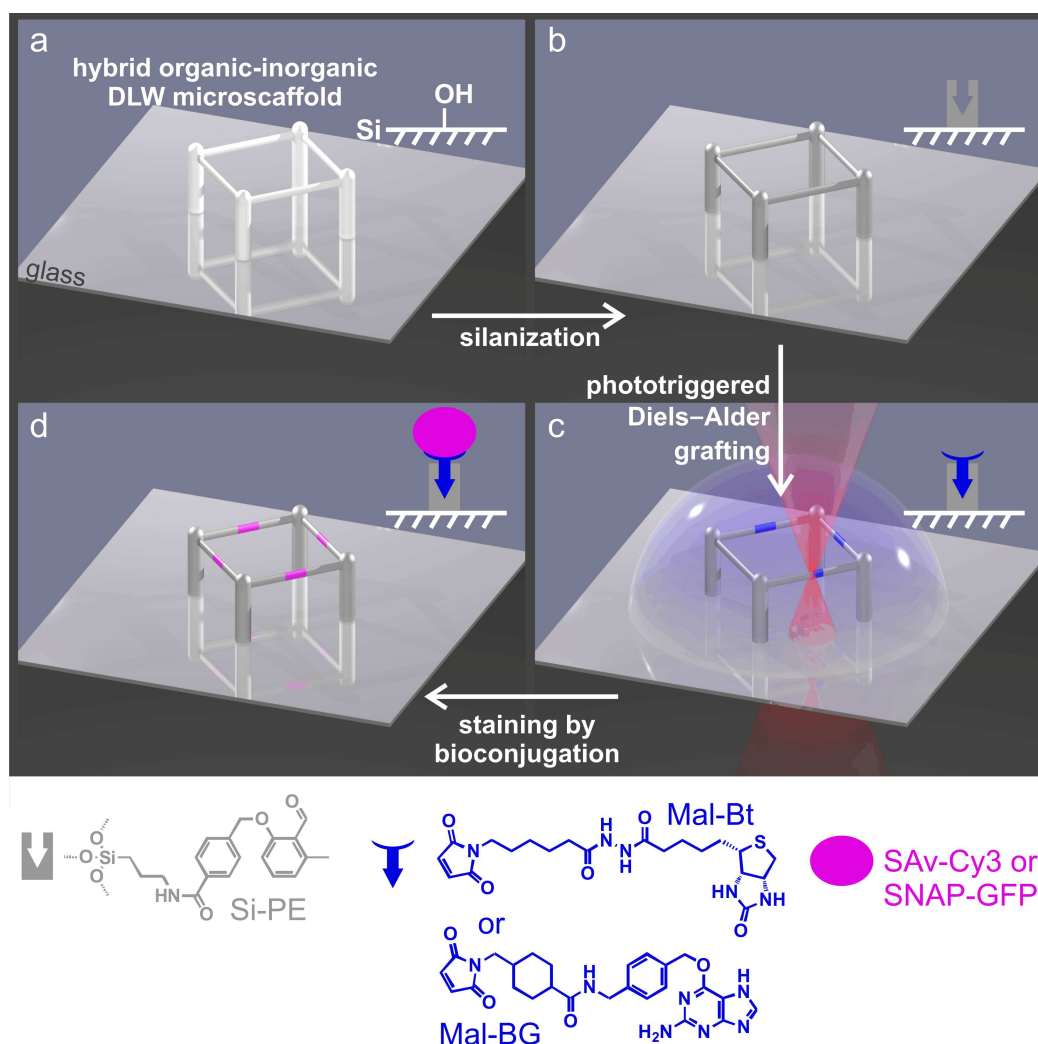


Figure 9.2 General chemical strategy towards the spatially controlled photochemical functionalization of three-dimensional organic-inorganic scaffolds. A three-dimensional micro scaffold made of Ormocomp is activated by plasma cleaning under argon (a) and covalently coated with photoenol moieties by silanization (b). The silanized micro scaffold is covered with a solution of maleimide derivative (Mal-Bt, maleimide-biotin or Mal-BG, maleimide-benzylguanamine). Maleimides are locally covalently attached to the scaffold by laser-triggered Diels-Alder cycloaddition (c). Finally the molecular 3D patterns are stained by non-covalent or covalent bioconjugation with fluorescent proteins (Cy3-labeled streptavidin, SAv-Cy3 or O^6 -alkylguanine-DNA alkyltransferase-green fluorescent protein fusion protein, SNAP-GFP, respectively) (d).

the photopatterning resolution does not significantly depend on the laser power, as opposed to that of the DLW process.^[9] Indeed, photoisomerization and coupling of reagents immobilized on a solid substrate occurs in the former, while a polymerization mechanism involving diffusion of the reactive centers (radicals) from the laser focus point through the resist is at work in the latter. Figure 9.4a evidences that the photoenol moiety could be activated – and subsequently react in a Diels-Alder cycloaddition – by a two-photon absorption process since its UV-Vis absorption spectrum shows no absorbance at the employed laser wavelengths, i.e., between

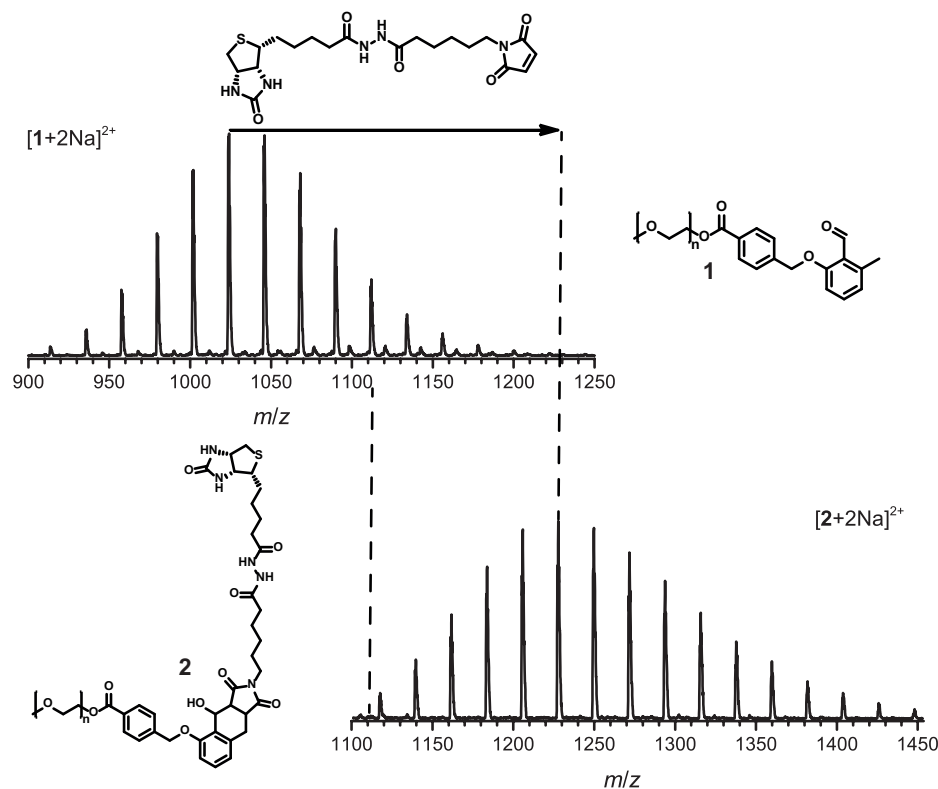


Figure 9.3 SEC/ESI-MS spectra of the phototriggered reaction of **1** with Mal-Bt in DMF to yield **2**. ESI-MS analysis confirmed full conversion within 2 h irradiation time ($\lambda_{\text{max}} = 320$ nm).

Table 9.1 Experimental and theoretical m/z values for the peak of highest intensity in Figure 9.3 in the m/z range between 900 and 1450.

$m/z_{\text{expt.}}$	ion assignment	formula	$m/z_{\text{theor.}}$	$\Delta m/z$
1045.6	1 + 2Na^{2+}	$[\text{C}_{97}\text{H}_{176}\text{Na}_2\text{O}_{44}]^{2+}$	1045.6	0.0
1227.3	2 + 2Na^{2+}	$[\text{C}_{113}\text{H}_{197}\text{N}_5\text{Na}_2\text{O}_{47}\text{S}]^{2+}$	1227.2	0.1

560 and 700 nm (see Figure 6.1). For an optimization of the patterning process it is important to determine the most efficient wavelength for surface patterning. Therefore, for each wavelength, the fluorescence intensity obtained after patterning at constant average laser power (4.75 mW) and staining was plotted. Figure 9.4c undoubtedly evidences that the two-photon-triggered surface cycloaddition/fluorescence staining sequence yield is well correlated to the UV absorption spectrum of the photoenol plotted on a 2λ scale. Consequently, the following 3D patterning experiments were performed at a wavelength of 640 nm, which in two-photon absorption would be equivalent to the maximum of absorption of the photoenol moiety in one-photon absorption. To demonstrate that the present approach could be utilized for 3D patterning, an Ormocomp microscaffold consisting of pillars (height 10 μm ; lateral lattice constant 20 μm) and connecting beams on two distinct vertical level separated by 5 μm (axis-to-axis distance) (see Figure 9.5a) was initially

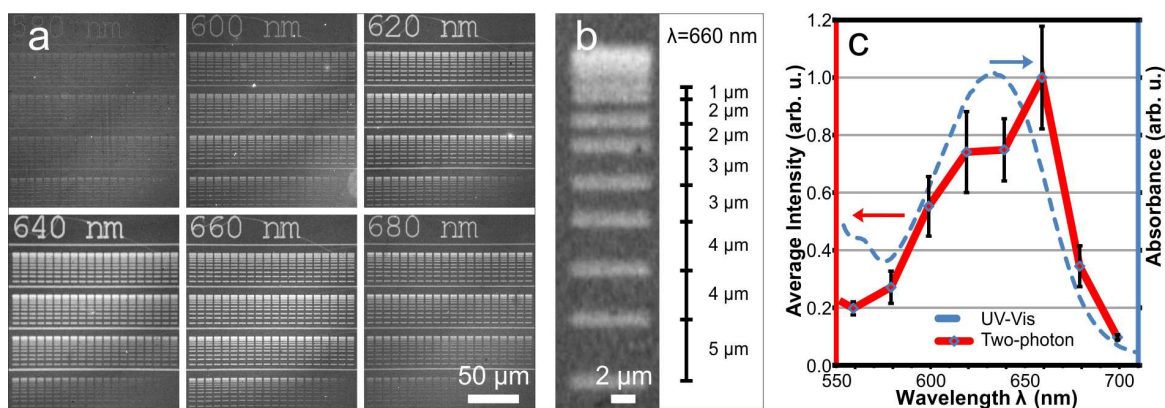


Figure 9.4 Confocal fluorescence image of a two-dimensional functionalized glass coverslip by two photon triggered Diels-Alder cycloaddition at different wavelengths (580-680 nm) and subsequent fluorescently-labeled protein supramolecular conjugation (Av-Rho) (a). Magnification of the pattern shown in (a) for $\lambda = 660$ nm and an average laser power of 4.75 mW (b). The shortest spacing that is clearly distinguishable between two lines is of 2 μm . Comparison between the fluorescence intensity obtained during the Diels-Alder cycloaddition/bioconjugation sequence on a glass coverslip using different activation wavelengths (see Figure 9.4a) (red full line) and the UV-Vis absorption spectrum of the photoenol precursor plotted on a 2λ scale (blue dashed line) (c).

fabricated by DLW. After silanization with Si-PE, the microscaffold was covered with a solution of Mal-Bt and irradiated by scanning ($200 \mu\text{m s}^{-1}$) with the pulsed laser at 5 mW on predetermined areas of the beams in such a way that the irradiated parts could not be located below or above one another, in order to demonstrate the fully three-dimensional character of the patterning. The remaining areas of the microscaffold were passivated by flood irradiation of the glass slide covered with a poly(oligo(ethylene glycol) methacrylate) bearing a maleimide moiety at its chain end (Mal-POEGMA, refer to Chapter 9.3 and Figure 9.1). After staining with

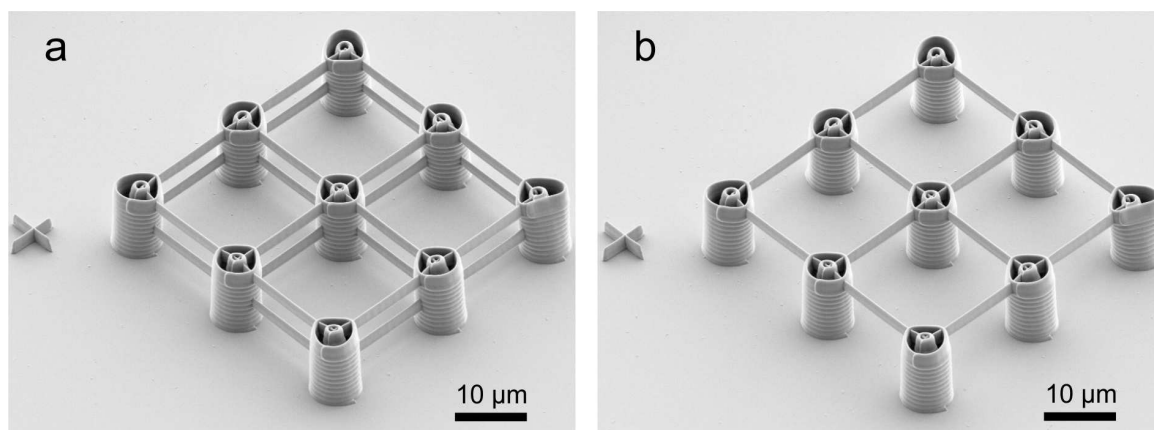


Figure 9.5 Scanning electron microscope (SEM) images of the scaffolds used for patterning experiments described and displayed in the main text: Figure 9.6 (a), Figure 9.8 and Figure 9.9 (b). The marker used to align the microscaffolds prior to the two-photon patterning can be seen on the left side of each image.

red fluorescent dye-labeled streptavidin (SAv-Cy3), the microstructure was imaged by confocal fluorescence microscopy (Figure 9.6a). It first appears that there is no unwanted functionalization of the beams in the axial direction (z). In relation to this aspect, Figure 9.6b depicts the focal intensity distributions of the 640 nm laser

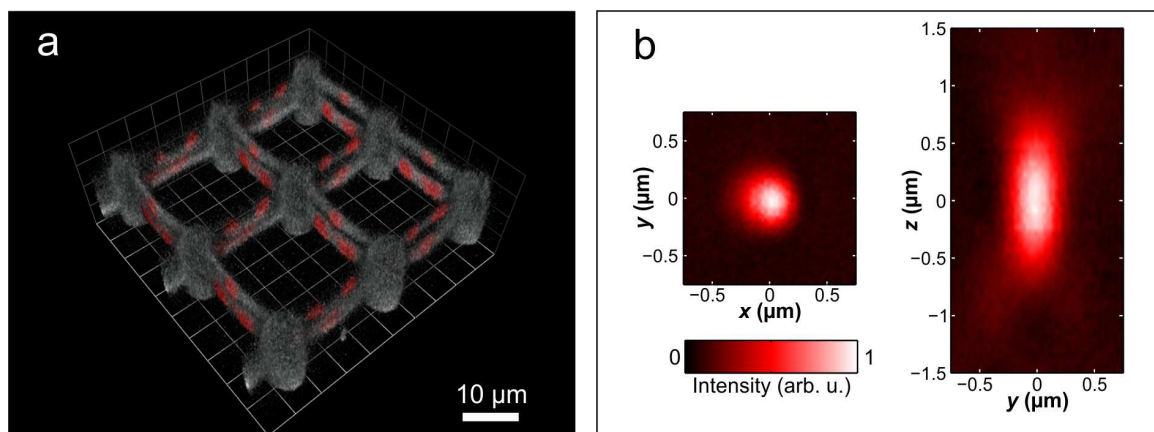


Figure 9.6 3D reconstruction of a confocal image stack depicting a three-dimensional DLW microscaffold patterned with biotin motifs on the beams and stained with SAv-Cy3 (red) (a). The beams are written in two distinct heights and functionalized alternatively in the axial direction to evidence the 3D character of the patterning, demonstrating the advantage of a two-photon process. The autofluorescence of the Ormocomp structure is shown in white. A scanning electron microscopy (SEM) image of the microscaffold and the 3D reconstruction of a confocal image stack of a wider patterned area can be seen in Figure 9.5a and Figure 9.10a, respectively (a). Measured intensity profiles of the laser beam used for photopatterning in the xy - and xz -planes ($\lambda = 640$ nm) (b).

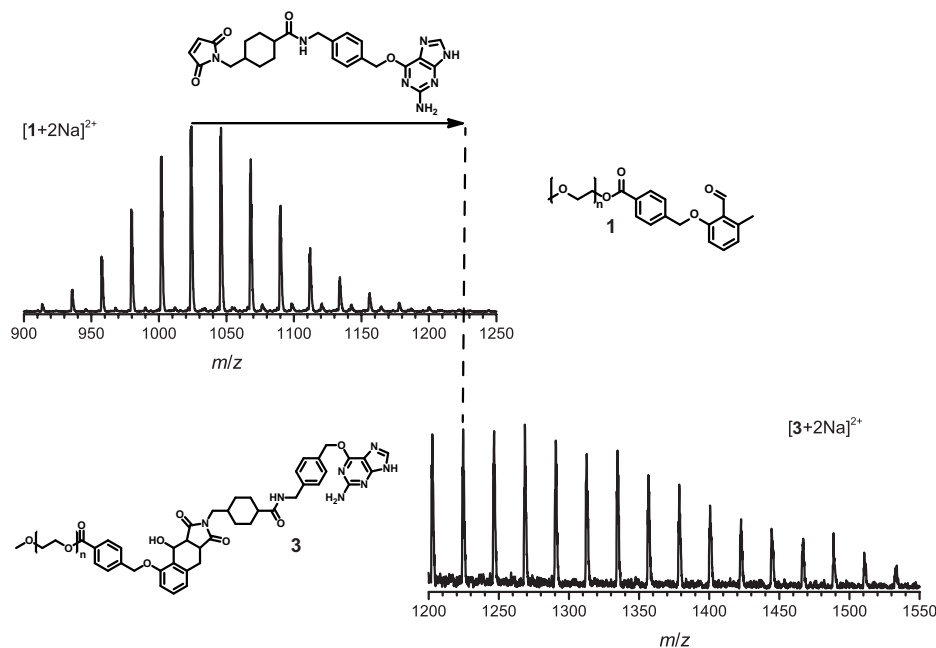


Figure 9.7 SEC/ESI-MS spectra of the phototriggered reaction of **1** with benzylguanine-maleimide in DMF to yield **3**. ESI-MS analysis confirmed full conversion within 2 h irradiation time ($\lambda_{\max} = 320$ nm).

Table 9.2 Experimental and theoretical m/z values for the peak of highest intensity in Figure 9.7 in the m/z range between 900 and 1500.

$m/z_{\text{expt.}}$	ion assignment	formula	$m/z_{\text{theor.}}$	$\Delta m/z$
1045.6	1 + 2Na ²⁺	[C ₉₇ H ₁₇₆ Na ₂ O ₄₄] ²⁺	1045.6	0.0
1224.1	3 + 2Na ²⁺	[C ₁₁₆ H ₁₉₁ N ₇ Na ₂ O ₄₅] ²⁺	1224.2	0.1

beam measured by scanning over a single gold bead (diameter 100 nm; suspended in pentaerythritol triacrylate) and recording the back-scattered light intensity.^[344] By this means an experimental resolution of about 300 nm in the lateral xy plane and 800 nm in the axial xz plane was determined. For 2D patterning, a lateral resolution between 1 and 2 μm was achieved, which is still in the range of the aforementioned optimal resolution (Figure 9.4a). In 3D chemical features with a lateral resolution of

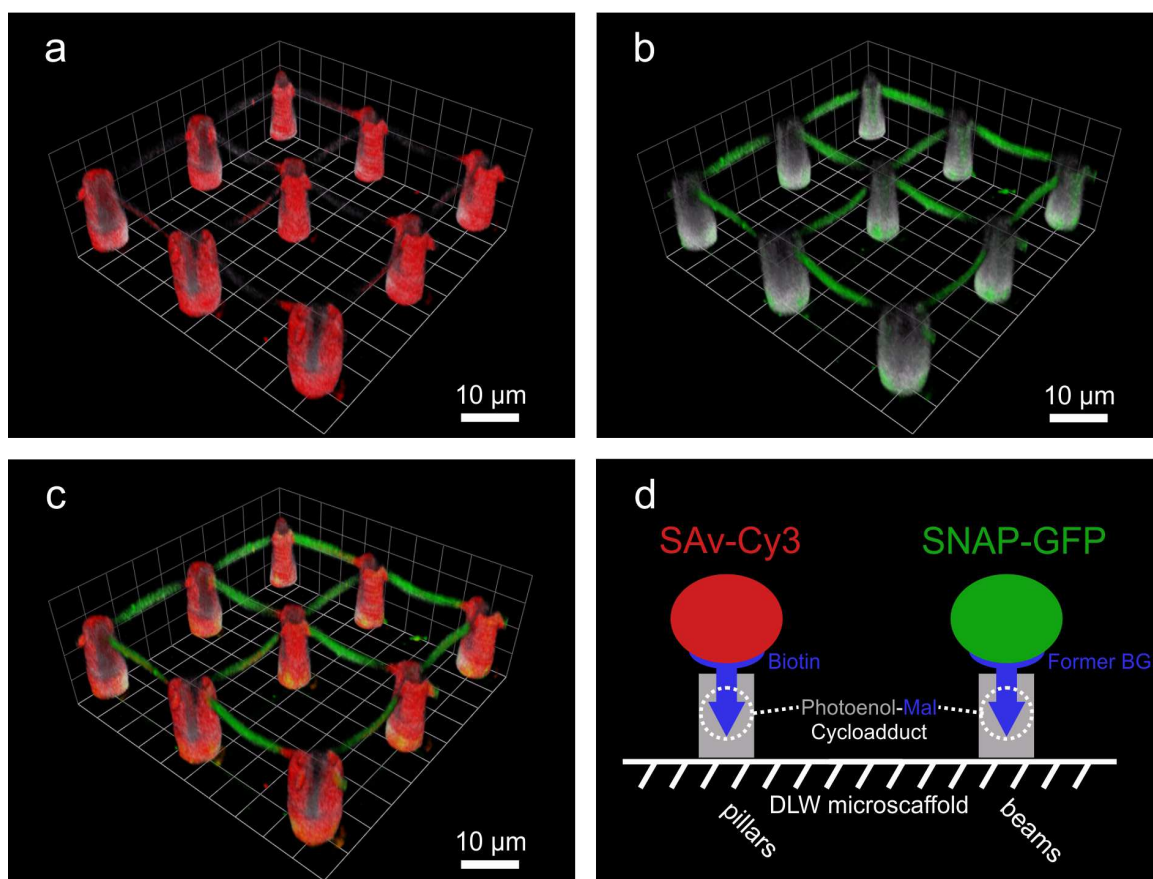


Figure 9.8 3D reconstruction of confocal image stacks representing a three-dimensional DLW scaffold selectively patterned with biotin (stained with SAv-Cy3, red) on the pillars and benzylguanidine (stained by GFP, green) on the beams. The autofluorescence of the Ormocomp structure is shown in white. White and red (a). White and green (note that the autofluorescence of the scaffold on the beams is too low to be detected) (b). Overlay of the red, green, and white channels (c). Schematic representation of the chemical functionalization of the DLW microstructure depicted in a-c (d). A SEM image of the microstructure can be seen in Figure 9.5b.

3 μm corresponding to the length of and the distance between the patterned areas were generated. In the axial direction, the current patterning reaches a resolution of at least 2.5 μm . Indeed, it can be clearly seen that there is no axial contamination of the beams, separated by 2.5 μm from surface to surface (5 μm axis to axis with a vertical dimension of 2.5 μm for each beam). Due to the low refractive index of the solvent used to dissolve Mal-Bt (*N,N*-dimethylformamide, $n_D = 1.430$) it is not possible to reach the aforementioned maximal resolution.^[355] Herein, biotin was used for the purpose of fluorescence imaging in order to provide a proof of concept. For precise applications, and consequently for other maleimide derivatives to be grafted, different solvents possessing a refractive index closer to that of glass, e.g., aromatic and/or halogenated solvents, could be envisaged to dissolve these molecules. In a second phase the possibility of precisely patterning more than one chemical entity in three dimensions was studied. For this purpose an orthogonal binding pair was chosen to avoid cross-contamination during the staining/imaging of the two chemically distinct patterns. A green fluorescent protein (GFP) was produced and fused with a SNAP tag, an enzyme which is able to covalently bind to the alkylated fragment of benzylguanine-containing substrates,^[356] notably surfaces,^[276,357] and employed a commercially available benzylguanine-maleimide derivative (Mal-BG, Figure 9.2) for surface patterning. The reactivity of Mal-BG towards photoenol derivatives was evidenced in solution (Figure 9.7 and Table 9.2). Therefore, the following experimental sequence (refer to Chapter 9.3 and Figure 9.1) was performed: deposition of a drop of Mal-Bt solution on a microscaffold-bearing glass slide (Figure 9.5b), laser

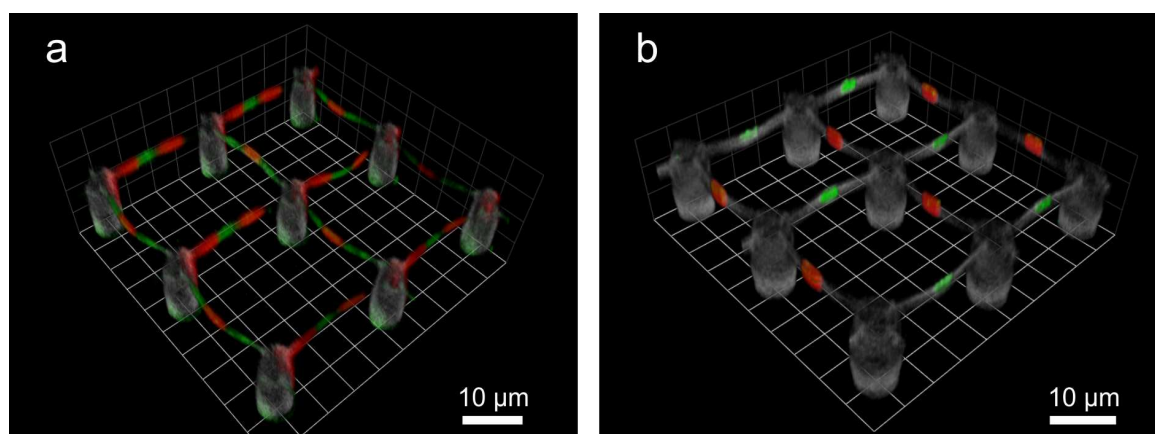


Figure 9.9 Overlay of the 3D reconstruction of confocal image stacks in the white, red, and green channels, depicting the dual functionalization of DLW 3D microscaffold. The beams are functionalized in an alternating fashion with biotin (stained with SAv-Cy3, red) and benzylguanine (stained with SNAP-GFP, green). The 3D reconstruction of a confocal image stack of a wider patterned area can be seen in Figure 9.10b (a). The beams are patterned in a discrete manner, highlighting the ability of precise positioning of multiple functional groups without altering the whole microscaffold surface (b).

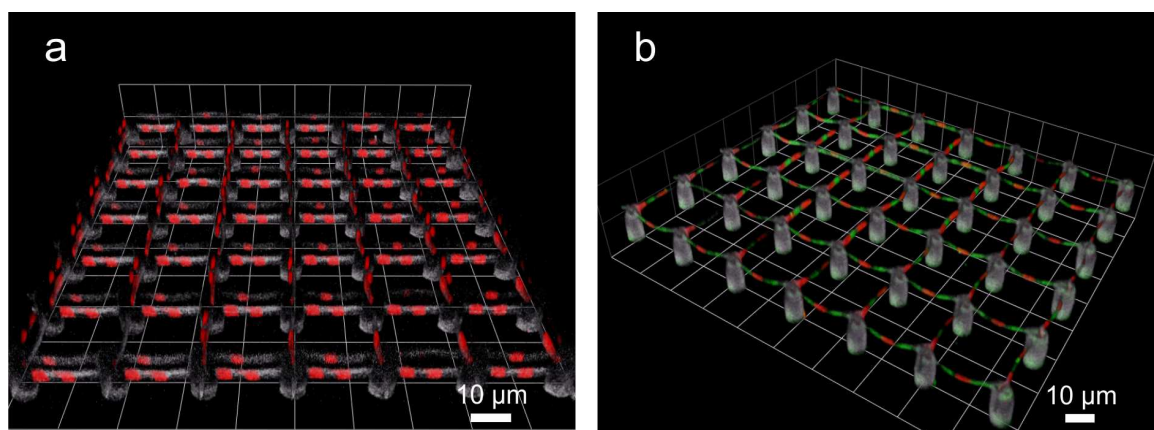


Figure 9.10 3D reconstruction of a confocal image stack depicting the full three-dimensional DLW microstructure patterned with biotin and benzylguanine motifs and stained with SAv-Cy3 and SNAP-GFP from Figure 9.6a (a) and Figure 9.9a (b).

writing of biotin onto the pillars, washing, deposition of a drop of Mal-BG, laser writing of benzylguanine onto the beams, washing, tagging with SAv-Cy3, washing, tagging with SNAP-GFP, and final washing. The 3D reconstruction of the confocal image stacks obtained by acquisition in two different channels – green (500-550 nm, for GFP) and red (580-650 nm, for Cy3) – is shown in Figure 9.8. A well-defined fluorescence pattern was observed with SAv-Cy3 mainly immobilized on the pillars (Figure 9.8a) and SNAP-GFP on the beams (Figure 9.8b). This experiment clearly demonstrates that patterning of multiple molecules, here biotin and benzylguanine, is possible via the herein described technique. In the present case the number of distinct molecules that is possible to investigate is limited since imaging them is rather challenging, notably in terms of fluorescence spectra diversity. Furthermore, in the case of protein immobilization – the present pattern revealing method – additional specific orthogonal binding pairs would be required, for instance affinity tag-based ones such as Ni-NTA/His-Tag^[358] and glutathione-GST.^[359] However, for other systems in which the molecules of interest can directly be patterned without the attachment of an intermediate (in the form of maleimide derivatives), their number would only be limited by the resolution of the laser-induced Diels-Alder grafting and would depend on the dimensions of the scaffolds. Ultimately, examples have been shown where the maximal resolution was exploited to yield microstructures in which only the beams were functionalized but this time with both biotin and benzylguanine (Figure 9.9). Again, the 3D reconstruction images highlight the high degree of spatial control achievable; in Figure 9.9a biotinylated areas neatly alternate with BG-functionalized ones with a pitch of approx. 3 µm, without major cross-contamination.

9.5 Conclusions

The present work is, presumably, the first report of a precise control of the chemical surface properties of three-dimensional free-standing microscaffolds. The combination of highly efficient yet simple photochemistries with direct laser writing holds significant promises for future nanomaterials design. Interestingly, the functionalization method involves the grafting of maleimide derivatives which are relatively widespread. Here, protein 3D patterns have been constructed since it constitutes a convenient way to reveal the chemical patterns by fluorescence microscopy and at the same time shows that the described method could possibly be employed for bio(techno)logical purposes, i.e., for studying single-cell behavior. Nevertheless, numerous technological fields such as microfluidics, MEMS, and photonics can benefit from this novel methodology. The current efforts are directed to further improving the resolution of both the microstructure writing and the chemical patterning, tuning the mechanical properties of the materials, and evaluating diverse photochemistries.

10

Concluding Remarks and Outlook

10.1 Concluding Remarks

The present body of work comprises a novel toolbox of photochemical approaches that bear testimony to the versatility and efficiency of light for the modular construction of advanced polymeric architectures as well as for the design of precisely tailored surface chemistry.

The rapid growth in demand for techniques involved in the preparation of macromolecular building blocks is largely attributed to a paradigm shift observed in the design of modern polymeric materials. However, the controlled incorporation of reactive moieties into polymer chains remains challenging since thiols, for instance, are common chain transfer agents in the radical polymerization process. Chapter 4 evidenced a sequential approach to resolve this issue: after initially imparting *o*-nitrobenzyl thioether moieties along the polymeric backbone, the *in situ* transformation of photoreleased thiols by a Michael-type acceptor was described. While the 2-nitrobenzyl cages are widely employed to enable the desired molecular cleavage, Chapter 5 further evidenced their applicability in the realm of oxime based conjugation chemistry by considering the usual photolysis by-product as the actual product. Furthermore, a novel *o*-nitrobenzyl acetale featuring extremely rapid photocleavage kinetics was developed to provide overall a facile means to confer spatial control by using mild photolysis conditions (370 nm, 3 minutes).

In this line, the successful generation of locally constrained surface patterns of (bio)molecules bearing a pendant hydroxylamine was evidenced and imaged within a ToF-SIMS investigation. Striving to provide a novel photochemical surface immobilization technique that would feature enhanced selectivity and efficiency, Chapter 7 has proven the feasibility of a photoconjugation strategy that is based on the cycloaddition of photogenerated *o*-quinodimethanes to a series of (bio)molecules bearing a pendant dienophile. Rather than providing merely unprecedented coupling performance, the potential of the described photochemical approach for modular conjugations in solution and for spatially resolved immobilizations onto surfaces goes far beyond that of classical ligation reactions. The light-based reaction provides inherently control over time and space, is applicable to two-photon-activation and avoids limitations associated with photoremovable protecting chemistry, the necessity to use a catalyst or elevated temperatures.

To date, photopatterning techniques require considerable efforts for the preparation of surface anchors and substrates bearing appropriate coupling moieties, thus limiting their scope in novel applications. To avoid expensive synthetic modifications, Chapter 7 and 8 addressed the design of novel photochemical platforms able to efficiently react with functionalities inherently present in many substrates. The relevant photoactive precursor in Chapter 7 – formed with ease by employing a Diels-Alder reaction – permitted the fast and very robust photoactivation even in an aqueous environment. The ability to perform photolysis under ambient atmosphere and solid state whilst generating only less reactive, gaseous byproducts (H_2 and CO) renders the system attractive for industrial micro array fabrication. Facilitated by the ring-opening reaction of the inherent amine functionality, the patterned immobilization of peptides strictly composed of natural residues was presented. Perhaps the most simple surface encoding protocol for the direct immobilization of nucleophiles was realized in Chapter 8. The light-directed functionalization methodology is based upon the efficient trapping of photogenerated thioaldehydes by substrates bearing pendant amine-, hydroxylamine-, or thiol moieties. The high reactivity of the intermediate translated into fast reaction kinetics but also into a rather limited chemical selectivity.

Having established an arsenal of light-driven conjugation techniques and bearing in mind the wide range of applications they might be employed in the broad categories depicted in Figure 10.1 serve as approximate performance indicators for selecting the most suitable one according to the concrete needs. By combining the high coupling performance and its applicability to two-photon

activation, for instance, the developed photoenol mediated immobilization technique (Chapter 7) was utilized in Chapter 9 for the successful generation of 3D resolved protein patterns with a resolution close to one micron on structurally complex microscaffolds. The significance lies in the fact that for the first time such a precise control over the chemical surface properties of three-dimensional microscaffolds has been achieved and the design of future nanomaterials can be envisaged.

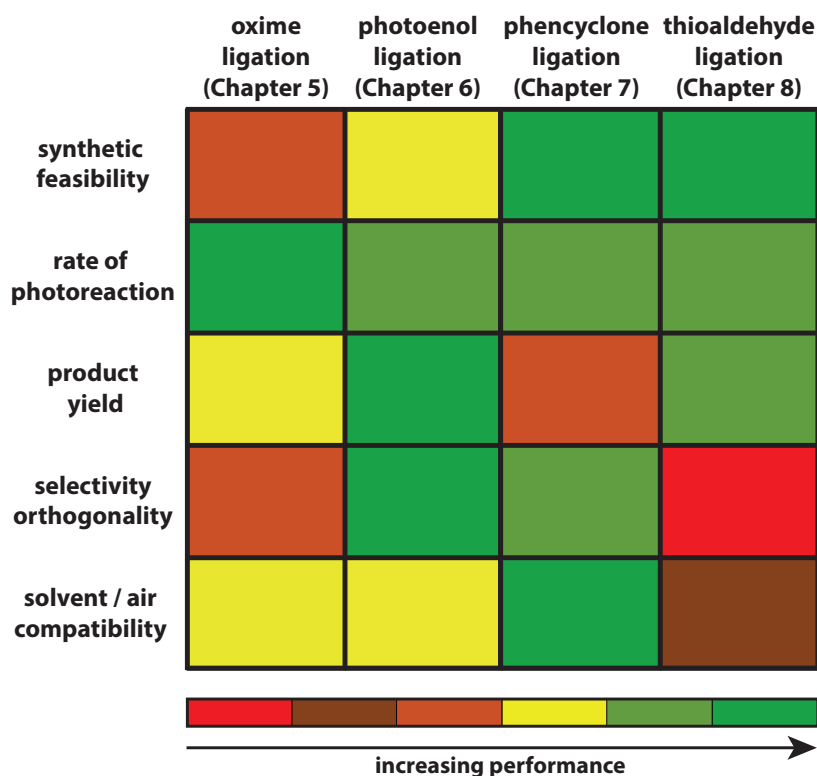


Figure 10.1 Schematic representation of the applicability of the developed photochemical approaches.

10.2 Outlook

An important benefit of photoinduced conjugation reactions – besides conferring spatial resolution – is their applicability orthogonal to most classical ligation strategies. The herein developed framework of photochemical reactions expands the existing repertoire of conjugations reactions from which the modern day chemist can choose. Photochemistry can also be tolerant to its own regime by employing wavelength-selective and thereby independently addressable light-triggered reactions. The challenge that should be addressed in future direction of research is to combine different photosensitive moieties by tuning them, e.g., via molecular

derivatization, with respect to their excitation wavelength and to identify spectral windows where each type of chromophore can be addressed without interfering with the others. Photosensitive moieties bearing red-shifted absorption maxima (above 400 nm) are particularly attractive since they would complement the excitation wavelengths of those described in Chapter 6 ($\lambda_{\text{max}} = 320$ nm), Chapter 8 ($\lambda_{\text{max}} = 355$ nm), and Chapter 5 (370 nm).

The precise modification of complex microstructures with proteins was achieved in Chapter 9 with a high spatial resolution (1 μm) and the applicability of these constructs to mimic cell environments can be envisaged. However, the fabrication of the microstructures themselves involve a two-photon initiated radical polymerization process that occurs from the laser focus point through the resist and translates into a rather limited resolution for the scaffold. In that respect, the use of efficient photoconjugation chemistry should be considered for the construction of the insoluble scaffold, e.g. by utilizing a multifunctional latent diene (based upon the photochemistry described in Chapter 6) in combination with a multifunctional dienophile. Both of the above noted challenges are currently being addressed in the Barner-Kowollik team.

Aside from the development of novel orthogonal and rapid conjugations, there is a growing demand for (polymeric) systems capable of reversibly switching between chemical states in response to external stimuli. Thermally driven reversibility of covalent bonds is usually limited to substrates insensitive to elevated temperatures and utilizing approaches based on photochemistry might be an attractive alternative. A foreseeable challenge is therefore to induce a covalent bond-cleaving and bond-forming event via (mild) light stimuli of different energies while still fulfilling *click* criteria. It should be taken into consideration that in the case where two substrates (A and B) bear the same photoactive moiety, the light-induced reformation would result in the (undesired) formation of three products (AA, AB, and BB). Besides investigating novel photoinduced ligation approaches, the development of suitable surface anchors is of equal importance to achieve a broadened scope for locally constrained surface immobilizations. Employing bioinspired surface coating technologies based upon polydopamine, for instance, would expand the applicability of the presented toolbox for photochemical surface design to a wide range of substrates, as is currently explored in our group.

The present body of work comprises a range of examples demonstrating the versatility and efficiency of light in modular conjugations. The significant benefits of photoinduced reactions described in the presented thesis are envisaged

to trigger a raising awareness of the high potential of photochemical reactions among chemists in general.

11

Materials and Characterization

11.1 Materials

11.1.1 Materials Used in Chapter 4

Copper(I) bromide (CuBr, Fluka) was purified via sequential washing with sulfurous acid, acetic acid, and ethanol followed by drying under reduced pressure. 2-nitrobenzyl bromide (98 %, ABCR), 3-mercaptopropionic acid (99 %, Acros), 4-dimethylaminopyridine (DMAP, 99 %, ABCR), α,α -dimethoxy- α -phenylacetophenone (DMPA, 99 %, Sigma-Aldrich), acetonitrile (HPLC grade, Acros), *N,N*-dimethylformamide (DMF, 99+ %, Alfa Aesar), anisole (>99 %, Fluka), dichloromethane (DCM, HPLC grade, Acros), dimethylphenylphosphine (DMPP, 99 %, Sigma Aldrich), dithiothreitol (DTT, 99 %, Alfa Aesar), ethyl 2-bromoisobutyrate (EBiB, 98 %, Acros), hydroxyethyl methacrylate (HEMA, 99 %, Sigma Aldrich), *N,N'*-dicyclohexylcarbodiimide (DCC, 99 %, Acros), *N,N,N',N'',N'''*-pentamethyldiethylenetriamine (PMDETA, 99+ %, Acros), tetrahydrofuran (THF, multisolvent, 250 ppm BHT, Scharlau), poly(ethylene glycol) methyl ether (PEG, Sigma Aldrich, average $M_n \approx 2000 \text{ g}\cdot\text{mol}^{-1}$) and triethylamine (TEA, 99 %, Alfa Aesar) were used as received. 1-(2-hydroxyethyl)-1*H*-pyrrole-2,5-dione **9** was synthesized according to a previously reported procedure.^[253]

11.1.2 Materials Used in Chapter 5

3-(Triethoxysilyl)propan-1-amine (98 %, Abcr), 3,4-dihydro-2H-pyran (97 %, Sigma Aldrich), 4-dimethylaminopyridine (DMAP, 99 %, Abcr), 4-hydroxy-3-methoxybenzaldehyde (99 %, Alfa Aesar), acetone (Normapur, VWR), acetonitrile (MeCN, HPLC grade, Acros), dichloromethane (DCM, 99.5 %, VWR for synthesis or HPLC grade, Acros for UV analysis), diethyl ether (99.9 %, VWR), ethanol (Normapur, VWR), ethyl acetate (Normapur grade, VWR), ethyl chloroformate (97 %, Acros), hydrogen peroxide (35 % v/v in water, Merck), hydroxylamine hydrochloride (99 %, Alfa Aesar), *N,N*-dimethylformamide (DMF, 99+ %, Alfa Aesar), *N,N'*-dicyclohexylcarbodiimide (DCC, 99 %, Acros), n-hexane (Normapur grade, VWR), nitric acid (Fischer, 70 % v/v in water), magnesium sulfate (> 99 %, Roth), methanol (chromasolv, Sigma Aldrich), methyl 4-bromobutanoate (97 %, Alfa Aesar), *O*-((perfluorophenyl)methyl)hydroxylamine hydrochloride (99+ %, Alfa Aesar), poly(ethylene glycol) methyl ether (PEG, Sigma Aldrich, average $M_n \approx 2000 \text{ g}\cdot\text{mol}^{-1}$), potassium carbonate (99 %, Merck), pyridinium chloride (98 %, Alfa Aesar), sodium borohydride (99 %, Acros), sodium hydroxide (> 99 %, Roth), sulfuric acid (95 %, Roth), tetrahydrofuran (THF, multisolvent, 250 ppm BHT, Scharlau), tetrahydrofuran (THF, 99.5 %, VWR), triethylamine (TEA, 99 %, Alfa Aesar), tosylic acid (>99 %, Merck) and toluene (99.8 %, Acros, extra dry) were used as received. Peptide synthesis carried out at the Humboldt Universität (Berlin): *N*- α -Fmoc protected amino acids (Fmoc-Gly OH, Fmoc-L-Arg(Pbf) OH, Fmoc-L-Ser(tBu) OH), 2-(1*H*-benzotriazole-1-yl)-1,1,3,3-tetramethyluroniumhexafluorophosphate (HBTU), (benzotriazol-1-yloxy) tripyrrolidinophosphonium-hexa-fluorophosphate (PyBOP), and Fmoc-Rink amide AM poly(styrene) resin (loading: $0.63 \text{ mmol}\cdot\text{g}^{-1}$) were used as received from IRIS Biotech GmbH (Marktredwitz, Germany). *N,N*-Diisopropylethylamine (DIPEA, Acros, peptide grade), piperidine (Acros, peptide grade), triethylsilane (TES, Alfa Aesar, 98+ %), and *t*Boc-2-(aminoxy)acetic acid (Aldrich Chemicals <98 %) have been used as received. *N*-methyl-2-pyrrolidone (NMP, 99.9+ %, peptide synthesis grade, IRIS Biotech) was purified by filtration through a column (10·60 cm) filled with aluminium oxide and silica gel at a rate of $2 \text{ mL}\cdot\text{min}^{-1}$. Trifluoroacetic acid (TFA, Acros, peptide grade) was distilled prior to use. Dichloromethane (DCM, IRIS Biotech GmbH, peptide grade) was distilled from CaH_2 prior to use.

11.1.3 Materials Used in Chapter 6

3-(Triethoxysilyl)propan-1-amine (98 %, Abcr), 4-(bromomethyl) benzoate (98 %, Alfa Aesar), aluminium chloride (99 %, Abcr), 4-dimethylaminopyridine (DMAP, 99 %, Abcr), acetonitrile (HPLC grade, Acros), 18-crown-6 (>95 %, VWR),

dichloromethane (DCM, HPLC grade, Acros), dimethylanisole (97 %, Alfa Aesar), ethyl chloroformate (97 %, Acros), fluoresceinamine isomer I (Sigma Aldrich), furan (99 %, Alfa Aesar), hydrogen peroxide 35 % (Merck), *N,N*-dimethylformamide (DMF, 99+ %, Alfa Aesar), *N,N'*-dicyclohexylcarbodiimide (DCC, 99 %, Acros), phosphate buffered saline (PBS, Sigma-Aldrich), poly(ethylene glycol) methyl ether (PEG, Sigma Aldrich, $M_n \approx 2000 \text{ g}\cdot\text{mol}^{-1}$), potassium persulfate (97 %, Alfa Aesar), succinic anhydride (>99 %, Sigma Aldrich), maleimide (98+ %, VWR), sulfuric acid (95 %, Roth), tetrahydrofuran (THF, multisolvent, 250 ppm BHT, Scharlau), triethylamine (TEA, 99 %, Alfa Aesar) and toluene (99.85 %, Acros) were used as received. Syntheses of bromine-containing maleimide derivative **7**, *N*-(5-fluoresceinyl)maleimide and ω -maleimido-poly(ethylene glycol) **8** were performed according to literature procedures.^[360–364] Peptide synthesis carried out at the Humboldt Universität (Berlin): *N*- α -Fmoc protected amino acids (Fmoc-Gly OH, Fmoc-L-Arg(Pbf)OH, Fmoc-L-Ser(tBu)OH), 2-(1*H*-benzotriazole-1-yl)-1,1,3,3-tertamethyluroniumhexafluorophosphate (HBTU), (benzotriazol-1-yloxy) tripyrrolidinophosphonium-hexa fluorophosphate (PyBOP) and Fmoc-Rink amide AM polystyrene resin (loading: $0.63 \text{ mmol}\cdot\text{g}^{-1}$) were used as received from IRIS Biotech GmbH (Marktredwitz, Germany). *N,N*-Diisopropylethylamine (DIPEA, Acros, peptide grade), piperidine (Acros, peptide grade), triethylsilane (TES, Alfa Aesar, 98+ %) and 3-maleimidopropionic succinimidyl ester (MPS, ABCR, 99 %) have also been used as received. *N*-methyl-2-pyrrolidone (NMP, 99.9+ %, peptide synthesis grade, IRIS Biotech) was purified by filtration through a column (10-60 cm) filled with aluminium oxide and silica gel at a rate of $2 \text{ mL}\cdot\text{min}^{-1}$. Trifluoroacetic acid (TFA, Acros, peptide grade) was distilled prior to use. Dichloromethane (DCM, IRIS Biotech GmbH, peptide grade) was distilled from CaH_2 prior to use.

11.1.4 Materials Used in Chapter 7

1-(3-Dimethylaminopropyl)-3-ethylcarbodiimide hydrochloride (98+ %, Alfa Aesar), 1,3-diphenylacetone (98+ %, Alfa Aesar), 2-(4-bromophenyl)ethanamine (99 %, Sigma Aldrich), 2-(4-fluorophenyl)ethanamine (98 %, Sigma Aldrich), 6-aminohexanoic acid (99 %, Alfa-Aesar), 1-ethyl-1*H*-pyrrole-2,5-dione (99+ %, Alfa Aesar), 1-hydroxy-2,5-pyrrolidinedione (98+ %, Alfa Aesar), 3-(triethoxysilyl)propan-1-amine (98 %, Abcr), 4-dimethylaminopyridine (DMAP, 99 %, Abcr), acetone (Normapur, VWR), acetonitrile (MeCN, HPLC grade, Acros), acetic acid (>99.7 %, Scharlau Chemie), 1,4-benzoquinone (>98 %, Merck), dichloromethane (DCM, 99.5 %, VWR for synthesis or HPLC grade, Acros for UV analysis), diethyl ether (99.9 %, VWR), ethanol (Normapur, VWR), ethyl acetate (Normapur grade, VWR), hydrochloric acid (37 % in water (v/v), reinst,

Roth), hydrogen peroxide (35 % v/v in water, Merck), *N,N*-dimethylformamide (DMF, 99+ %, Alfa Aesar), *N,N'*-dicyclohexylcarbodiimide (DCC, 99 %, Acros), *n*-hexane (Normapur grade, VWR), *N,N*-diisopropylethylamine (DIPEA, 99 %, Alfa Aesar), magnesium sulfate (>99 %, Roth), methanol (chromasolv, Roth), phenanthrene-9,10-dione (95 %, Alfa Aesar), phencyclone (97 %, Alfa Aesar), phenylacetic acid (99 %, Sigma Aldrich), phenylacetic acid ethyl ester (99 %, Sigma Aldrich), potassium carbonate (99 %, Merck), potassium hydroxide (>86 % pellets, Fluka), sodium bicarbonate (>99 %, Roth), sodium hydroxide (>99 %, Roth), sulfuric acid (95 %, Roth), tetrahydrofuran (THF, multisolvent, 250 ppm BHT, Scharlau), tetrahydrofuran (THF, 99.5 %, VWR), and toluene (99.8 %, Acros, extra dry) were used as received. Syntheses of 2-(2,5-dioxo-2,5-dihydro-1*H*-pyrrol-1-yl)ethyl 2-bromo-2-methylpropanoate was performed according to a literature procedure.^[361] Peptide synthesis carried out at the Humboldt Universität (Berlin): *N*- α -Fmoc protected amino acids (Fmoc-L-Asp-OAll, Fmoc-Gly-OH, Fmoc-L-Arg(Pbf)-OH, Fmoc-L-Lys(Boc)-OH, Fmoc-D-Phe-OH), 2-(1*H*-benzotriazole-1-yl)-1,1,3,3-tetramethyluronium hexafluorophosphate (HBTU) were used as received from IRIS Biotech GmbH (Marktredwitz, Germany). Standard TentaGel Resin with hydroxytrityl linker, 0.25 mmol·g⁻¹ loading, (TentaGel S Trt-OH, RAPP Polymere, Tuebingen, Germany) have been used as described. *N*-methylmorpholine (Acros, 99 %), palladium-tetrakis (triphenylphosphine) (Pd(PPh₃)₄, Sigma-Aldrich, 99 %), diethyldithiocarbamic acid sodium salt trihydrate (Acros, 98 %), 7-azabenzotriazol-1-yloxytris(pyrrolidino)phosphoniumhexafluorophosphate (PyAOP, Applied Biosystems), triethylsilane (TES, Alfa Aesar, 98+ %), dimethylformamid (DMF, IRIS, peptid grade) have been used as received. Piperidine (Alfa Aesar, 99 %) and *N,N*-diisopropylethylamine (DIPEA, IRIS Biotech, 99.96 %) were distilled from KOH prior to use. Acetyl chloride (Fluka, 98+ %) was freshly distilled. *N*-methyl-2-pyrrolidone (NMP, 99.9+ %, peptide synthesis grade, IRIS Biotech) was purified by filtration through a column (10·60 cm) filled with aluminium oxide and silica gel at a rate of 2 mL·min⁻¹. Trifluoroacetic acid (TFA, IRIS Biotech, peptide grade) was distilled prior to use. Dichloromethane (DCM, IRIS Biotech, peptide grade) was distilled from CaH₂ prior to use. 3-(2,5-dioxo-2,5-dihydro-1*H*-pyrrol-1-yl)propanoic acid (maleimidopropionic acid (MPA)) and Fmoc-4-(2-(2-(2-aminoethoxy)ethoxy)ethyl amino)-4-oxobutanoic acid) were synthesized according to literature procedures.^[365,366]

11.1.5 Materials Used in Chapter 8

2-(4-Bromophenyl)ethanamine (98 %, Sigma Aldrich), 1-ethyl-3-(3-dimethylamino-propyl)carbodiimid hydrochloride (EDC hydrochloride, 98 %, Alfa Aesar),

3-(triethoxysilyl)propan-1-amine (98 %, Abcr), (4-bromophenyl)methanethiol (98 %, Alfa Aesar), 4-dimethylaminopyridine (DMAP, 99 %, Abcr), acetone (Normapur, VWR), acetonitrile (MeCN, HPLC grade, Acros), dichloromethane (DCM, 99.5 %, VWR for synthesis), diethyl ether (99.9 %, VWR), ethanol (Normapur, VWR), ethyl acetate (Normapur grade, VWR), hydrochloric acid (37 % in water (v/v), reinst, Roth), hydrogen peroxide (35 % v/v in water, Merck), *N,N'*-dicyclohexylcarbodiimide (DCC, 99 %, Acros), n-hexane (Normapur grade, VWR), *N,N*-diisopropylethylamine (DIPEA, 99 %, Alfa Aesar), magnesium sulfate (> 99 %, Roth), methanol (chromasolv, Roth), mono-functional amino end-capped poly(ethylene)glycol methyl ether (mPEG-amine, $M_n \approx 1000 \text{ g}\cdot\text{mol}^{-1}$, Alfa Aesar), octadecan-1-amine (98 %, Alfa Aesar), O-(2,3,4,5,6-pentafluorobenzyl)hydroxylamine hydrochloride (Alfa Aesar, 99+ %), potassium carbonate (99 %, Merck), potassium hydroxide (> 86 % pellets, Fluka), sodium bicarbonate (> 99 %, Roth), sodium hydroxide (> 99 %, Roth), sulfuric acid (95 %, Roth), tetrahydrofuran (THF, multisolvent, 250 ppm BHT, Scharlau), tetrahydrofuran (THF, 99.5 %, VWR), and toluene (99.8 %, Acros, extra dry) were used as received. Synthesis of (phenacylthio)acetic acid was synthesized according to a literature procedure (purification by recrystallization from chloroform).^[328,367] The synthesis of 2-((2-oxo-2-phenylethyl)thio)-*N*-(3-(triethoxysilyl)propyl)acetamide was performed according to a literature procedure.^[328]

11.1.6 Materials Used in Chapter 9

3-(Trimethoxysilyl) propyl methacrylate (Sigma-Aldrich, $\geq 98 \%$), Ormocomp (Micro Resist Technology GmbH), copper(I) chloride (CuCl, Acros, 99.99 %), 2,2'-bipyridine (BPy, Sigma-Aldrich, $\geq 99 \%$), poly(dimethylsiloxane) (PDMS, Dow Corning), biotin-maleimide (Mal-Bt, Sigma-Aldrich, $\geq 95 \%$), avidin-rhodamine (Av-Rho, Molecular Probes), streptavidin-Cy3 (SAv-Cy3, Sigma-Aldrich), benzylguanine-maleimide (Mal-BG, New England BioLabs Inc., 98 %), Pluronic[®] F-108 ($M_n \approx 14600 \text{ g}\cdot\text{mol}^{-1}$, Sigma-Aldrich), 4-methyl-2-pentanone (Roth), isopropyl alcohol (Roth), *N,N*-dimethylformamide (DMF, for organic and macromolecular synthesis: Alfa Aesar, 99+ %, for microstructure functionalization: Roth), ethanol (Normapur, VWR), and toluene (for organic and macromolecular synthesis: Normapur, VWR, for microstructure functionalization: Roth) were used as received. Oligo(ethylene glycol) methacrylate (OEGMA, $M_n \approx 300 \text{ g}\cdot\text{mol}^{-1}$, Sigma-Aldrich) was de-inhibited by elution through a short plug of basic alumina. The photoenol-functionalized silane (Si-PE),^[3] the photoenol-functionalized poly(ethylene glycol) **1**,^[3] 2-bromo-2-methylpropionic acid 2-(3,5-dioxo-10-oxa-4-azatricyclo[5.2.1.0^{2,6}]dec-8-en-4-yl) ethyl ester (Fur-Mal-ATRP),^[361] maleimide-

functionalized poly(ethylene glycol) ($DP_n \approx 11.8$, Mal-PEG),^[368] and the GFP fused with a modified O^6 -alkylguanine-DNA alkyltransferase (SNAP-GFP)^[276] were prepared according to previously reported procedures.

11.2 Photoreactions

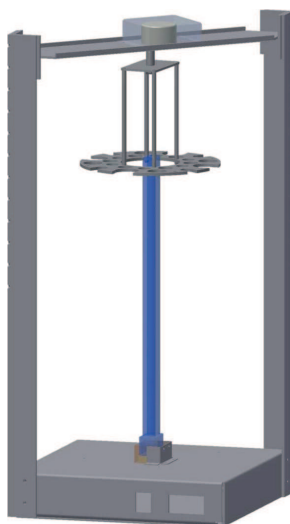


Figure 11.1 Drawing of the custom-built photoreactor employed for all photoreactions. The setup of the custom built photoreactor has been described previously.^[144]

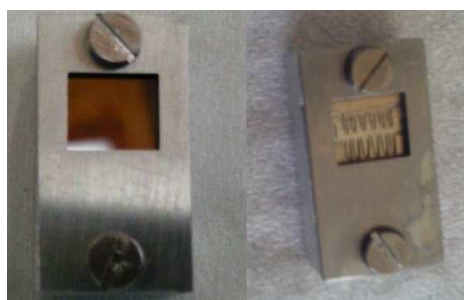


Figure 11.2 Shadow mask for the photoenol patterning on surface with a square cut into a metal plate (left) and a shadow mask featuring waved structures (right).

11.3 Characterization

^1H Nuclear Magnetic Resonance (NMR) and ^{13}C NMR Spectroscopy

The NMR spectra of all molecules – except of the peptides – depicted in Chapters 5, 6, 7, and 9 were recorded using a Bruker AM 250 or Bruker AM 400 spectrometers

at 250 MHz or 400 MHz for hydrogen nuclei and 101 MHz for carbon nuclei. ^1H NMR spectra of peptides were carried out at the Humboldt Universität (Berlin) in the group of Prof. Dr. Hans Börner on an AvanceIII-500 spectrometer from Bruker BioSpin GmbH (Rheinstetten, Germany) at 500 MHz in d-TFA at ambient temperature. The NMR spectra depicted in Chapter 8 were recorded on a Bruker Avance III Microbay spectrometer at 400 MHz. All samples were dissolved in CDCl_3 , acetone- d^6 or DMSO- d^6 . The δ (ppm)-scale is referenced to chemical shift of the residual solvent resonances.

Attenuated Total Reflection Fourier Transform Infrared Spectroscopy (ATR-FTIR)

Attenuated total reflection Fourier transform infrared spectroscopy (ATR-FTIR) for all analyzed compounds except for the peptides were recorded on a Vertrex 80 Fourier Transform Infrared Spectrometer from Bruker (Karlsruhe, Germany). ATR-FTIR of peptides were carried out at the Humboldt Universität (Berlin) in the group of Prof. Dr. Hans Börner on a Jasco FT/IR-4200 fourier transform infrared spectrometer (Golden gate) from Jasco Ltd. (Easton, USA).

Confocal Fluorescence Microscopy

To analyze the samples a confocal laser scanning microscope (LSM 510 Meta, Zeiss) with a high NA Objective ($63\times$, NA 1.4) was employed. For the 3D reconstruction of the confocal image stacks we used the Volocity software package (version 4.3.2, Perkin Elmer). Fluorescence detection was carried out through three different channels:

- white, corresponding to the autofluorescence of the Ormocomp microscaffolds ($\lambda_{\text{excitation}} = 405 \text{ nm}$; $\lambda_{\text{detection}} = 420\text{-}480 \text{ nm}$);
- red, corresponding to rhodamine-labeled avidin (Av-Rho) or Cy3-labeled streptavidin (SAv-Cy3) ($\lambda_{\text{excitation}} = 561 \text{ nm}$; $\lambda_{\text{detection}} = 580\text{-}650 \text{ nm}$);
- green, corresponding to the SNAP-GFP ($\lambda_{\text{excitation}} = 488 \text{ nm}$; $\lambda_{\text{detection}} = 500\text{-}550 \text{ nm}$).

For the quantification of the fluorescence intensity of the Av-Rho-stained biotin 2D patterns (Figure 9.4a), maximum projections of confocal z-slices were analyzed using the ImageJ software package (version 1.46q, National Institutes of Health). Average pixel intensity of areas where a laser power of 4.75 mW (in front of the objective) was used for the immobilization and the background average pixel intensity very

close to these areas was subtracted. This was carried out for a wavelength between 500 nm and 700 nm with a step size of 20 nm and a maximal laser power of 20 mW in front of the objective. For the wavelength of 700 nm the maximal laser power was 10 mW in front of the objective regarding a higher absorption of a beam splitter in the optical path.

Elemental Analysis

Elemental analysis (C, N, H analysis) was performed with an Elementar Vario Micro Cube device (Elementar, Hanau, Germany).

Electrospray Ionization-Mass Spectrometry (ESI-MS)

Electrospray ionization-mass spectrometry (ESI-MS) spectra were recorded on a LXQ mass spectrometer (ThermoFisher Scientific) equipped with an atmospheric pressure ionization source operating in the nebulizer-assisted electrospray mode. The instrument was calibrated in the m/z range 195-1822 using a standard comprising caffeine, Met-Arg-Phe-Ala acetate (MRFA), and a mixture of fluorinated phosphazenes (Ultramark 1621, all from Aldrich). A constant spray voltage of 4.5 kV and a dimensionless sweep gas flow rate of 2 and a dimensionless sheath gas flow rate of 8 were applied. The capillary voltage, the tube lens offset voltage, and the capillary temperature were typically set to 40 V, 100 V, and 325 °C, respectively.

Scanning Electron Microscopy

Images were acquired with a Zeiss SUPRA 55VP.

Size Exclusion Chromatography (SEC)

Size exclusion chromatography (SEC) measurements were performed on a Polymer Laboratories (Varian) PL-GPC 50 Plus Integrated System, comprising an autosampler, a PLgel 5 mm bead-size guard column (50×7.5 mm), one PLgel 5 mm Mixed E column (300×7.5 mm), three PLgel 5 mm Mixed C columns (300×7.5 mm), and a differential refractive index detector using THF as the eluent at 35 °C with a flow rate of 1 mL min⁻¹. The SEC system was calibrated using linear poly(styrene) standards ranging from 160 to 6·10⁶ g mol⁻¹ and linear poly(methyl methacrylate) standards ranging from 700 to 2·10⁶ g mol⁻¹. The resulting molecular weight distributions were determined by universal calibration using Mark Houwink parameters for PMMA ($K=12.8 \cdot 10^{-5}$ dL g⁻¹, $\alpha = 0.69$).^[369] Molecular weights relative to PMMA are reported in Chapter 4.

Size-Exclusion Chromatography Coupled to Electrospray Ionization-Mass Spectrometry (SEC/ESI-MS)

Size-exclusion chromatography coupled to electrospray ionization-mass spectrometry (SEC/ESI-MS) spectra were recorded on a LXQ mass spectrometer (ThermoFisher Scientific) equipped with an atmospheric pressure ionization source operating in the nebulizer-assisted electrospray mode. The instrument was calibrated in the m/z range 195 – 1822 using a standard comprising caffeine, Met-Arg-Phe-Ala acetate (MRFA), and a mixture of fluorinated phosphazenes (Ultramark 1621, all from Aldrich). A constant spray voltage of 4.5 kV and a dimensionless sweep gas flow rate of 2 and a dimensionless sheath gas flow rate of 12 were applied. The capillary voltage, the tube lens offset voltage, and the capillary temperature were set to 60 V, 110 V, and 275 °C, respectively. The LXQ was coupled to a Series 1200 HPLC system (Agilent) that consisted of a solvent degasser (G1322A), a binary pump (G1312A) and a high-performance autosampler (G1367B), followed by a thermostated column compartment (G1316A). Separation was performed on two mixed-bead GPC columns (Polymer Laboratories, Mesopore 250 × 4.6 mm, particle diameter 3 μm) with pre-column (Mesopore 50 × 4.6 mm) operating at 30 °C. THF at a flow rate of 0.3 mL·min⁻¹ was used as the eluent. The mass spectrometer was coupled to the column in parallel to an RI detector (G1362A with SS420 × A/D) in a setup described previously.^[166] A 0.27 mL·min⁻¹ aliquot of the eluent was directed through the RI detector and 30 μL·min⁻¹ infused into the electrospray source after postcolumn addition of a 0.1 mM solution of sodium iodide in methanol at 20 μL·min⁻¹ by a micro flow HPLC syringe pump (Teledyne ISCO, Model 100DM). The polymer solutions (20 μL) with a concentration of ≈ 1.0 mg·mL⁻¹ were injected into the HPLC system.

Time-of-flight Secondary Ion Mass Spectrometry (ToF-SIMS)

ToF-SIMS (time-of-flight secondary ion mass spectrometry) was performed on a ToF-SIMS instrument (ION-TOF GmbH, Münster, Germany) equipped with a Bi cluster liquid metal primary ion source and a non-linear time of flight analyzer. Samples were rinsed and sonicated in HPLC grade water (Carl Roth) prior to analysis. The Bi source was operated in “bunched” mode providing Bi₁⁺ or Bi₃⁺ ion pulses at 25 keV energy and a lateral resolution of approx. 4 μm. The short pulse length allowed for high mass resolution to analyze the complex mass spectra of the immobilized organic layers. Images larger than the maximum deflection range of the primary ion gun of 500 × 500 μm² were obtained using the manipulator stage scan mode. Negative polarity spectra were calibrated on the C⁻, CH⁻, CH₂⁻ peaks.

Positive polarity spectra were calibrated on C⁺, Si⁺ and small hydrocarbon peaks. Primary ion doses were kept below 10¹¹ ions · cm⁻² (static SIMS limit).

X-ray Photoelectron Spectroscopy (XPS)

X-ray photoelectron spectroscopy (XPS) measurements were performed using a K-Alpha XPS spectrometer (ThermoFisher Scientific, East Grinstead, UK). All the samples were analyzed using a microfocused, monochromated Al K α X-ray source (400 μ m spot size). The kinetic energy of the electrons was measured by a 180 ° hemispherical energy analyzer operated in the constant analyzer energy mode (CAE) at 50 eV pass energy for elemental spectra. Data acquisition and processing using the Thermo Avantage software is described elsewhere.^[370] The spectra were fitted with one or more Voigt profiles (BE uncertainty: \pm 0.2 eV). The analyzer transmission function, Scofield sensitivity factors,^[371] and effective attenuation lengths (EALs) for photoelectrons were applied for quantification. EALs were calculated using the standard TPP-2M formalism.^[372] All spectra were referenced to the C1s peak of hydrocarbon at 285.0 eV binding energy controlled by means of the well-known photoelectron peaks of metallic Cu, Ag, and Au.

12

List of Abbreviations

λ	wavelength
ϕ	quantum yield
2D	two-dimensional
3D	three-dimensional
7-MCM	7-methoxycoumarin-4-ylmethyl
A	absorption
ADIBO	aza-dibenzocyclooctyne
APCI	atmospheric pressure chemical ionization
ATRP	atom transfer radical polymerization
Av-Rho	rhodamine-labeled avidin
BARAC	biarylazacyclooctynone
BCMCM	6,7-bis(carboxymethoxy)coumarin-4-ylmethyl
BHT	butylated hydroxytoluene
BHCM	6-bromo-7-hydroxycoumarin-4-ylmethyl
BP _y	2,2'-bipyridine
CDMNB	α -carboxy-4,5-dimethoxy-2-nitrobenzyl
CI	chemical ionization
CID	collision-induced decay
COMBO	carboxymethylmonobenzocyclooctyne
CPDB	2-cyanopropyl dithiobenzoate
Da	dalton

DA	Diels-Alder
DCC	dicyclohexylcarbodiimide
DCM	dichloromethane
DEACM	7-(diethylamino)coumarin-4-ylmethyl
DESI	desorption electrospray ionization
DIBO	dibenzocyclooctyne
DIFO	difluorinated cyclooctyne
DIPEA	<i>N,N</i> -diisopropylethylamine
DLW	direct laser writing
DMAP	4-dimethylaminopyridine
DMB	3',5'-dimethoxybenzoin
DMNB	4,5-dimethoxy-2-nitrobenzyl
DMNPE	4,5-dimethoxy-2-nitrophenethyl
DMP	2,5-dimethylphenacyl
DMSO	dimethyl sulfoxide
DTT	dithiothreitol
E	energy
e.g.	exempli gratia (for example)
EBiB	ethyl 2-bromoisobutyrate
EI	electron ionization
eq.	equivalent
ESI	electrospray ionization
ESI-MS	electrospray ionization-mass spectrometry
eV	electron volt
F	fluorescence
FAB	fast atom bombardment
FAS	phenacyl sulfide
FI	field ionization
FT-ICR	fourier transform-ion cyclotron resonance
FMO	frontier molecular orbital
FMP	2-formyl-3-methylphenoxy
FRET	Förster resonance energy transfer
Fur-Mal-ATRP	2-(1,3-dioxo-3a,4,7,7a-tetrahydro-1 <i>H</i> -4,7-epoxyisoindol-2 (3 <i>H</i>)-yl)ethyl 2-bromo-2-methylpropanoate
HDA	hetero Diels-Alder
HEMA	(hydroxyethyl)methacrylate
HOMO	highest occupied molecular orbital
IC	internal conversion
ICR	ion-cyclotron resonance

i.e.	id est (that is)
IMS	imaging mass spectrometry
ISC	intersystem crossing
k_{IC}	rate coefficient of internal conversion
k_{ISC}	rate coefficient of intersystem crossing
k_{Ph}	rate coefficient of phosphorescence
k_{vib}	rate coefficient of vibrational relaxation
L	liter
LC	liquid chromatography
LACCC	liquid adsorption chromatography at critical conditions
LSM	laser scanning microscope
LUMO	lowest unoccupied molecular orbital
Mal	maleimide
Mal-PEG	maleimide-functionalized poly(ethylene glycol)
Mal-POEGMA	poly(oligo(ethylene glycol) methacrylate) bearing a maleimide moiety
MALDI	matrix-assisted laser desorption ionization
MALDI-ToF	matrix-assisted laser desorption ionization - time-of-flight
MCPO	1,3-bis(4-methoxyphenyl)-2 <i>H</i> -cyclopenta[<i>l</i>]phenanthren-2-one
MeNPOC	α -methyl-6-nitro-piperonyloxycarbonyl
M_n	number-average molecular weight
Mal-Bt	maleimide-functionalized biotin
Mal-BG	benzylguanine-maleimide
MEMS	microelectromechanical systems
MO	molecular orbital
mPEG-amine	mono-functional amino end-capped poly(ethylen)glycol methyl ether
MS	mass spectrometry
m/z -ratio	mass-to-charge ratio
n	number of charges per polymer chain
NMR	nuclear magnetic resonance
NOTP	2-[(4,5-dimethoxy-2-nitrobenzyl)oxy]tetrahydro-2 <i>H</i> -pyranyl
NVOC	6-nitroveratryloxycarbonyl
NVOC-Cl	6-nitroveratryloxycarbonyl chloride
OCT	cyclooctyne
PDI	polydispersity index
PEG	poly(ethylene glycol)
PDMS	poly(dimethylsiloxane)
GFP	green fluorescent protein

PG	protecting group
pHP	<i>p</i> -hydroxyphenacyl
PPG	photoremovable protecting group
PMMA	poly(methyl methacrylate)
PMDETA	<i>N,N,N',N'',N''</i> -pentamethyldiethylenetriamine
PTFE	poly(tetrafluoroethylene)
PyAOP	(7-azabenzotriazol-1-yloxy)tripyrrolidinophosphonium hexafluorophosphate
PyBOP	(benzotriazol-1-yloxy)tripyrrolidinophosphonium hexafluorophosphate
RAFT	reversible addition-fragmentation chain transfer
rDA	retro-Diels-Alder
RI	refractive index
S	singlet state
SAv-Cy3	red fluorescent dye-labeled streptavidin
SBR	styrene butadiene rubber
SEC	size-exclusion chromatography
SEC/ESI-MS	size-exclusion chromatography-electrospray ionization-mass spectrometry
SEM	scanning electron microscopy
Si-PE	photoenol-functionalized silane
SIMS	secondary ion mass spectrometry
SNAP-GFP	GFP fused with a modified <i>O</i> ⁶ -alkylguanine-DNA alkyltransferase
SOP	single oligomer profile
SPAAC	strain-promoted azide-alkyne cycloadditions
T	triplet state
TEA	triethylamine
THF	tetrahydrofuran
ToF	time-of-flight
UV	ultraviolet
UV-Vis	ultraviolet/visible
V	voltage
XPS	X-ray photoelectron spectroscopy

Bibliography

- [1] Kolb, H. C.; Finn, M. G.; Sharpless, K. B. *Angew. Chem., Int. Ed.* **2001**, *40*, 2004–2021.
- [2] Barner-Kowollik, C.; Du Prez, F. E.; Espeel, P.; Hawker, C. J.; Junkers, T.; Schlaad, H.; Van Camp, W. *Angew. Chem., Int. Ed.* **2011**, *50*, 60–62.
- [3] Pauloehrl, T.; Delaittre, G.; Winkler, V.; Welle, A.; Bruns, M.; Börner, H. G.; Greiner, A. M.; Bastmeyer, M.; Barner-Kowollik, C. *Angew. Chem., Int. Ed.* **2012**, *51*, 1071–1074.
- [4] Park, E. J.; Carroll, G. T.; Turro, N. J.; Koberstein, J. T. *Soft Matter* **2009**, *5*, 36–50.
- [5] Albin, A.; Germani, L. *Handbook of Synthetic Photochemistry*; Wiley-VCH Verlag GmbH & Co. KGaA, **2010**; pp 1–24.
- [6] Horner, L.; Christmann, A. *Angew. Chem. Int. Ed.* **1963**, *2*, 599–608.
- [7] Kawata, S.; Sun, H.-B.; Tanaka, T.; Takada, K. *Nature* **2001**, *412*, 697–698.
- [8] Deubel, M.; von Freymann, G.; Wegener, M.; Pereira, S.; Busch, K.; Soukoulis, C. M. *Nature Mater.* **2004**, *3*, 444–447.
- [9] Fischer, J.; Wegener, M. *Laser Photon. Rev.* **2013**, *7*, 22–44.
- [10] Ciamician, G.; Silber, P. *Chem. Ber.* **1901**, *34*, 2040–2046.
- [11] Ciamician, G.; Silber, P. *Chem. Ber.* **1907**, *40*, 2415–2424.
- [12] Ciamician, G. *Science* **1912**, *36*, 385–394.
- [13] Ciamician, G.; Silber, P. *Chem. Ber.* **1903**, *36*, 1575–1583.
- [14] Moore, W. M.; Hammond, G. S.; Foss, R. P. *J. Am. Chem. Soc.* **1961**, *83*, 2789–2794.
- [15] Paternò, E.; Chieffi, G. *Gazz. Chim. Ital.* **1909**, *39*, 341–361.

- [16] Büchi, G.; Inman, C. G.; Lipinsky, E. S. *J. Am. Chem. Soc.* **1954**, *76*, 4327–4331.
- [17] Hoffmann, N. *Chem. Rev.* **2008**, *108*, 1052–1103.
- [18] Conradi, M.; Junkers, T. *Macromolecules* **2011**, *44*, 7969–7976.
- [19] Jablonski, A. *Nature* **1933**, *131*, 839–840.
- [20] Sharma, V. P.; Kumar, R. *Pragati's pericyclic reactions and organic photochemistry*; Pragati Prakashan: Meerut, India, **2008**; pp 1–333.
- [21] Bixon, M.; Jortner, J. *J. Chem. Phys.* **1968**, *48*, 715–726.
- [22] Kuhlman, T. S.; Pittelkow, M.; Sølling, T. I.; Møler, K. B. *Angew. Chem. Int. Ed.* **2013**, *52*, 2247–2250.
- [23] Oxtoby, D. W. *Annu. Rev. Phys. Chem.* **1981**, *32*, 77–101.
- [24] Marian, C. M. *WIREs: Comput. Mol. Sci.* **2012**, *2*, 187–203.
- [25] Singh, J. *Photochemistry And Pericyclic Reactions*; New Age International (P) Ltd., **2005**; pp 1–400.
- [26] Itoh, T. *Chem. Rev.* **2012**, *112*, 4541–4568.
- [27] Maciejewski, A.; Steer, R. P. *Chem. Rev.* **1993**, *93*, 67–98.
- [28] Sekar, R. B.; Periasamy, A. *J. Cell. Biol.* **2003**, *160*, 629–633.
- [29] Norrish, R. G. W.; Bamford, C. H. *Nature* **1936**, *138*, 1016–1016.
- [30] Norrish, R. G. W.; Bamford, C. H. *Nature* **1937**, *140*, 195–196.
- [31] Voll, D.; Hufendiek, A.; Junkers, T.; Barner-Kowollik, C. *Macromol. Rapid Commun.* **2012**, *33*, 47–53.
- [32] Marciniak, B. *J. Chem. Educ.* **1988**, *65*, 832.
- [33] Wagner, P. J. *Acc. Chem. Res.* **1971**, *4*, 168–177.
- [34] Yang, N. C.; Yang, D.-D. H. *J. Am. Chem. Soc.* **1958**, *80*, 2913–2914.
- [35] del Campo, A.; Boos, D.; Spiess, H. W.; Jonas, U. *Angew. Chem., Int. Ed.* **2005**, *44*, 4707–4712.
- [36] Cui, J.; Miguel, V. S.; del Campo, A. *Macromol. Rapid Commun.* **2013**, *34*, 310–329.

- [37] Bochet, C. G. *J. Chem. Soc., Perkin Trans. 1* **2002**, 0, 125–142.
- [38] Kessler, M.; Glatthar, R.; Giese, B.; Bochet, C. G. *Org. Lett.* **2003**, 5, 1179–1181.
- [39] Holmes, C. P. *J. Org. Chem.* **1997**, 62, 2370–2380.
- [40] Pauloehrl, T.; Delaittre, G.; Bruns, M.; Meißler, M.; Börner, H. G.; Bastmeyer, M.; Barner-Kowollik, C. *Angew. Chem., Int. Ed.* **2012**, 51, 9181–9184.
- [41] Pelliccioli, A. P.; Wirz, J. *Photochem. Photobiol. Sci.* **2002**, 1, 441–458.
- [42] Patchornik, A.; Amit, B.; Woodward, R. B. *J. Am. Chem. Soc.* **1970**, 92, 6333–6335.
- [43] Suyama, K.; Shirai, M. *Prog. Polym. Sci.* **2009**, 34, 194 – 209.
- [44] Zhao, H.; Sterner, E. S.; Coughlin, E. B.; Theato, P. *Macromolecules* **2012**, 45, 1723–1736.
- [45] Hoffmann, N. *Photochem. Photobiol. Sci.* **2012**, 11, 1613–1641.
- [46] Kramer, R. H.; Chambers, J. J.; Trauner, D. *Nat. Chem. Biol.* **2005**, 1, 360–365.
- [47] Mayer, G.; Heckel, A. *Angew. Chem.* **2006**, 118, 5020–5042.
- [48] Ellis-Davies, G. C. R. *Nat. Methods* **2007**, 4, 619–628.
- [49] Delaittre, G.; Greiner, A. M.; Pauloehrl, T.; Bastmeyer, M.; Barner-Kowollik, C. *Soft Matter* **2012**, 8, 7323–7347.
- [50] Yu, H.; Li, J.; Wu, D.; Qiu, Z.; Zhang, Y. *Chem. Soc. Rev.* **2010**, 39, 464–473.
- [51] Fehrentz, T.; Schönberger, M.; Trauner, D. *Angew. Chem., Int. Ed.* **2011**, 50, 12156–12182.
- [52] Lovell, J. F.; Liu, T. W. B.; Chen, J.; Zheng, G. *Chem. Rev.* **2010**, 110, 2839–2857.
- [53] Warther, D.; Gug, S.; Specht, A.; Bolze, F.; Nicoud, J.-F.; Mourot, A.; Goeldner, M. *Bioorg. Med. Chem.* **2010**, 18, 7753–7758.
- [54] Park, C.-H.; Givens, R. S. *J. Am. Chem. Soc.* **1997**, 119, 2453–2463.
- [55] Zabadal, M.; Pelliccioli, A. P.; à, P.; Wirz, J. *J. Phys. Chem. A* **2001**, 105, 10329–10333.
- [56] Sheehan, J. C.; Wilson, R. M.; Oxford, A. W. *J. Am. Chem. Soc.* **1971**, 93, 7222–7228.

- [57] Klàn, P.; Šolomek, T.; Bochet, C. G.; Blanc, A.; Givens, R.; Rubina, M.; Popik, V.; Kostikov, A.; Wirz, J. *Chem. Rev.* **2012**, *113*, 119–191.
- [58] Il'ichev, Y. V.; Schwörer, M. A.; Wirz, J. *J. Am. Chem. Soc.* **2004**, *126*, 4581–4595.
- [59] Dunkin, I. R.; Gebicki, J.; Kiszka, M.; Sanin-Leira, D. *J. Chem. Soc., Perkin Trans. 2* **2001**, *0*, 1414–1425.
- [60] Il'ichev, Y. V.; Wirz, J. *J. Phys. Chem. A* **2000**, *104*, 7856–7870.
- [61] Marriott, G.; Heidecker, M. *Biochemistry* **1996**, *35*, 3170–3174.
- [62] Avlonitis, N.; Chalmers, S.; McDougall, C.; Stanton-Humphreys, M. N.; Brown, C. T. A.; McCarron, J. G.; Conway, S. J. *Mol. BioSyst.* **2009**, *5*, 450–457.
- [63] Stanton-Humphreys, M. N.; Taylor, R. D. T.; McDougall, C.; Hart, M. L.; Brown, C. T. A.; Emptage, N. J.; Conway, S. J. *Chem. Commun.* **2012**, *48*, 657–659.
- [64] Ghosn, B.; Haselton, F. R.; Gee, K. R.; Monroe, W. T. *Photochem. Photobiol.* **2005**, *81*, 953–959.
- [65] Dyer, R. G.; Turnbull, K. D. *J. Org. Chem.* **1999**, *64*, 7988–7995.
- [66] Griffin, D. R.; Kasko, A. M. *J. Am. Chem. Soc.* **2012**, *134*, 13103–13107.
- [67] Gautier, A.; Nguyen, D. P.; Lusic, H.; An, W.; Deiters, A.; Chin, J. W. *J. Am. Chem. Soc.* **2010**, *132*, 4086–4088.
- [68] McGall, G. H.; Barone, A. D.; Diggelmann, M.; Fodor, S. P. A.; Gentalen, E.; Ngo, N. J. *J. Am. Chem. Soc.* **1997**, *119*, 5081–5090.
- [69] Kotzur, N.; Briand, B.; Beyermann, M.; Hagen, V. *Chem. Commun.* **2009**, *0*, 3255–3257.
- [70] Gilbert, D.; Funk, K.; Dekowski, B.; Lechler, R.; Keller, S.; Möhrle, F.; Frings, S.; Hagen, V. *ChemBioChem* **2007**, *8*, 89–97.
- [71] Russell, A. G.; Ragoussi, M.-E.; Ramalho, R.; Wharton, C. W.; Carteau, D.; Bassani, D. M.; Snaith, J. S. *J. Org. Chem.* **2010**, *75*, 4648–4651.
- [72] Fodor, S.; Read, J.; Pirrung, M.; Stryer, L.; Lu, A.; Solas, D. *Science* **1991**, *251*, 767–773.

- [73] Reichmanis, E.; Smith, B. C.; Gooden, R. J. *Polym. Sci. Polym. Chem. Ed.* **1985**, *23*, 1–8.
- [74] Young, D. D.; Deiters, A. *Bioorg. Med. Chem. Lett.* **2006**, *16*, 2658–2661.
- [75] Russell, A. G.; Sadler, M. J.; Laidlaw, H. J.; Gutierrez-Loriente, A.; Whar-ton, C. W.; Carreau, D.; Bassani, D. M.; Snaith, J. S. *Photochem. Photobiol. Sci.* **2012**, *11*, 556–563.
- [76] Kawano, Y.; Takada, T.; Nakamura, M.; Yamana, K. *Nucleic Acids Symp. Ser.* **2009**, *53*, 173–174.
- [77] Barltrop, J. A.; Plant, P. J.; Schofield, P. *Chem. Commun. (London)* **1966**, *0*, 822–823.
- [78] Givens, R. S.; Matuszewski, B. J. *Am. Chem. Soc.* **1984**, *106*, 6860–6861.
- [79] Schade, B.; Hagen, V.; Schmidt, R.; Herbrich, R.; Krause, E.; Eckardt, T.; Bendig, J. J. *Org. Chem.* **1999**, *64*, 9109–9117.
- [80] Hagen, V.; Kilic, F.; Schaal, J.; Dekowski, B.; Schmidt, R.; Kotzur, N. *J. Org. Chem.* **2010**, *75*, 2790–2797.
- [81] Hagen, V.; Frings, S.; Bendig, J.; Lorenz, D.; Wiesner, B.; Kaupp, U. B. *Angew. Chem., Int. Ed.* **2002**, *41*, 3625–3628.
- [82] Takaoka, K.; Tatsu, Y.; Yumoto, N.; Nakajima, T.; Shimamoto, K. *Bioorg. Med. Chem.* **2004**, *12*, 3687–3694.
- [83] Pinheiro, A. V.; Baptista, P.; Lima, J. C. *Nucleic Acids Res.* **2008**, *36*, e90.
- [84] Shembekar, V. R.; Chen, Y.; Carpenter, B. K.; Hess, G. P. *Biochemistry* **2007**, *46*, 5479–5484.
- [85] Skwarczynski, M.; Noguchi, M.; Hirota, S.; Sohma, Y.; Kimura, T.; Hayashi, Y.; Kiso, Y. *Bioorg. Med. Chem. Lett.* **2006**, *16*, 4492–4496.
- [86] Givens, R. S.; Rubina, M.; Wirz, J. *Photochem. Photobiol. Sci.* **2012**, *11*, 472–488.
- [87] Moses, J. E.; Moorhouse, A. D. *Chem. Soc. Rev.* **2007**, *36*, 1249–1262.
- [88] Avinash, M. B.; Govindaraju, T. *Adv. Mater.* **2012**, *24*, 3905–3922.
- [89] van Dijk, M.; Rijkers, D. T. S.; Liskamp, R. M. J.; van Nostrum, C. F.; Hen-nink, W. E. *Bioconjugate Chem.* **2009**, *20*, 2001–2016.
- [90] Binder, W. H.; Sachsenhofer, R. *Macromol. Rapid Commun.* **2008**, *29*, 952–981.

- [91] Hein, C.; Liu, X.-M.; Wang, D. *Pharm. Res.* **2008**, *25*, 2216–2230.
- [92] Kolb, H. C.; Sharpless, K. *Drug Discov. Today* **2003**, *8*, 1128–1137.
- [93] Le Droumaguet, B.; Velonia, K. *Macromol. Rapid Commun.* **2008**, *29*, 1073–1089.
- [94] Barner-Kowollik, C.; Inglis, A. J. *Macromol. Chem. Phys.* **2009**, *210*, 987–992.
- [95] Wang, Y.; Song, W.; Hu, W.; Lin, Q. *Angew. Chem., Int. Ed.* **2009**, *48*, 5330–5333.
- [96] Devaraj, N.; Upadhyay, R.; Haun, J.; Hilderbrand, S.; Weissleder, R. *Angew. Chem., Int. Ed.* **2009**, *48*, 7013–7016.
- [97] Bahta, M.; Burke, T. R. *ChemMedChem* **2011**, *6*, 1363–1370.
- [98] Hoyle, C.; Bowman, C. *Angew. Chem., Int. Ed.* **2010**, *49*, 1540–1573.
- [99] Inglis, A.; Sinnwell, S.; Stenzel, M.; Barner-Kowollik, C. *Angew. Chem., Int. Ed.* **2009**, *48*, 2411–2414.
- [100] Meldal, M.; Tornøe, C. W. *Chem. Rev.* **2008**, *108*, 2952–3015.
- [101] Becer, C. R.; Hoogenboom, R.; Schubert, U. *Angew. Chem., Int. Ed.* **2009**, *48*, 4900–4908.
- [102] Paulöhr, T.; Inglis, A. J.; Barner-Kowollik, C. *Adv. Mater.* **2010**, *22*, 2788–2791.
- [103] Tornøe, C. W.; Christensen, C.; Meldal, M. *J. Org. Chem.* **2002**, *67*, 3057–3064.
- [104] Rostovtsev, V. V.; Green, L. G.; Fokin, V. V.; Sharpless, K. B. *Angew. Chem., Int. Ed.* **2002**, *41*, 2596–2599.
- [105] Hein, J. E.; Fokin, V. V. *Chem. Soc. Rev.* **2010**, *39*, 1302–1315.
- [106] Sohn, C. H.; Agnew, H. D.; Lee, J. E.; Sweredoski, M. J.; Graham, R. L.; Smith, G. T.; Hess, S.; Czerwieńiec, G.; Loo, J. A.; Heath, J. R.; Deshaies, R. J.; Beauchamp, J. L. *Anal. Chem.* **2012**, *84*, 2662–2669.
- [107] Brantley, J. N.; Wiggins, K. M.; Bielawski, C. W. *Science* **2011**, *333*, 1606–1609.
- [108] Leibfarth, F. A.; Hawker, C. J. *Science* **2011**, *333*, 1582–1583.
- [109] Wittig, G.; Krebs, A. *Chem. Ber.* **1961**, *94*, 3260–3275.
- [110] Agard, N. J.; Prescher, J. A.; Bertozzi, C. R. *J. Am. Chem. Soc.* **2004**, *126*, 15046–15047.
- [111] Gold, B.; Dudley, G. B.; Alabugin, I. V. *J. Am. Chem. Soc.* **2012**, *135*, 1558–1569.

- [112] Varga, B. R.; Kállay, M.; Hegyi, K.; Béni, S.; Kele, P. *Chem.–Eur. J.* **2012**, *18*, 822–828.
- [113] Codelli, J. A.; Baskin, J. M.; Agard, N. J.; Bertozzi, C. R. *J. Am. Chem. Soc.* **2008**, *130*, 11486–11493.
- [114] Ning, X.; Guo, J.; Wolfert, M. A.; Boons, G.-J. *Angew. Chem., Int. Ed.* **2008**, *47*, 2253–2255.
- [115] Debets, M. F.; van Berkel, S. S.; Schoffelen, S.; Rutjes, F. P. J. T.; van Hest, J. C. M.; van Delft, F. L. *Chem. Commun.* **2010**, *46*, 97–99.
- [116] Kuzmin, A.; Poloukhtine, A.; Wolfert, M. A.; Popik, V. V. *Bioconjugate Chem.* **2010**, *21*, 2076–2085.
- [117] Jewett, J. C.; Sletten, E. M.; Bertozzi, C. R. *J. Am. Chem. Soc.* **2010**, *132*, 3688–3690.
- [118] Gold, B.; Shevchenko, N. E.; Bonus, N.; Dudley, G. B.; Alabugin, I. V. *J. Org. Chem.* **2012**, *77*, 75–89.
- [119] Inglis, A. J.; Barner-Kowollik, C. *Complex Macromolecular Architectures*; John Wiley & Sons (Asia) Pte Ltd, **2011**; pp 21–52.
- [120] Zheng, T.; Jiang, H.; Gros, M.; Soriano del Amo, D.; Sundaram, S.; Lauvau, G.; Marlow, F.; Liu, Y.; Stanley, P.; Wu, P. *Angew. Chem., Int. Ed.* **2011**, *50*, 4113–4118.
- [121] Jewett, J. C.; Bertozzi, C. R. *Org. Lett.* **2011**, *13*, 5937–5939.
- [122] Brocksom, T. J.; Nakamura, J.; Ferreira, M. L. A.; Brocksom, U. J. *Braz. Chem. Soc.* **2001**, *12*, 597 – 622.
- [123] Nicolaou, K. C.; Snyder, S. A.; Montagnon, T.; Vassilikogiannakis, G. *Angew. Chem., Int. Ed.* **2002**, *41*, 1668–1698.
- [124] Diels, O.; Alder, K. *Justus Liebigs Ann. Chem.* **1928**, *460*, 98–122.
- [125] Sauer, J.; Sustmann, R. *Angew. Chem., Int. Ed.* **1980**, *19*, 779–807.
- [126] Fleming, I. *Molecular Orbitals and Organic Chemical Reactions*; John Wiley & Sons, Ltd, **2010**; pp 69–125.
- [127] Cooley, J. H.; Williams, R. V. *J. Chem. Ed.* **1997**, *74*, 582.
- [128] García, J. I.; Mayoral, J. A.; Salvatella, L. *Acc. Chem. Res.* **2000**, *33*, 658–664.

- [129] Glassner, M.; Blinco, J. P.; Barner-Kowollik, C. *Macromol. Rapid Commun.* **2011**, *32*, 724–728.
- [130] Devaraj, N. K.; Weissleder, R.; Hilderbrand, S. A. *Bioconjugate Chem.* **2008**, *19*, 2297–2299.
- [131] Blackman, M. L.; Royzen, M.; Fox, J. M. *J. Am. Chem. Soc.* **2008**, *130*, 13518–13519.
- [132] Inglis, A. J.; Sinnwell, S.; Davis, T. P.; Barner-Kowollik, C.; Stenzel, M. H. *Macromolecules* **2008**, *41*, 4120–4126.
- [133] Nebhani, L.; Gerstel, P.; Atanasova, P.; Bruns, M.; Barner-Kowollik, C. *J. Polym. Sci., Part A: Polym. Chem.* **2009**, *47*, 7090–7095.
- [134] Nebhani, L.; Sinnwell, S.; Inglis, A. J.; Stenzel, M. H.; Barner-Kowollik, C.; Barner, L. *Macromol. Rapid Commun.* **2008**, *29*, 1431–1437.
- [135] Inglis, A. J.; Stenzel, M. H.; Barner-Kowollik, C. *Macromol. Rapid Commun.* **2009**, *30*, 1792–1798.
- [136] Inglis, A. J.; Barner-Kowollik, C. *Polym. Chem.* **2011**, *2*, 126–136.
- [137] Inglis, A. J.; Nebhani, L.; Altintas, O.; Schmidt, F. G.; Barner-Kowollik, C. *Macromolecules* **2010**, *43*, 5515–5520.
- [138] Zhou, J.; Guimard, N. K.; Inglis, A. J.; Namazian, M.; Lin, C. Y.; Coote, M. L.; Spyrou, E.; Hilf, S.; Schmidt, F. G.; Barner-Kowollik, C. *Polym. Chem.* **2012**, *3*, 628–639.
- [139] Inglis, A. J.; Paulöhr, T.; Barner-Kowollik, C. *Macromolecules* **2010**, *43*, 33–36.
- [140] Glassner, M.; Delaittre, G.; Kaupp, M.; Blinco, J. P.; Barner-Kowollik, C. *J. Am. Chem. Soc.* **2012**, *134*, 7274–7277.
- [141] Porter, G.; Tchir, M. F. *J. Chem. Soc. D* **1970**, *0*, 1372–1373.
- [142] Yang, N. C.; Rivas, C. *J. Am. Chem. Soc.* **1961**, *83*, 2213–2213.
- [143] Sammes, P. G. *Tetrahedron* **1976**, *32*, 405–422.
- [144] Gruending, T.; Oehlenschlaeger, K. K.; Frick, E.; Glassner, M.; Schmid, C.; Barner-Kowollik, C. *Macromol. Rapid Commun.* **2011**, *32*, 807–812.
- [145] Oehlenschlaeger, K. K.; Mueller, J. O.; Heine, N. B.; Glassner, M.; Guimard, N. K.; Delaittre, G.; Schmidt, F. G.; Barner-Kowollik, C. *Angew. Chem., Int. Ed.* **2013**, *52*, 762–766.

- [146] Porter, G.; Tchir, M. F. *J. Chem. Soc. A* **1971**, 0, 3772–3777.
- [147] Wilson, R. M.; Hannemann, K.; Heineman, W. R.; Kirchhoff, J. R. *J. Am. Chem. Soc.* **1987**, 109, 4743–4745.
- [148] Moorthy, J. N.; Samanta, S. *ARKIVOC* **2007**, 8, 324–340.
- [149] Small, R. D.; Scaiano, J. C. *J. Phys. Chem.* **1978**, 82, 2662–2664.
- [150] Arumugam, S.; Popik, V. V. *J. Am. Chem. Soc.* **2009**, 131, 11892–11899.
- [151] Arumugam, S.; Orski, S. V.; Locklin, J.; Popik, V. V. *J. Am. Chem. Soc.* **2012**, 134, 179–182.
- [152] Arumugam, S.; Popik, V. V. *J. Am. Chem. Soc.* **2011**, 133, 15730–15736.
- [153] Arumugam, S.; Popik, V. V. *J. Am. Chem. Soc.* **2011**, 133, 5573–5579.
- [154] Arumugam, S.; Popik, V. V. *J. Am. Chem. Soc.* **2012**, 134, 8408–8411.
- [155] Thomson, J. J. *Proc. Roy. Soc. A* **1913**, 89, 1–20.
- [156] Kandiah, M.; Urban, P. L. *Chem. Soc. Rev.* **2013**, 42, 5299–5322.
- [157] Barner-Kowollik, C.; Falkenhagen, J.; Gruending, T.; Weidner, S. *Mass Spectrometry in Polymer Chemistry*; Wiley-VCH Verlag GmbH & Co. KGaA, **2011**; pp 1–4.
- [158] Hanton, S. D. *Chem. Rev.* **2001**, 101, 527–570.
- [159] Gies, A. P. *Mass Spectrometry in Polymer Chemistry*; Wiley-VCH Verlag GmbH & Co. KGaA, **2011**; pp 33–56.
- [160] Barner-Kowollik, C.; Falkenhagen, J.; Gruending, T.; Weidner, S. *Mass Spectrometry in Polymer Chemistry*; Wiley-VCH Verlag GmbH & Co. KGaA, **2011**; pp 1–483.
- [161] Hart-Smith, G.; Barner-Kowollik, C. *Macromol. Chem. Phys.* **2010**, 211, 1507–1529.
- [162] Gruending, T.; Weidner, S.; Falkenhagen, J.; Barner-Kowollik, C. *Polym. Chem.* **2010**, 1, 599–617.
- [163] Dole, M.; Mack, L. L.; Hines, R. L.; Mobley, R. C.; Ferguson, L. D.; Alice, M. B. *J. Chem. Phys.* **1968**, 49, 2240–2249.
- [164] Mack, L. L.; Kralik, P.; Rheude, A.; Dole, M. *J. Chem. Phys.* **1970**, 52, 4977–4986.

- [165] Fenn, J.; Mann, M.; Meng, C.; Wong, S.; Whitehouse, C. *Science* **1989**, *246*, 64–71.
- [166] Gruending, T.; Guilhaus, M.; Barner-Kowollik, C. *Anal. Chem.* **2008**, *80*, 6915–6927.
- [167] Banerjee, S.; Mazumdar, S. *Int. J. Anal. Chem.* **2012**, 1–40.
- [168] Smith, R. *Int. J. Mass spectrom.* **2000**, *200*, 509–544.
- [169] Manisali, I.; Chen, D.; Schneider, B. *TrAC, Trends Anal. Chem.* **2006**, *25*, 243–256.
- [170] Karas, M.; Bachmann, D.; Hillenkamp, F. *Anal. Chem.* **1985**, *57*, 2935–2939.
- [171] Tanaka, K.; Waki, H.; Ido, Y.; Akita, S.; Yoshida, Y.; Yoshida, T.; Matsuo, T. *Rapid Commun. Mass Spectrom.* **1988**, *2*, 151–153.
- [172] Hillenkamp, F.; Karas, M. *MALDI MS*; Wiley-VCH Verlag GmbH & Co. KGaA, **2007**; pp 1–28.
- [173] Hanton, S. D.; Owens, K. G. *Mass Spectrometry in Polymer Chemistry*; Wiley-VCH Verlag GmbH & Co. KGaA, **2011**; pp 119–147.
- [174] Hart-Smith, G.; Blanksby, S. J. *Mass Spectrometry in Polymer Chemistry*; Wiley-VCH Verlag GmbH & Co. KGaA, **2011**; pp 5–32.
- [175] Jonscher, K. R.; Yates III, J. R. *Anal. Biochem.* **1997**, *244*, 1–15.
- [176] Marshall, A. G.; Hendrickson, C. L.; Jackson, G. S. *Mass Spectrom. Rev.* **1998**, *17*, 1–35.
- [177] Perry, R. H.; Cooks, R. G.; Noll, R. J. *Mass Spectrom. Rev.* **2008**, *27*, 661–699.
- [178] Wollnik, H. *Mass Spectrom. Rev.* **1993**, *12*, 89–114.
- [179] Weickhardt, C.; Moritz, F.; Grotemeyer, J. *Mass Spectrom. Rev.* **1996**, *15*, 139–162.
- [180] Glish, G. L.; Vachet, R. W. *Nat. Rev. Drug Discov.* **2003**, *2*, 140–150.
- [181] Michael, S. M.; Chien, M.; Lubman, D. M. *Rev. Sci. Instrum.* **1992**, *63*, 4277–4284.
- [182] Mamyrin, B.; Karataev, V.; Shmikk, D.; Zagulin, V. *Sov. Phys. JETP* **1973**, *37*, 45–48.
- [183] Chughtai, K.; Heeren, R. M. A. *Chem. Rev.* **2010**, *110*, 3237–3277.
- [184] Schriemer, D. C.; Li, L. *Anal. Chem.* **1996**, *68*, 2721–2725.

- [185] Miller, P. E.; Denton, M. B. *J. Chem. Educ.* **1986**, *63*, 617–622.
- [186] McDonnell, L. A.; Heeren, R. M. *Mass Spectrom. Rev.* **2007**, *26*, 606–643.
- [187] Pól, J.; Strohal, M.; Havlíček, V.; Volný, M. *Histochem Cell Biol.* **2010**, *134*, 423–443.
- [188] Mahoney, C. M.; Weidner, S. M. *Mass Spectrometry in Polymer Chemistry*; Wiley-VCH Verlag GmbH & Co. KGaA, **2011**; pp 149–207.
- [189] Franck, J.; Longuespée, R.; Wisztorski, M.; Van Remoortere, A.; Van Zeijl, R.; Deelder, A.; Salzet, M.; McDonnell, L.; Fournier, I. *Med. Sci. Monit.* **2010**, *16*, BR293–BR299.
- [190] Salter, T. L.; Green, F. M.; Gilmore, I. S.; Seah, M. P.; Stokes, P. *Surf. Interface Anal.* **2011**, *43*, 294–297.
- [191] Bletsos, I. V.; Hercules, D. M.; VanLeyen, D.; Benninghoven, A. *Macromolecules* **1987**, *20*, 407–413.
- [192] Caprioli, R. M.; Farmer, T. B.; Gile, J. *Anal. Chem.* **1997**, *69*, 4751–4760.
- [193] Castellino, S.; Groseclose, M. R.; Wagner, D. *Bioanalysis* **2011**, *3*, 2427–2441.
- [194] Burrell, M.; Earnshaw, C.; Clench, M. J. *Exp. Bot.* **2007**, *58*, 757–763.
- [195] Cornett, D. S.; Reyzer, M. L.; Chaurand, P.; Caprioli, R. M. *Nat. Methods* **2007**, *4*, 828–833.
- [196] Benninghoven, A. *Angew. Chem., Int. Ed.* **1994**, *33*, 1023–1043.
- [197] Belu, A. M.; Graham, D. J.; Castner, D. G. *Biomaterials* **2003**, *24*, 3635–3653.
- [198] Benninghoven, A. *Surf. Sci.* **1973**, *35*, 427–457.
- [199] Benninghoven, A. *Surf. Interface Anal.* **2011**, *43*, 2–11.
- [200] Cyriac, J.; Pradeep, T.; Kang, H.; Souda, R.; Cooks, R. G. *Chem. Rev.* **2012**, *112*, 5356–5411.
- [201] Heeren, R.; McDonnell, L.; Amstalden, E.; Luxembourg, S.; Altelaar, A.; Piersma, S. *Appl. Surf. Sci.* **2006**, *252*, 6827–6835.
- [202] Takás, Z.; Wiseman, J. M.; Gologan, B.; Cooks, R. G. *Science* **2004**, *306*, 471–473.
- [203] Cooks, R. G.; Ouyang, Z.; Takats, Z.; Wiseman, J. M. *Science* **2006**, *311*, 1566–1570.

- [204] Costa, A. B.; Cooks, R. G. *Chem. Commun.* **2007**, 0, 3915–3917.
- [205] Ifa, D. R.; Wu, C.; Ouyang, Z.; Cooks, R. G. *Analyst* **2010**, 135, 669–681.
- [206] Badu-Tawiah, A. K.; Eberlin, L. S.; Ouyang, Z.; Cooks, R. G. *Annu. Rev. Phys. Chem.* **2013**, 64, 481–505.
- [207] Wiseman, J. M.; Ifa, D. R.; Venter, A.; Cooks, R. G. *Nat. Protoc.* **2008**, 3, 517–524.
- [208] Pauloehrl, T.; Delaittre, G.; Bastmeyer, M.; Barner-Kowollik, C. *Polym. Chem.* **2012**, 3, 1740–1749.
- [209] Campos, L. M.; Killops, K. L.; Sakai, R.; Paulusse, J. M. J.; Damiron, D.; Drockenmuller, E.; Messmore, B. W.; Hawker, C. J. *Macromolecules* **2008**, 41, 7063–7070.
- [210] Sinnwell, S.; Inglis, A. J.; Stenzel, M. H.; Barner-Kowollik, C. *Click Chemistry for Biotechnology and Materials Science*; John Wiley & Sons, Ltd, **2009**; pp 89–117.
- [211] Hawker, C. J.; Wooley, K. L. *Science* **2005**, 309, 1200–1205.
- [212] Kade, M. J.; Burke, D. J.; Hawker, C. J. *J. Polym. Sci., Part A: Polym. Chem.* **2010**, 48, 743–750.
- [213] Hoyle, C. E.; Lee, T. Y.; Roper, T. J. *Polym. Sci., Part A: Polym. Chem.* **2004**, 42, 5301–5338.
- [214] Lowe, A. B. *Polym. Chem.* **2010**, 1, 17–36.
- [215] Killops, K. L.; Campos, L. M.; Hawker, C. J. *J. Am. Chem. Soc.* **2008**, 130, 5062–5064.
- [216] Campos, L. M.; Meinel, I.; Guino, R. G.; Schierhorn, M.; Gupta, N.; Stucky, G. D.; Hawker, C. J. *Adv. Mater.* **2008**, 20, 3728–3733.
- [217] Koo, S. P. S.; Stamenović, M. M.; Prasath, R. A.; Inglis, A. J.; Du Prez, F. E.; Barner-Kowollik, C.; Van Camp, W.; Junkers, T. J. *Polym. Sci., Part A: Polym. Chem.* **2010**, 48, 1699–1713.
- [218] Kim, B. J.; Given-Beck, S.; Bang, J.; Hawker, C. J.; Kramer, E. J. *Macromolecules* **2007**, 40, 1796–1798.
- [219] Jana, N. R.; Erathodiyil, N.; Jiang, J.; Ying, J. Y. *Langmuir* **2010**, 26, 6503–6507.
- [220] Garamszegi, L.; Donzel, C.; Carrot, G.; Nguyen, T. Q.; Hilborn, J. *React. Funct. Polym.* **2003**, 55, 179–183.

- [221] Liras, M.; Garcóa, O.; Quijada-Garrido, I.; París, R. *Macromolecules* **2011**, *44*, 1335–1339.
- [222] Uygun, M.; Tasdelen, M. A.; Yagci, Y. *Macromol. Chem. Phys.* **2010**, *211*, 103–110.
- [223] Boyer, C.; Soeriyadi, A. H.; Roth, P. J.; Whittaker, M. R.; Davis, T. P. *Chem. Commun.* **2011**, *47*, 1318–1320.
- [224] Trollsås, M.; Hawker, C. J.; Hedrick, J. L.; Carrot, G.; Hilborn, J. *Macromolecules* **1998**, *31*, 5960–5963.
- [225] Stenzel, M. H.; Davis, T. P.; Barner-Kowollik, C. *Chem. Commun.* **2004**, 1546–1547.
- [226] Xu, J.; He, J.; Fan, D.; Wang, X.; Yang, Y. *Macromolecules* **2006**, *39*, 8616–8624.
- [227] Boyer, C.; Granville, A.; Davis, T. P.; Bulmus, V. J. *Polym. Sci., Part A: Polym. Chem.* **2009**, *47*, 3773–3794.
- [228] Sumerlin, B. S.; Lowe, A. B.; Stroud, P. A.; Zhang, P.; Urban, M. W.; McCormick, C. L. *Langmuir* **2003**, *19*, 5559–5562.
- [229] Nebhani, L.; Barner-Kowollik, C. *Macromol. Rapid Commun.* **2010**, *31*, 1298–1305.
- [230] Chong, S.-F.; Chandrawati, R.; Städler, B.; Park, J.; Cho, J.; Wang, Y.; Jia, Z.; Bulmus, V.; Davis, T. P.; Zelikin, A. N.; Caruso, F. *Small* **2009**, *5*, 2601–2610.
- [231] Chan, J. W.; Hoyle, C. E.; Lowe, A. B. *J. Am. Chem. Soc.* **2009**, *131*, 5751–5753.
- [232] Chan, J. W.; Hoyle, C. E.; Lowe, A. B.; Bowman, M. *Macromolecules* **2010**, *43*, 6381–6388.
- [233] Li, G.-Z.; Randev, R. K.; Soeriyadi, A. H.; Rees, G.; Boyer, C.; Tong, Z.; Davis, T. P.; Becer, C. R.; Haddleton, D. M. *Polym. Chem.* **2010**, *1*, 1196–1204.
- [234] Syrett, J. A.; Jones, M. W.; Haddleton, D. M. *Chem. Commun.* **2010**, *46*, 7181–7183.
- [235] Johnson, J. A.; Finn, M. G.; Koberstein, J. T.; Turro, N. J. *Macromolecules* **2007**, *40*, 3589–3598.
- [236] Kang, M.; Moon, B. *Macromolecules* **2008**, *42*, 455–458.
- [237] Katz, J. S.; Zhong, S.; Ricart, B. G.; Pochan, D. J.; Hammer, D. A.; Burdick, J. A. *J. Am. Chem. Soc.* **2010**, *132*, 3654–3655.

- [238] Braun, F.; Eng, L.; Trogisch, S.; Voit, B. *Macromol. Chem. Phys.* **2003**, *204*, 1486–1496.
- [239] Xie, Z.; Hu, X.; Chen, X.; Sun, J.; Shi, Q.; Jing, X. *Biomacromolecules* **2007**, *9*, 376–380.
- [240] Bajpai, U. D. N.; Bajpai, A. K.; Bajpai, J. J. *Appl. Polym. Sci.* **1991**, *42*, 2005–2012.
- [241] Odian, G. *Principles of Polymerization*; John Wiley & Sons, Inc., **2004**; pp 198–349.
- [242] He, Y. Z.; Cui, J. P.; Mallard, W. G.; Tsang, W. J. *Am. Chem. Soc.* **1988**, *110*, 3754–3759.
- [243] Delaittre, G.; Pauloehrl, T.; Bastmeyer, M.; Barner-Kowollik, C. *Macromolecules* **2012**, *45*, 1792–1802.
- [244] Kice, J. L. *J. Am. Chem. Soc.* **1954**, *76*, 6274–6280.
- [245] Schumers, J.-M.; Fustin, C.-A.; Can, A.; Hoogenboom, R.; Schubert, U. S.; Gohy, J.-F. *J. Polym. Sci., Part A: Polym. Chem.* **2009**, *47*, 6504–6513.
- [246] Borman, C. D.; Jackson, A. T.; Bunn, A.; Cutter, A. L.; Irvine, D. J. *Polymer* **2000**, *41*, 6015–6020.
- [247] Jackson, A. T.; Bunn, A.; Priestnall, I. M.; Borman, C. D.; Irvine, D. J. *Polymer* **2006**, *47*, 1044–1054.
- [248] Gruending, T.; Guilhaus, M.; Barner-Kowollik, C. *Macromol. Rapid Commun.* **2009**, *30*, 589–597.
- [249] Marriott, G.; Miyata, H.; Kinoshita Jr., K. *Biochem. Int.* **1992**, *26*, 943–951.
- [250] Bennet, F.; Hart-Smith, G.; Gruending, T.; Davis, T. P.; Barker, P. J.; Barner-Kowollik, C. *Macromol. Chem. Phys.* **2010**, *211*, 1083–1097.
- [251] Hall, D. J.; Van Den Berghe, H. M.; Dove, A. P. *Polym. Int.* **2011**, *60*, 1149–1157.
- [252] Stanford, M. J.; Pflughaupt, R. L.; Dove, A. P. *Macromolecules* **2010**, *43*, 6538–6541.
- [253] Gramlich, W. M.; Robertson, M. L.; Hillmyer, M. A. *Macromolecules* **2010**, *43*, 2313–2321.
- [254] Khan, M. N. *J. Pharm. Sci.* **1984**, *73*, 1767–1771.

- [255] Kammari, L.; Šolomek, T.; Ngoy, B. P.; Heger, D.; Klàan, P. J. *Am. Chem. Soc.* **2010**, *132*, 11431–11433.
- [256] Sundberg, S. A.; Barrett, R. W.; Pirrung, M.; Lu, A. L.; Kiangsoontra, B.; Holmes, C. P. *J. Am. Chem. Soc.* **1995**, *117*, 12050–12057.
- [257] Yamaguchi, S.; Yamahira, S.; Kikuchi, K.; Sumaru, K.; Kanamori, T.; Nagamune, T. *Angew. Chem., Int. Ed.* **2012**, *51*, 128–131.
- [258] Luo, Y.; Shoichet, M. S. *Nature Mater.* **2004**, *3*, 249–253.
- [259] Young, D. D.; Deiters, A. *Org. Biomol. Chem.* **2007**, *5*, 999–1005.
- [260] DeForest, C. A.; Anseth, K. S. *Nat. Chem.* **2011**, *3*, 925–931.
- [261] DeForest, C. A.; Anseth, K. S. *Angew. Chem., Int. Ed.* **2012**, *51*, 1816–1819.
- [262] Yesilyurt, V.; Ramireddy, R.; Thayumanavan, S. *Angew. Chem., Int. Ed.* **2011**, *50*, 3038–3042.
- [263] Schumers, J.-M.; Vlad, A.; Huynen, I.; Gohy, J.-F.; Fustin, C.-A. *Macromol. Rapid Commun.* **2012**, *33*, 199–205.
- [264] Minkwitz, R.; Meldal, M. *QSAR Comb. Sci.* **2005**, *24*, 343–353.
- [265] McMinn, D. L.; Greenberg, M. M. *Tetrahedron* **1996**, *52*, 3827–3840.
- [266] Pirrung, M. C.; Lee, Y. R.; Park, K.; Springer, J. B. *J. Org. Chem.* **1999**, *64*, 5042–5047.
- [267] Lemieux, G. A.; Bertozzi, C. R. *Trends Biotechnol.* **1998**, *12*, 506–513.
- [268] Christman, K. L.; Broyer, R. M.; Tolstyka, Z. P.; Maynard, H. D. *J. Mater. Chem.* **2007**, *17*, 2021–2027.
- [269] Christman, K. L.; Broyer, R. M.; Schopf, E.; Kolodziej, C. M.; Chen, Y.; Maynard, H. D. *Langmuir* **2011**, *27*, 1415–1418.
- [270] Broyer, R. M.; Schopf, E.; Kolodziej, C. M.; Chen, Y.; Maynard, H. D. *Soft Matter* **2011**, *7*, 9972–9977.
- [271] Dietrich, M.; Delaittre, G.; Blinco, J. P.; Inglis, A. J.; Bruns, M.; Barner-Kowollik, C. *Adv. Funct. Mater.* **2012**, *22*, 304–312.
- [272] Bodnar, B. S.; Miller, M. J. *Angew. Chem.* **2011**, *123*, 5746–5764.

- [273] Prompinit, P.; Achalkumar, A. S.; Han, X.; Bushby, R. J.; Wälti, C.; Evans, S. D. *J. Phys. Chem. C* **2009**, *113*, 21642–21647.
- [274] Alang Ahmad, S. A.; Wong, L. S.; ul Haq, E.; Hobbs, J. K.; Leggett, G. J.; Micklefield, J. *J. Am. Chem. Soc.* **2011**, *133*, 2749–2759.
- [275] Hunger, R.; Jaegermann, W.; Merson, A.; Shapira, Y.; Pettenkofer, C.; Rappich, J. *J. Phys. Chem. B* **2006**, *110*, 15432–15441.
- [276] Engin, S.; Trouillet, V.; Franz, C. M.; Welle, A.; Bruns, M.; Wedlich, D. *Langmuir* **2010**, *26*, 6097–6101.
- [277] Ferraria, A. M.; Lopes da Silva, J. D.; Botelho do Rego, A. M. *Polymer* **2003**, *44*, 7241–7249.
- [278] Mantus, D. S.; Ratner, B. D.; Carlson, B. A.; Moulder, J. F. *Anal. Chem.* **1993**, *65*, 1431–1438.
- [279] Wagner, M. S.; Castner, D. G. *Langmuir* **2001**, *17*, 4649–4660.
- [280] Canavan, H. E.; Graham, D. J.; Cheng, X.; Ratner, B. D.; Castner, D. G. *Langmuir* **2007**, *23*, 50–56.
- [281] Kazanis, S.; McClelland, R. A. *J. Am. Chem. Soc.* **1992**, *114*, 3052–3059.
- [282] Adzima, B. J.; Tao, Y.; Kloxin, C. J.; DeForest, C. A.; Anseth, K. S.; Bowman, C. N. *Nat. Chem.* **2011**, *3*, 256–259.
- [283] Hoogenboom, R. *Angew. Chem., Int. Ed.* **2010**, *49*, 3415–3417.
- [284] Orski, S. V.; Poloukhine, A. A.; Arumugam, S.; Mao, L.; Popik, V. V.; Locklin, J. *J. Am. Chem. Soc.* **2010**, *132*, 11024–11026.
- [285] Song, W.; Wang, Y.; Qu, J.; Madden, M.; Lin, Q. *Angew. Chem., Int. Ed.* **2008**, *47*, 2832–2835.
- [286] Clovis, J. S.; Eckell, A.; Huisgen, R.; Sustmann, R. *Chem. Ber.* **1967**, *100*, 60–70.
- [287] Glassner, M.; Oehlenschlaeger, K. K.; Gruending, T.; Barner-Kowollik, C. *Macromolecules* **2011**, *44*, 4681–4689.
- [288] Hauser, F. M.; Ellenberger, S. R. *Synthesis* **1987**, 1987, 723,724.
- [289] Senthilmurugan, A.; Aidhen, I. S. *Eur. J. Org. Chem.* **2010**, 2010, 555–564.
- [290] Charlton, J. L.; Alauddin, M. M. *Tetrahedron* **1987**, *43*, 2873–2889.

- [291] Segura, J. L.; Martín, N. *Chem. Rev.* **1999**, *99*, 3199–3246.
- [292] Mellows, S. M.; Sammes, P. G. *J. Chem. Soc. D* **1971**, *1*, 21–22.
- [293] Lock, E. H.; Petrovykh, D. Y.; Mack, P.; Carney, T.; White, R. G.; Walton, S. G.; Fernsler, R. F. *Langmuir* **2010**, *26*, 8857–8868.
- [294] Mrabet, B.; Nguyen, M. N.; Majbri, A.; Mahouche, S.; Turmine, M.; Bakhrouf, A.; Chehimi, M. M. *Surf. Sci.* **2009**, *603*, 2422–2429.
- [295] Wu, Y.; Huang, Y.; Ma, H. *J. Am. Chem. Soc.* **2007**, *129*, 7226–7227.
- [296] Lee, C.-Y.; Harbers, G. M.; Grainger, D. W.; Gamble, L. J.; Castner, D. G. *J. Am. Chem. Soc.* **2007**, *129*, 9429–9438.
- [297] Charleux, B.; D'Agosto, F.; Delaître, G. In *Hybrid Latex Particles*; Herk, A. M., Landfester, K., Eds.; Adv. Polym. Sci.; Springer Berlin Heidelberg, **2011**; Vol. 233; pp 125–183.
- [298] Nie, Z.; Kumacheva, E. *Nature Mater.* **2008**, *7*, 277–290.
- [299] Nan Cheng, X. C. *J. Colloid Interface Sci.* **2010**, *348*, 71–79.
- [300] Mathieu, H. J. *Surf. Interface Anal.* **2001**, *32*, 3–9.
- [301] Pauloehrl, T.; Welle, A.; Bruns, M.; Linkert, K.; Börner, H. G.; Bastmeyer, M.; Delaître, G.; Barner-Kowollik, C. *Angew. Chem.* **2013**, doi:10.1002/anie.201302040.
- [302] Martin, T. A.; Herman, C. T.; Limpoco, F. T.; Michael, M. C.; Potts, G. K.; Bailey, R. C. *ACS Appl. Mater. Interfaces* **2011**, *3*, 3762–3771.
- [303] Fan, R.; Vermesh, O.; Srivastava, A.; Yen, B. K. H.; Qin, L.; Ahmad, H.; Kwong, G. A.; Liu, C.-C.; Gould, J.; Hood, L.; Heath, J. R. *Nat. Biotechnol.* **2008**, *26*, 1373–1378.
- [304] Braunschweig, A. B.; Huo, F.; Mirkin, C. A. *Nat. Chem.* **2009**, *1*, 353–358.
- [305] Bach, T.; Hehn, J. P. *Angew. Chem., Int. Ed.* **2011**, *50*, 1000–1045.
- [306] Carroll, G. T.; Wang, D.; Turro, N. J.; Koberstein, J. T. *Langmuir* **2006**, *22*, 2899–2905.
- [307] Takahashii, K.; Seio, K.; Sekine, M.; Hino, O.; Esashi, M. *Sens. Actuators, B* **2002**, *83*, 67–76.

- [308] Kloxin, A. M.; Kasko, A. M.; Salinas, C. N.; Anseth, K. S. *Science* **2009**, *324*, 59–63.
- [309] Lutolf, M. P. *Nature* **2012**, *482*, 477–478.
- [310] Levskaya, A.; Weiner, O. D.; Lim, W. A.; Voigt, C. A. *Nature* **2009**, *461*, 997–1001.
- [311] Poloukhtine, A. A.; Mbua, N. E.; Wolfert, M. A.; Boons, G.-J.; Popik, V. V. *J. Am. Chem. Soc.* **2009**, *131*, 15769–15776.
- [312] Verho, O.; Johnston, E. V.; Karlsson, E.; Bäckvall, J.-E. *Chem.–Eur. J.* **2011**, *17*, 11216–11222.
- [313] Chaudhuri, D.; Wettach, H.; van Schooten, K. J.; Liu, S.; Sigmund, E.; Höger, S.; Lupton, J. M. *Angew. Chem., Int. Ed.* **2010**, *49*, 7714–7717.
- [314] Wettach, H.; Jester, S. S.; Colsmann, A.; Lemmer, U.; Rehmann, N.; Meerholz, K.; Höger, S. *Synth. Met.* **2010**, *160*, 691–700.
- [315] Chan, W.; White, P. *Fmoc Solid Phase Peptide Synthesis: A Practical Approach*, 1st ed.; Oxford University Press, USA, **2000**; pp 1–371.
- [316] Legigan, T.; Clarhaut, J.; Renoux, B.; Tranoy-Opalinski, I.; Monvoisin, A.; Berjeaud, J.-M.; Guilhot, F.; Papot, S. *J. Med. Chem.* **2012**, *55*, 4516–4520.
- [317] Song, H. Y.; Ngai, M. H.; Song, Z. Y.; MacAry, P. A.; Hogley, J.; Lear, M. J. *Org. Biomol. Chem.* **2009**, *7*, 3400–3406.
- [318] Choithani, J.; Kumar, P.; Gupta, K. C. *Anal. Biochem.* **2006**, *357*, 240–248.
- [319] Broyer, R. M.; Grover, G. N.; Maynard, H. D. *Chem. Commun.* **2011**, *47*, 2212–2226.
- [320] Christman, K. L.; Enriquez-Rios, V. D.; Maynard, H. D. *Soft Matter* **2006**, *2*, 928–939.
- [321] Fuchs, B. J. *Chem. Soc. C* **1968**, *0*, 68–71.
- [322] Hargreaves, M. K.; Pritchard, J. G.; Dave, H. R. *Chem. Rev.* **1970**, *70*, 439–469.
- [323] Sedman, V. L.; Adler-Abramovich, L.; Allen, S.; Gazit, E.; Tendler, S. J. B. *J. Am. Chem. Soc.* **2006**, *128*, 6903–6908.
- [324] Pauloehrl, T.; Welle, A.; Oehlschlaeger, K. K.; Barner-Kowollik, C. *Chem. Sci.* **2013**, *4*, 3503–3507.

- [325] Huo, F.; Zheng, Z.; Zheng, G.; Giam, L. R.; Zhang, H.; Mirkin, C. A. *Science* **2008**, *321*, 1658–1660.
- [326] McNitt, C. D.; Popik, V. V. *Org. Biomol. Chem.* **2012**, *10*, 8200–8202.
- [327] Vedejs, E.; Eberlein, T. H.; Varie, D. L. *J. Am. Chem. Soc.* **1982**, *104*, 1445–1447.
- [328] Glassner, M.; Oehlenschlaeger, K. K.; Welle, A.; Bruns, M.; Barner-Kowollik, C. *Chem. Commun.* **2013**, *49*, 633–635.
- [329] Zavarzin, I. V.; Yarovenko, V. N.; Shirokov, A. V.; Smirnova, N. G.; Es'kov, A. A.; Krayushkin, M. M. *ARKIVOC* **2003**, *8*, 205–223.
- [330] Duchenet, V.; Vallee, Y. *J. Chem. Soc., Chem. Commun.* **1993**, *0*, 806–807.
- [331] Vedejs, E.; Reid, J. G. *J. Am. Chem. Soc.* **1984**, *106*, 4617–4618.
- [332] Norrman, K.; Papra, A.; Kamounah, F. S.; Gadegaard, N.; Larsen, N. B. *J. Mass Spectrom.* **2002**, *37*, 699–708.
- [333] Artel, V.; Cohen, R.; Aped, I.; Ronen, M.; Gerber, D.; Sukenik, C. N. *Langmuir* **2012**, *29*, 191–198.
- [334] Dirksen, A.; Hackeng, T. M.; Dawson, P. E. *Angew. Chem.* **2006**, *118*, 7743–7746.
- [335] Richter, B.; Pauloehrl, T.; Kaschke, J.; Fichtner, D.; Fischer, J.; Greiner, A. M.; Wedlich, D.; Wegener, M.; Delaittre, G.; Barner-Kowollik, C. *Adv. Mater.* **2013**, doi:10.1002/adma.201302678.
- [336] Zhou, X.; Boey, F.; Huo, F.; Huang, L.; Zhang, H. *Small* **2011**, *7*, 2273–2289.
- [337] Leggett, G. J. *Nanoscale* **2012**, *4*, 1840–1855.
- [338] Wendeln, C.; Ravoo, B. J. *Langmuir* **2012**, *28*, 5527–5538.
- [339] Chou, S. Y.; Krauss, P. R.; Renstrom, P. J. *Science* **1996**, *272*, 85–87.
- [340] Vieu, C.; Carcenac, F.; Pépin, A.; Chen, Y.; Mejias, M.; Lebib, A.; Manin-Ferlazzo, L.; Couraud, L.; Launois, H. *Appl. Surf. Sci.* **2000**, *164*, 111–117.
- [341] Mirkin, C. A. *ACS Nano* **2007**, *1*, 79–83.
- [342] LaFratta, C.; Fourkas, J.; Baldacchini, T.; Farrer, R. *Angew. Chem., Int. Ed.* **2007**, *46*, 6238–6258.
- [343] Li, L.; Gattass, R. R.; Gershgoren, E.; Hwang, H.; Fourkas, J. T. *Science* **2009**, *324*, 910–913.

- [344] Fischer, J.; von Freymann, G.; Wegener, M. *Adv. Mater.* **2010**, *22*, 3578–3582.
- [345] Scott, T. F.; Kloxin, C. J.; Forman, D. L.; McLeod, R. R.; Bowman, C. N. *J. Mater. Chem.* **2011**, *21*, 14150–14155.
- [346] Quick, A. S.; Fischer, J.; Richter, B.; Pauloehrl, T.; Trouillet, V.; Wegener, M.; Barner-Kowollik, C. *Macromol. Rapid Commun.* **2013**, *34*, 335–340.
- [347] Nimmo, C. M.; Shoichet, M. S. *Bioconjugate Chem.* **2011**, *22*, 2199–2209.
- [348] Hahn, M.; Miller, J.; West, J. *Adv. Mater.* **2006**, *18*, 2679–2684.
- [349] Wosnick, J. H.; Shoichet, M. S. *Chem. Mater.* **2007**, *20*, 55–60.
- [350] DeForest, C. A.; Polizzotti, B. D.; Anseth, K. S. *Nature Mater.* **2009**, *8*, 659–664.
- [351] Klein, F.; Richter, B.; Striebel, T.; Franz, C. M.; Freymann, G. v.; Wegener, M.; Bastmeyer, M. *Adv. Mater.* **2011**, *23*, 1341–1345.
- [352] Farrer, R. A.; LaFratta, C. N.; Li, L.; Praino, J.; Naughton, M. J.; Saleh, B. E. A.; Teich, M. C.; Fourkas, J. T. *J. Am. Chem. Soc.* **2006**, *128*, 1796–1797.
- [353] Klein, F.; Striebel, T.; Fischer, J.; Jiang, Z.; Franz, C. M.; von Freymann, G.; Wegener, M.; Bastmeyer, M. *Adv. Mater.* **2010**, *22*, 868–871.
- [354] Fischer, J.; Wegener, M. *Opt. Mater. Express* **2011**, *1*, 614–624.
- [355] Booth, M. J.; Wilson, T. J. *Biomed. Opt.* **2001**, *6*, 266–272.
- [356] Keppler, A.; Gendreizig, S.; Gronemeyer, T.; Pick, H.; Vogel, H.; Johnsson, K. *Nat. Biotechnol.* **2003**, *21*, 86–89.
- [357] Kindermann, M.; George, N.; Johnsson, N.; Johnsson, K. *J. Am. Chem. Soc.* **2003**, *125*, 7810–7811.
- [358] Hochuli, E.; Bannwarth, W.; Dobeli, H.; Gentz, R.; Stuber, D. *Nat. Biotechnol.* **1988**, *6*, 1321–1325.
- [359] Smith, D. B.; Johnson, K. S. *Gene* **1988**, *67*, 31–40.
- [360] Reddy, P. Y.; Kondo, S.; Fujita, S.; Toru, T. *Synthesis* **1998**, *7*, 999–1002.
- [361] Mantovani, G.; Lecolley, F.; Tao, L.; Haddleton, D. M.; Clerx, J.; Cornelissen, J. J. L. M.; Velonia, K. *J. Am. Chem. Soc.* **2005**, *127*, 2966–2973.
- [362] Schmidt, J.; Garambois, V.; Rocheblave, L.; Martinez, J.; Pèlerin, A.; Cavellier, F.; Vivès, E. *ChemBiochem* **2010**, *11*, 1083–1092.

- [363] Durmaz, H.; Karatas, F.; Tunca, U.; Hizal, G. *J. Polym. Sci., Part A: Polym. Chem.* **2006**, *44*, 3947–3957.
- [364] Dag, A.; Durmaz, H.; Hizal, G.; Tunca, U. *J. Polym. Sci., Part A: Polym. Chem.* **2008**, *46*, 302–313.
- [365] Soriano, A.; Ventura, R.; Molero, A.; Hoen, R.; Casadoó, V.; Cortés, A.; Fanelli, F.; Albericio, F.; Lluís, C.; Franco, R.; Royo, M. *J. Med. Chem.* **2009**, *52*, 5590–5602.
- [366] Kassianidis, E.; Pearson, R. J.; Philp, D. *Chem. Eur. J.* **2006**, *12*, 8798–8812.
- [367] Vedejs, E.; Eberlein, T. H.; Wilde, R. G. *J. Org. Chem.* **1988**, *53*, 2220–2226.
- [368] Glassner, M.; Kempe, K.; Schubert, U. S.; Hoogenboom, R.; Barner-Kowollik, C. *Chem. Commun.* **2011**, *47*, 10620–10622.
- [369] Rudin, A.; Hoegy, H. L. W. *J. Polym. Sci., Part A: Polym. Chem.* **1972**, *10*, 217–235.
- [370] Parry, K. L.; Shard, A. G.; Short, R. D.; White, R. G.; Whittle, J. D.; Wright, A. *Surf. Interface Anal.* **2006**, *38*, 1497–1504.
- [371] Scofield, J. H. *J. Electron Spectrosc. Relat. Phenom.* **1976**, *8*, 129–137.
- [372] Tanuma, S.; Powell, C. J.; Penn, D. R. *Surf. Interface Anal.* **1994**, *21*, 165–176.

Curriculum Vitae

Date of Birth 10. April 1985
Place of Birth Ulm, Germany
Nationality German

Education

15.09.2010 - Present **Doctoral Studies in Chemistry funded by the Fonds der Chemischen Industrie**
Under the supervision of Prof. Dr. Christopher Barner-Kowollik
Karlsruhe Institute of Technology (KIT), Germany

12.06.2012 **DWI/RWTH Aachen Young Scientist Award sponsored by LANXESS**

24.06.2010 **Award for the best diploma thesis sponsored by Procter & Gamble**

07.01.2010 **Diploma in Chemistry mark: 1.0 (passed with highest distinction, "mit Auszeichnung")**
Synthesis of Novel Cyclopentadienyl-Capped Polymers and their Utilization in Temperature Guided Color Switching
Under the supervision of Prof. Dr. Christopher Barner-Kowollik
Universität Karlsruhe (TH), Germany

01.04.2005 - 07.01.2010 **Studies of Chemistry**
Universität Karlsruhe (TH), Karlsruhe, Germany

25.06.2004 **High School Certificate**

1996 - 2004 Illertal-Gymnasium-Vöhringen, Gmynasium, Illerzell, Germany

Employment History

- 09/2010 - Present **Institut für Technische Chemie und Polymer Chemie**
Karlsruhe Institute of Technology (KIT), Karlsruhe, Germany
Scientific Co-worker
- 07/2004 - 03/2005 **Civilian Service**
Arbeiter-Samariter-Bund, Ulm, Germany

Scholarships

- 09/2010 - 09/2012 **Fonds der Chemischen Industrie**
PhD Scholarship

Awards

- 12.06.2012 **LANXESS (DWI/RWTH Aachen) Young Scientist Award**
- 24.06.2010 **Award for the best diploma thesis sponsored by Procter & Gamble**

List of Publications and Conference Contributions

Refereed Journal Publications arising from the Thesis

- [9] *Three-Dimensional Microscaffolds Exhibiting Spatially Resolved Surface Chemistry*
Richter, B.;* **Pauloehrl, T.**;* Kaschke, J.; Fichtner, D.; Fischer, J.; Greiner, A. M.; Wedlich, D.; Wegener, M.; Delaittre, G.; Barner-Kowollik, C. *Adv. Mater.* **2013**, doi:10.1002/adma.201302678. *These authors contributed equally to this work.
- [8] *Spatially Controlled Surface Immobilization of Nucleophiles via Trapping of of Photo-Generated Thioaldehydes*
Pauloehrl, T.; Welle, A.; Oehlenschlaeger, K. K.; Barner-Kowollik, C. *Chem. Sci.* **2013**, 4, 3503–3507.
- [7] *Spatially Controlled Surface Immobilization of Non-Modified Peptides*
Pauloehrl, T.; Welle, A.; Bruns, M.; Linkert, K.; Börner, H. G.; Bastmeyer, M.; Delaittre, G.; Barner-Kowollik, C. *Angew. Chem., Int. Ed.* **2013**, doi:10.1002/anie.201302040.
- [6] *Preparation of Reactive Three-Dimensional Microstructures via Direct Laser Writing and Thiol-ene Chemistry*
Quick, A. S.; Fischer J.; Richter B.; **Pauloehrl, T.**; Trouillet, V.; Wegener, M.; Barner-Kowollik, C. *Macromol. Rapid Commun.* **2013**, 34, 335–340.
- [5b] *(Bio)Molecular Surface Patterning by Phototriggered Oxime Ligation*
Pauloehrl, T.; Delaittre, G.; Bruns M.; Meißler M.; Börner, H. G.; Bastmeyer, M.; Barner-Kowollik, C. *Angew. Chem., Int. Ed.* **2012**, 51, 9181–9184.

- [5a] *(Bio)Molekulare Oberflächenmuster durch photoinduzierte Oxime Ligation*
Pauloehrl, T.; Delaittre, G.; Bruns M.; Meißler M.; Börner; H. G.; Bastmeyer, M.; Barner-Kowollik, C. *Angew. Chem.* **2012**, *124*, 9316–9319.
- [4] *Chemical Approaches to Synthetic Polymer Surface Biofunctionalization for Targeted Cell Adhesion using Small Binding Motifs*
Delaittre, G., Greiner, A. M.; **Pauloehrl, T.**; Bastmeyer, M.; Barner-Kowollik, C. *Soft Matter* **2012**, *8*, 7323–7347.
- [3b] *Adding Spatial Control to Click Chemistry: Phototriggered Diels-Alder Surface (Bio)functionalization at Ambient Temperature*
Pauloehrl, T.; Delaittre, G.; Winkler, M.; Welle, A.; Bruns, M.; Börner, H. G.; Greiner, A. M.; Bastmeyer, M.; Barner-Kowollik, C. *Angew. Chem., Int. Ed.* **2012**, *51*, 1071–1074.
- [3a] *Klick-Chemie mit räumlicher Kontrolle: Biofunktionalisierung von Oberflächen durch photoinduzierte Diels-Alder-Reaktionen bei Umgebungstemperatur*
Pauloehrl, T.; Delaittre, G.; Winkler, M.; Welle, A.; Bruns, M.; Börner, H. G.; Greiner, A. M.; Bastmeyer, M.; Barner-Kowollik, C. *Angew. Chem.* **2012**, *124*, 1096–1099.
- [2] *Acrylamide-Based Copolymers Bearing Photoreleasable Thiols for Subsequent Thiol-Ene Functionalization*
Delaittre, G.; **Pauloehrl, T.**; Bastmeyer, M.; Barner-Kowollik, C. *Macromolecules* **2012**, *45*, 1792–1802.
- [1] *Ambient Temperature Polymer Modification by in situ Phototriggered Deprotection and Thiol-Ene Chemistry*
Pauloehrl, T.; Delaittre, G.; Bastmeyer, M.; Barner-Kowollik, C. *Polym. Chem.* **2012**, *3*, 1740–1749.

Other refereed Journal Publications

- [2] *Reversible Diels-Alder Chemistry as a Modular Polymeric Color Switch*
Paulöhrl, T.; Inglis, A. J.; Barner-Kowollik, C. *Adv. Mater.* **2010**, *22*, 2788–2791.
- [1] *Ambient Temperature Synthesis of a Versatile Macromolecular Building Block: Cyclopentadienyl-Capped Polymers*
Inglis, A. J.; **Pauloehrl, T.**; Barner-Kowollik, C. *Macromolecules* **2010**, *43*, 33–36.

Book Chapters

- [1] *Elucidation of Reaction Mechanisms and Polymer Structure: Living/Controlled Radical Polymerization*
Barner-Kowollik, C.; Delaittre, G.; Gruendling, T.; **Pauloehrl, T.** in *Mass Spectrometry in Polymer Chemistry*, Wiley-VCH Verlag GmbH & Co. KGaA, **2011**, 373–403.

Conference Contributions

- [3] *Shining Light on Click Chemistry*
Pauloehrl, T.; Delaittre, G.; Richter, B.; Bruns, M.; Bastmeyer, M.; Barner-Kowollik, C.; **Warwick Polymer Chemistry 2012**, Warwick, UK, June 09-12, 2012. (Poster)
- [2] *Polymer Surface Modification for Targeted Cell Attachment*
G. Delaittre, G.; **Pauloehrl, T.**; Richter, B.; Wegener, M.; Bastmeyer, M.; Barner-Kowollik, C.; **Symposium Celebrating the Tenth Anniversary of the CFN**, Karlsruhe, Germany, December 02-03, 2011 (Poster Presentation).
- [1] *Towards regiospecific and micro-/nano-resolved surface biofunctionalization*
Pauloehrl, T.; Delaittre, G.; Dietrich, M.; Bruns, M.; Bastmeyer, M.; Barner-Kowollik, C.; **Nano-Biology-Summerschool**, Karlsruhe, Bad Herrenalb, September 07-10, 2011 (Poster Presentation).

Acknowledgment

First, and foremost, I want to thank Prof. Dr. Christopher Barner-Kowollik for giving me the chance to work on such an exciting project and to pursue my own ideas in a self-directed manner. Your support and guidance throughout the course of my doctoral research as well as your inexhaustible energy, enthusiasm, and optimism created an excellent and motivating working environment.

I am particularly grateful to Dr. Guillaume Delaitre, Benjamin Richter, Dr. Joachim Fischer, and Prof. Dr. Martin Bastmeyer for scientific discussions and a friendly collaboration within the CFN. For an equally fruitful collaboration, I am thankful to Katharina Linkert, Maria Meißler and Prof. Dr. Hans Börner (Humboldt University of Berlin) for the just-in-time delivery of the many precisely designed peptides.

The Fonds of the Chemical Industry is sincerely acknowledged for the generous funding of my phd studies for two years. I also want to thank the DWI/RWTH for the professional organization of the Summer School in Aachen and the Lanxess AG for sponsoring the prize money. I feel honored to have received the Young Scientist Talent Award.

I also wish to express my particular gratitude to Dr. Michael Bruns and Dr. Alexander Welle for performing the many surface related characterizations. Much of the success of the presented light-driven methodologies are due to their intensive commitment to XPS- and, specifically, ToF-SIMS measurements. Many thanks also to those who performed additional measurements: Dr. Hartmut Gliemann (AFM), Dr. Alexandra Goldyn-Greiner and Benjamin Richter (fluorescence microscopy), Volker Winkler (XPS), Pia Lang and Tanja Ohmer (NMR). Michael Kaupp and Astrid Hirschbiel are acknowledged for SEC-MS measurements and for keeping the mass-spectrometer in good condition.

I am also very thankful to Johannes Willenbacher for being such an outstanding 'Vertiefer' student.

Furthermore I am grateful to Dr. Andrew Inglis. Although having not directly supervised my phd studies, you still have had a great impact on them. During my diploma thesis under your supervision I have learnt so much from you in the ways of presentation of data and scientific thinking.

I thank Jan Müller, Alexander Quick, Kim Öhlenschläger and Dr. Mathias Glassner for scientific discussions and some great joking as well as Corinna Preuß, Elena Frick and Anja Goldman for promoting the social aspects. Dr. Dominik Voll is furthermore acknowledged for his support with Latex.

Evelyn Stühling, Gabriele Herrmann, Peter Gerstel and Dr. Maria Schneider are thanked for 'the many things that need to be done' in and outside of the laboratory. I also wish to extend a big thank you to all the past and present members of the macroarc team. It was for me a great pleasure to work with all of you.

Finally, I am very thankful to my parents, my sisters and grandparents for their continues support and encouragement. My special gratitude is for Imane. Your support has always been my source of strength and inspiration and I am looking forward to many more great years together with you.